

ADA 085982

UNCLASSIFIED

SECURITY CLASSIFICATION OF THIS PAGE (When Data Entered)

19 REPORT DOCUMENTATION PAGE		READ INSTRUCTIONS BEFORE COMPLETING FORM	
18 1. REPORT NUMBER SAM TR-79-31-VOL-2	2. GOVT ACCESSION NO. AD-A085 982	3. RECIPIENT'S CATALOG NUMBER	
4. TITLE (and Subtitle) PROCEDURAL TESTS FOR ANTI-G PROTECTIVE DEVICES Volume II: G-Sensitivity Tests		5. TYPE OF REPORT & PERIOD COVERED Final rept. 1 Oct 76 - 30 Jun 78	
6. AUTHOR(s) Roy W. Thompson, Carmen E. Galvan B.A.; James E. Allred, Larry J. Meeker B.S.; Paul E. Love, and Arnold G. Kraeger		7. PERFORMING ORG. REPORT NUMBER	
8. CONTRACT OR GRANT NUMBER(s) F33615-77-C-0610		9. PROGRAM ELEMENT, PROJECT, TASK AREA & WORK UNIT NUMBERS 62202F 793012-13	
10. PERFORMING ORGANIZATION NAME AND ADDRESS Technology Incorporated 511 W. Rhapsody Dr. San Antonio, Texas 78216		11. REPORT DATE December 1979	
11. CONTROLLING OFFICE NAME AND ADDRESS USAF School of Aerospace Medicine (VNB) Aerospace Medical Division (AFSC) Brooks Air Force Base, Texas 78235		12. NUMBER OF PAGES 200	
14. MONITORING AGENCY NAME & ADDRESS (if different from Controlling Office)		15. SECURITY CLASS. (of this report) UNCLASSIFIED	
16. DISTRIBUTION STATEMENT (of this Report) Approved for public release; distribution unlimited.		15a. DECLASSIFICATION/DOWNGRADING SCHEDULE	
17. DISTRIBUTION STATEMENT (of the abstract entered in Block 20, if different from Report)			
18. SUPPLEMENTARY NOTES Appendix A applies to both volumes.			
19. KEY WORDS (Continue on reverse side if necessary and identify by block number) Acceleration Control systems--Centrifuge Performance of Acceleration sensitivity Data acquisition anti-G valve Accelerometers ECG recording Aircrew protection Equipment failure Anti-G valve Equipment in jet aircraft			
20. ABSTRACT (Continue on reverse side if necessary and identify by block number) In this second volume of a two-volume study report, an examination of anti-G valve failures is reported, as well as the results of 9 short-term investigations dealing with acceleration protection equipment and studies on the USAFSAM Human Centrifuge. These studies involved: the CWU-9/P undergarments; the Statham PM131TC pressure transducer; the Ready Pressure Anti-G valve; the ALAR "High flow" and "Special" anti-G valves; accelerometer calibration; continuous ECG recording; control-center data distribution; closed-loop centrifuge control; and the Medilog recorder.			

DD FORM 1 JAN 73 1473A

UNCLASSIFIED

SECURITY CLASSIFICATION OF THIS PAGE (When Data Entered)

401650

LHW

CONTENTS

<u>Section No.</u>		<u>Page</u>
1.	ANTI-G VALVE (AGV) FAILURES	9
1.1	Historical Data	9
1.1.1	Limitations of the Data	9
1.1.2	Explanation of the Data Used	10
1.1.3	Pertinent Notes	10
1.2	Analysis of the Historical Failure Data	11
1.2.1	Description of Illustrations	11
1.2.2	Suggestions for Future Data Collection on AGV Failures	33
1.3	Induced AGV Failure Analysis	33
1.3.1	Failure Analysis of Bendix AGV FR139A2	34
1.3.2	Failure Analysis of ALAR AGV 8400A	36
1.4	Standardized AGV Test Protocol (SVTP) Testing of Failures	37
1.4.1	Test of Bendix AGV Failure #1	37
1.4.2	Test of Bendix AGV Failure #2	44
1.4.3	Testing of ALAR AGV Failure	64
1.4.4	Failure Testing Conclusions	109
2.	SPECIFIC EQUIPMENT EVALUATIONS	110
2.1	CWU-9/P Undergarment G-Effects Tests	110
2.1.1	Test Instrumentation and Calibration	110
2.1.2	Test Methods	110
2.1.3	Data Presentation	111
2.1.4	Discussion and Conclusions	111
2.2	G-Sensitivity Evaluation of the Statham PM131TC Pressure Transducer	123
2.2.1	Test Configuration	123
2.2.2	Test Protocol	123
2.2.3	Data-handling Techniques for Performance Evaluation	123
2.2.4	Performance Evaluation	142
2.3	Ready Pressure AGV Mannequin Test	142
2.3.1	Test Protocol	142
2.3.2	Description of the Test Data	143
2.3.3	Data Analysis	144
2.3.4	Data Presentation	145
2.3.5	Test Conclusions	156
2.4	ALAR "High Flow" and "Special" Examinations	156
2.4.1	Design Modifications	156
2.4.2	Open-flow Capacity of "High Flow"	157
2.4.3	First-stage Regulator Shim Effect	157
2.5	Accelerometer Calibration	157
2.5.1	Gondola Acceleration Environment	157
2.5.2	Dynamic Calibration	170

CONTENTS (cont'd.)

<u>Section No.</u>		<u>Page</u>
2.6	Continuous ECG Recordings in Primates	171
2.6.1	Objective	171
2.6.2	ECG from Chronically Implanted Electrodes	171
2.6.3	Animal Instrumentation	175
2.6.4	Conclusions	176
2.6.5	References	176
2.7	Control Center Data Distribution System Study	177
2.7.1	Undesirable Characteristics	177
2.7.2	Recommendations	178
2.8	Closed-loop Centrifuge Control Study	179
2.8.1	Objective	179
2.8.2	Normal Centrifuge Operation	182
2.8.3	Closed-loop Control System Developed by the Air Force	183
2.8.4	Design Modifications	183
2.9	Medilog Recorder G-sensitivity Tests	189
2.9.1	Introduction	189
2.9.2	Test Protocol and Configurations	189
2.9.3	Test Results	192
2.9.4	Conclusions	196
	ABBREVIATIONS, ACRONYMS, AND SYMBOLS	198

FIGURES

<u>Figure No.</u>		
1	Number of failures for Bendix and ALAR anti-G valves for July 1974 to June 1977 . .	12
2	Number of OTH/MAL's for Bendix and ALAR anti-G valves for July 1974 to June 1977 . .	13
3	Total number of failures and OTH/MAL's for Bendix and ALAR anti-G valves for July 1974 to June 1977	14
4	Rate of occurrence of failures	15
5	Rate of occurrence of OTH/MAL's	16
6	Rate of occurrence of failures and OTH/MAL's	17
	<u>Distribution of:</u>	
7	F-111-A failures per 1000 flight hrs	18
8	F-111-A OTH/MAL's per 1000 flight hrs	19
9	F-111-A total failures and OTH/MAL's per 1000 flight hrs	20
10	F-111-D failures per 1000 flight hrs	21
11	F-111-D OTH/MAL's per 1000 flight hrs	22

CONTENTS ("Distribution of," cont'd.)

<u>Figure No.</u>		<u>Page</u>
12	F-111-D total failures and OTH/MAL's per 1000 flight hrs	23
13	F-111-E failures per 1000 flight hrs	24
14	F-111-E OTH/MAL's per 1000 flight hrs	25
15	F-111-E total failures and OTH/MAL's per 1000 flight hrs	26
16	F-111-F failures per 1000 flight hrs	27
17	F-111-F OTH/MAL's per 1000 flight hrs	28
18	F-111-F total failures and OTH/MAL's per 1000 flight hrs	29
19	T-38 failures per 10,000 flight hrs	30
20	T-38 OTH/MAL's per 10,000 flight hrs	31
21	T-38 total failures and OTH/MAL's per 10,000 flight hrs	32
22	Exploded view of the FR139A2 anti-G valve	35
23	Exploded view of the ALAR 8400A anti-G valve	38
	<u>Bendix Failure #1:</u>	
24	flow as a function of source pressure	42
25	variation (three sigma) in flow as a function of source pressure	43
26	0.1 G/sec suit pressure profile as a function of source pressure	45
27	0.1 G/sec suit pressure variation as a function of source pressure	46
28	0.1 G/sec decreasing suit pressure profile as a function of source pressure	47
29	0.1 G/sec suit pressure hysteresis as a function of source pressure	48
30	suit pressure profile comparison as a function of onset rate	49
31	suit pressure profile as a function of G-onset rate	50
32	dP/dG as a function of G-onset rate	51
33	1.5 G/sec suit pressure profile as a function of source pressure	52
34	1.5 G/sec suit pressure variation as a function of source pressure	53
35	-1.5 G/sec decreasing suit pressure profile as a function of source pressure	54
36	1.5 G/sec suit pressure hysteresis as a function of source pressure	55
37	SACM suit pressure profile comparison with minimum source pressure and maximum suit volume	56
38	suit pressure deviation and dG/dt for the minimum source pressure, maximum suit volume SACM	57
39	SACM suit pressure profile comparison with maximum source pressure and minimum suit volume	58

CONTENTS ("Bendix Failure #1," cont'd.)

<u>Figure No.</u>		<u>Page</u>
40	suit pressure deviation and dG/dt for the maximum source pressure, minimum suit volume SACM	59
41	SACM suit pressure profile comparison with median source pressure and suit volume	60
42	suit pressure deviation and dG/dt for the median source pressure and suit volume SACM	61
43	SACM suit pressure profile comparison with G vector misalignment	62
44	suit pressure deviation and dG/dt for the G vector misalignment SACM	63
<u>Bendix Failure #2:</u>		
45	flow as a function of source pressure	66
46	variation (three sigma) in flow as a function of source pressure	67
47	0.1 G/sec suit pressure profile as a function of source pressure	68
48	0.1 G/sec suit pressure variation as a function of source pressure	69
49	0.1 G/sec decreasing suit pressure profile as a function of source pressure	70
50	0.1 G/sec suit pressure hysteresis as a function of source pressure	71
51	suit pressure profile comparison as a function of onset rate	72
52	suit pressure profile as a function of G-onset rate	73
53	dP/dG as a function of G-onset rate	74
54	1.5 G/sec suit pressure profile as a function of source pressure	75
55	1.5 G/sec suit pressure variation as a function of source pressure	76
56	-1.5 G/sec decreasing suit pressure profile as a function of source pressure	77
57	1.5 G/sec suit pressure hysteresis as a function of source pressure	78
58	SACM suit pressure profile comparison with minimum source pressure and maximum suit volume	79
59	suit pressure deviation and dG/dt for the minimum source pressure, maximum suit volume SACM	80
60	SACM suit pressure profile comparison with maximum source pressure and minimum suit volume	81
61	suit pressure deviation and dG/dt for the maximum source pressure, minimum suit volume SACM	82
62	SACM suit pressure profile comparison with median source pressure and suit volume	83
63	suit pressure deviation and dG/dt for the median source pressure and suit volume SACM	84
64	SACM suit pressure profile comparison with G vector misalignment	85
65	suit pressure deviation and dG/dt for the G vector misalignment SACM	86

CONTENTS (cont'd.)

<u>Figure No.</u>		<u>Page</u>
	<u>ALAR Failure #1:</u>	
66	flow as a function of source pressure	88
67	variation (three sigma) in flow as a function of source pressure	89
68	0.1 G/sec suit pressure profile as a function of source pressure	90
69	0.1 G/sec suit pressure variation as a function of source pressure	91
70	0.1 G/sec decreasing suit pressure profile as a function of source pressure	92
71	0.1 G/sec suit pressure hysteresis as a function of source pressure	93
72	suit pressure profile comparison as a function of onset rate	94
73	suit pressure profile as a function of G-onset rate	95
74	dP/dG as a function of G-onset rate	96
75	1.5 G/sec suit pressure profile as a function of source pressure	97
76	1.5 G/sec suit pressure variation as a function of source pressure	98
77	-1.5 G/sec decreasing suit pressure profile as a function of source pressure	99
78	1.5 G/sec suit pressure hysteresis as a function of source pressure	100
79	SACM suit pressure profile comparison with minimum source pressure and maximum suit volume	101
80	suit pressure deviation and dG/dt for the minimum source pressure, maximum suit volume SACM	102
81	SACM suit pressure profile comparison with maximum source pressure and minimum suit volume	103
82	suit pressure deviation and dG/dt for the maximum source pressure, minimum suit volume SACM	104
83	SACM suit pressure profile comparison with median source pressure and suit volume	105
84	suit pressure deviation and dG/dt for the median source pressure and suit volume SACM	106
85	SACM suit pressure profile comparison with G vector misalignment	107
86	suit pressure deviation and dG/dt for the G vector misalignment SACM	108
	<u>Normalized Exposure Suit:</u>	
87	abdomen force	118
88	right thigh force	119
89	left thigh force	120
90	right calf force	121
91	left calf force	122

CONTENTS (cont'd.)

Figure No.

Page

Acceleration Influence on the:

92	+Z axis of the PM131TC-3644 transducer with 0-psig stimulus	124
93	-Z axis of the PM131TC-3644 transducer with 0-psig stimulus	125
94	+Y axis of the PM131TC-3644 transducer with 0-psig stimulus	126
95	-Y axis of the PM131TC-3644 transducer with 0-psig stimulus	127
96	+X axis of the PM131TC-3644 transducer with 0-psig stimulus	128
97	-X axis of the PM131TC-3644 transducer with 0-psig stimulus	129
98	+Z axis of the PM131TC-3644 transducer with 10-psig stimulus	130
99	-Z axis of the PM131TC-3644 transducer with 10-psig stimulus	131
100	+Y axis of the PM131TC-3644 transducer with 10-psig stimulus	132
101	-Y axis of the PM131TC-3644 transducer with 10-psig stimulus	133
102	+X axis of the PM131TC-3644 transducer with 10-psig stimulus	134
103	-X axis of the PM131TC-3644 transducer with 10-psig stimulus	135
104	+Z axis of the PM131TC-3644 transducer with 18-psig stimulus	136
105	-Z axis of the PM131TC-3644 transducer with 18-psig stimulus	137
106	+Y axis of the PM131TC-3644 transducer with 18-psig stimulus	138
107	-Y axis of the PM131TC-3644 transducer with 18-psig stimulus	139
108	+X axis of the PM131TC-3644 transducer with 18-psig stimulus	140
109	-X axis of the PM131TC-3644 transducer with 18-psig stimulus	141

RPV Mannequin Test:

110	suit pressure response for four test cases	147
111	abdominal force response for four test cases	149
112	left thigh force response for four test cases	151
113	left calf force response for four test cases	153
114	right thigh force response for four test cases	155
115	suit pressure residuals	159
116	abdominal force residuals	161
117	left thigh force residuals	163
118	left calf force residuals	165
119	right thigh force residuals	167
120	Recommended arrangement of new patchcord programming system	180

CONTENTS (cont'd.)

<u>Figure No.</u>		<u>Page</u>
121	New patchcord programming system	181
122	Electrical rotor arm drive subsystem (Part I)	184
123	Electrical rotor arm drive subsystem (Part II)	185
124	Hydraulic rotor arm drive subsystem (Part I)	186
125	Hydraulic rotor arm drive subsystem (Part II)	187
126	Air Force closed-loop control circuit	188
127	Time base expansion test configuration	190
128	Recorder axis orientation	191
129	Medilog recorder test configuration	191
130	Oxford reproduce and re-record test configuration	193

TABLES

<u>Table No.</u>		
1	Bendix AGV failure #1 performance evaluation table	40
2	Key to symbols in figures 24 to 86	41
3	Bendix AGV failure #2 performance evaluation table	65
4	ALAR AGV failure #1 performance evaluation table	109
5	First set of runs <u>without</u> exposure suit	112
6	Second set of runs <u>without</u> exposure suit	113
7	Third set of runs <u>without</u> exposure suit	114
8	First set of runs <u>with</u> exposure suit	115
9	Second set of runs <u>with</u> exposure suit	116
10	Third set of runs <u>with</u> exposure suit	117
	<u>RPV Mannequin Test:</u>	
11	suit pressure response (psig)	146
12	abdominal force response (psi)	148
13	left thigh force response (psi)	150
14	left calf force response (psi)	152
15	right thigh force response (psi)	154
16	suit pressure residuals (psig)	158

CONTENTS ("RPV Mannequin Test," cont'd.)

<u>Table No.</u>		<u>Page</u>
17	abdominal force residuals (psi)	160
18	left thigh force residuals (psi)	162
19	left calf force residuals (psi)	164
20	right thigh force residuals (psi)	166
21	ALAR "high-flow" and "special" design modifications	168
22	ALAR "high-flow" and "special" open-flow capacities	169
23	ALAR 8400A first-stage regulator shim effect	169
24	Accelerometer calibration values for location 13 ft. 9 in. \pm 0.1 in. from the cent. of rotation	172
25	Order of axis testing and test signals	192
26	Oxford reproduce test setup	193
27	Time base expansion accuracy	194
28	Reproduced frequency (mean)	194
29	Percent error in frequency reproduction at 1-G start of run	195
30	Percent error channel 1 reproduce normalized to 1-G start of run	195

PROCEDURAL TESTS FOR ANTI-G PROTECTIVE DEVICES

VOLUME II:

G-SENSITIVITY TESTS

1. ANTI-G VALVE FAILURES

Two lines of investigation were taken to develop an anti-gravity valve (AGV) failure analysis for predicting lifetime expectations and reasons for failure of respective valves. In the first of these investigations, historical anti-G valve failure data were obtained for analysis. In the second, failures were induced in functional AGV's; and these "failed" valves were tested. Test results then were analyzed using the GVALVPGM (described in Appendix A).

1.1 Historical Data

Data on AGV failure were sought. Because the most frequently used valve (i.e., the ALAR 8000 series--which includes the 8400A, 8000A, and 8000B) is considered to be a low-cost (or throw-away) item, only two repositories of AGV failure data were found: The Naval Aviation Integrated Logistics Support Center (NAILSC), Naval Air Station, Patuxent River, Maryland 20670; and The Department of the Air Force Headquarters, Air Force Logistics Command, Wright-Patterson AFB, Ohio 45433.

1.1.1 Limitations of the Data

The data available through NAILSC were most pertinent to this study. Because a major overhaul of the computer programs used to access this data repository was in process, however, the data were inaccessible for the period of this contract. Any followup work should consider this NAILSC source.

For this report, the data were provided by the Wright-Patterson Logistics Command, and were more limited than the NAILSC data. The limitations of the Wright-Patterson AFB data are as follows:

- (a) Data were available on only two valves, the ALAR and the Bendix.
- (b) Each of these valves was used in only one type of aircraft--the ALAR AGV in the T-38, and the Bendix AGV in four models of the F-111.

EDITOR'S NOTE: Appendix A applies to, and supplements, Volumes I and II. (Information on how to order this Appendix appears at the close of each volume.)

(c) Both the T-38 and the F-111 are low-G aircraft. No data are available on AGV failures in high-G aircraft.

(d) At the time of the study, the repository contained only three years of monthly data (July 1974 - June 1977).

(e) The failures were classified in such a manner that neither the reasons for failure nor the time of failure (whether preflight or inflight) could be determined.

1.1.2 Explanation of the Data Used

The original data used in the following analysis were recorded in columns headed: (1) month; (2) op time (or flight hrs); and (3) occurrences, both fail (failures) and OTH/MAL (other malfunctions). [NOTE: These raw data are not included in this report.] The classifications under occurrences, failures, other malfunctions, and total can be interpreted as follows:

- 1) Failures means any Type 1 HOW MALFUNCTION CODE--which indicates that the item can no longer meet the minimum specified performance requirements due to its own internal failure pattern.
- 2) Other Malfunctions (OTH/MAL) means any Type 2 HOW MALFUNCTION CODE--which indicates that the item can no longer meet the minimum specified performance requirements due to some induced condition and not due to its own internal failure pattern.
- 3) Total included, inexplicitly in the total for this column along with Failures and OTH/MAL's are Type 6 HOW MALFUNCTION CODES--which indicate that maintenance resources were extended due to policy, modification, location, or cannibalization, and no defect existed at the time of maintenance. Because Type 6 HOW MALFUNCTION CODES were not considered pertinent to this investigation, they were not included in the report. All figures of Totals, therefore, refer to the sum of the failures and OTH/MAL columns only. For a more detailed explanation on these three classifications, the reader is referred to:

AFLC Regulation 66-15
23 August 1974
Equipment Maintenance/Product Performance
Ch 5 and 13

1.1.3 Pertinent Notes

A. In general, operating time (or flight hrs) for the T-38 is approximately 18 times that for the F-111.

B. Moisture accumulation on the internal surface of a valve can affect the way it functions. Therefore, climate conditions of the geographic region in which the valve is used may be of importance.

EDITOR'S NOTE: Available, on pp. 198-199, is a selective list (plus definitions) of the "Abbreviations, Acronyms, and Symbols" used throughout this volume.

1.2 Analysis of the Historical Failure Data

Due to the limited nature of the data obtained, the following analysis is strictly descriptive of the data. Sufficient data are not yet available for a predictive study.

1.2.1 Description of Illustrations

Two types of descriptive figures are presented in the following pages. In the first sets (Figs. 1 - 6), schematics are used to reflect the distributions of the five data sets, their means, medians, ranges, extremes, etc. [NOTE: This form of analysis was developed by J. W. Tukey in Exploratory Data Analysis, Addison-Wesley, Reading, Mass., July 1977.] In each of these figures, the five sets are plotted side by side, so that comparisons can be readily made. In Figures 1 - 3, raw counts, or the numbers of failures, OTH/MAL's, or totals are presented. The mean flight hours, shown below each of the box-and-whisker plots, are an important part of these figures. It is immediately apparent that the ALAR valve performed comparably with the Bendix, even though the ALAR sustained approximately 18 times more flight hours per month.

In Figures 4 - 6, the failures, OTH/MAL's, and totals per 1,000 flight hours are presented, also in side-by-side box-and-whisker plots. Again, the ALAR performance was much more reliable than the Bendix. On the right side of Figures 4 - 6 are expansions of the ALAR failures, OTH/MAL's, or totals over 10,000 flight hours (i.e., a 10-to-1 expansion), to give the reader a clearer indication of the numbers involved.

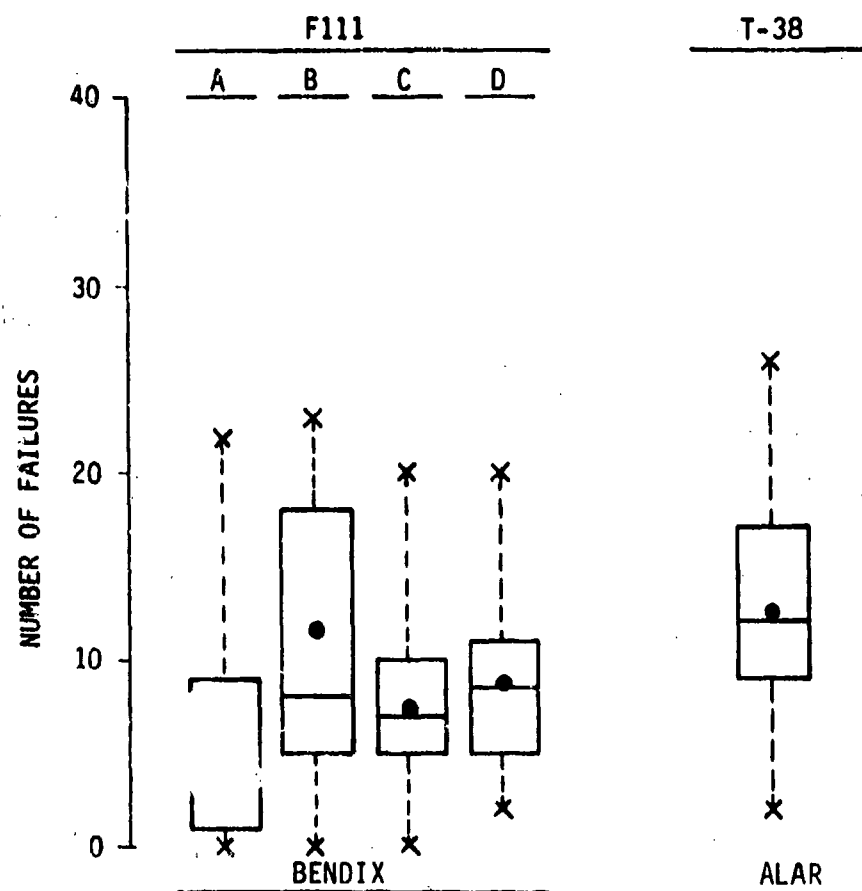
The conclusions that can be drawn from these figures are:

- a) Over the same number of flight hours, Bendix malfunctions and failures are relatively consistent in the four F-111 models.
- b) The ALAR valve is approximately 10 times more reliable than the Bendix in terms of flight hours sustained before malfunction or failure.

In the second set of figures (Figs. 7 - 21), data set means and medians are used to indicate monthly variation and yearly trend. These figures are only descriptive, for too few years of data are available to draw conclusions about monthly or yearly patterns. Several important facts should be noted about these figures.

- a) For trend, the years 1974 and 1977 are biased toward the last six months and the first six months, respectively.
- b) The bias in a) may carry over to monthly variation if the years 1974 and 1977 are significantly different.
- c) The Bendix failures, other malfunctions, and totals are over 1,000 flight hours, while the ALAR figures are over 10,000 flight hours.

Again, stress is placed on the fact that these figures are strictly descriptive of the data. No conclusion can be drawn about the monthly or yearly patterns.



MEAN OP TIME (Flight Hrs) Per Month	1415	1308	1640	1868	28,373
--	------	------	------	------	--------

Figure 1. Number of failures for Bendix and ALAR anti-G valves for July 1974 to June 1977.

Key: • = Arithmetic mean
 Middle bar = Median
 Upper & Lower Bar = Upper & Lower Quartile
 x = Extremes of Data Set
 OP = operating

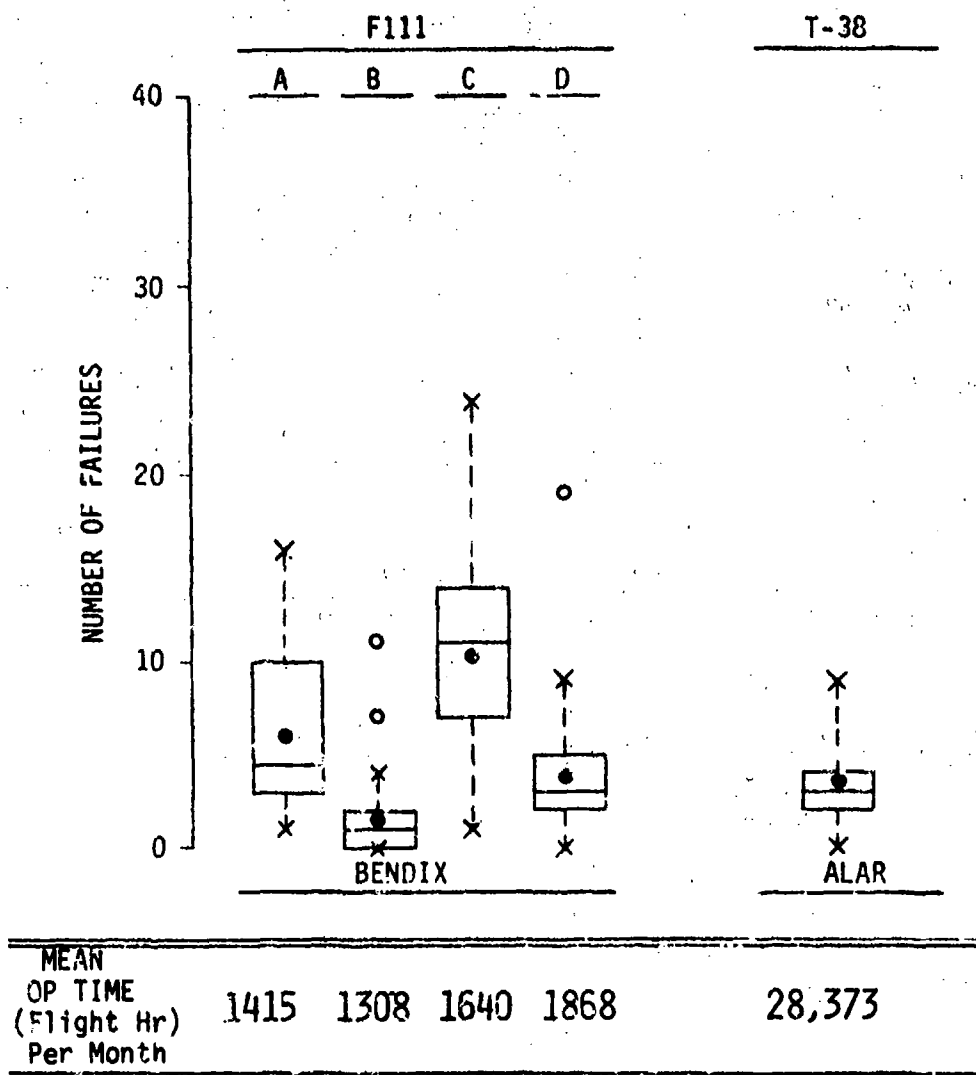
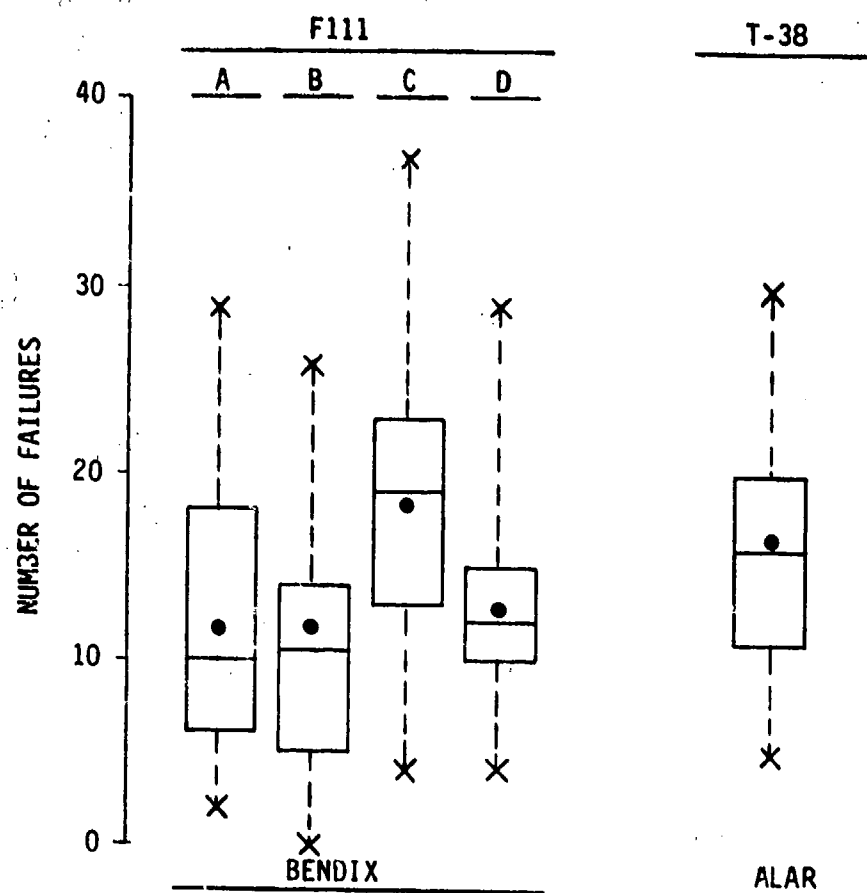


Figure 2. Number of OTH/MAL's for Bendix and ALAR anti-G valves for July 1974 to June 1977.

Key: ● = Arithmetic mean
 Middle bar = Median
 Upper & Lower Bars = Upper & Lower Quartiles
 o = Separate Values
 x = Extremes of Data Set (excluding separate values)



MEAN					
OP TIME					
(Flight Hrs)	1415	1308	1640	1868	28,373
Per Month					

Figure 3. Total number of failures and OTH/MAL's for Bendix and ALAR anti-G valves for July 1974 to June 1977.

Key: • = Arithmetic mean
 Middle bar = Median
 Upper & Lower bars = Upper & Lower Quartiles
 x = Extremes of Data Sets

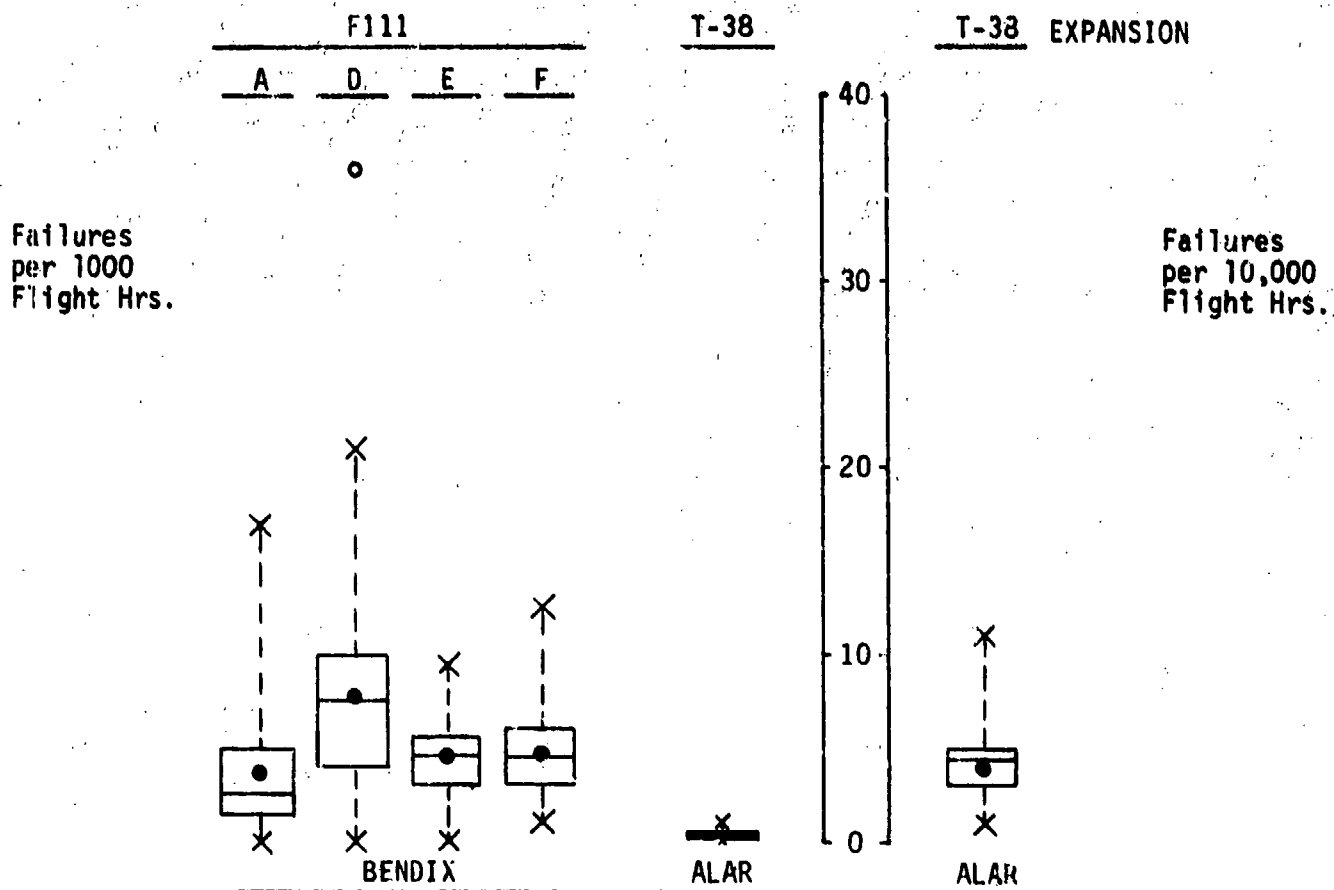


Figure 4. Rate of occurrence of failures.

Key: • = Arithmetic mean
 Middle bar = Median
 Upper & Lower bar = Upper & Lower Quartiles
 o = Separate values
 x = Extremes of Data (excluding separate values)

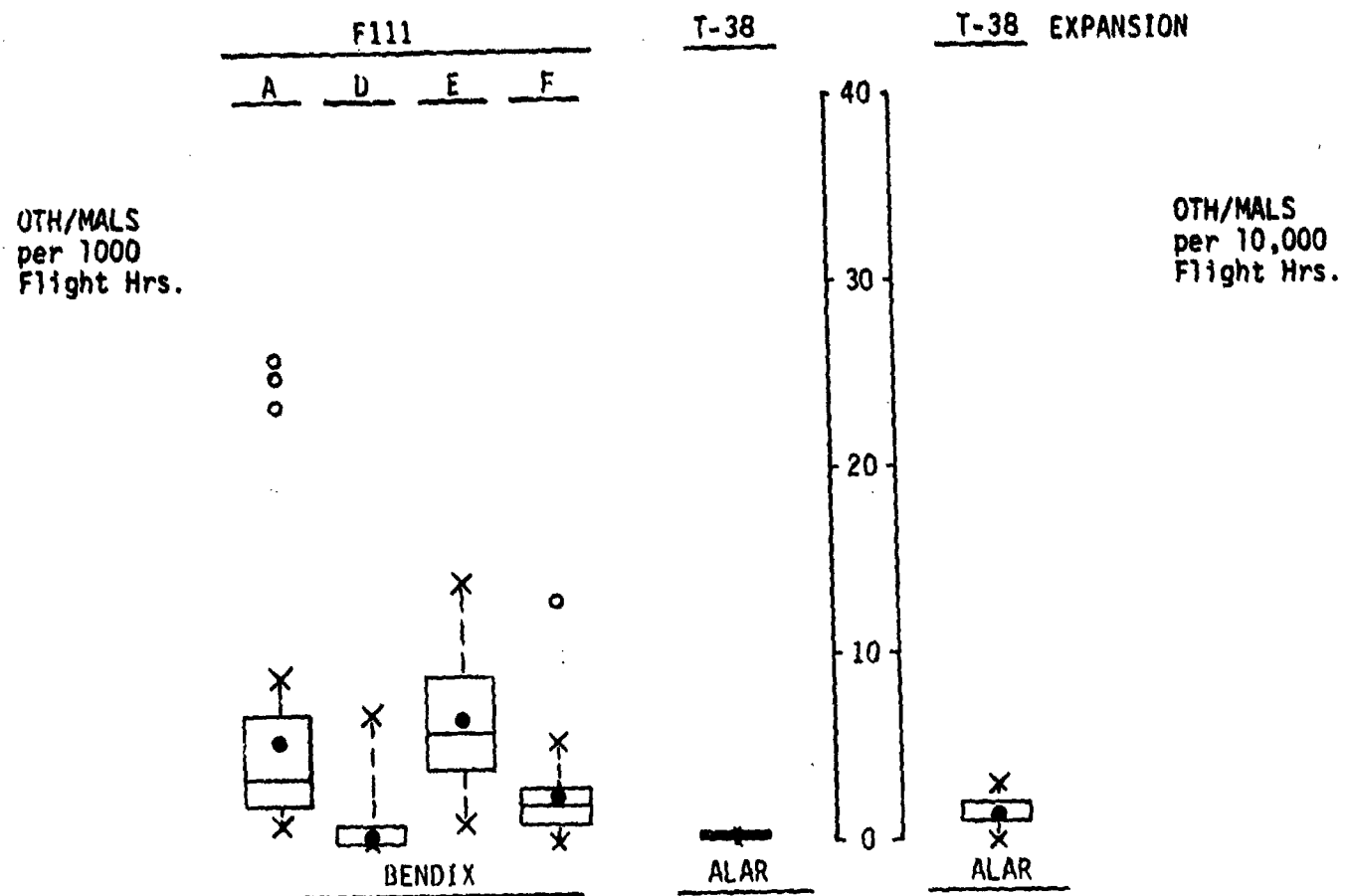


Figure 5. Data of occurrence of OTH/MAL's.

Key:

- = Arithmetic mean
- Middle bar = Median
- Upper & Lower bar = Upper & Lower Quartiles
- o = Separate values
- x = Extremes of Data (excluding separate values)

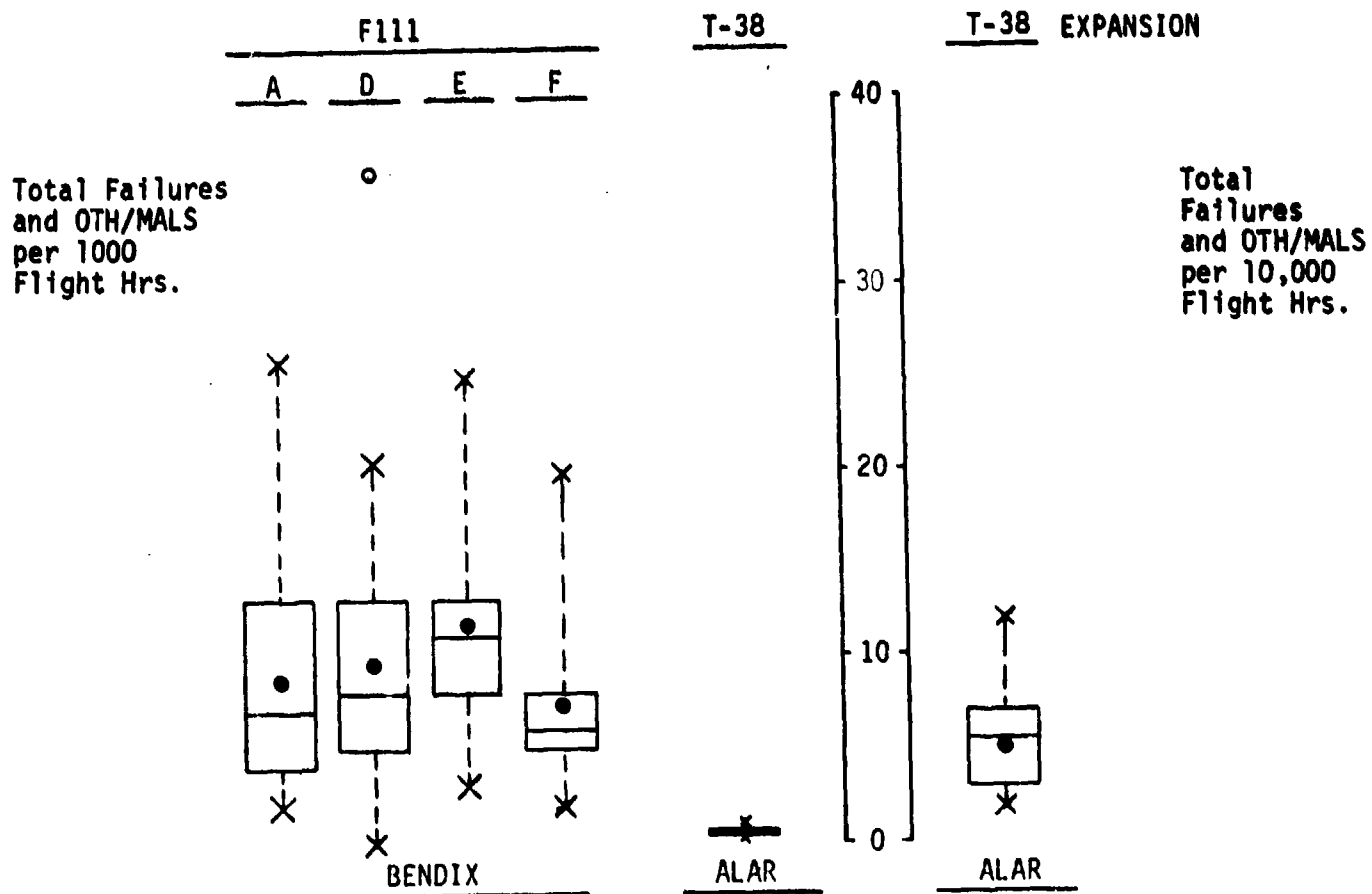
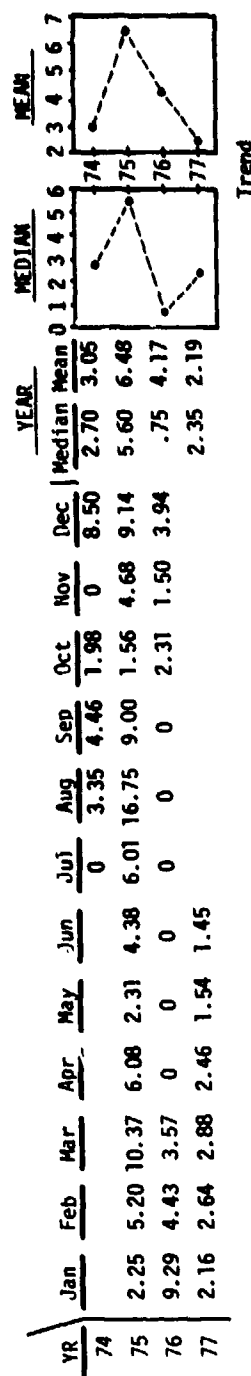


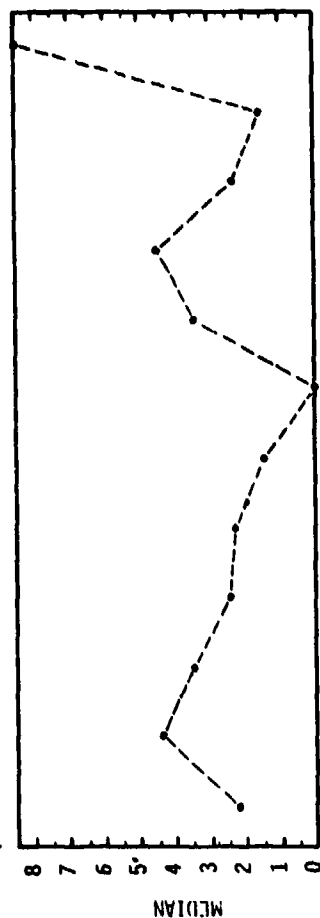
Figure 6. Rate of occurrence of failures and OTH/MAL's.

Key: • = Arithmetic mean
 Middle bar = Median
 Upper & Lower bar = Upper and Lower Quartile
 o = Separate values
 x = Extremes of Data (excluding separate values)



Trend

MO.	MONTHLY VARIATION											
	Jan	Feb	Mar	Apr	May	Jun	Jul	Aug	Sep	Oct	Nov	Dec
MEDIAN	2.25	4.43	3.57	2.46	2.31	1.45	0	3.35	4.46	2.31	1.50	8.50
MEAN	4.57	4.09	5.61	2.85	1.28	1.94	2.00	6.70	4.49	1.95	2.06	7.19



MONTHLY VARIATION

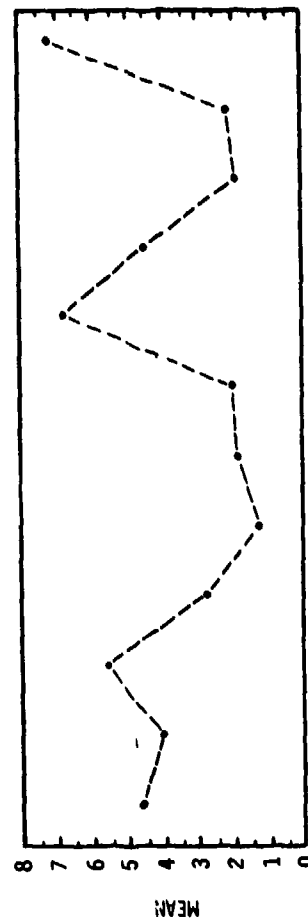
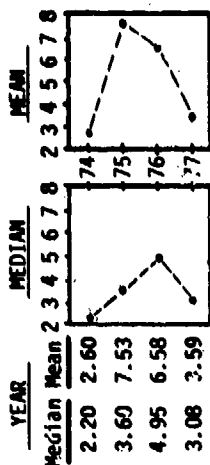
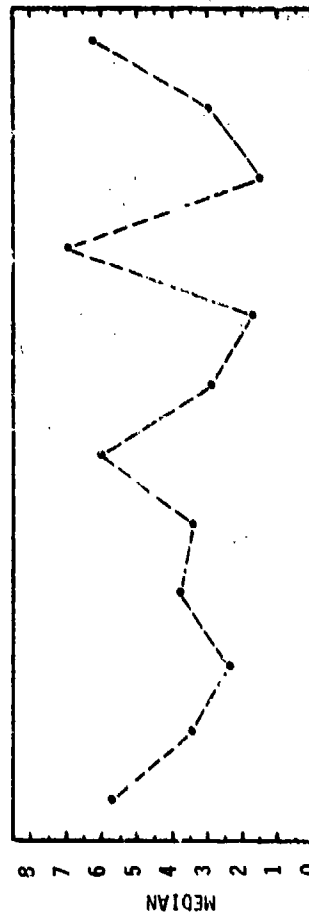


Figure 7. Distribution of F-111-A failures per 1000 flight hrs.



Trend

MO.	YEAR											
	Jan	Feb	Mar	Apr	May	Jun	Jul	Aug	Sep	Oct	Nov	Dec
MEDIAN	5.75	3.46	2.36	3.74	3.43	5.79	2.84	1.68	6.80	1.48	2.99	6.07
MEAN	5.12	4.77	3.42	4.44	2.89	5.13	3.26	9.61	5.89	9.23	9.44	5.59



MONTHLY VARIATION

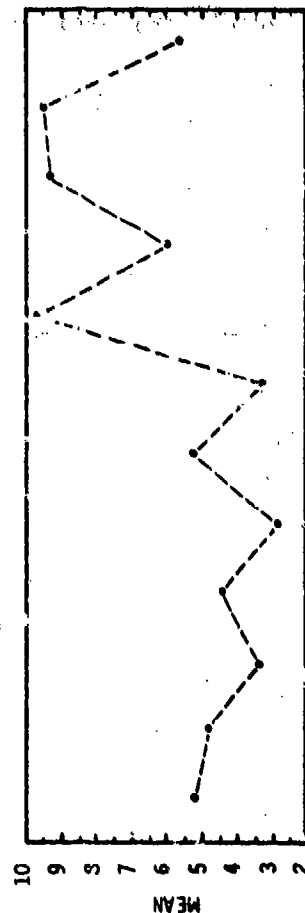
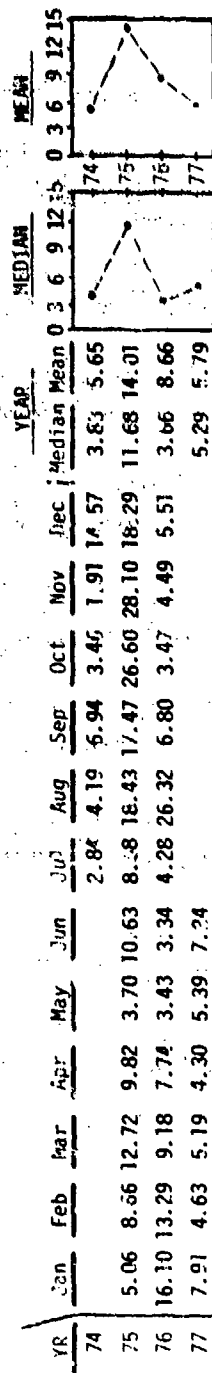
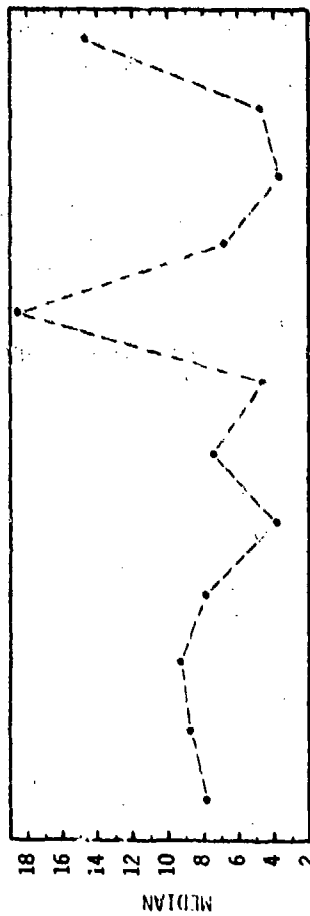


Figure 6. Distribution of F-111-A OTT/MAJ's per 1000 flight hrs.



Trend

MO	JAN	FEB	MAR	APR	MAY	JUN	JUL	AUG	SEP	OCT	NOV	DEC
MEDIAN	7.91	8.66	9.18	7.74	3.70	1.24	4.28	18.43	6.94	3.47	4.49	14.57
MEAN	9.69	8.86	9.03	7.29	4.17	7.07	5.27	16.31	10.40	11.18	11.50	12.79



MONTHLY VARIATION

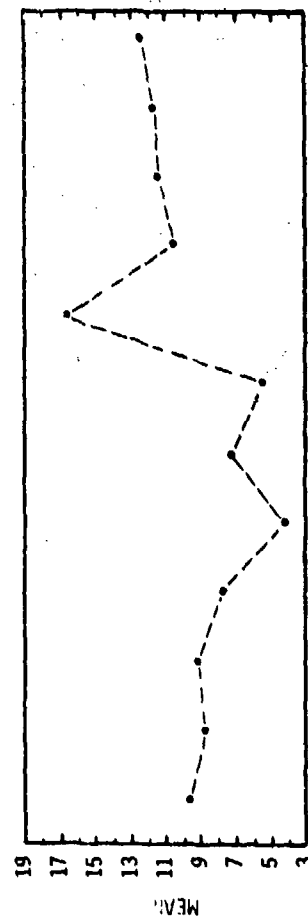
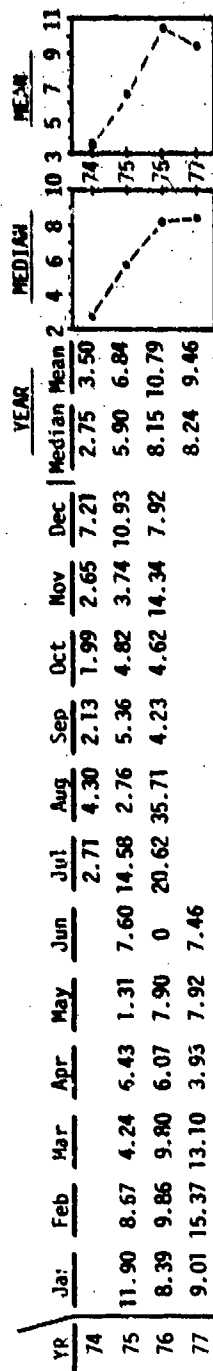
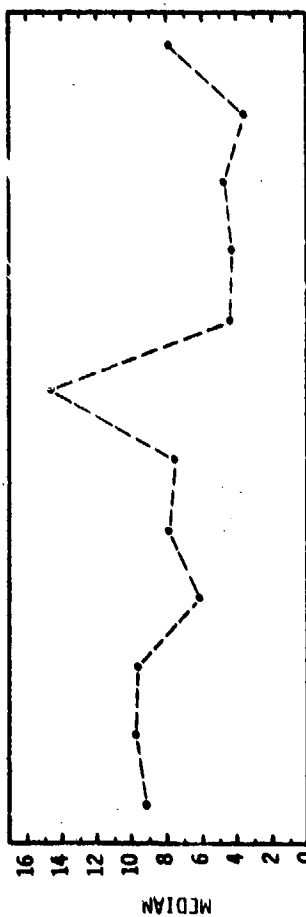


Figure 9. Distribution of F-111-A total failures and OTH/MAL's per 1000 flight hrs.



Trend

MO.	MEDIAN	9.01	9.85	9.80	6.07	7.90	7.46	14.58	4.30	4.23	4.62	3.74	7.92
	MEAN	9.77	11.30	9.05	5.48	5.71	5.02	12.64	14.26	3.91	3.81	6.91	8.62



MONTHLY VARIATION

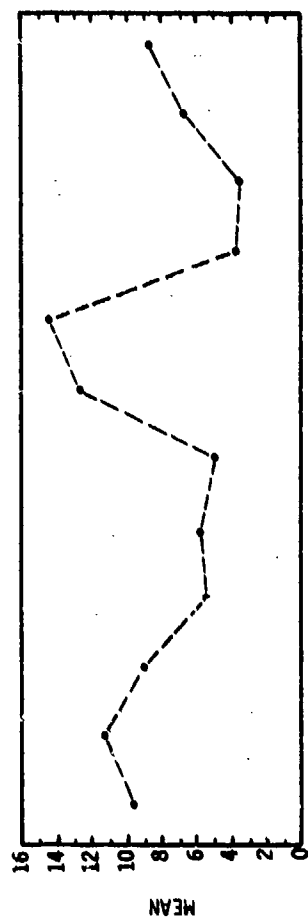
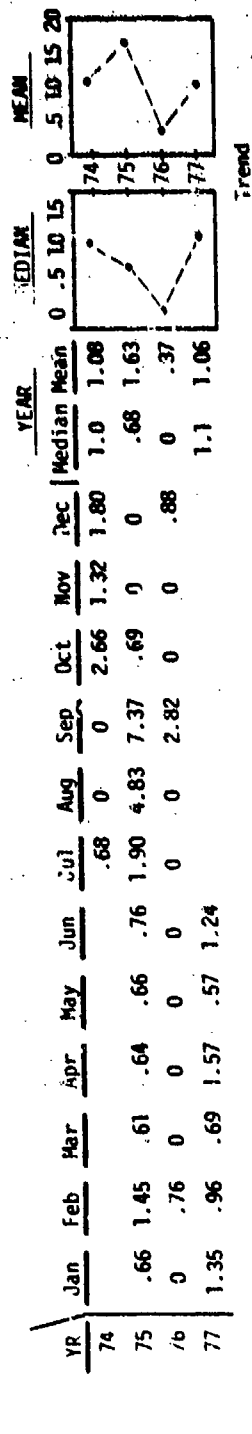


Figure 10. Distribution of F-111-D failures per 1000 flight hrs.



MO.	MONTHLY VARIATION											
	Jan	Feb	Mar	Apr	May	Jun	Jul	Aug	Sep	Oct	Nov	Dec
MEDIAN	.66	.96	.61	.64	.57	.76	.68	0	2.82	.69	0	.88
MEAN	.67	1.06	.43	.74	.41	.67	.86	1.61	3.40	1.12	.44	.89

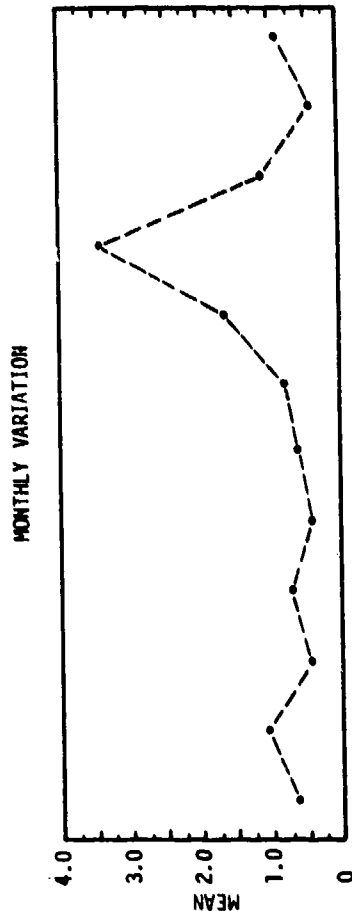
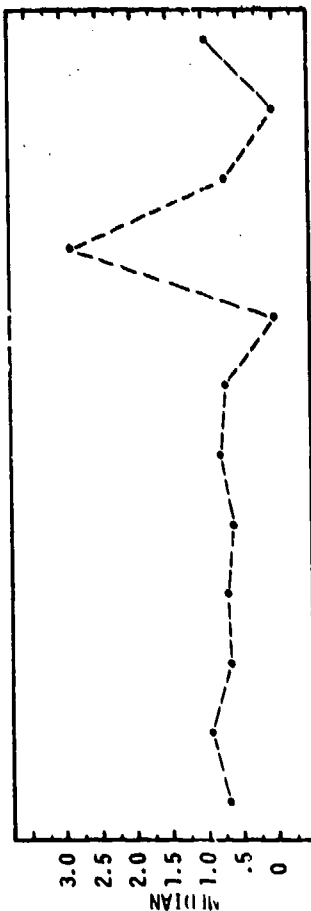
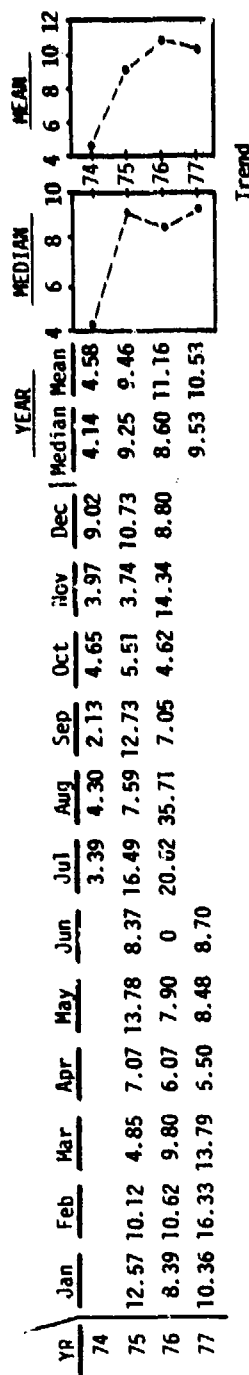


Figure 11. Distribution of F-111-D OTH/MAL's per 1000 flight hrs.



Trend

MO.	MONTHLY VARIATION											
	Jan	Feb	Mar	Apr	May	Jun	Jul	Aug	Sep	Oct	Nov	Dec
MEDIAN	10.36	10.12	9.80	6.07	8.48	8.37	16.49	7.59	7.05	4.65	3.97	9.02
MEAN	10.44	12.36	9.48	6.21	10.05	5.69	13.50	15.87	7.30	4.93	7.35	9.52

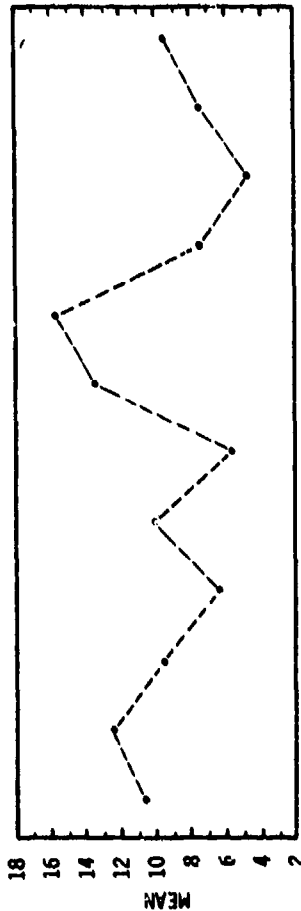
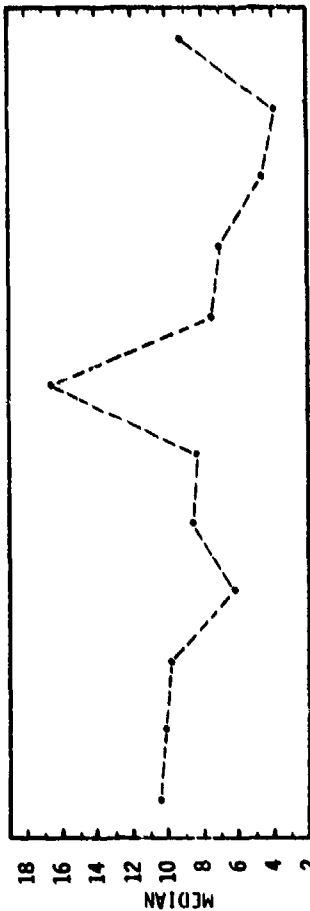
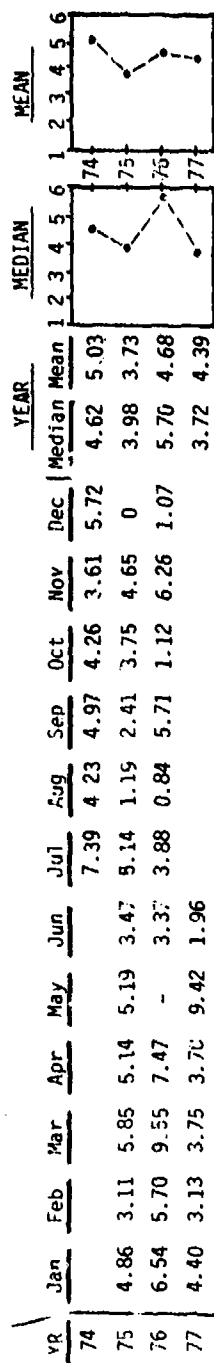


Figure 12. Distribution of F-111-D total failures and OTH/MAL's per 1000 flight hrs.



Trend

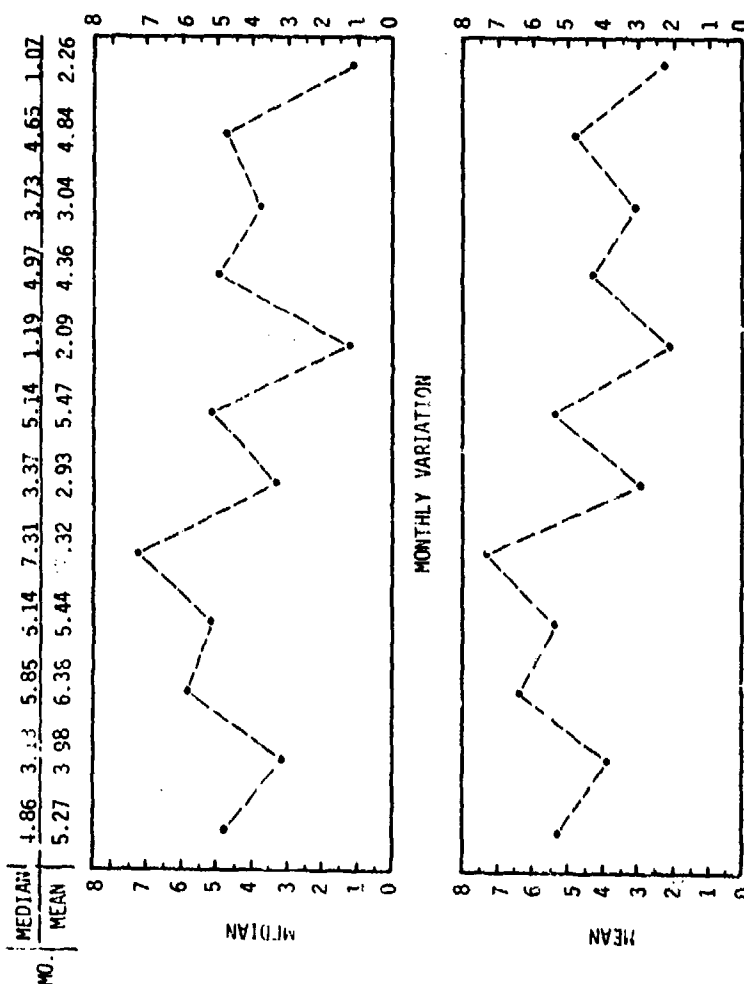


Figure 13. Distribution of F-111-E failures per 1000 flight hrs.

YR	YEAR												MEDIAN										MEAN									
	Jan	Feb	Mar	Apr	May	Jun	Jul	Aug	Sep	Oct	Nov	Dec	Median	Mean	4	5	6	7	8	9	10	4	5	6	7	8	9	10				
74							2.27	5.87	9.32	4.26	12.64	2.45		6.13																		
75	2.78	6.18	2.34	6.16	7.49	4.62	5.14	4.77	3.38	9.64	7.97	3.19		5.31																		
76	9.80	11.46	5.25	6.32	--	.67	4.52	8.40	7.43	3.92	9.04	4.29		6.46																		
77	8.79	8.78	6.97	7.92	13.81	8.82								8.79	9.18																	

Trend

MO	MEDIAN												MEAN											
	8.79	8.78	5.25	6.32	10.65	4.62	4.52	5.81	7.43	4.26	9.04	3.19	7.12	8.80	4.85	6.80	10.65	4.70	3.98	6.33	6.71	5.94	9.88	3.31

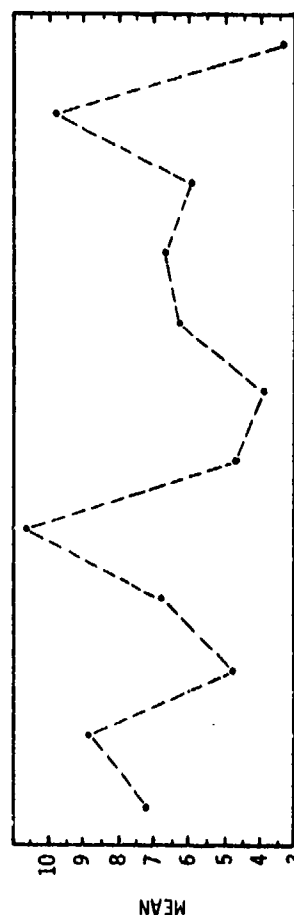
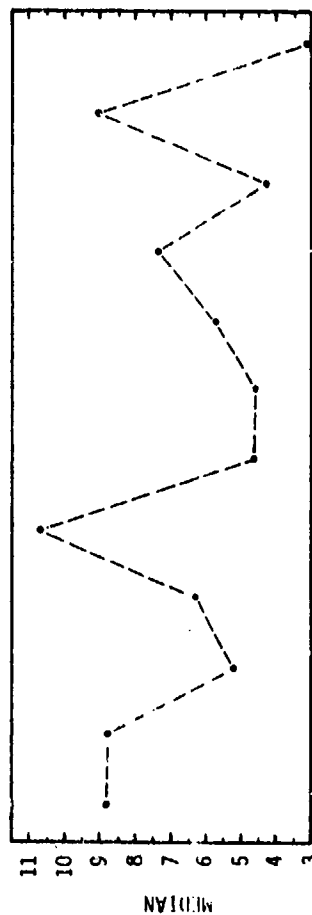
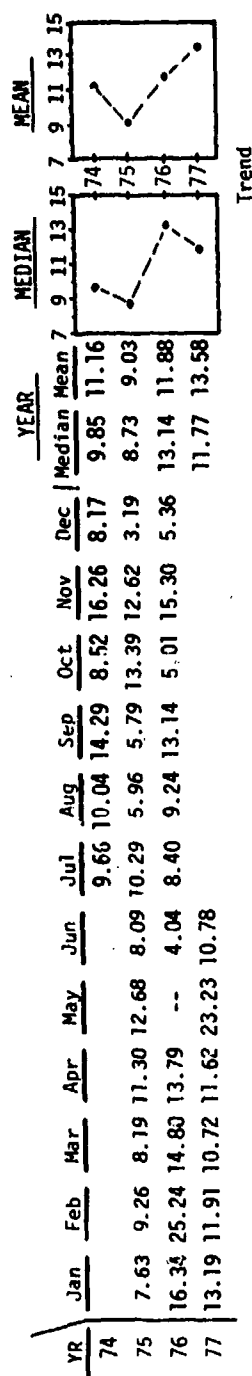


Figure 14. Distribution of F-111-E OTH/MAL's per 1000 flight hrs.



MO	MONTHLY VARIATION											
	Jan	Feb	Mar	Apr	May	Jun	Jul	Aug	Sep	Oct	Nov	Dec
MEDIAN	13.19	11.91	10.72	11.62	17.96	8.09	9.66	9.24	13.14	8.52	12.62	5.36
MEAN	12.39	15.47	11.24	12.24	17.96	7.64	9.45	8.41	11.07	8.98	14.73	5.57

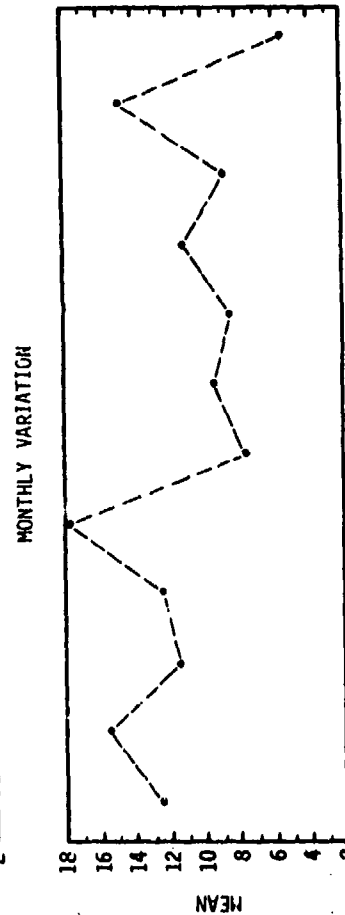
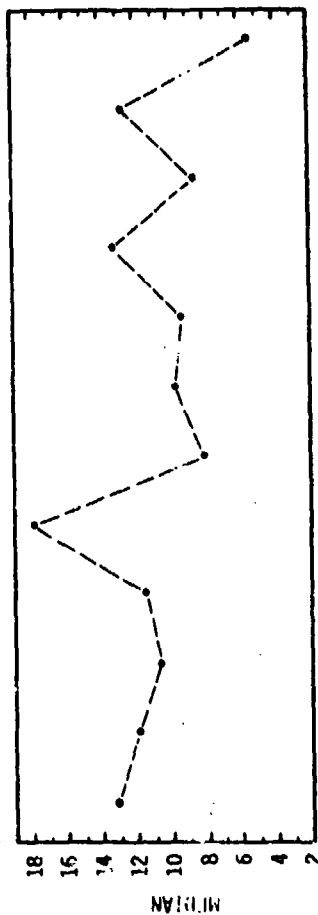
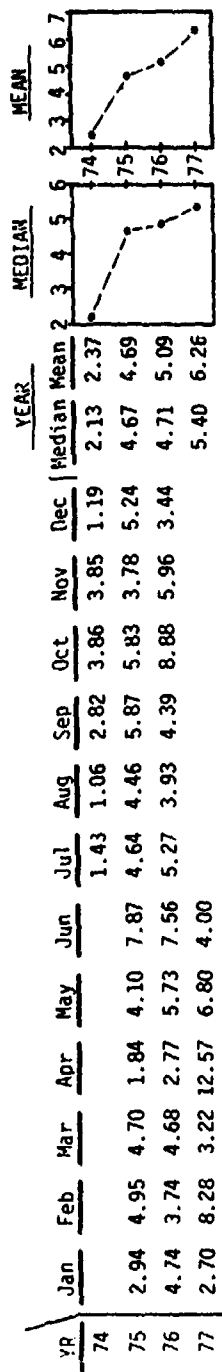
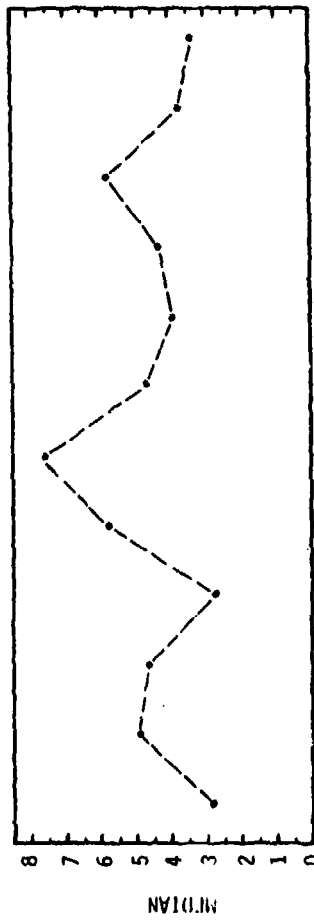


Figure 15. Distribution of F-111-E total failures and OTH/MAL's per 1000 flight hrs.



Trend

MO.	YEAR											
	Jan	Feb	Mar	Apr	May	Jun	Jul	Aug	Sep	Oct	Nov	Dec
MEDIAN	2.94	4.95	4.68	2.77	5.73	7.56	4.64	3.93	4.39	5.83	3.85	3.44
MEAN	3.46	5.66	4.20	5.73	5.54	6.48	3.78	3.15	4.36	6.19	4.53	3.29



MONTHLY VARIATION

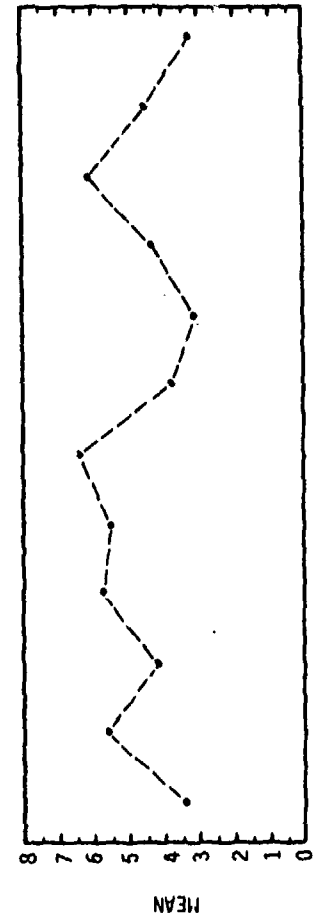
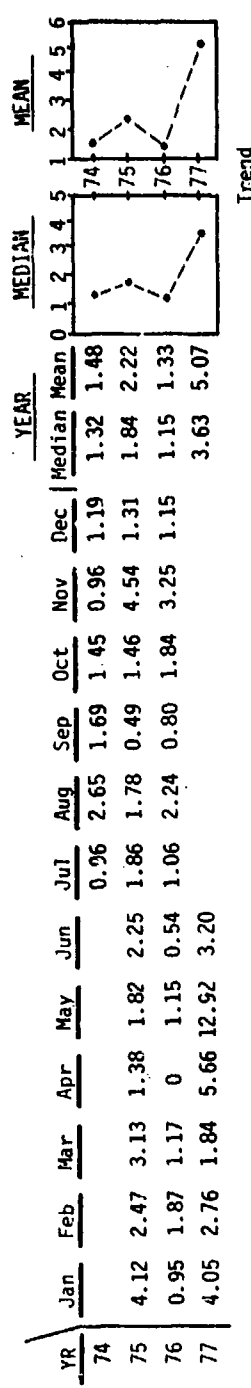


Figure 16. Distribution of F-111-F failures per 1000 flight hrs.



MO.	YEAR											
	Jan	Feb	Mar	Apr	May	Jun	Jul	Aug	Sep	Oct	Nov	Dec
MEDIAN	4.05	2.47	1.84	1.38	1.2	2.25	1.05	2.24	0.80	1.46	3.25	1.19
MEAN	3.05	2.37	2.04	2.35	5.30	2.00	1.29	2.22	0.99	1.58	2.92	1.22

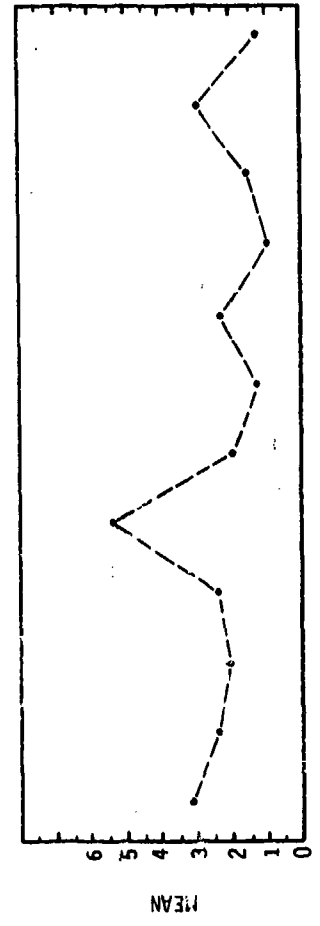
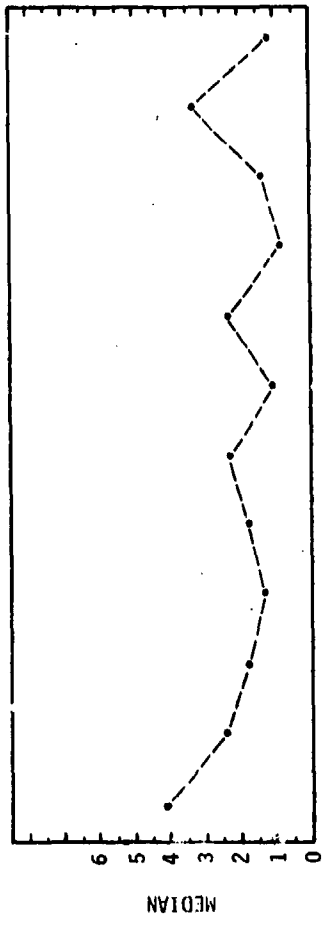


Figure 17. Distribution of F-111-F OTH/MAL's per 1000 flight hrs.

YR	YEAR												MEDIAN												MEAN																
	Jan	Feb	Mar	Apr	May	Jun	Jul	Aug	Sep	Oct	Nov	Dec	Median	Mean	4	5	6	7	8	9	10	11	12	13	14	Median	Mean	4	5	6	7	8	9	10	11	12	13	14			
74	7.05	7.42	7.84	3.21	5.93	10.12	6.50	6.24	6.36	7.29	8.32	6.55	4.11	3.85												74															
75	5.68	5.61	5.85	2.77	6.88	8.10	6.33	6.17	5.19	10.07	9.20	5.73	6.80	6.90												75															
76	6.76	11.04	5.07	18.23	19.71	7.19							6.01	6.47												76															
77																										77															

Trend

MO.	MEDIAN												MEAN											
	Jan	Feb	Mar	Apr	May	Jun	Jul	Aug	Sep	Oct	Nov	Dec	Jan	Feb	Mar	Apr	May	Jun	Jul	Aug	Sep	Oct	Nov	Dec
74	6.76	7.42	5.85	3.21	6.88	8.10	6.33	6.17	5.19	7.29	8.32	5.73	6.50	8.02	6.25	8.07	10.84	8.47	5.07	5.37	5.33	7.55	7.44	4.88
75	5.68	5.61	5.85	2.77	6.88	8.10	6.33	6.17	5.19	7.29	8.32	5.73	6.50	8.02	6.25	8.07	10.84	8.47	5.07	5.37	5.33	7.55	7.44	4.88
76	6.76	11.04	5.07	18.23	19.71	7.19							6.50	8.02	6.25	8.07	10.84	8.47	5.07	5.37	5.33	7.55	7.44	4.88
77																								

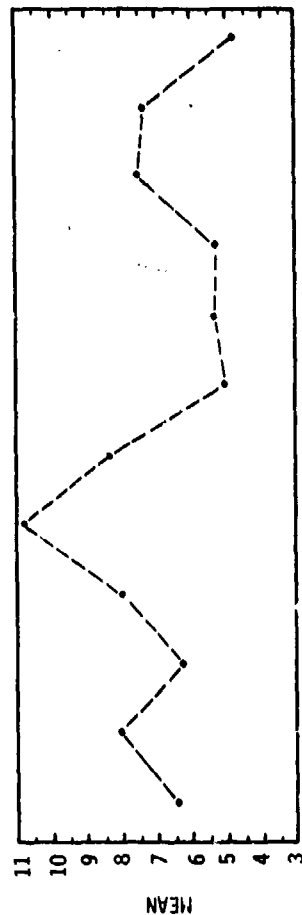
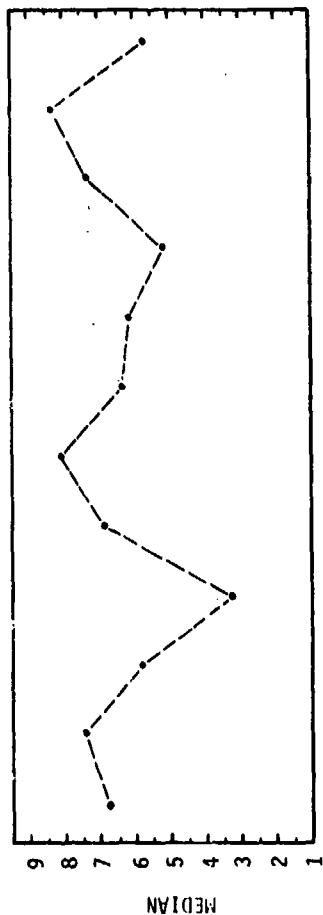
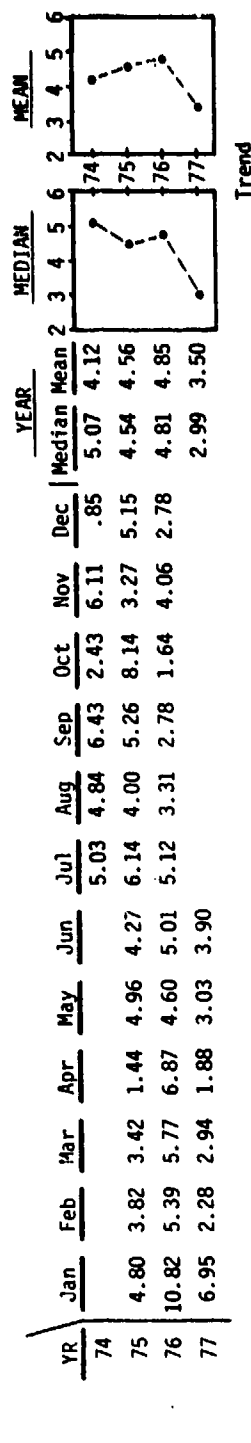


Figure 18. Distribution of F-111-F total failures and OTH/MAL's per 1000 flight hrs.



MO.	MONTHLY VARIATION											
	Jan	Feb	Mar	Apr	May	Jun	Jul	Aug	Sep	Oct	Nov	Dec
MEDIAN	6.95	3.82	3.42	1.88	4.60	4.27	5.12	4.00	5.26	2.43	4.06	2.78
MEAN	7.52	3.83	4.04	3.40	4.20	4.39	5.43	4.05	4.82	4.07	4.15	2.93

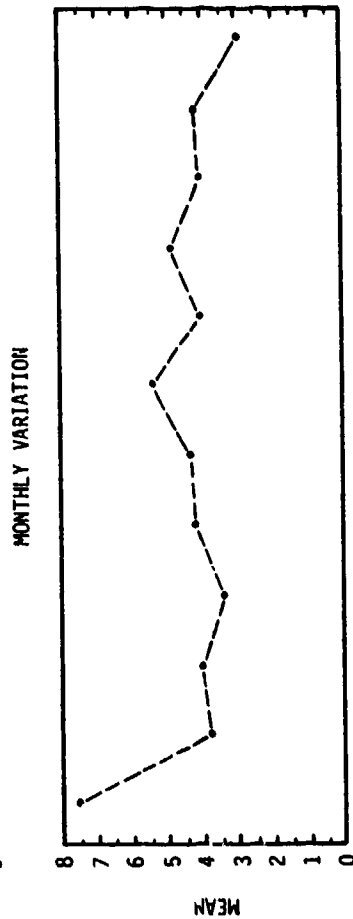
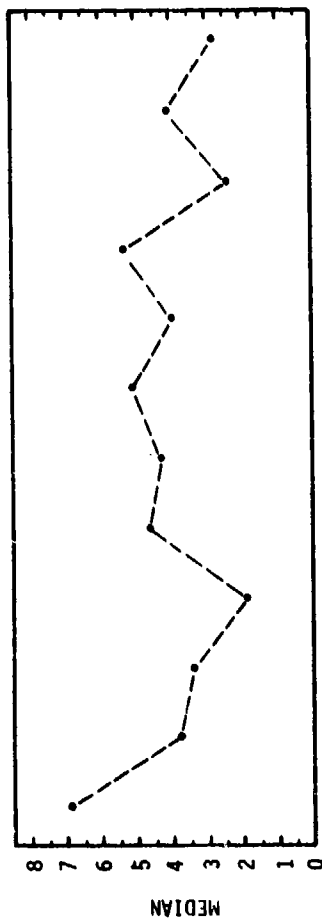
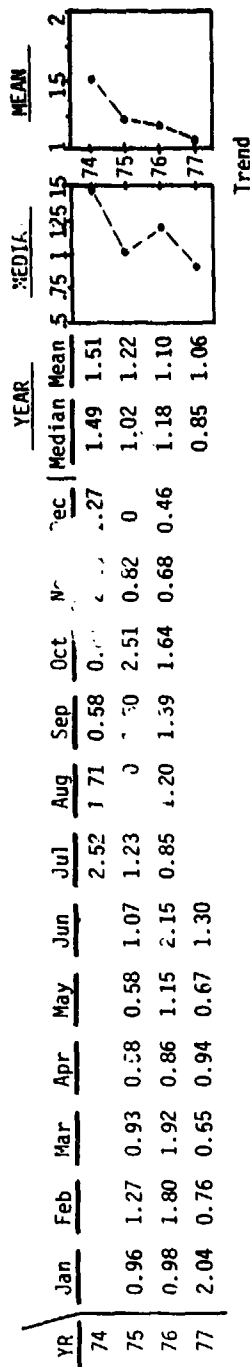
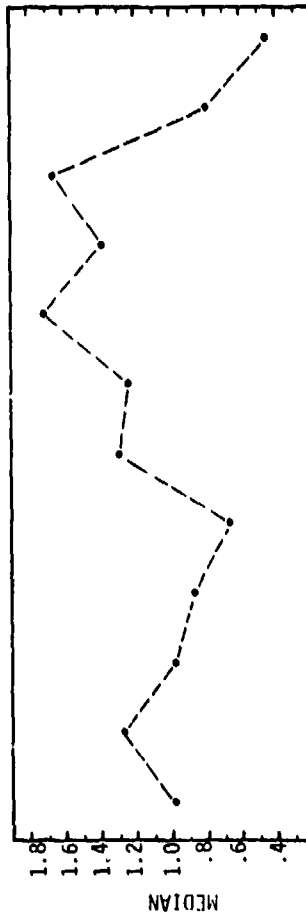


Figure 19. Distribution of T-38 failures per 10,000 flight hrs.



Trend

MO.	MONTHLY VARIATION											
	Jan	Feb	Mar	Apr	May	Jun	Jul	Aug	Sep	Oct	Nov	Dec
MEDIAN	0.98	1.27	0.93	0.86	0.67	1.30	1.23	1.71	1.39	1.64	0.86	0.46
MEAN	1.33	1.28	1.17	0.79	0.80	1.51	1.54	2.04	1.16	1.65	1.22	0.58



MONTHLY VARIATION

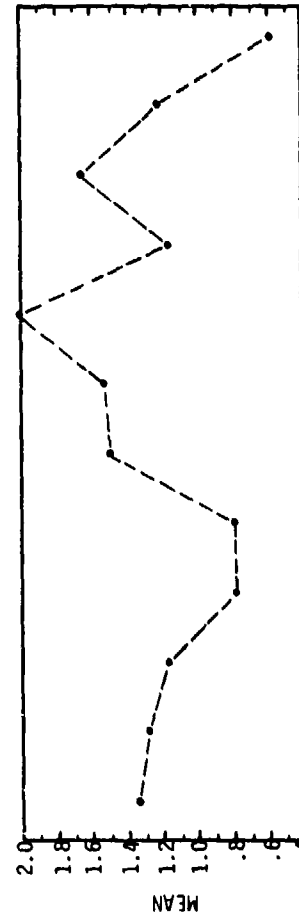
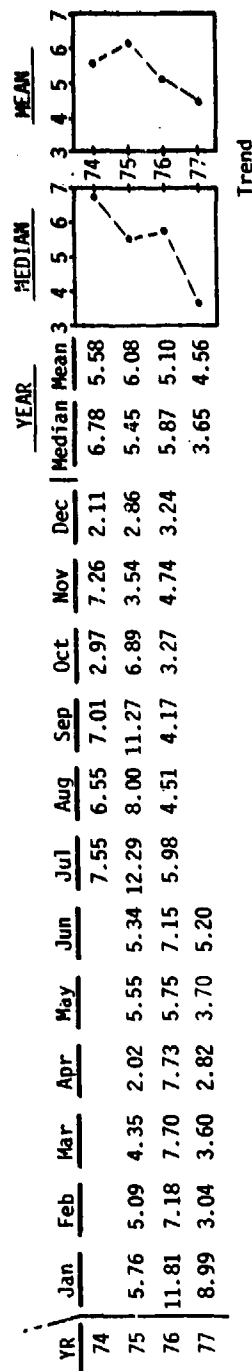
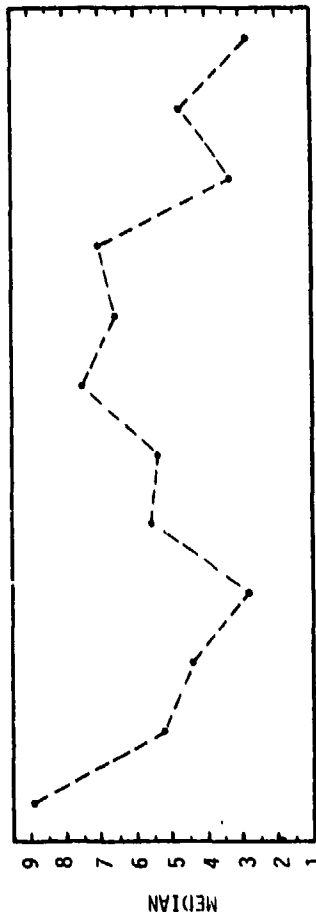


Figure 20. Distribution of T-38 OTH/MAL's per 10,000 flight hrs.



Trend

MO.	MEDIAN												MEAN											
	Jan	Feb	Mar	Apr	May	Jun	Jul	Aug	Sep	Oct	Nov	Dec	Jan	Feb	Mar	Apr	May	Jun	Jul	Aug	Sep	Oct	Nov	Dec
74	8.99	5.09	4.35	2.82	5.55	5.34	7.55	6.55	7.01	3.27	4.74	2.86	8.85	5.10	5.22	4.19	5.00	5.90	8.61	6.35	7.48	4.38	5.18	2.74



MONTHLY VARIATION

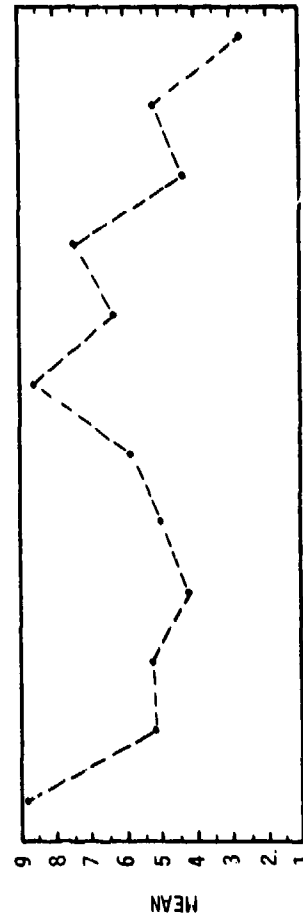


Figure 21. Distribution of T-38 total failures and OTH/MAL's per 10,000 flight hrs.

1.2.2 Suggestions for Future Data Collection on AGV Failures

Even over the limited three-year period, the following types of data collected on the anti-G valves could have generated more meaningful information:

- a) The name and model of the valve
- b) Type of aircraft
- c) Climate conditions and G-stress the valve sustained
- d) Length of time valve was in service (both full-time and actual flight hours)
- e) Reason for failure (as specifically as possible)
- f) Indication of a preflight or inflight failure
- g) Data from all (especially, high-performance) aircraft.

1.3 Induced AGV Failure Analysis

One of the primary objectives of the PTAP program was to obtain information on AGV failures. To supplement the limited data available, an engineering evaluation of potential failure modes on selected AGV's was undertaken. This study, which was limited to failures existing in the valve before preflight testing, concentrated on insidious failures which might not be noted on preflight tests.

For this study, the selected AGV was completely disassembled and arranged sequentially on a work table. Starting at the inlet port, each part and sub-assembly was examined for possible failure modes. As each potential failure was identified, it was listed, along with the expected results of such a failure. During this phase of the evaluation, potential failures were listed without regard to probability of occurrence, or to the fact that such a failure would be readily apparent on preflight examination, or to the fact that such a failure would have little effect on AGV performance. No double failures were considered, except in cases where one failure precipitated another. After each part and subassembly of the valve had been examined and all failure cases listed, each case was analyzed to determine the relative likelihood or practicality of such a failure, and its effect on function. Failure cases which were deemed improbable, or which had slight effect on valve performance, were deleted from the list. The remaining candidate failure cases were then examined to determine which ones would be immediately apparent to the pilot during the preflight check of the AGV, and which failures were insidious in nature and would probably pass the preflight test, but would result in degraded performance during flight. The

failure cases which would be detected on the preflight test were removed from the list. Finally, the remaining cases were examined to determine if a way could be devised to simulate this failure in an AGV in a reversible manner.

The final list, of AGV failures which were to be candidates for testing, included only those failures which were believed to be probably degrading to AGV performance, not readily apparent on preflight test, and producible in the AGV in a reversible manner.

The test portion of this study was accomplished in two phases. The first phase was a static test of the AGV which was accomplished by inducing the selected failure in the valve and testing by use of the press-to-test button. During this phase, data were recorded only on oscillograph charts and were analyzed by inspection. Several of the candidate failure cases yielded results other than those predicted during the initial study of the valve. This finding was anticipated; for the AGV are reasonably complex, and all of the interactive effects are difficult to anticipate. This uncertainty was therefore one of the primary reasons for the static testing.

The second phase of testing was the performance of a full SVTP on those failure cases not deleted during the first phase.

The results of the study and the first phase of testing are listed on the following pages. The results of the final (SVTP) phase of testing are given in section 1.4.

1.3.1 Failure Analysis of Bendix AGV FR139A2

A Bendix AGV FR139A2 was completely disassembled and minutely examined. The function of each individual element and subsystem was cataloged, and possible failure modes were listed. A total of 28 failure modes were postulated and reviewed. Where any doubt existed concerning the effect of a postulated failure, the failure was simulated and statically tested. Only two failures were judged worthy of further (SVTP) investigation. [In the following description, the item numbers in brackets refer to the part-identification Key to Fig. 22.]

1.3.1.1 FR139A2 (Bendix AGV) Failure Case 1

Failure: Mass valve seat [Item 40] leaking

Result: Reduced AGV function

Simulation: Scratch valve seat.

Discussion: Research on the Bendix valve failure history revealed that one common failure was caused by the mass valve seat [Item 40] falling out of the valve cover body. This failure makes the valve

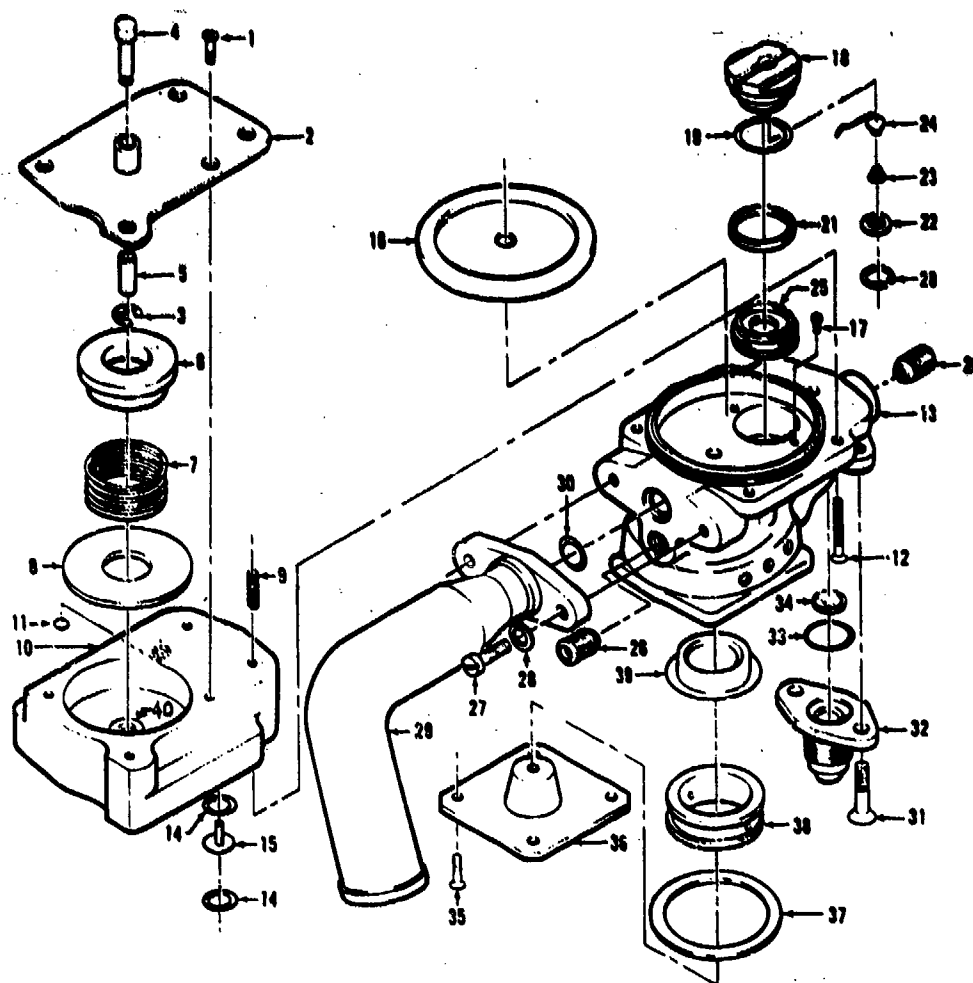


Figure 22. Exploded view of the FR139A2 anti-G valve.
[TO 15X8-7-21-2, Tinker AFB, Okla.]

- | | | |
|----------------------------|-------------------------------------|----------------------------|
| 1. Screw (two) | 15. Inlet Filter & Orifice Assembly | 27. Screw (two) |
| 2. Cover | 16. Breathing Diaphragm | 28. Washer (two) |
| 3. Retainer Ring | 17. Screw (two) | 29. Air Regulating Outlet |
| 4. Press-to-test Button | 18. Pilot Valve | 30. Packing |
| 5. Sleeve | 19. Packing | 31. Screw (two) |
| 6. Mass | 20. Retainer Ring | 32. Inlet Fitting |
| 7. Compression Spring | 21. Flat Washer | 33. Packing |
| 8. Spring Bearing Washer | 22. Spring Retainer Plate | 34. Inlet Filter |
| 9. Helicoil Insert (three) | 23. Conical Spring | 35. Screw (four) |
| 10. Mass Housing | 24. Valve & Lever Assembly | 36. Relief Valve Cover |
| 11. Packing | 25. Diaphragm Outlet Lever | 37. Packing |
| 12. Screw (four) | 26. Plug (two) | 38. Relief Valve Ring |
| 13. Valve Housing | | 39. Relief Valve Diaphragm |
| 14. Packing | | 40. Mass Valve Seat |

entirely inoperative, and is therefore easily discovered. However, since a leaking valve seat may be a cause of failure, the valve seat should be tested.

In order to simulate this failure, a leak rate had to be established which was large enough to degrade AGV performance, but would not render the valve inoperative. Since the Bendix AGV design is such that a constant, though very small, flow is present through the valve when the system is at constant pressure, the initial baseline flow rate had to be measured. This measuring was accomplished by fabricating a set of weights to simulate G forces, and by measuring the flow through the valve at various G loads and source pressures. Once the baseline flow was established, the valve seat was "nicked" with a fine file, and flows were again measured. A final flow of approximately 700 cc/min, or about twice the unmodified flow at 70-psig source pressure, was established.

The valve was then subjected to the SVTP, and results are listed in section 1.4.1.

1.3.1.2 FRI39A2 (Bendix AGV) Failure Case 2

Failure: Orifice or screen (Fig. 22: Item 15) contaminated

Result: Increased AGV response time

Simulation: Partially block orifice

Discussion: This case is the most likely and most common failure in this AGV. It was decided that this failure should be thoroughly tested using the SVTP; therefore, static tests were not considered to be useful. The failure was simulated by inserting a number 46 AWG (American Wire Gage) wire, of 0.0018 in. diam., through the orifice and screen. This wire blocked 51.8% of the area of the orifice. Results of SVTP testing of this failure are listed in section 1.4.2.

1.3.2 Failure Analysis of ALAR AGV 8400A

The failure analysis of the ALAR AGV 8400A was approached in the same manner as that of the Bendix AGV. In the ALAR AGV case, 24 failures were postulated; and only one was judged worthy of SVTP investigation.

1.3.2.1 8400A (ALAR AGV) Failure Case 1

Failure: Leaking bellows (Fig. 23: Item 18)

Result: Exhaust valve control of suit pressure

Simulation: Bellows plugs (Fig. 23: Items 13, 14, and 15) were replaced by screw with small hole drilled through the center. Failure simulator was manufactured with the same physical dimensions as Item 15.

The position of Item 15 was then carefully measured when the bellows spring [Item 16] was properly adjusted, and the failure simulator was positioned identically.

Discussion: Under normal operating conditions, a hole in the top of the bellows maintains the interior bellows pressure identical to the suit pressure. With a leaking bellows, the interior bellows pressure more closely resembled the first-stage regulation pressure. Two conditions result: First, the air from the first-stage regulator bleeds through the bellows directly into the suit without control. Control is established by the exhaust valve. Second, the mass [Item 3] must overcome a greater force to open the normal second-stage regulator control port sealed by Item 19 (an "O" ring).

Under normal operating conditions, the force generated by the action of acceleration on the mass must overcome the force of two springs [Items 5 and 16] and the natural stiffness of the bellows. In this failure case, it must additionally overcome the force generated by the difference in pressure between first-stage regulated pressure and suit pressure acting across an area equal to the top of the bellows. The result is a late pressurization start on the pressure-G profile. The results of SVTP testing of this failure mode are discussed in section 1.4.3.

1.4 Standardized AGV Test Protocol (SVTP) Testing of Failures

Those induced failures judged worthy of serious consideration were subjected to SVTP testing and GVALVPGM analysis. In the absence of adequate data on failures in the field, the failures tested were derived from engineering evaluation. They were, by design, "soft failures" (those which did not render the valve inoperative). Emphasis was placed on those failures which, in addition, might not be detected during normal preflight checkout.

1.4.1 SVTP Test of Bendix AGV Failure #1

Bendix Failure #1 is especially insidious because it will pass all normally prescribed static tests, including that performed after overhaul. The nature of the failure is described, in detail, in section 1.3.1.1. For specific comparisons of the effect of this failure, all graphs and tables in this section may be compared directly to those in section 5.2 of PTAP Volume I. Comparison of the total performance scores, shown on line 33 of the two PET's (i.e., 200.3 for the failure #1, compared with a normal 111.2), gives a quick indication of the effect (PET, Vol. I, Table 3; and PET, Vol. II, Table 1). The reader is reminded that the lower score indicates more desirable operating characteristics, and that the Ready Pressure Valve's (RPV) performance score of 25.4 sets the standard for this report.

1.4.1.1 Bendix AGV Failure #1 Flow Characteristics (Figs. 24 and 25)

Very little difference exists between the normal flow characteristics and the failure flow characteristics. The difference

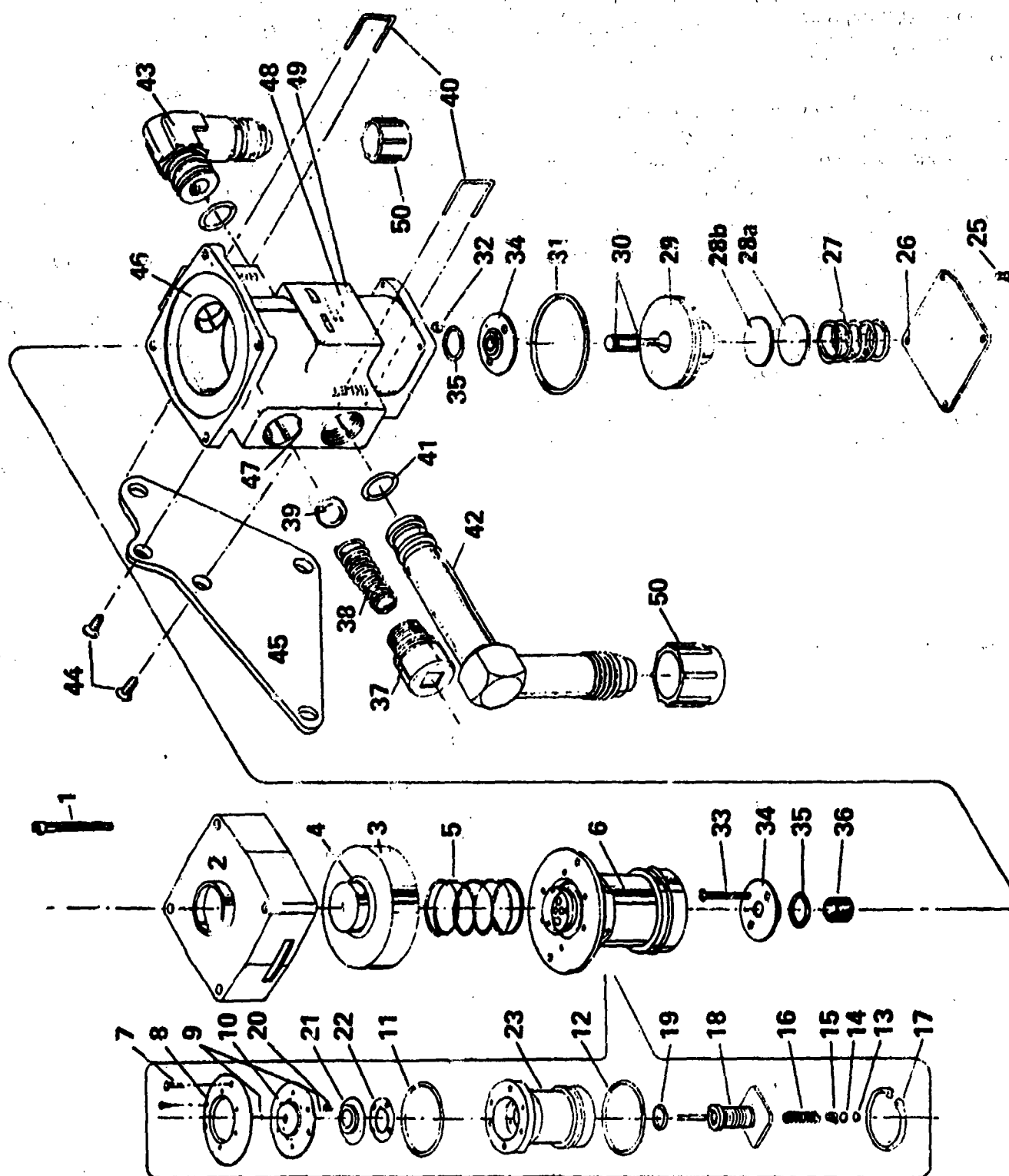


Figure 23. Exploded view of the ALAR 8400A anti-G valve.
 [TO 15X8-7-5-3, Wright-Patterson AFB, Ohio]
 [Key is on facing page]

-- Key to Figure 23 --

ITEM NO.	DESCRIPTION	ITEM NO.	DESCRIPTION
1	Bolt	27	Spring
2	Housing, weight	28	Shim
3	Weight assembly	29	Spool assembly
4	Packing, preformed	30	Packing, preformed
5	Spring, weight	31	Packing, preformed
6	Second-stage assembly	32	Nut
7	Screw	33	Screw
8	Plate, diaphragm	34	Seat
9	Ring, retaining	35	Packing, preformed
10	Diaphragm assembly	36	Screen assembly
11	Packing, preformed	37	Body, relief valve
12	Packing, preformed	38	Spring
13	Screw, bellows sealing	39	Ball
14	Seal	40	Retaining clip
15	Screw, bellows setting	41	Packing, preformed
16	Spring, bellows	42	Fitting, inlet
17	Ring, retaining bellows	43	Fitting, outlet
18	Bellows assembly	44	Screw
19	Packing, preformed	45	Plate assembly, mounting
20	Screw	46	Body assembly, main
21	Seat	47	Lock plug
22	Gasket	48	Nameplate
23	Body, second-stage	49	Drive screws
24	First-stage assembly	50	Protector cap
25	Screw		
26	Cover		

TABLE 1: BENDIX AGV FAILURE #1 PERFORMANCE EVALUATION TABLE

TEST STANDARDS:

1. SPMIN = 40. PSIG
2. SPMID = 70. PSIG
3. SPMAX = 120. PSIG
4. THETA = 20. DEGREES
5. SVMIN = 6. LITERS
6. SVMID = 10. LITERS
7. SVMAX = 14. LITERS

CHARACTERISTIC NUMBERS:

8. XSPMX = 2.5000
9. XSPMN = 1.3333
10. XTHTA = 1.0000
11. DESIGN TOTAL: 4.833
12. XFLBR = 3.771
13. XDOLF = 2.136
14. XDDL F = 2.156
15. XSIGF = 0.234
16. FLOW TOTAL: 8.297
17. XCCP1 = 26.238
18. XCDP1 = 36.986
19. XSGP1 = 1.453
20. XDPP1 = 1.464
21. LOW-ONSET TOTAL: 66.140
22. XCCP2 = 10.817
23. XDDP2 = 37.910
24. XDGP2 = 5.444
25. XDPP2 = 5.294
26. XTD P2 = 13.242
27. HIGH-ONSET TOTAL: 72.706
28. XIDPA = 9.548
29. XIDPB = 15.983
30. XIDPC = 5.119
31. XIDPD = 17.586
32. SACM TOTAL: 48.337
33. VALVE: BENDIX FAILURE #1 TOTAL: 200.313

TABLE 2. KEY TO SYMBOLS IN FIGURES 24 TO 86
[Symbols are shown as data points
on the curves. See footnote.]

- 1 = 0.1 G/SEC G-ONSET RATE
- 2 = 0.5 G/SEC G-ONSET RATE
- 3 = 1.0 G/SEC G-ONSET RATE
- 4 = 1.5 G/SEC G-ONSET RATE
- A = MAXIMUM DESIGN ANGLE
- D = MEDIUM SOURCE PRESSURE, OR DECREASING
(WITH RESPECT TO G)
- I = INCREASING (WITH RESPECT TO G) OR P-IDEAL
(ACMS)
- N = MINIMUM SOURCE PRESSURE
- R = P-REAL (ACMS ONLY)
- X = MAXIMUM SOURCE PRESSURE
- * = P-REAL LESS P-IDEAL OR G-ONSET

EDITOR'S NOTE: Due to the limitations of the technique initially used, these symbols are not always discernible on the respective curves. In such cases, however, the symbols are insignificant as compared with the close relationship obvious between the curves in each figure.

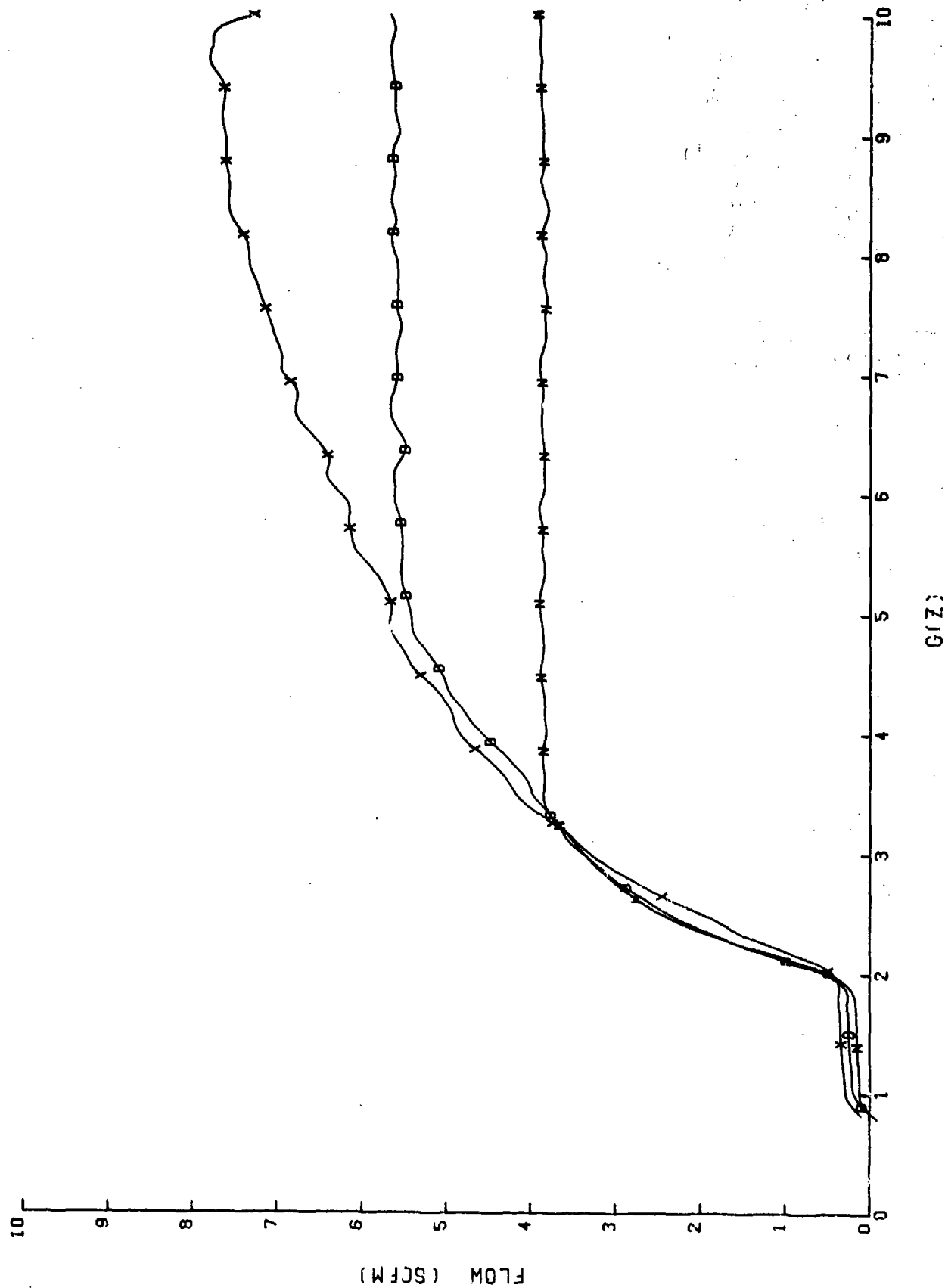


Figure 24. Bendix failure #1: Flow as a function of source pressure.
 [Curves are: N, D, and X. For "Key," refer to Table 2.]

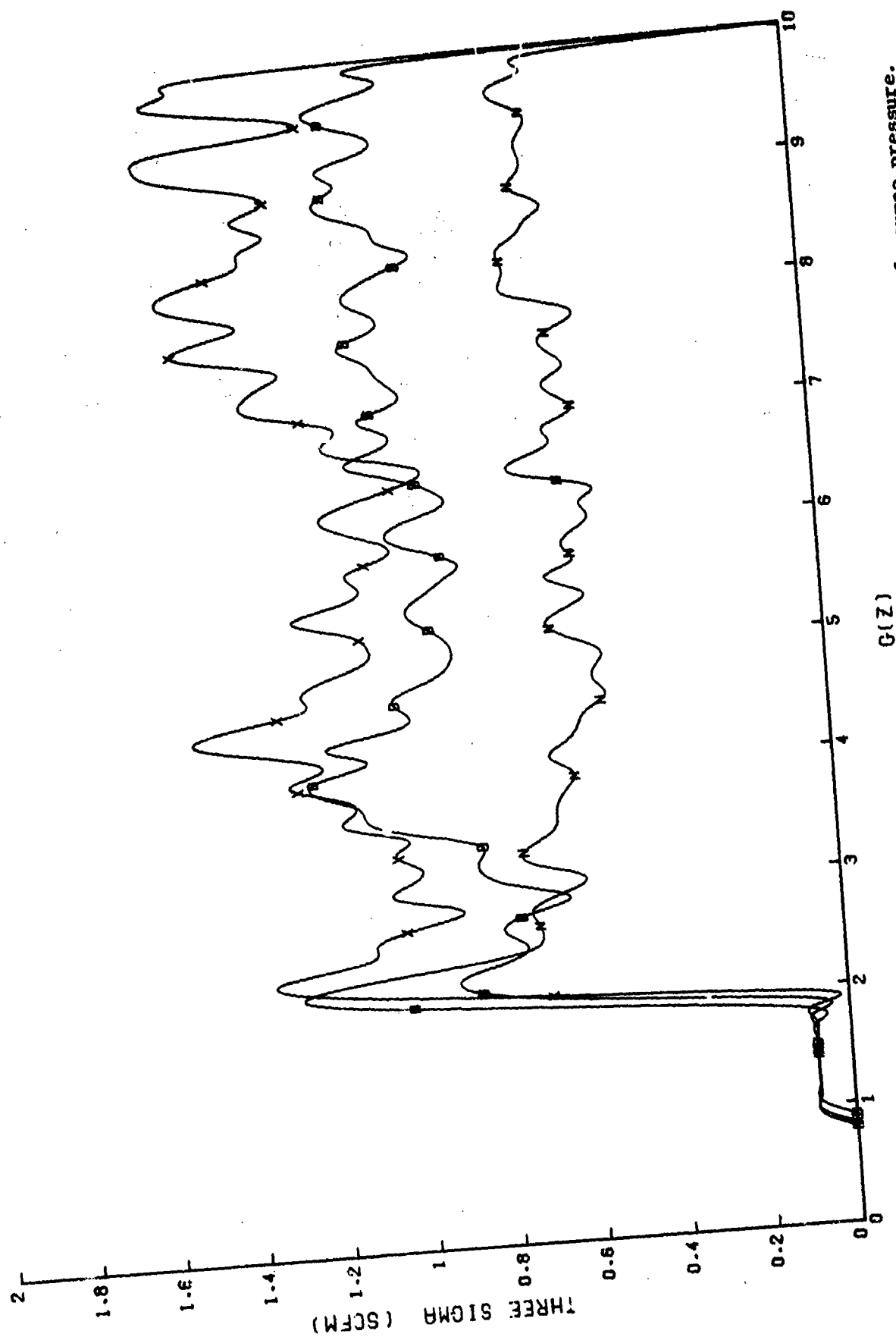


Figure 25. Bendix failure #1: Variation (three sigma) in flow as a function of source pressure.
[Curves are: N, D, and X. For "Key," refer to Table 2.]

between a normal 7.147 (Vol. I, Table 3, line 16) and 8.297 (Vol. II, Table 1, line 16) is primarily reflected in the source pressure influence scored on lines 13 and 14. The same effect is apparent in Figure 26 (Vol. I) of the normal case and Figure 24 (Vol. II) of the failed case, with the saturating median-source-pressure open-flow curve.

1.4.1.2 Bendix AGV Failure #1: Low-Onset-Rate Characteristics (Figs. 26 - 29)

Approximately 60% of the PET performance score difference occurred in the low-onset-rate test, and the majority of this change occurred on line 17 (indicating poor linearity) and line 18 (indicating a large source pressure influence). The cause of these high (undesirable) scores may be readily seen in a comparison of Figure 28 (Vol. I) and Figure 26 (Vol. II). The inability of the low and median source pressures to outrun the mass valve leak rate (i.e., drive the output pressure above 3 psig and 6 psig, respectively) degraded both linearity and source pressure response. Lines 19 and 20 of the PET actually improved over the normal valve score. The saturated pressures actually reduced the 3 sigma of the data (in Fig. 27 of Vol. II compared to that in Fig. 29 of Vol. I), and the hysteresis (in Fig. 29 of Vol. II, compared to that in Fig. 31 of Vol. I).

1.4.1.3 Bendix AGV Failure #1: High-Onset-Rate Characteristics (Figs. 30 - 36)

Approximately 20% of the performance degradation, reflected in the PET (Table 1), occurs in lines 22 through 27. The failure case scores actually improved in the tests for 3 sigma (line 24), hysteresis (line 25), and profile lag due to onset rate (line 26). In each case, saturated output at high-onset rates was essentially identical to the low-onset-rate output. However, the poorer performance shows dramatically on lines 22 (doubled linearity score) and 23 (tripled source-pressure influence score). Figures 30-36 graphically represent these results.

1.4.1.4 Bendix AGV Failure #1 SACM Characteristics (Figs. 37 - 44)

The Simulated Aerial Combat Maneuver (SACM) test is almost entirely self-comparative. Since the standard for comparison is generated in the earlier tests, even very poor performance may score reasonably well if it is consistent. As a result, only 17% of the PET score degradation appears in this section. Figures 37 - 44 support these results.

1.4.2 SVTP Test of Bendix AGV Failure #2

Bendix Failure #2 is an extremely probable failure. Probably, the weakest link in the Bendix AGV system design is the minute orifice which supplies pilot pressure to the regulator. Even though multiple filters were used during SVTP testing, this orifice had to be cleaned frequently by the PTAP crew. The exact nature of the induced failure is described in detail in section 1.3.1.2. For specific comparisons of the effect of this

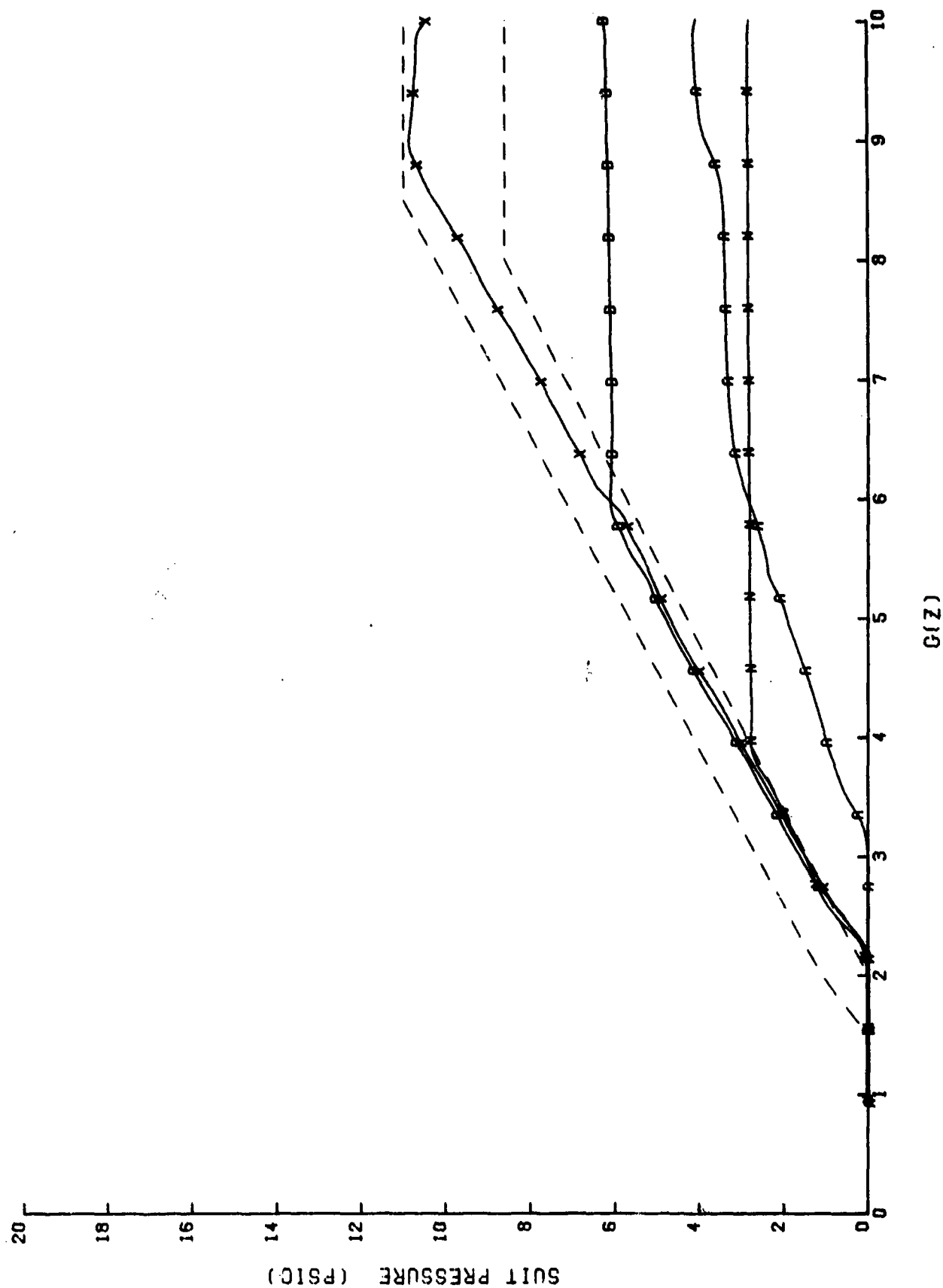


Figure 26. Bendix failure #1: 0.1 G/sec suit pressure profile as a function of source pressure.
 [Curves are: N, D, X, and A. For "Key," refer to Table 2.]

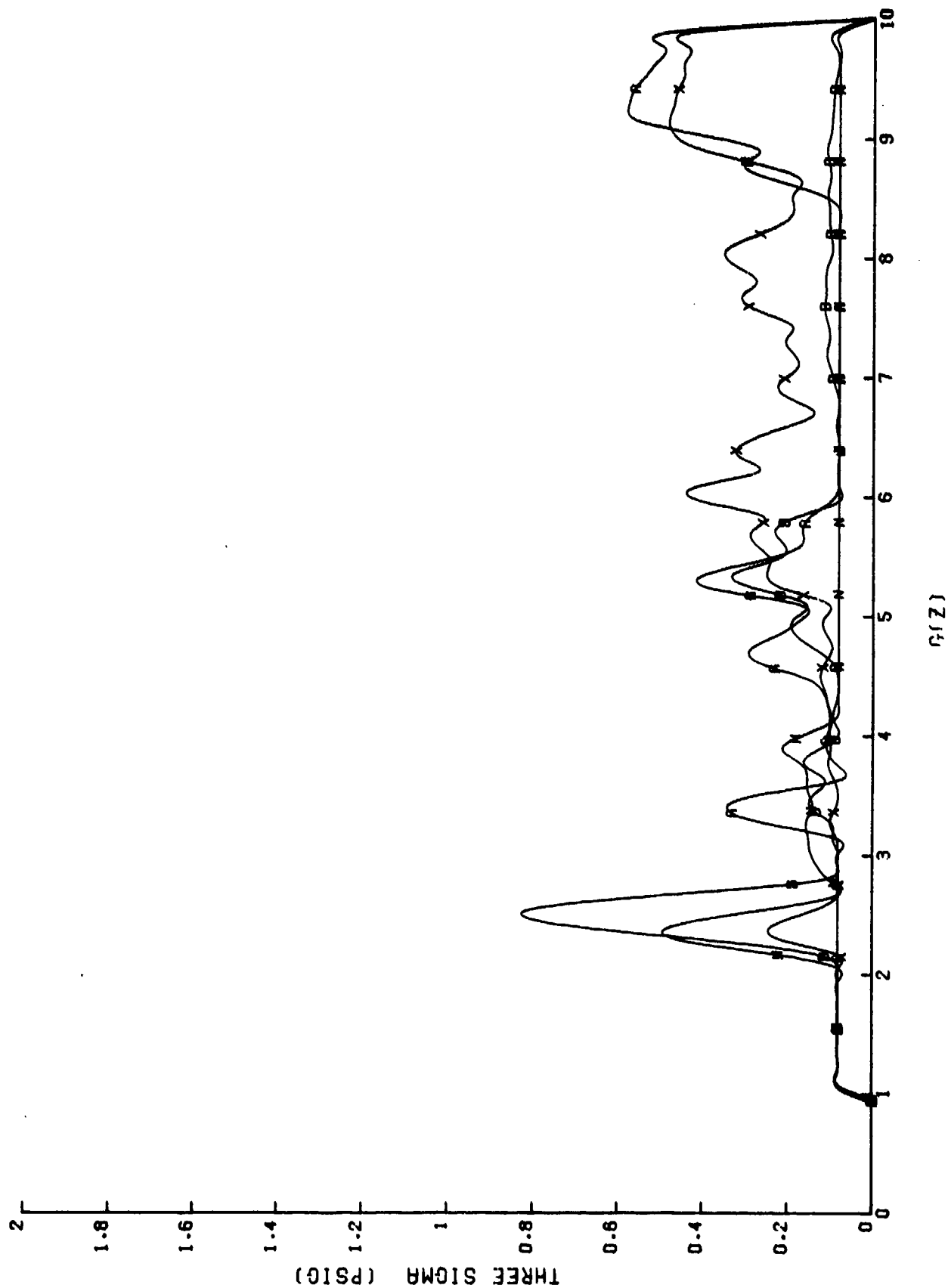


Figure 27. Bendix failure #1: 0.1 G/sec suit pressure variation as a function of source pressure.
[Curves are: N, D, X, and A. For "Key," refer to Table 2.]

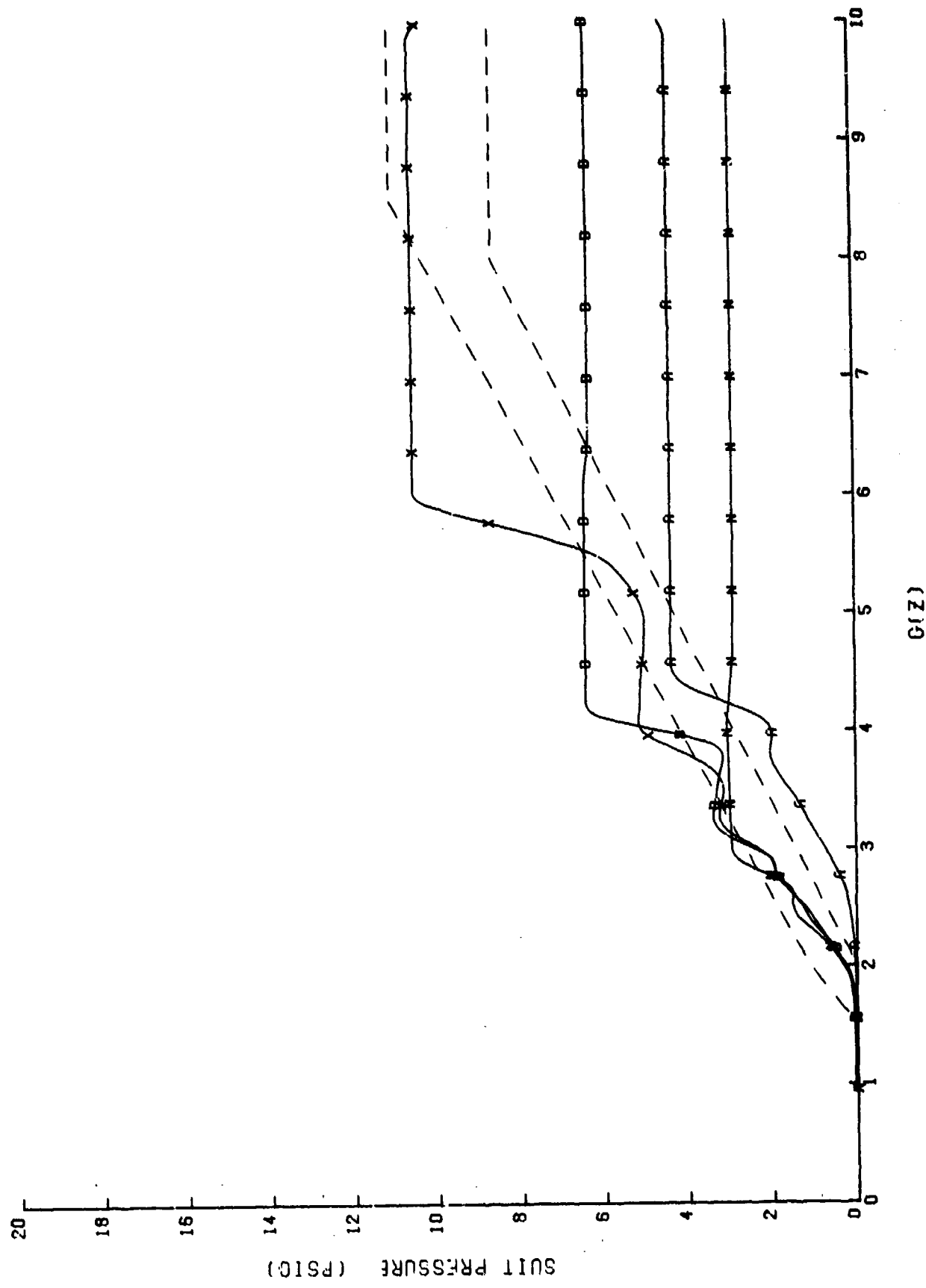
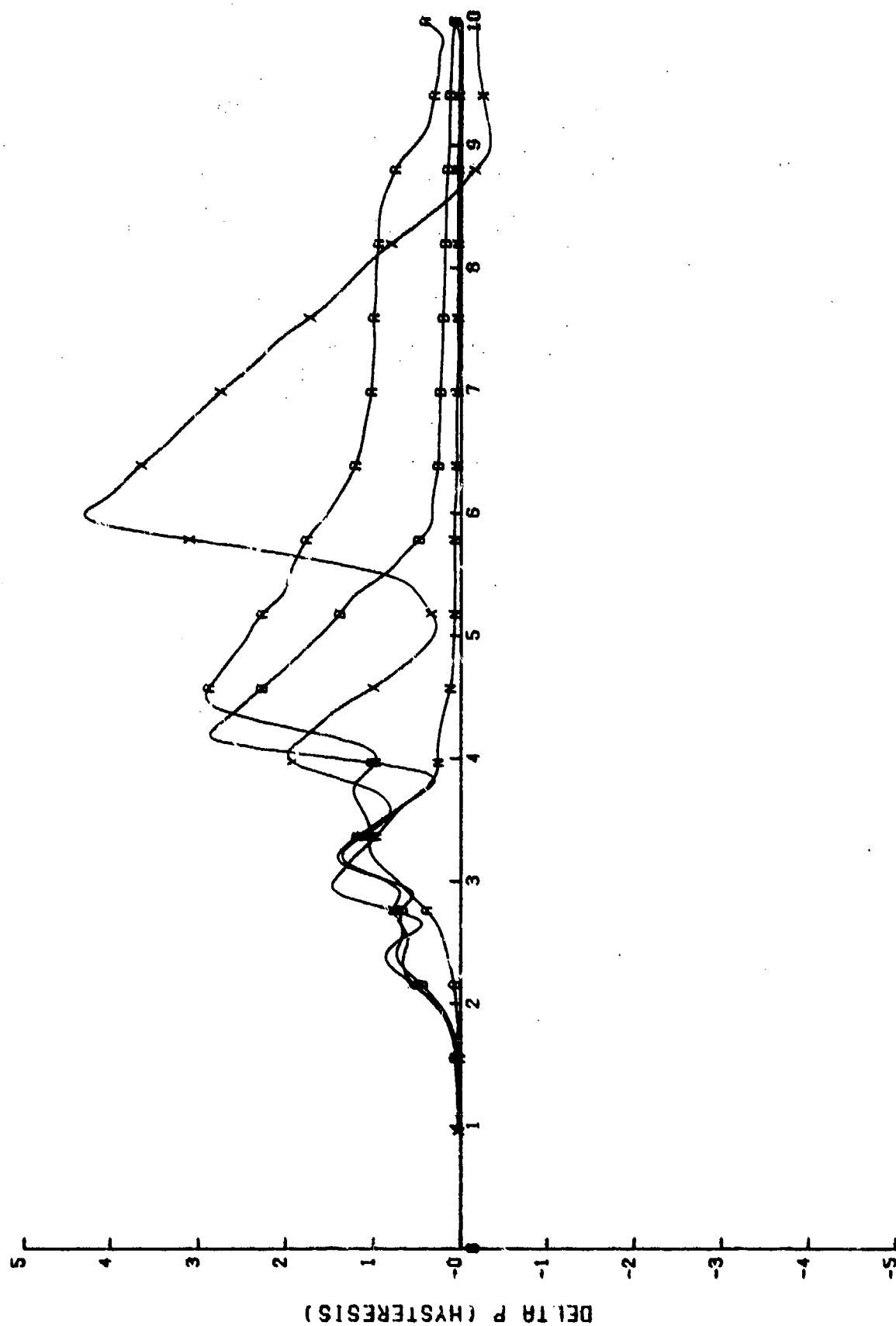


Figure 28. Bendix failure #1: 0.1 G/sec decreasing suit pressure profile as a function of source pressure. [Curves are: N, D, X, and A. For "Key," refer to Table 2.]



$G(Z)$

Figure 29. Bendix failure #1: 0.1 G/sec suit pressure hysteresis as a function of source pressure.
[Curves are: N, D, X, and A. For "Key." refer to Table 2.1]

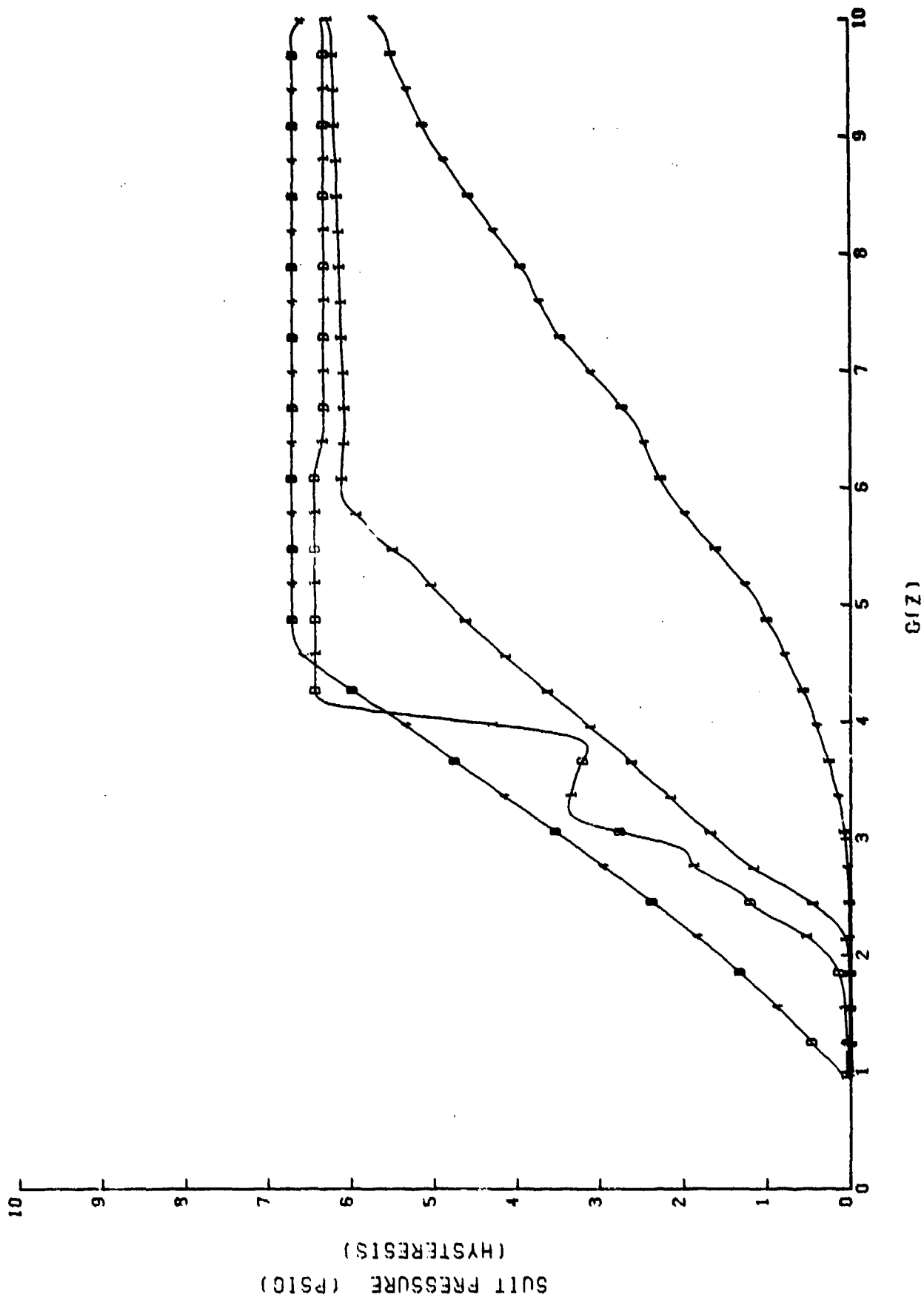


Figure 30. Bendix failure #1: Suit pressure profile comparison as a function of onset rate.
[Curves are: 1I, 4I, 1D, and 4D. For "Key," refer to Table 2.]

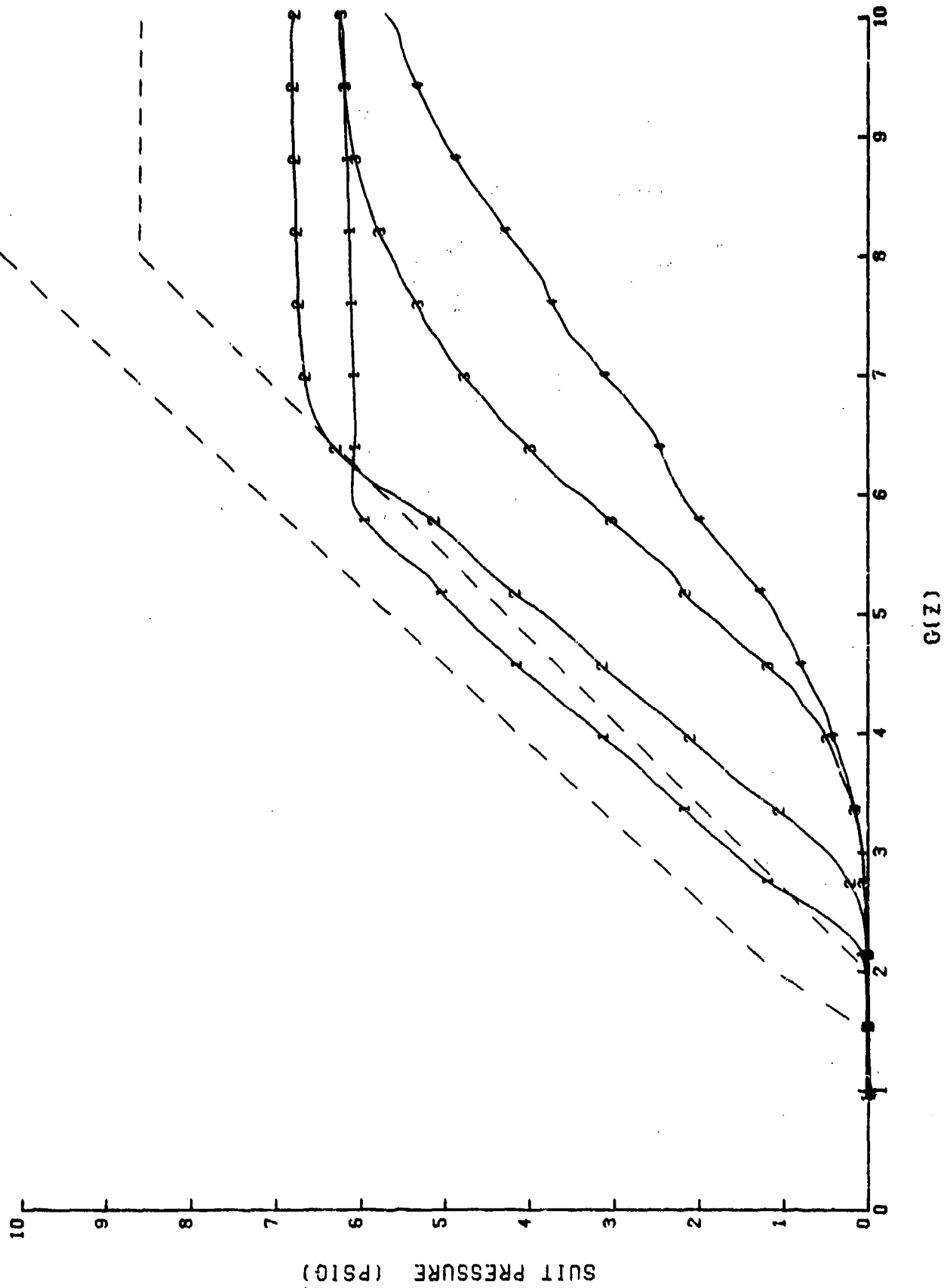


Figure 31. Bendix failure #1: Suit pressure profile as a function of G-onset rate.
[Curves are: 1, 2, 3, and 4. For "Key," refer to Table 2.]

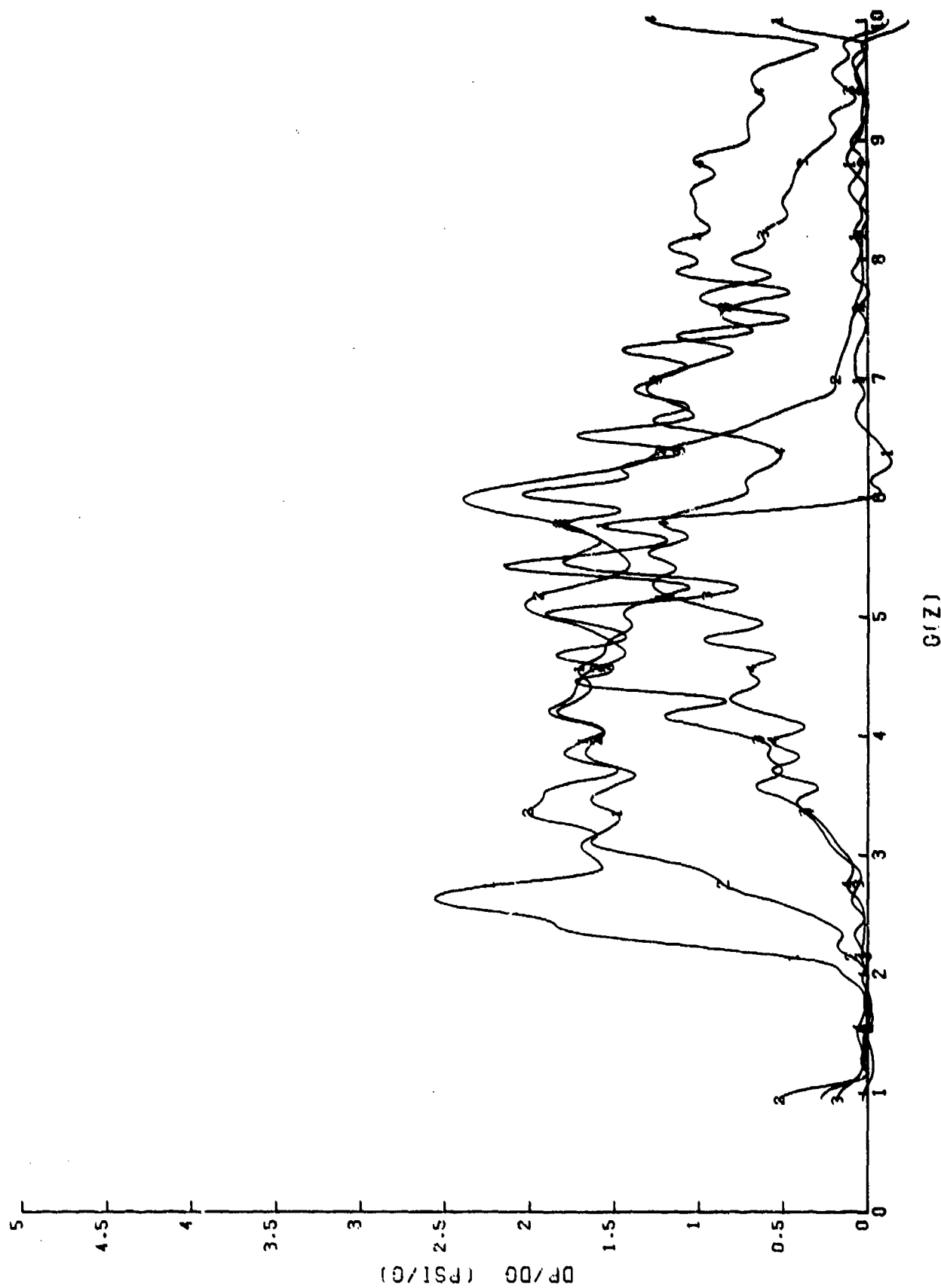


Figure 32. Bendix failure #1: dP/dG as a function of G -onset rate.
 [Curves are: 1, 2, 3, and 4. For "Key," refer to Table 2.]

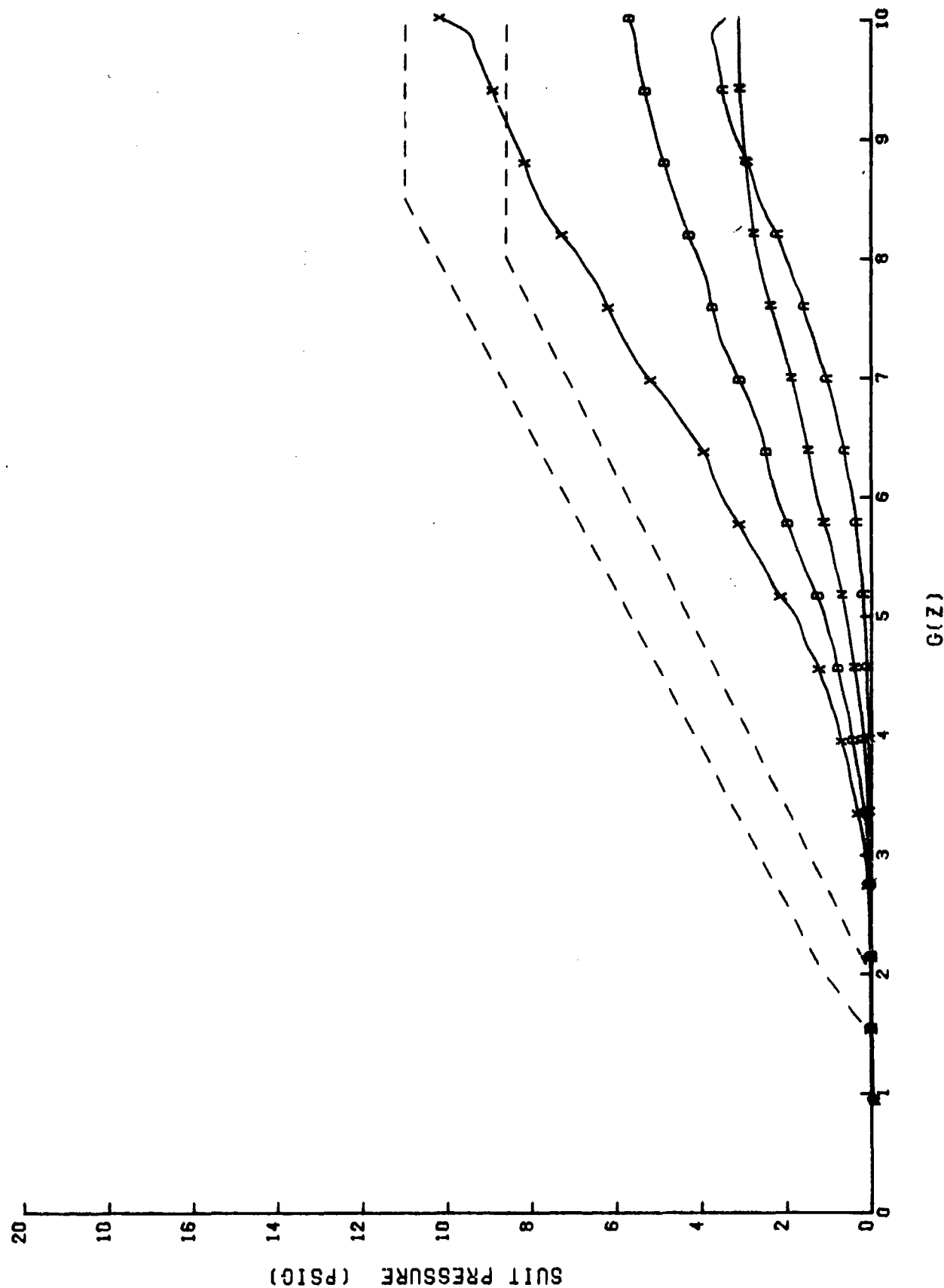


Figure 33. Bendix failure #1: 1.5 G/sec suit pressure profile as a function of source pressure.
 [Curves are: N, D, X, and A. For "Key," refer to Table 2.]

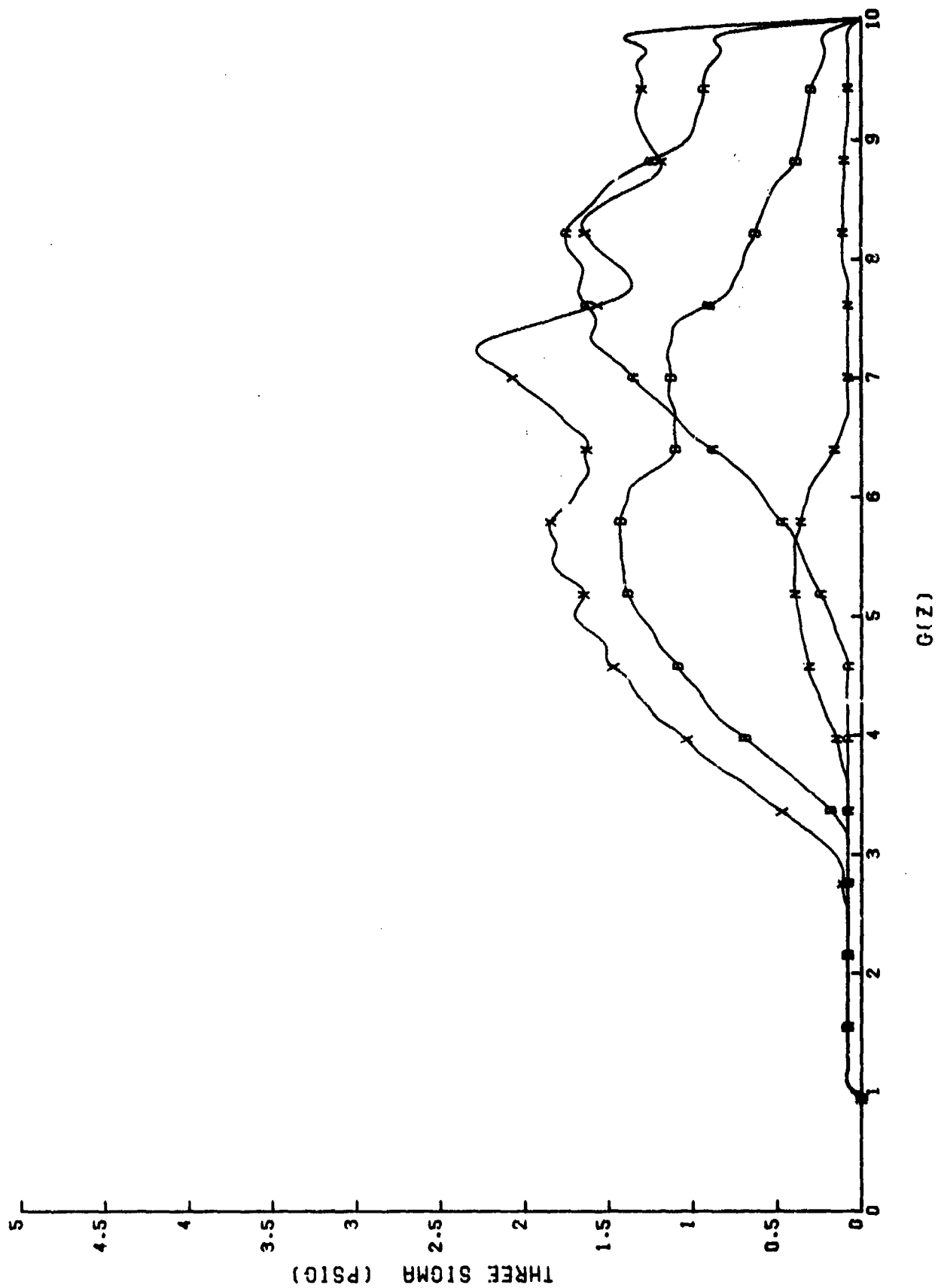


Figure 34. Bendix failure #1: 1.5 G/sec suit pressure variation as a function of source pressure.
 [Curves are: N, D, X, and A. For "Key," refer to Table 2.]

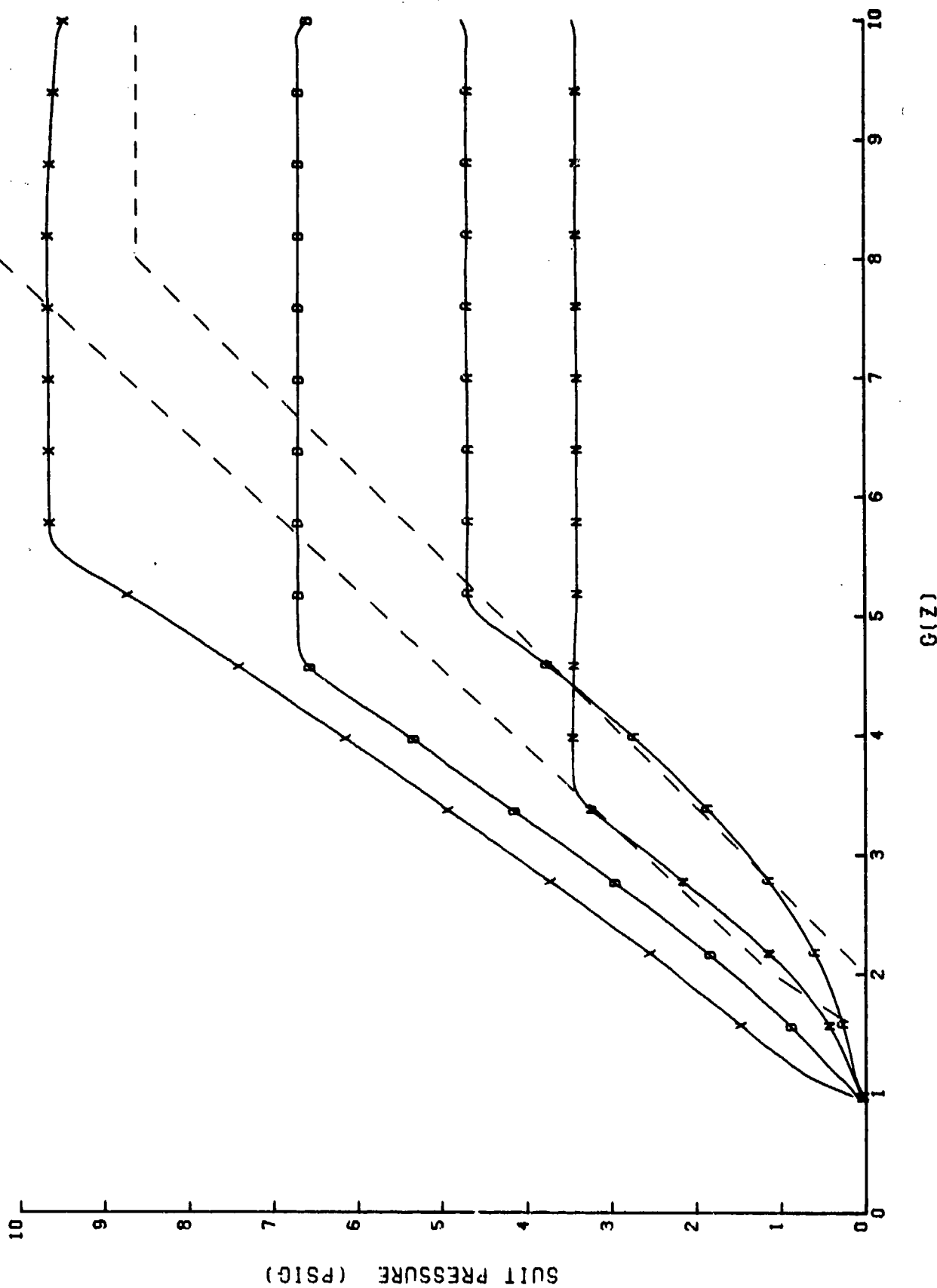
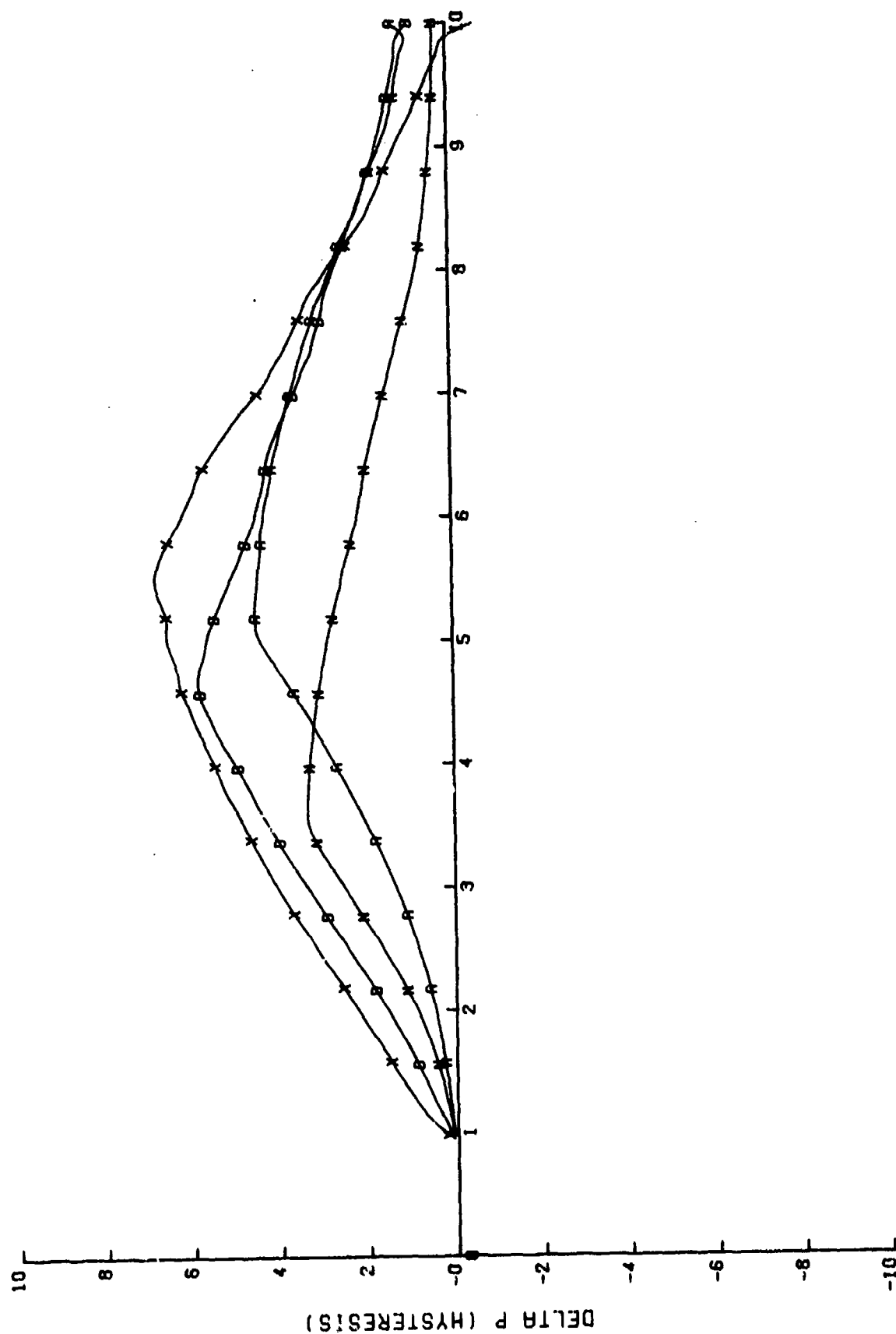


Figure 35. Bendix failure #1: -1.5 G/sec decreasing suit pressure profiles of test #1



G(Z)

Figure 36. Bendix failure #1: 1.5 G/sec suit pressure hysteresis as a function of source pressure.
[Curves are: N, D, X, and A. For "Key," refer to Table 2.]

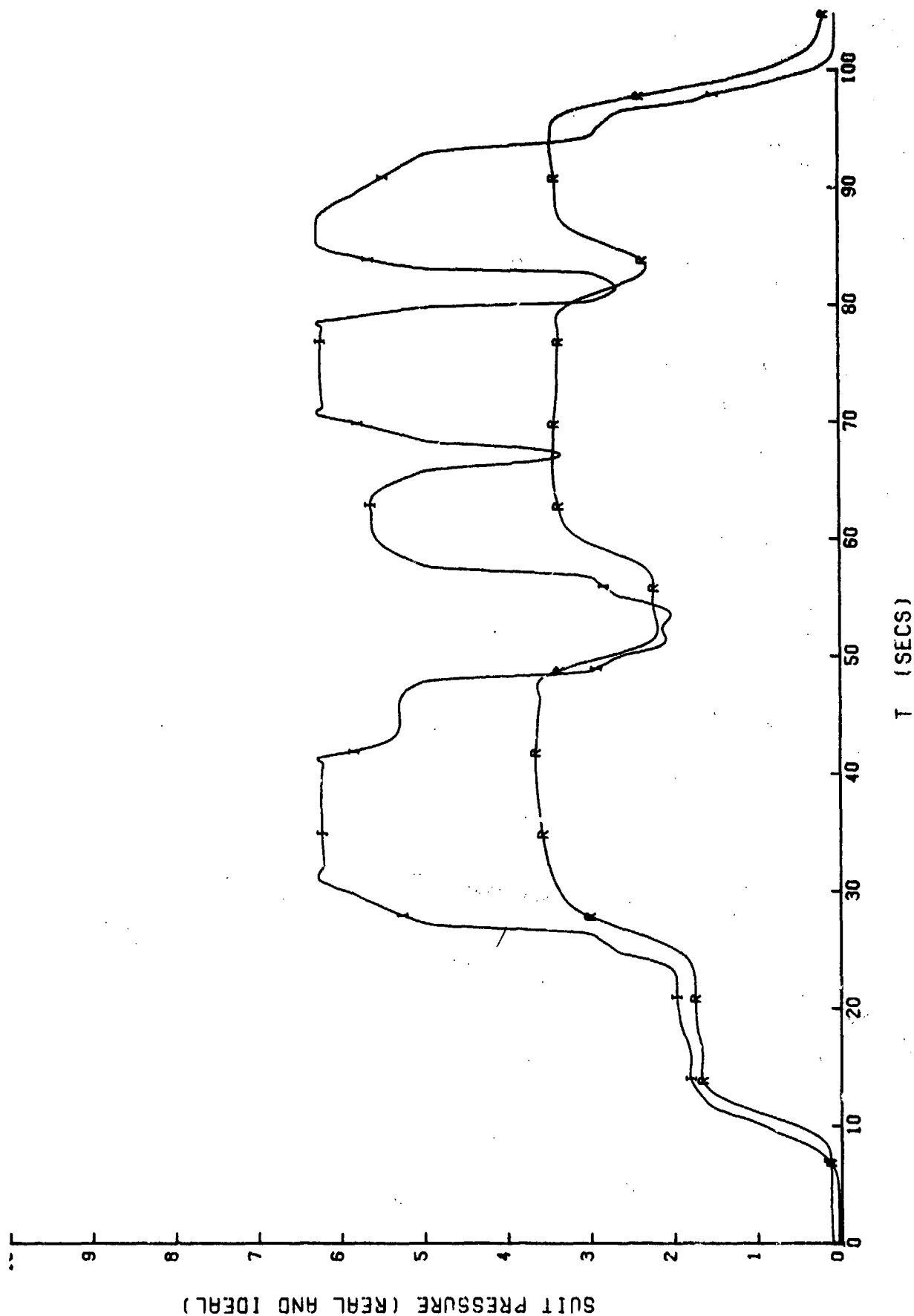
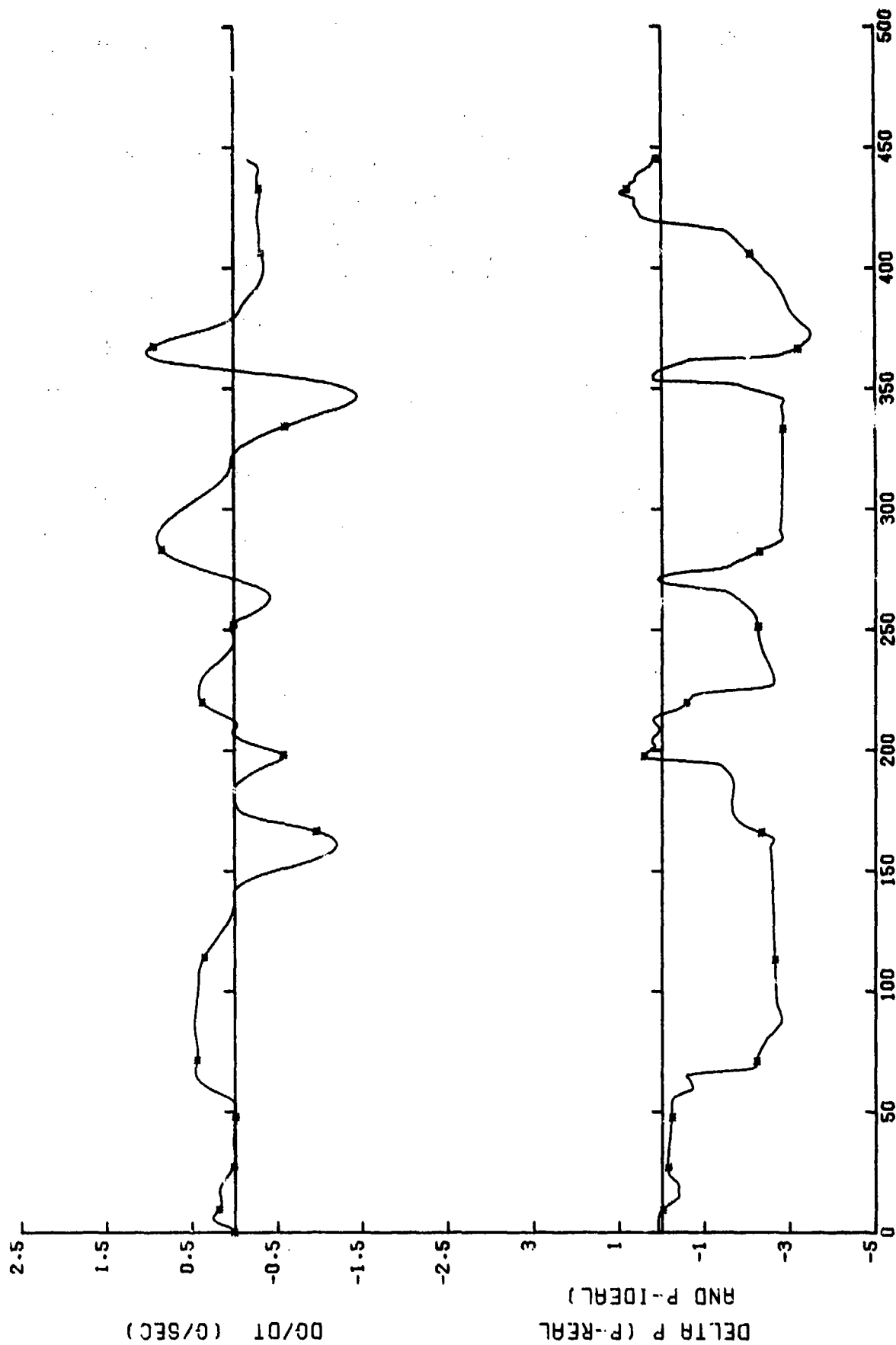


Figure 37. Bendix failure #1: SACM suit pressure profile comparison with minimum source pressure and maximum suit volume. [Curves are: R and I. For "Key," refer to Table 2.]



INTEGRAL OF $G \, DT$ FROM 0 TO T

Figure 38. Bendix failure #1: Suit pressure deviation and dg/dt for the minimum source pressure, maximum suit volume SACM. [Curves are: *. For "key," refer to Table 2.]

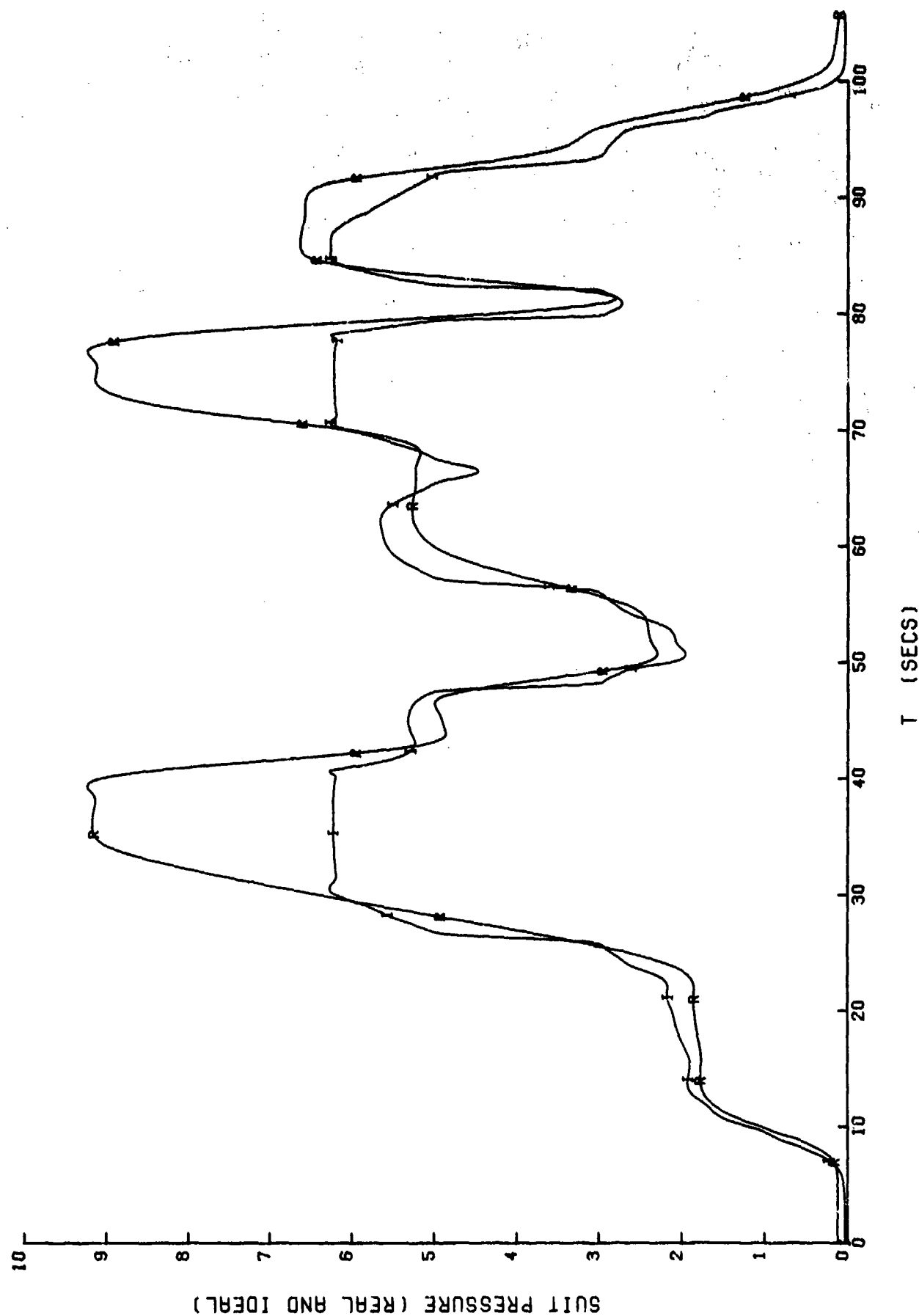
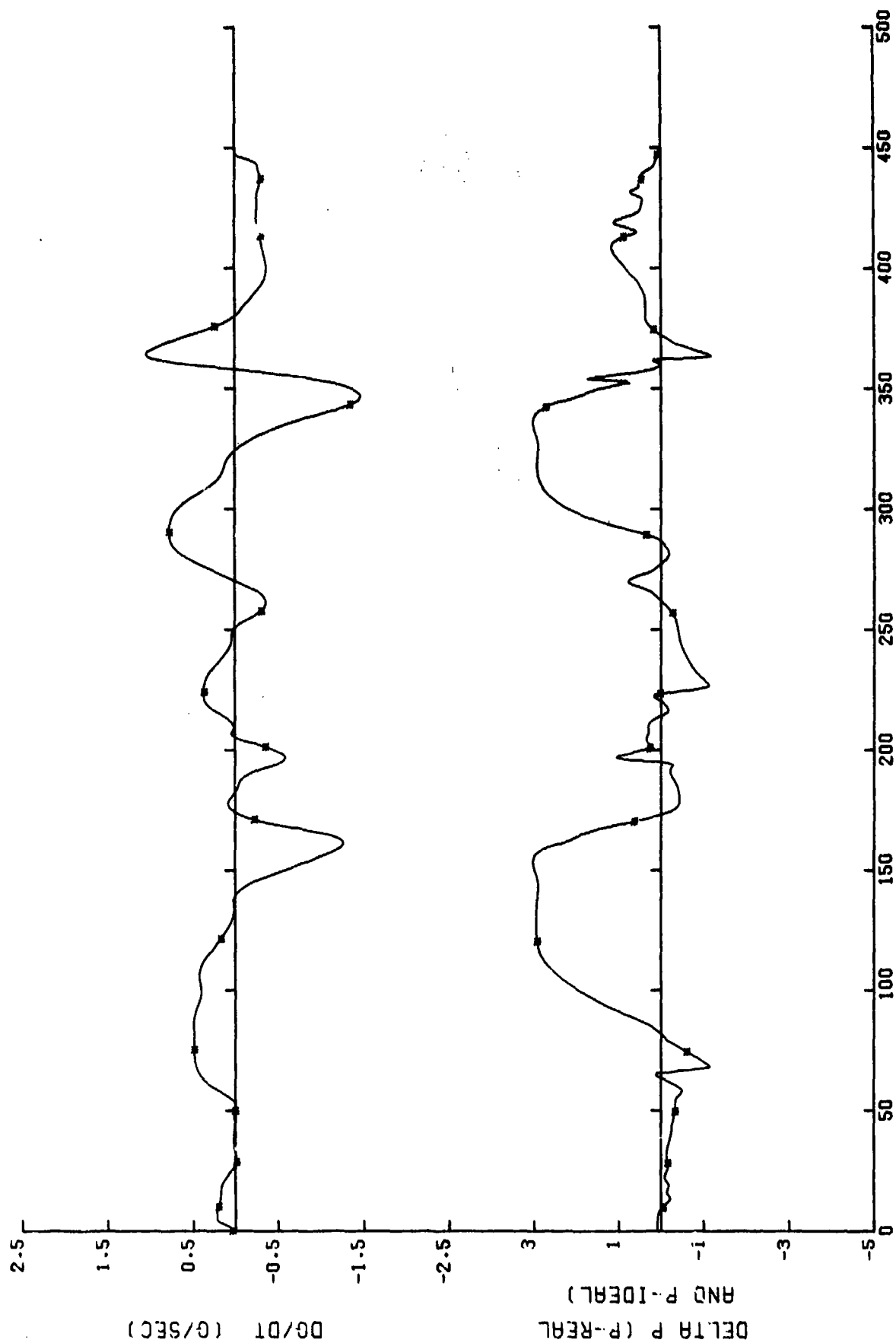


Figure 39. Bendix failure #1: SACM suit pressure profile comparison with maximum source pressure and minimum suit volume. [Curves are: R and I. For "Key," refer to Table 2.]



INTEGRAL OF \dot{G} DT FROM 0 TO T

Figure 40. Bendix failure #1: Suit pressure deviation and dG/dt for the maximum source pressure, minimum suit volume SACM. [Curves are: *. For "Key," refer to Table 2.]

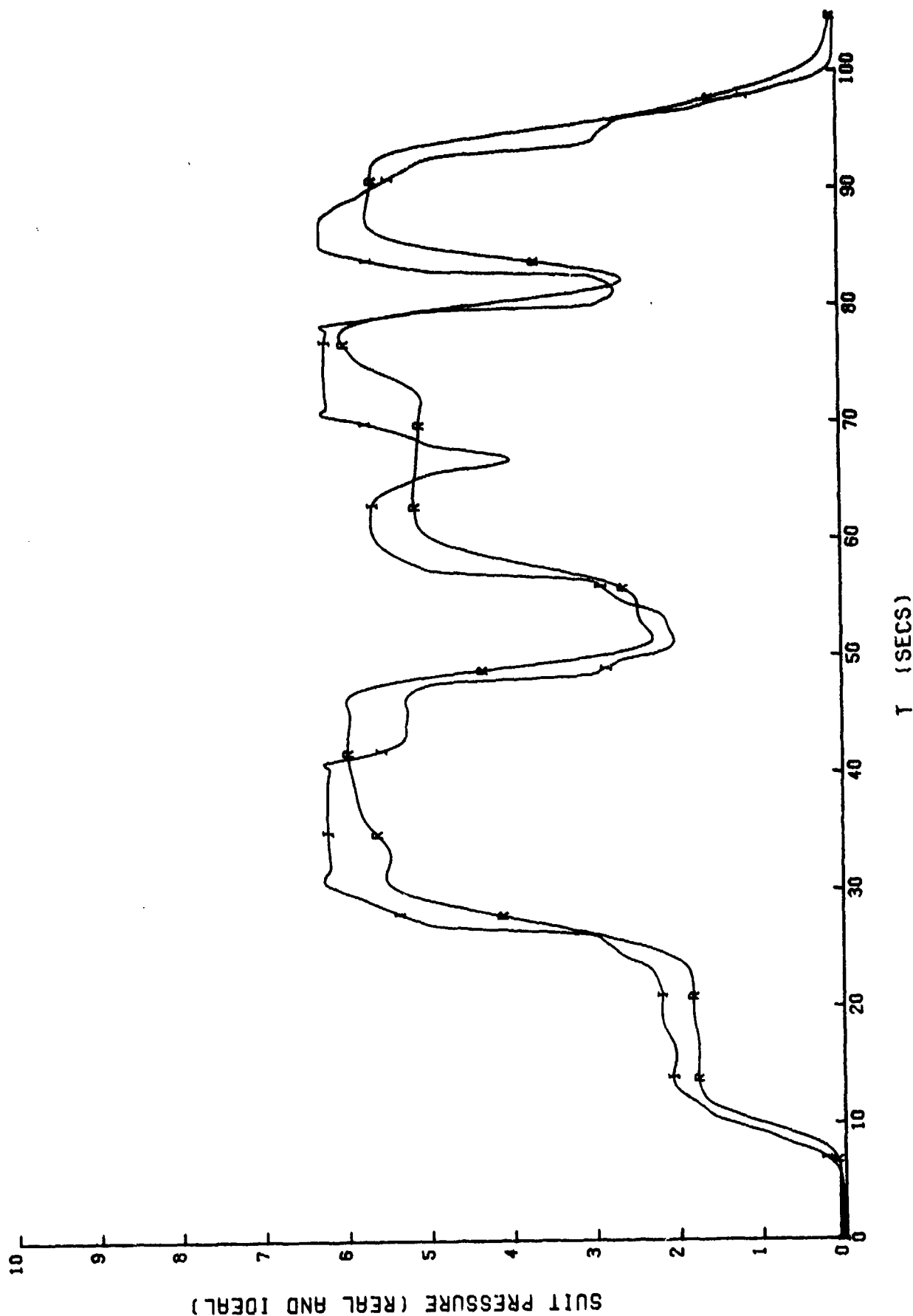
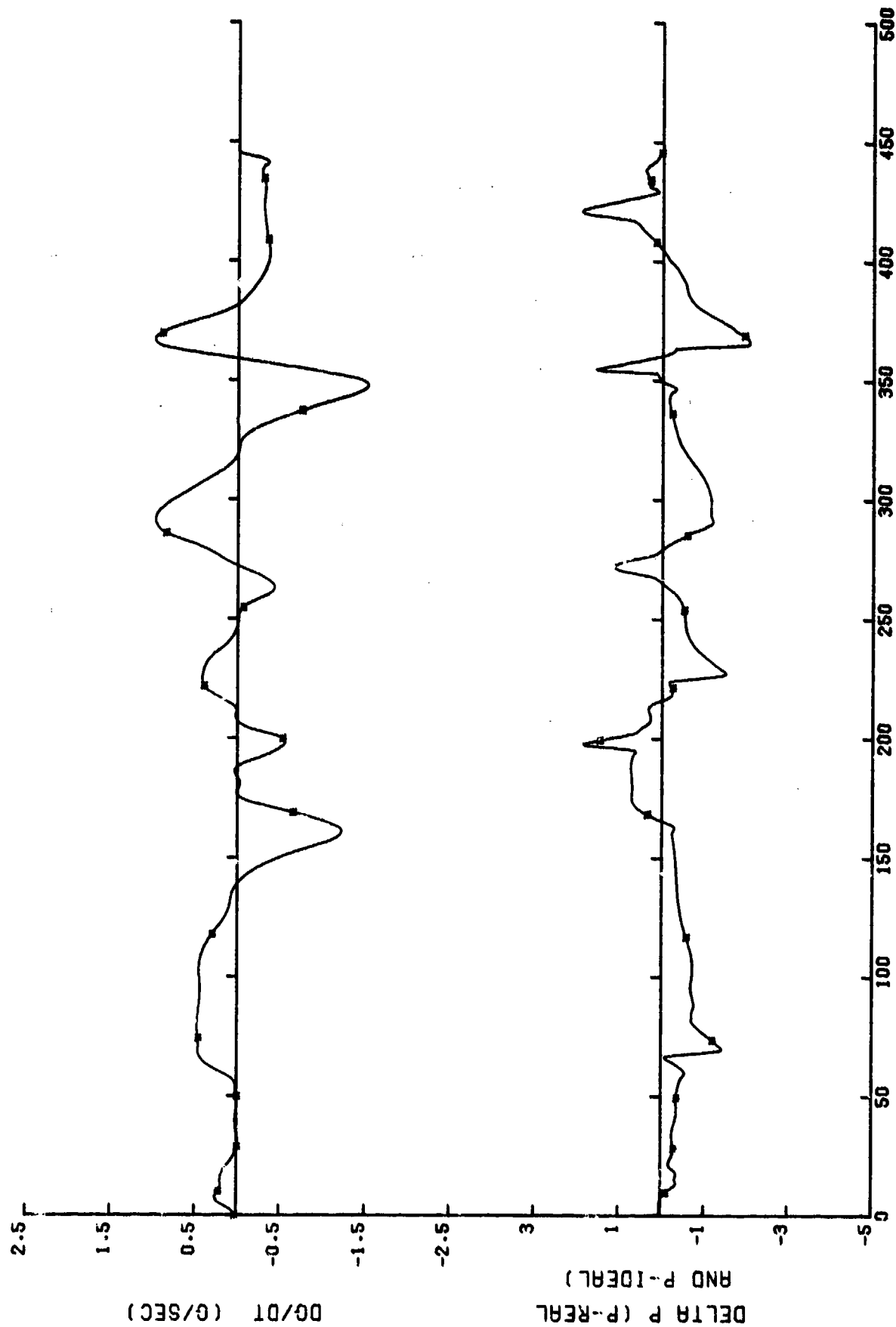


Figure 41. Bendix failure #1: SACM suit pressure profile comparison with median source pressure and suit volume. [Curves are: R and I. For "Key," refer to Table 2.]



INTEGRAL OF $G \cdot DT$ FROM 0 TO T

Figure 42. Bendix failure #1: Suit pressure deviation and dG/dt for the median source pressure and suit volume SACM. [Curves are: *. For "Key," refer to Table 2.]

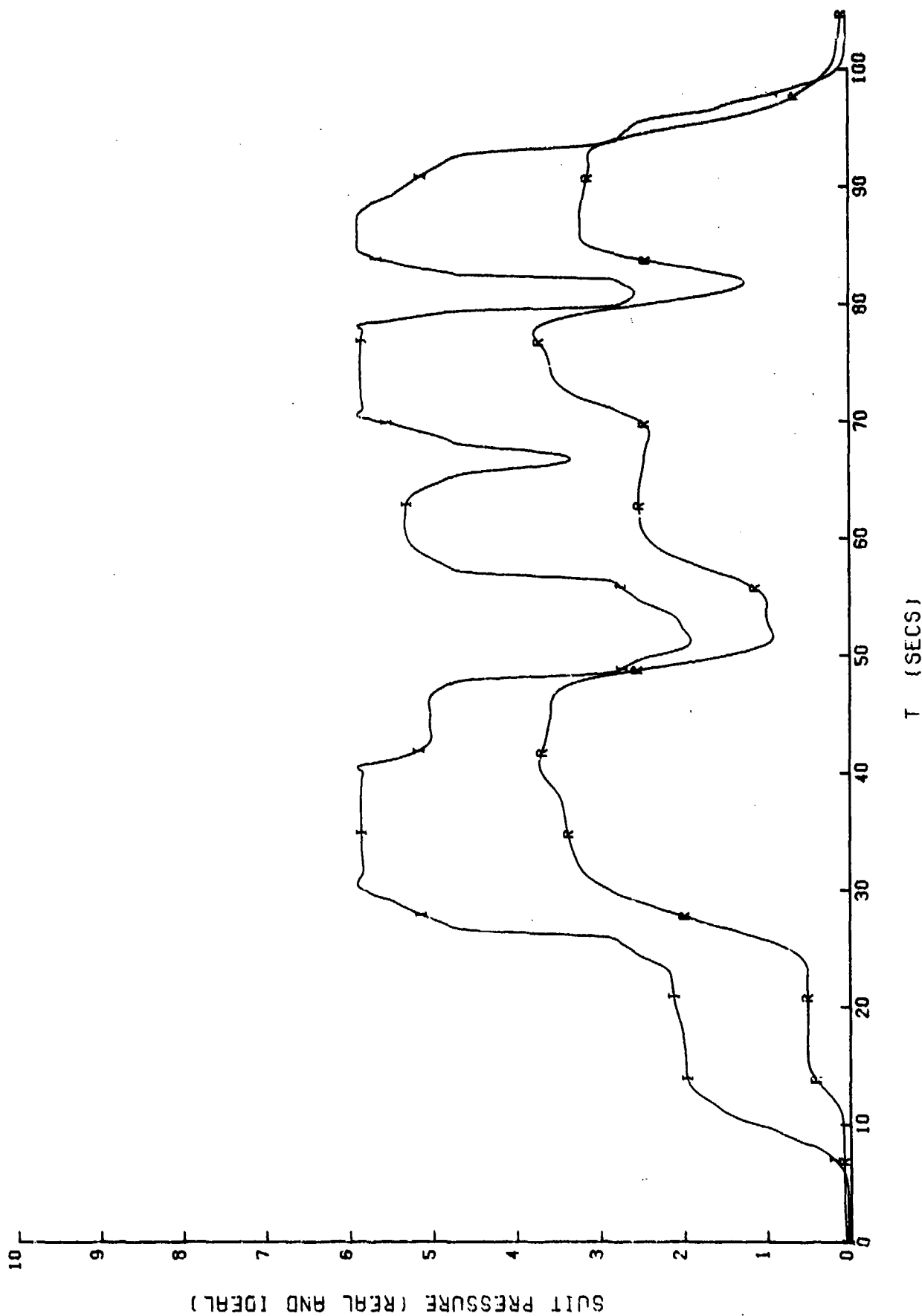
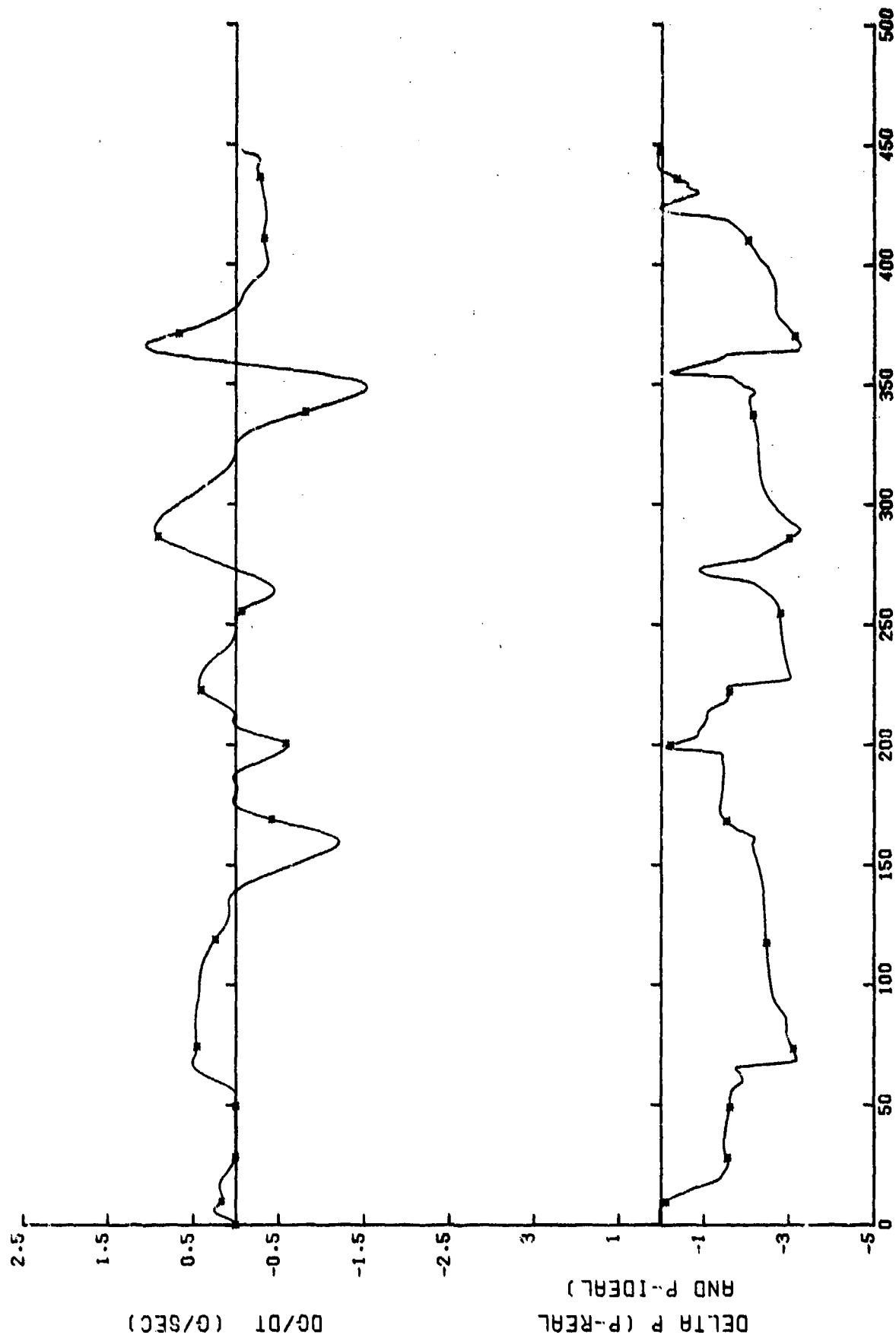


Figure 43. Rendix failure #1: SACM suit pressure profile comparison with G vector misalignment.
[Curves are: R and I. For "Key," refer to Table 2.]



INTEGRAL OF G DT FROM 0 TO T

Figure 44. Bendix failure #1: Suit pressure deviation and dG/dt for G vector misalignment SACH.
[Curves are: *. For "Key," refer to Table 2.]

failure, all graphs and tables may be directly compared with those of section 5.2 in Volume I. A comparison of the total performance scores shown on line 33 of the two PET's (i.e., 144.9 for failure #2, Table 3 compared to a normal 111.2, Fig. 3, Vol. I) gives a quick indication of the effect. The reader is reminded that the lower score indicates the more desirable operating characteristics, and that the RPV's performance score of 25.4 sets the standard for this report.

1.4.2.1 Bendix AGV Failure #2 Flow Characteristics
(Figs. 45 - 46)

Very little effect of the failure is apparent in the flow characteristics, as evidenced by lines 12 through 16 of Table 3 (corresponding to Table 3, Vol. I), and the open-flow curves in Figures 45 and 46.

1.4.2.2 Bendix AGV Failure #2 Low-Onset-Rate Characteristics
(Figs. 47 - 50)

Examination of lines 17 through 21 of Table 3 indicates Bendix Failure #2 exhibited an only slightly better performance than a normally operating valve. It is doubtful this improvement is real. The reader is reminded that the nature of this failure has absolutely no effect in static situations. The pilot "pressure" is not restricted, only the flow into the chamber containing that pressure. As a result, the 52% occlusion did not prevent pilot pressure from reaching required levels on the 0.1 G/sec profiles. Figures 47-50 graphically represent these results.

1.4.2.3 Bendix AGV Failure #3 High-Onset-Rate Characteristics
(Figs. 51 - 57)

The majority of the performance decrement (71% according to the PET, Table 3), resulting from Bendix Failure #2, occurs in the high G-onset tests. The reduced rate of flow into the pilot pressure chamber is apparent in increasing delays as the onset rate increases (Fig. 52). These increasing delays naturally affect linearity (line 22 of the PET) and source pressure influence (line 23 of the PET, and Fig. 54).

1.4.2.4 Bendix AGV Failure #2 SACM Characteristics
(Figs. 58 - 65)

The late pressure rise characteristic of this failure is very apparent in the SACM tests. Approximately 32% of the PET score decrement occurs in these tests. The self-comparison did not mask this failure, since its effect was not apparent at low G-onset rates.

1.4.3 SVTP Testing of ALAR AGV Failure

The exact nature of ALAR Failure is described in detail in section 1.3.2. For specific comparisons of the effect of this failure, all graphs and tables in this section may be compared directly to those in section 5.1 of Volume I. A comparison of the total performance scores on line 33 of the

TABLE 3. BENDIX AGV FAILURE #2 PERFORMANCE EVALUATION TABLE

TEST STANDARDS:

1. SPMIN = 40. PSIG
2. SPMID = 70. PSIG
3. SPMAX = 120. PSIG
4. THETA = 20. DEGREES
5. SVMIN = 6. LITERS
6. SVMID = 10. LITERS
7. SVMAX = 14. LITERS

CHARACTERISTIC NUMBERS:

8. XSPMX = 2.5000
9. XSPMN = 1.3333
10. XTHTA = 1.0000
11. DESIGN TOTAL: 4.833
12. XFLBR = 3.668
13. XDELf = 2.186
14. XDDLf = 2.175
15. XSIGf = 0.216
16. FLOW TOTAL: 8.245
17. XCCP1 = 2.520
18. XDDP1 = 2.594
19. XSGP1 = 1.771
20. XDPP1 = 2.431
21. LOW-ONSET TOTAL: 9.316
22. XCCP2 = 9.837
23. XDDP2 = 30.250
24. XSGP2 = 9.273
25. XDPP2 = 8.790
26. XTDP2 = 20.415
27. HIGH-ONSET TOTAL: 78.566
28. XIDPA = 5.460
29. XIDPB = 9.032
30. XIDPC = 6.338
31. XIDPD = 23.108
32. SACM TOTAL: 43.938
33. VALVE: BENDIX FAILURE #2 TOTAL: 144.898

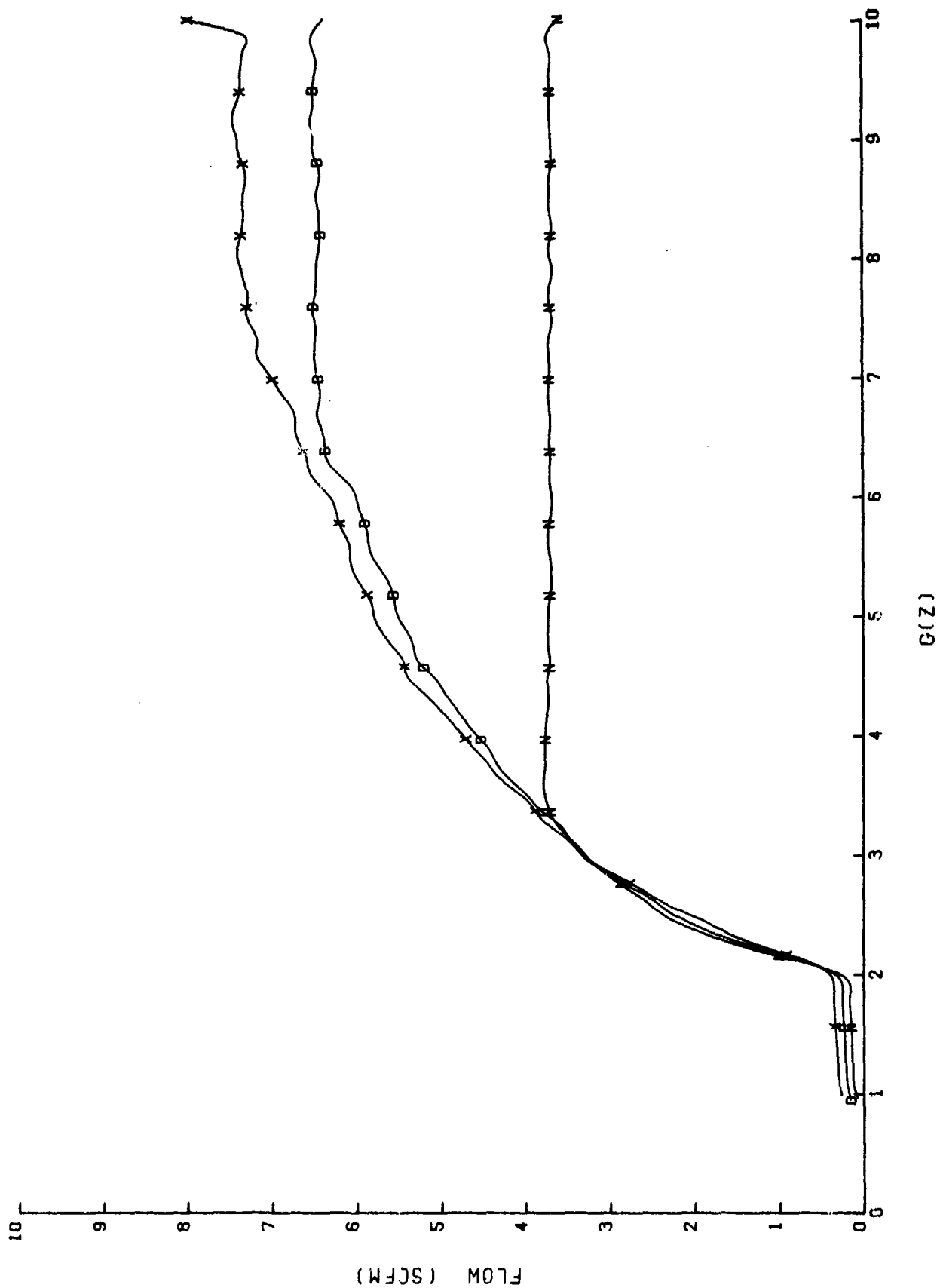


Figure 45. Bendix failure #2: flow as a function of source pressure.
[Curves are: N, D, and X. For "Key," refer to Table 2.]

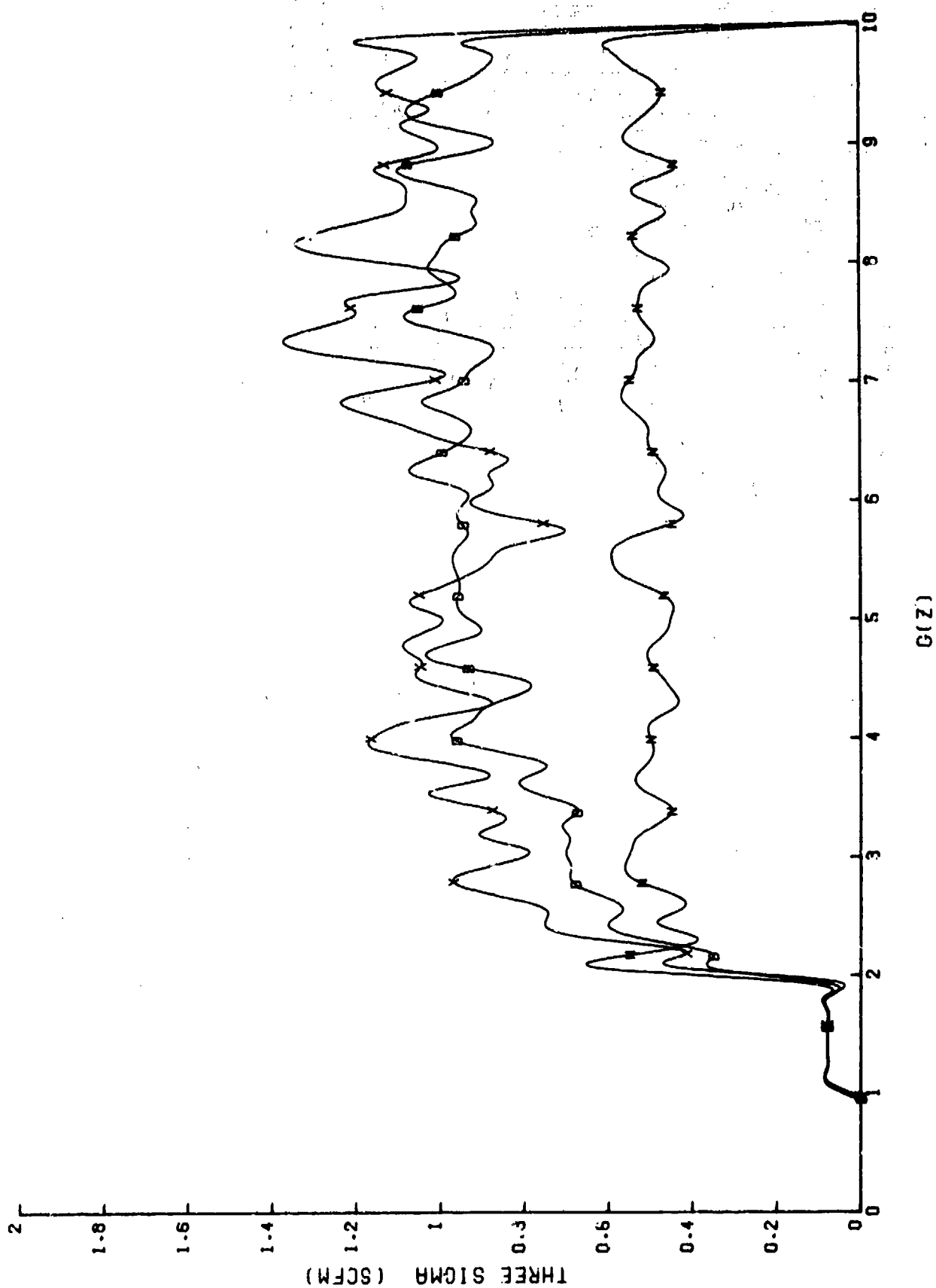


Figure 46. Bendix failure #2 variation (three sigma) in flow as a function of source pressure.
 [Curves are: N, D, and X. For "Key," refer to Table 2.]

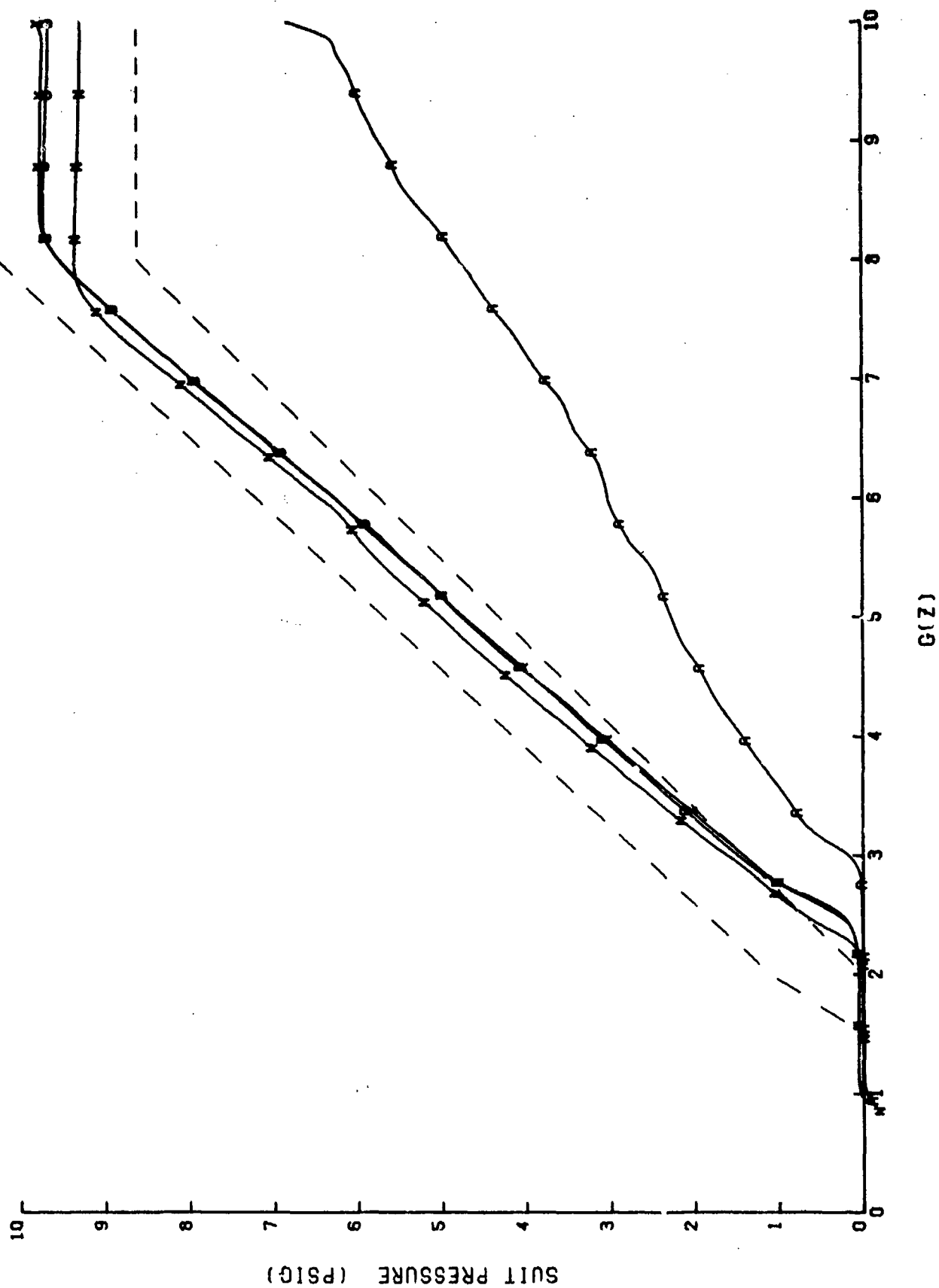


Figure 47. Bendix failure #2: 0.1 G/sec suit pressure profile as a function of source pressure.
[Curves are: N, D, X, and A. For "Key," refer to Table 2.]

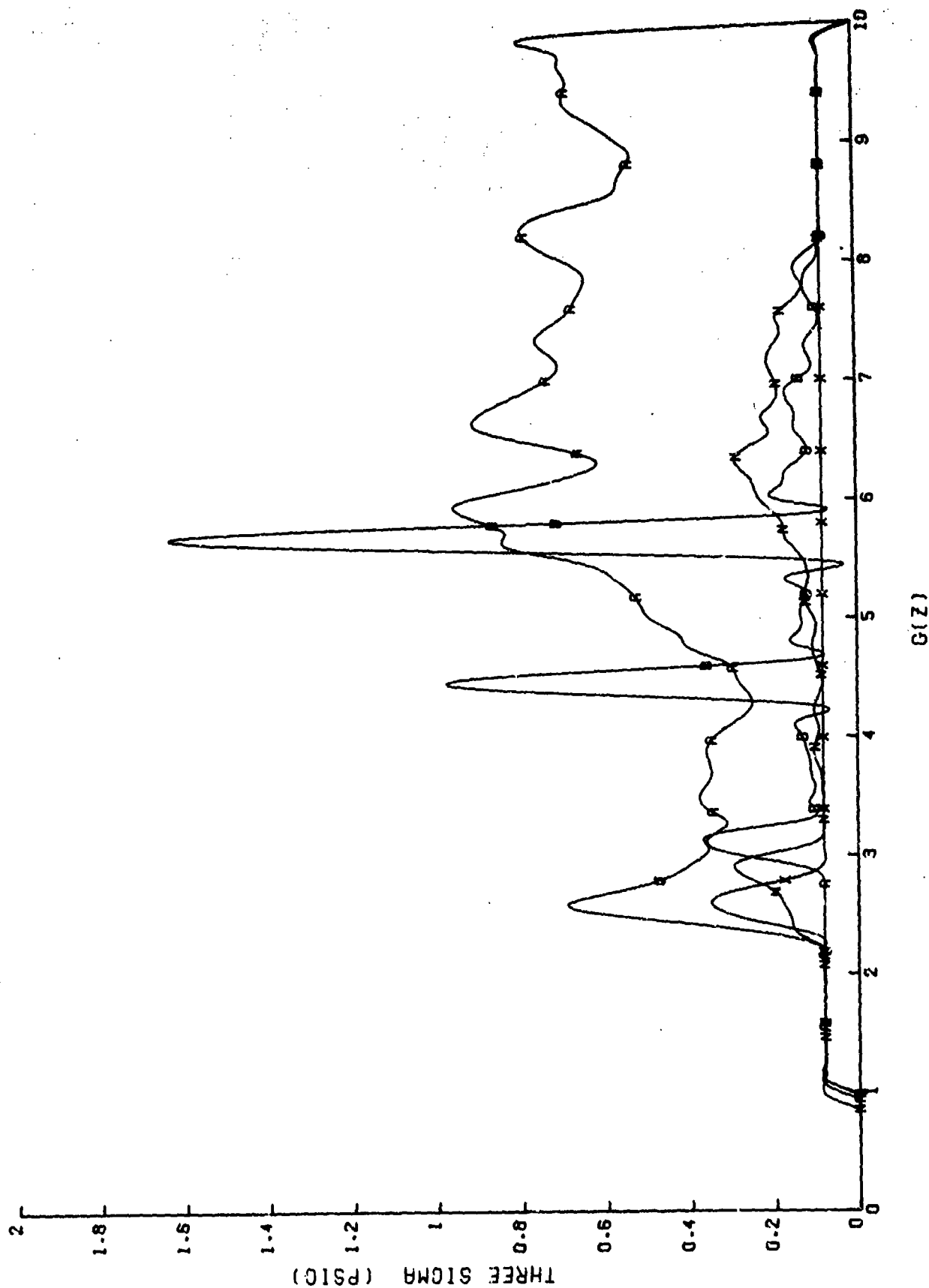


Figure 48. Bendix failure #2: 0.1 G/sec suit pressure variation as a function of source pressure.
[Curves are: N, D, X, and A. For "Key," refer to Table 2.]

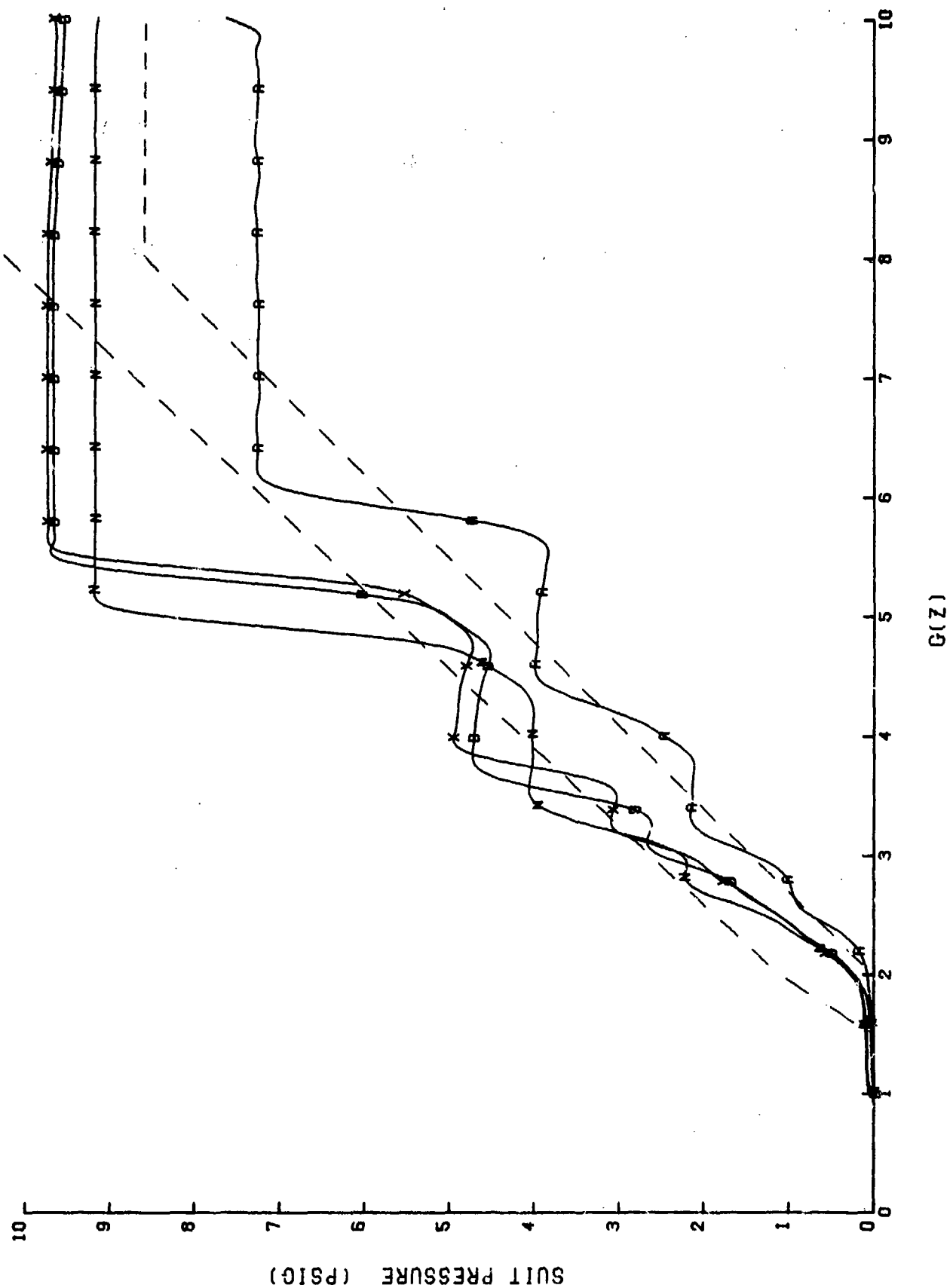
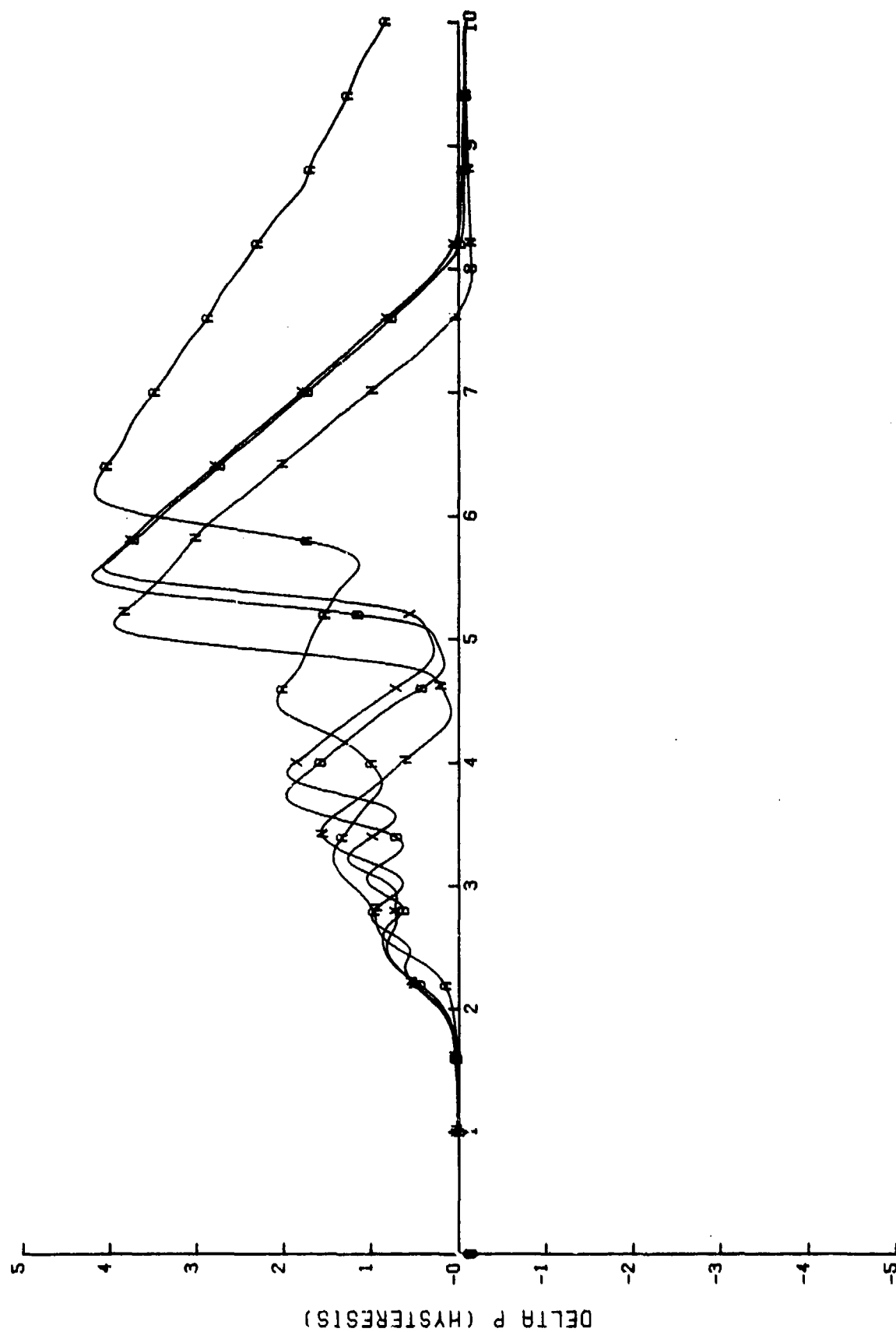


Figure 49. Bendix failure #2: 0.1 G/sec decreasing suit pressure profile as a function of source pressure. [Curves are: N, D, X, and A. For "Key," refer to Table 2.]



$G(Z)$

Figure 50. Bendix failure #2: 0.1 G/sec suit pressure hysteresis as a function of source pressure.
[Curves are: N, D, X, and A. For "Key," refer to Table 2.]

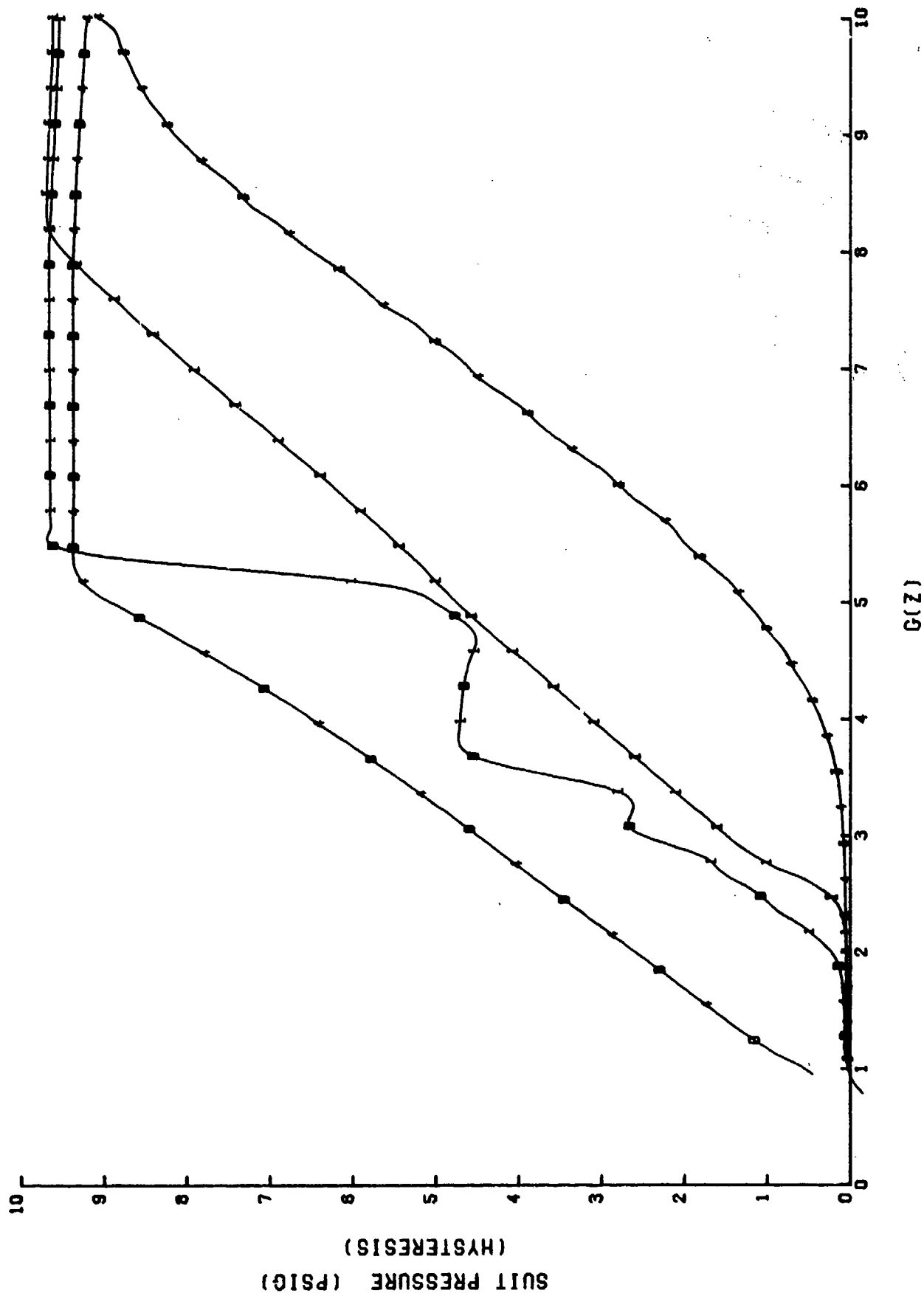


Figure 51. Bend: failure #2: suit pressure profile comparison as a function of onset rate.
[Curves are: 1I, 4I, 1D, and 4D. For "Key," refer to Table 2.]

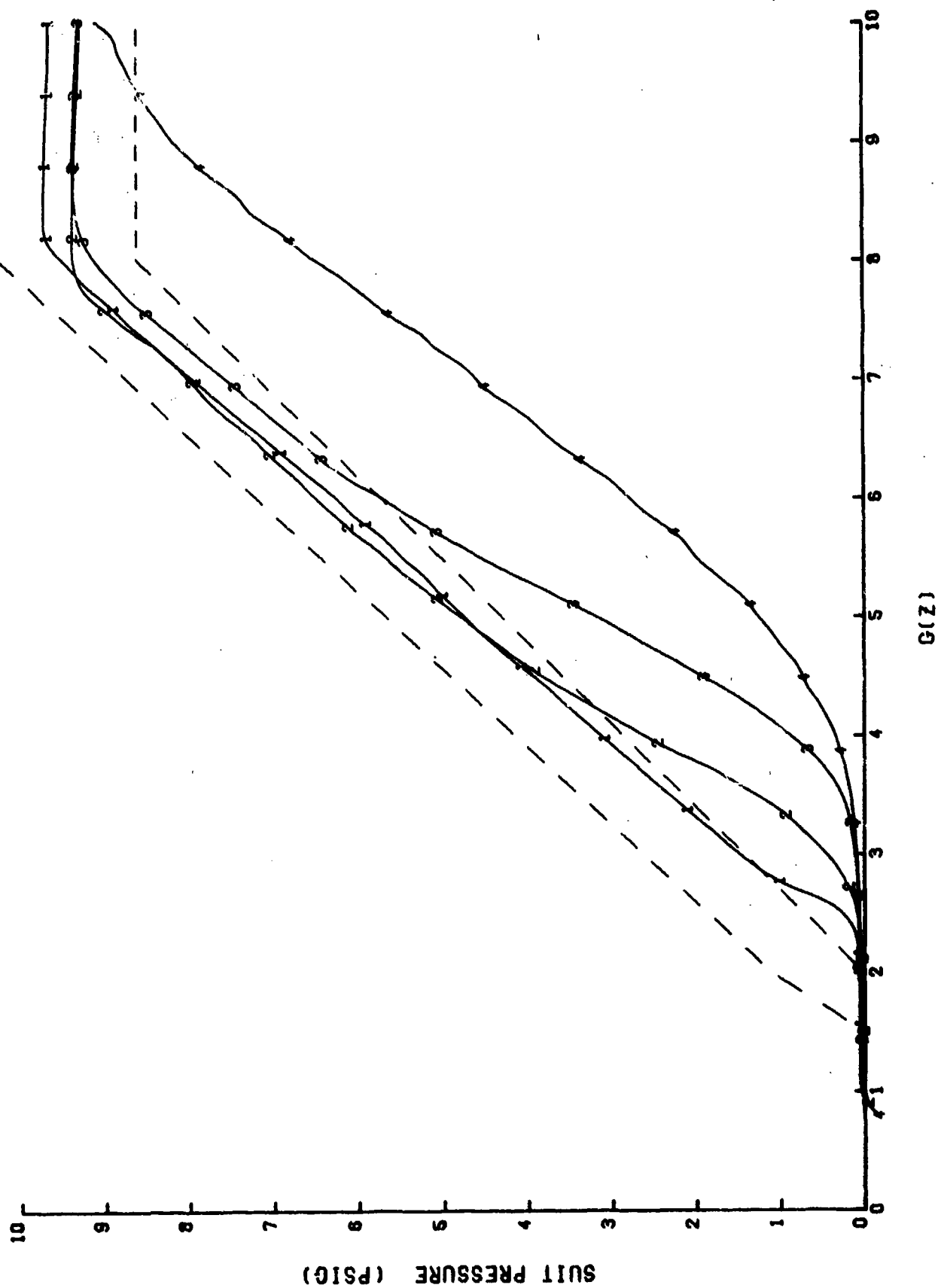


Figure 52. Bendix failure #2: suit pressure profile as a function of G-onset rate.
[Curves are: 1, 2, 3, and 4. For "Key," refer to Table 2.]

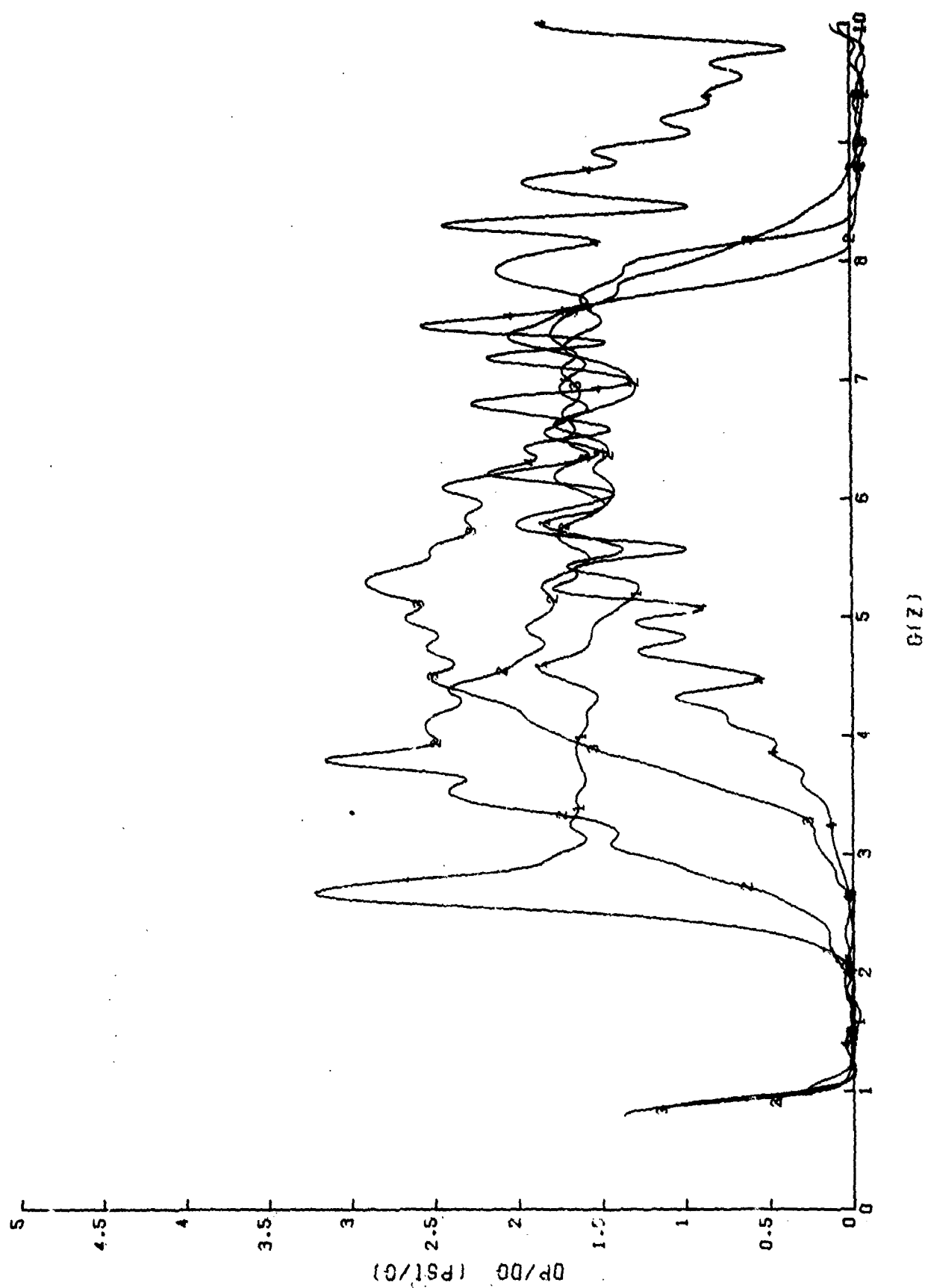


Figure 53. Bendix failure #2: dP/dG as a function of G -onset rate.
[Curves are: 1, 2, 3, and 4. For "Key," refer to Table 2.]

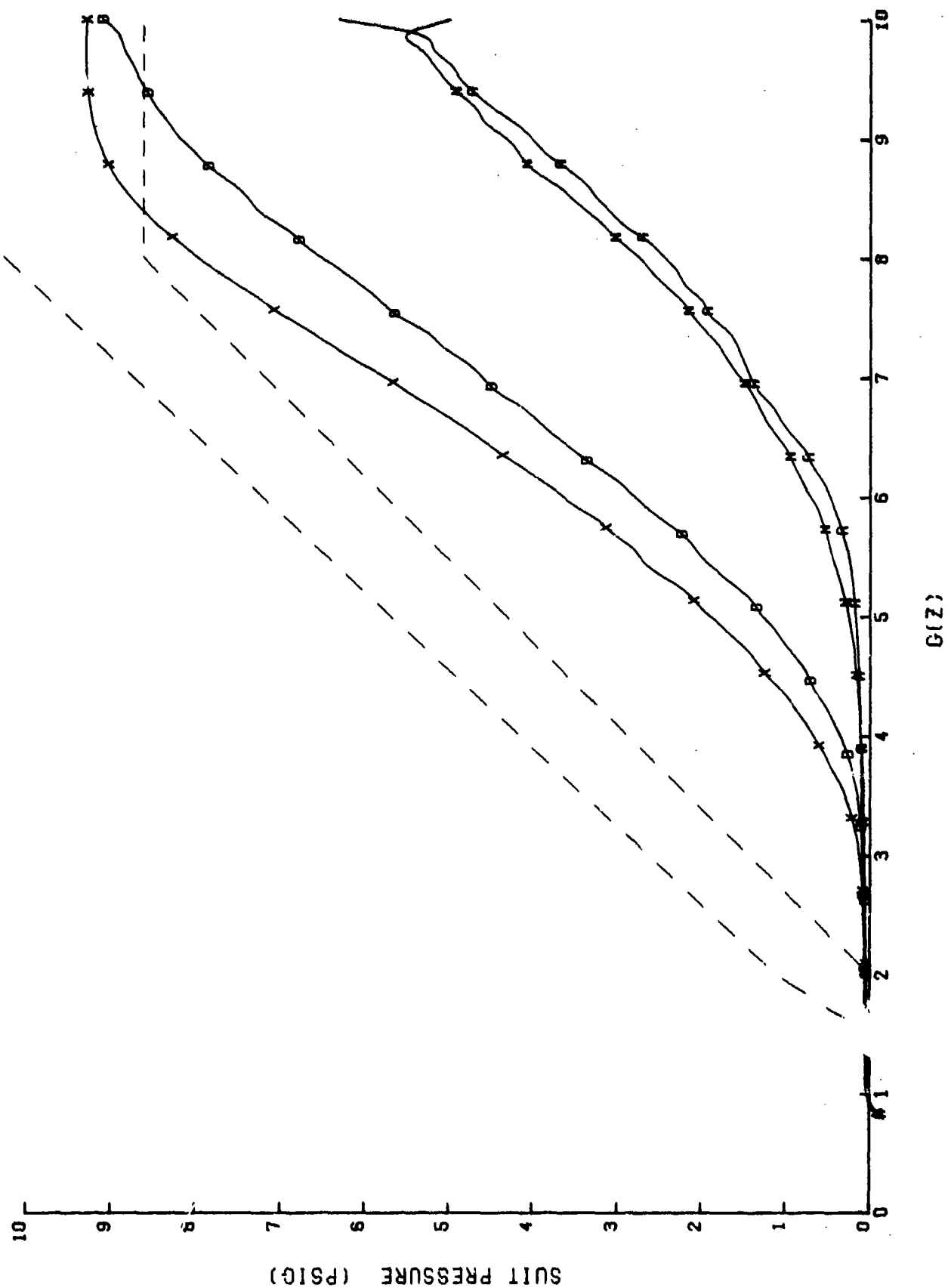


Figure 54. Bendix failure #2: 1.5 G/sec suit pressure profile as a function of source pressure.
[Curves are: N, D, X, and A. For "Key," refer to Table 2.]

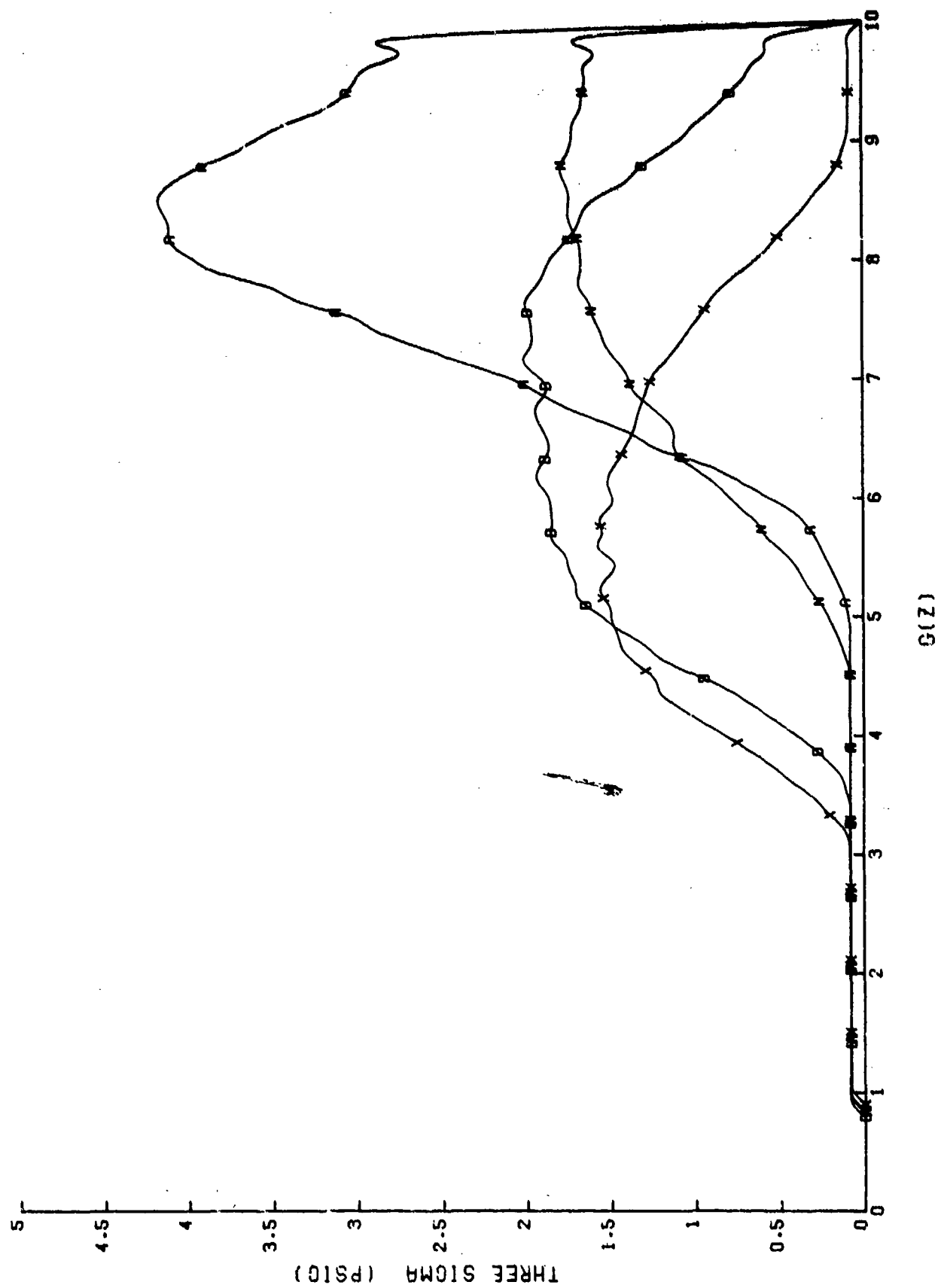


Figure 55. Bendix Failure #2: 1.5 G/sec suit pressure variation as a function of source pressure.

[Curves are: A, B, C, D, E, F, G, H, I, J, K, L, M, N, O, P, Q, R, S, T, U, V, W, X, Y, Z]

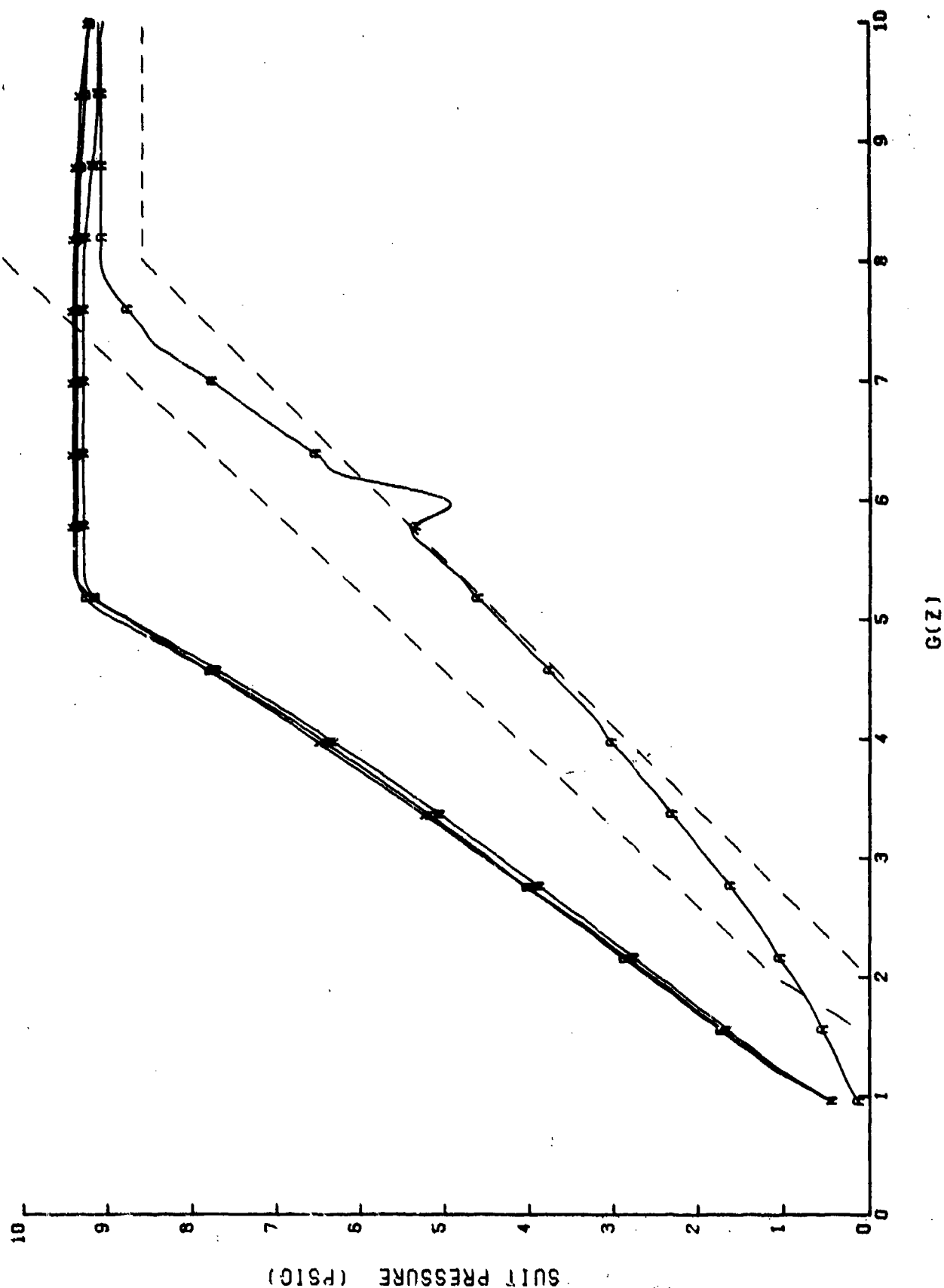


Figure 56. Bendix failure #2: -1.5 G/sec decreasing suit pressure profile as a function of source pressure. [Curves are: N, D, X, and A. For "Key," refer to Table 2.]

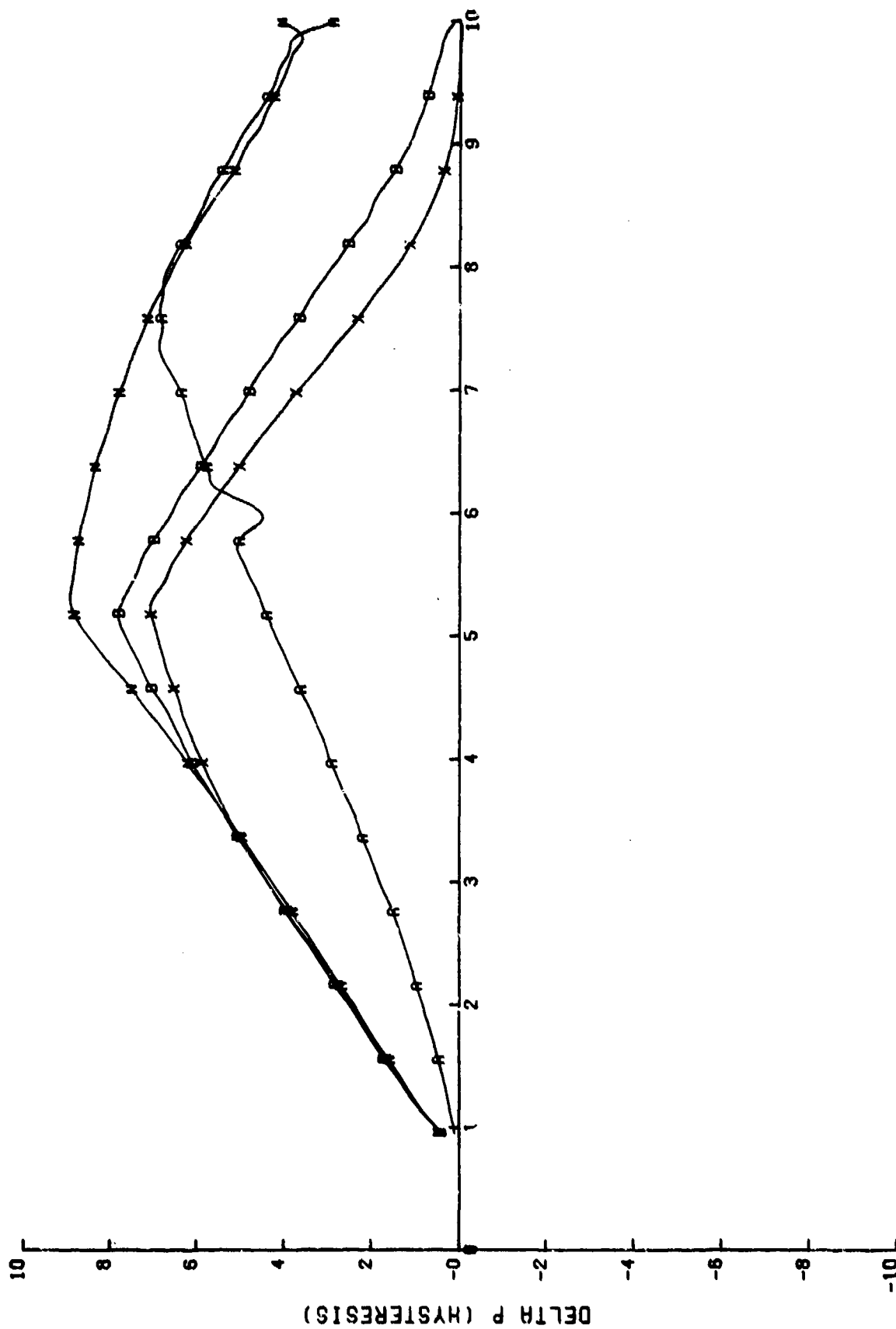


Figure 57. Bendix failure #2: 1.5 G/sec suit pressure hysteresis as a function of source pressure.
[Curves are: N, D, X, and A. For "Key," refer to Table 2.]

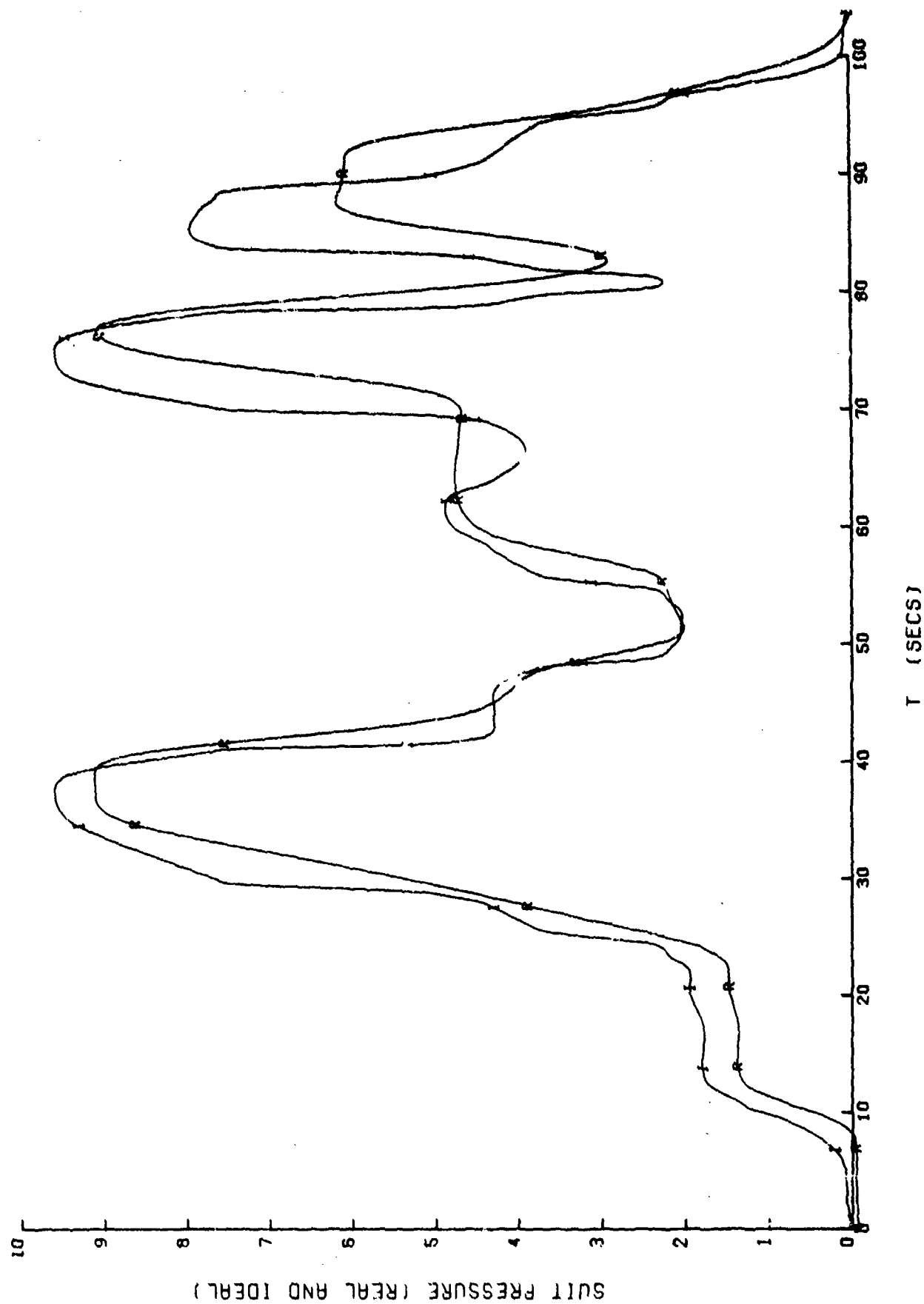
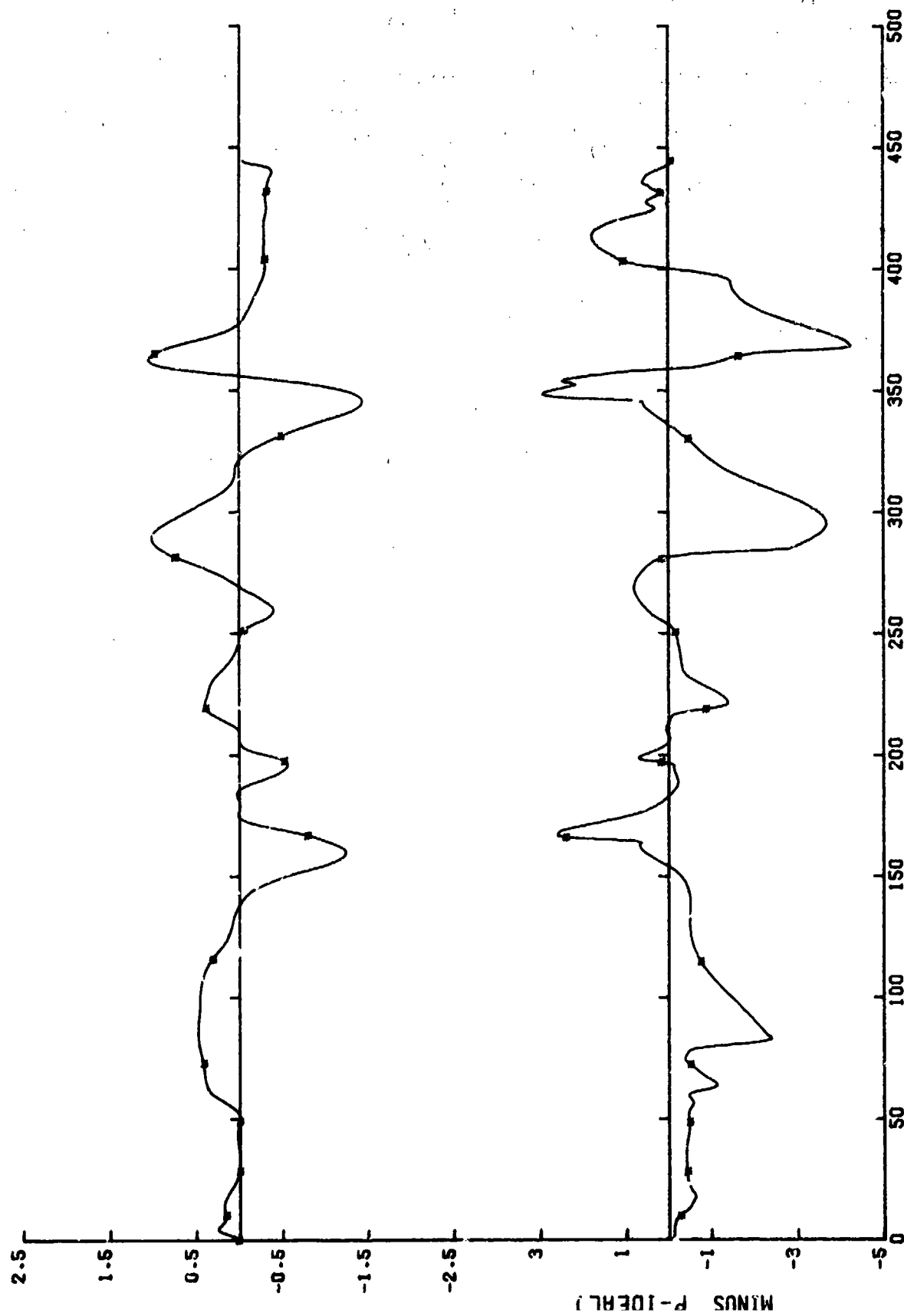


Figure 58. Bendix failure #2: SACH suit pressure profile comparison with minimum source pressure and maximum suit volume. [Curves are: I and R. For "Key," refer to Table 2.]



INTEGRAL OF G DT FROM 0 TO T

Figure 59. Bendix failure #2: suit pressure deviation and dC/dt for the minimum source pressure, maximum suit volume SACM. [Curves are: *. For "Key," refer to Table 2.]

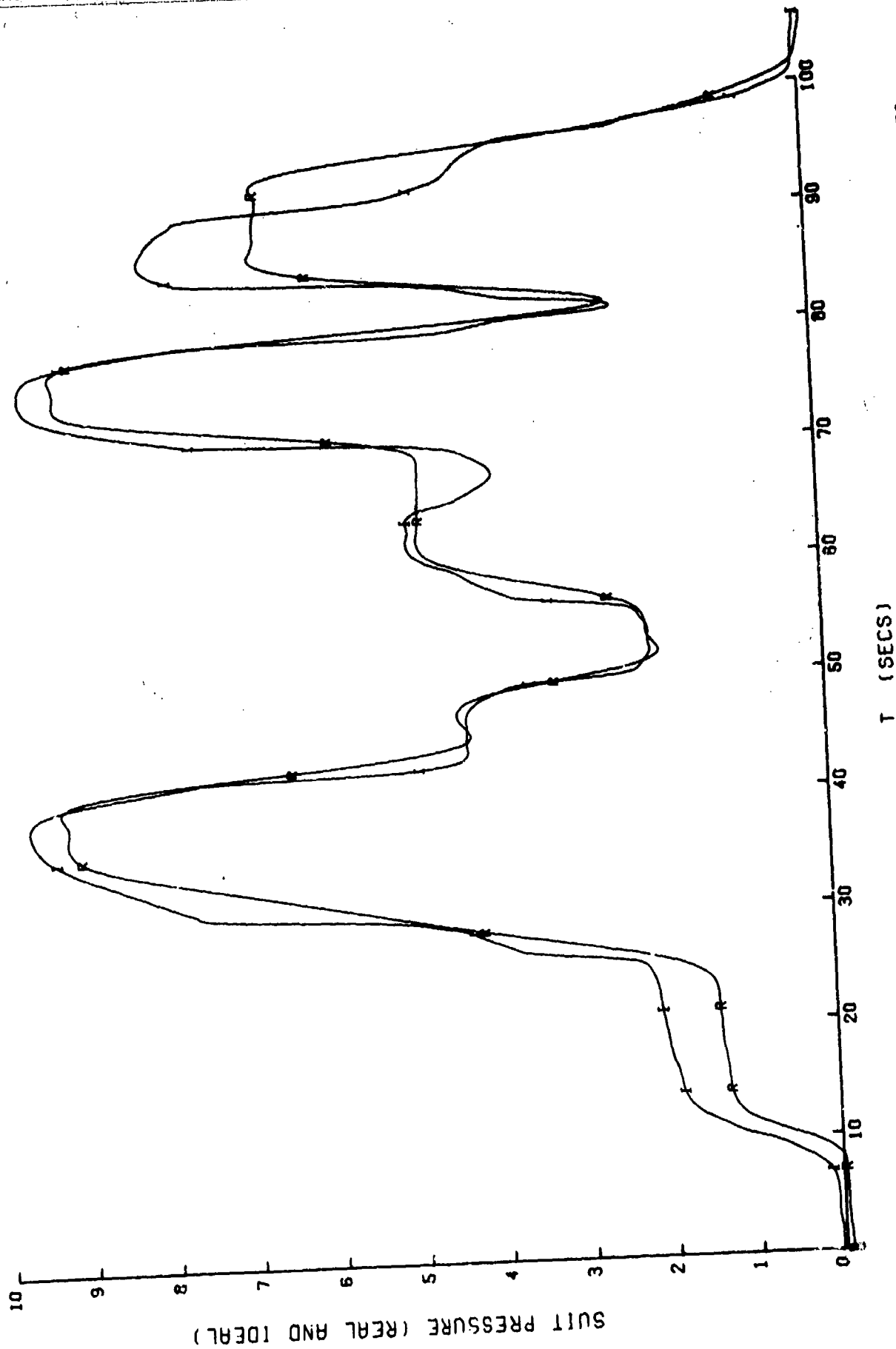


Figure 60. Bendix failure #2: SACM suit pressure profile comparison with maximum source pressure and minimum suit volume. [Curves are: J and R. For "Key," refer to Table 2.]

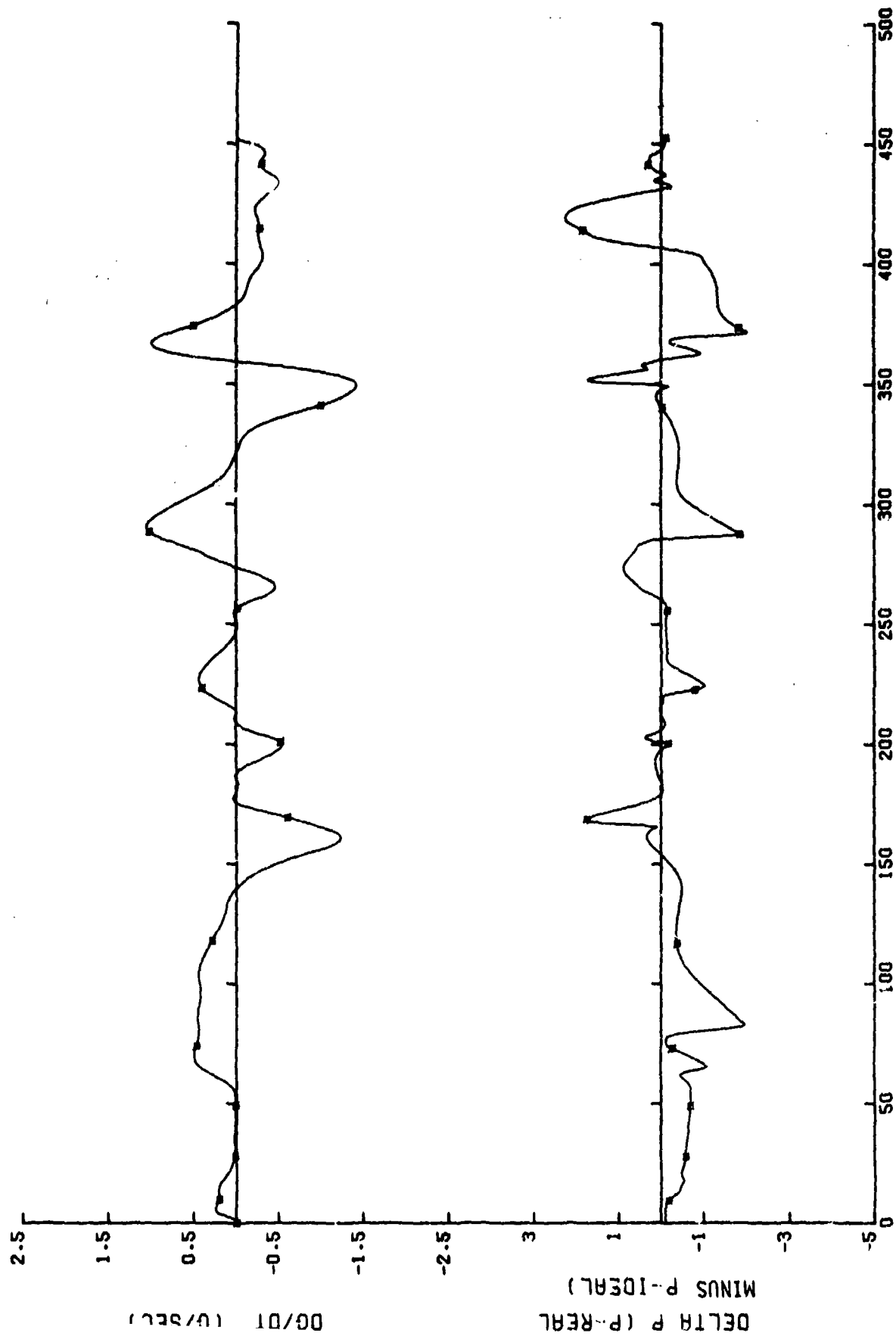


Figure 61. Bendix failure #2: suit pressure deviation and $\Delta G/\Delta t$ for the maximum source pressure, for "Key" refer to Table 2.1

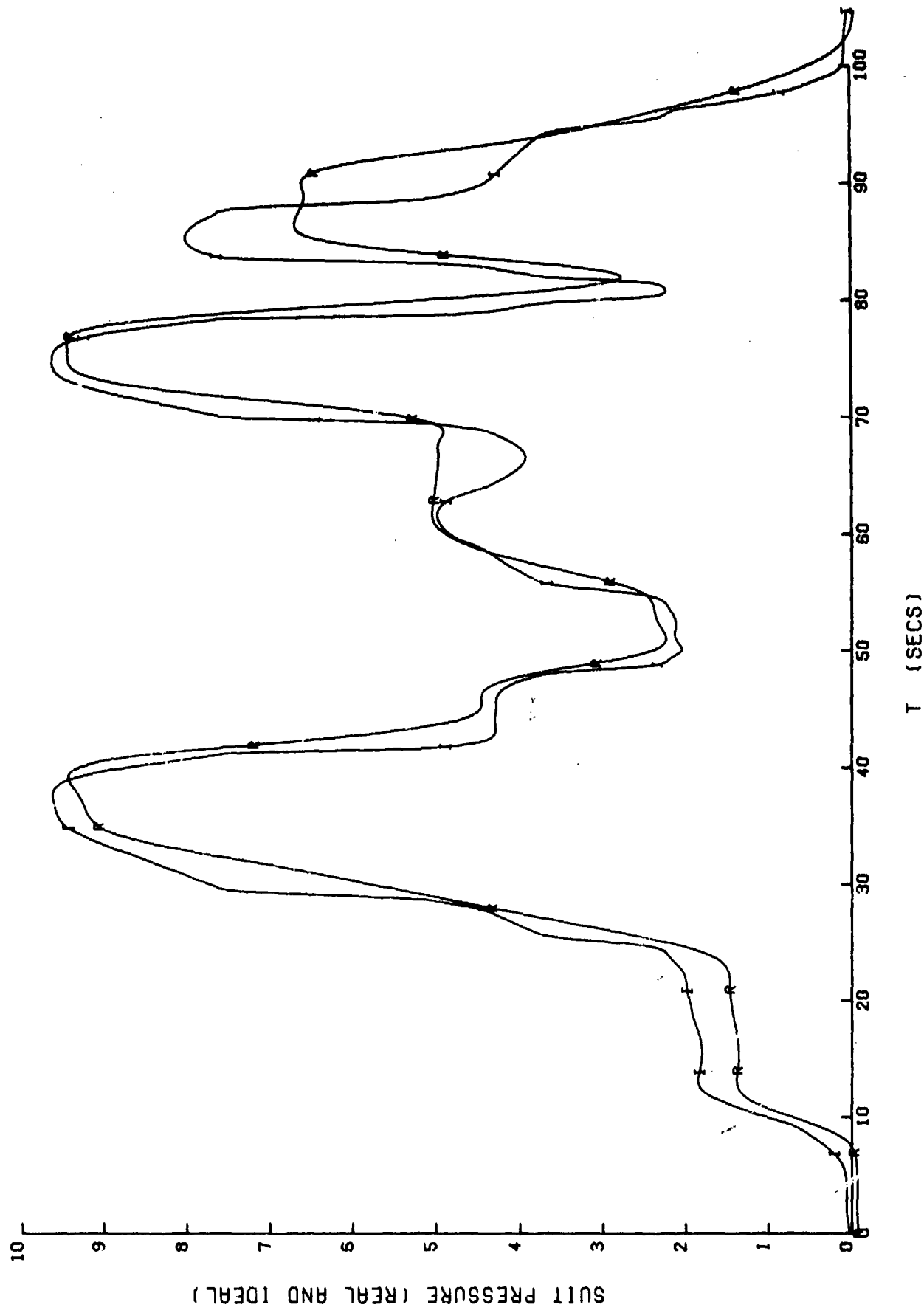
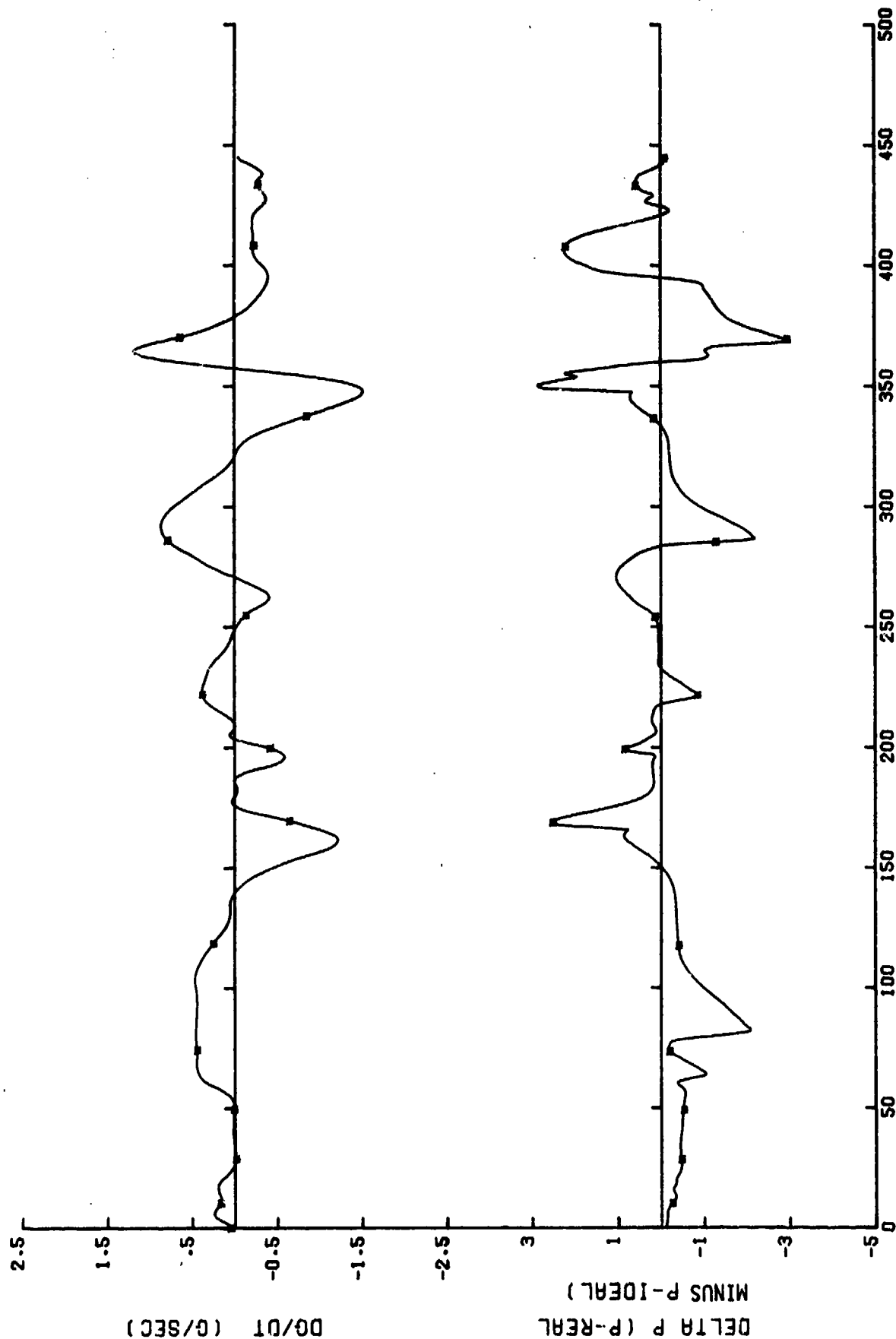


Figure 62. Bendix failure #2: SACM suit pressure profile comparison with median source pressure and suit volume. [Curves are: I and R. For "Key," refer to Table 2.]



INTEGRAL OF G DT FROM 0 TO T

Figure 63. Bendix failure #2: suit pressure deviation and dC/dt for the reaction

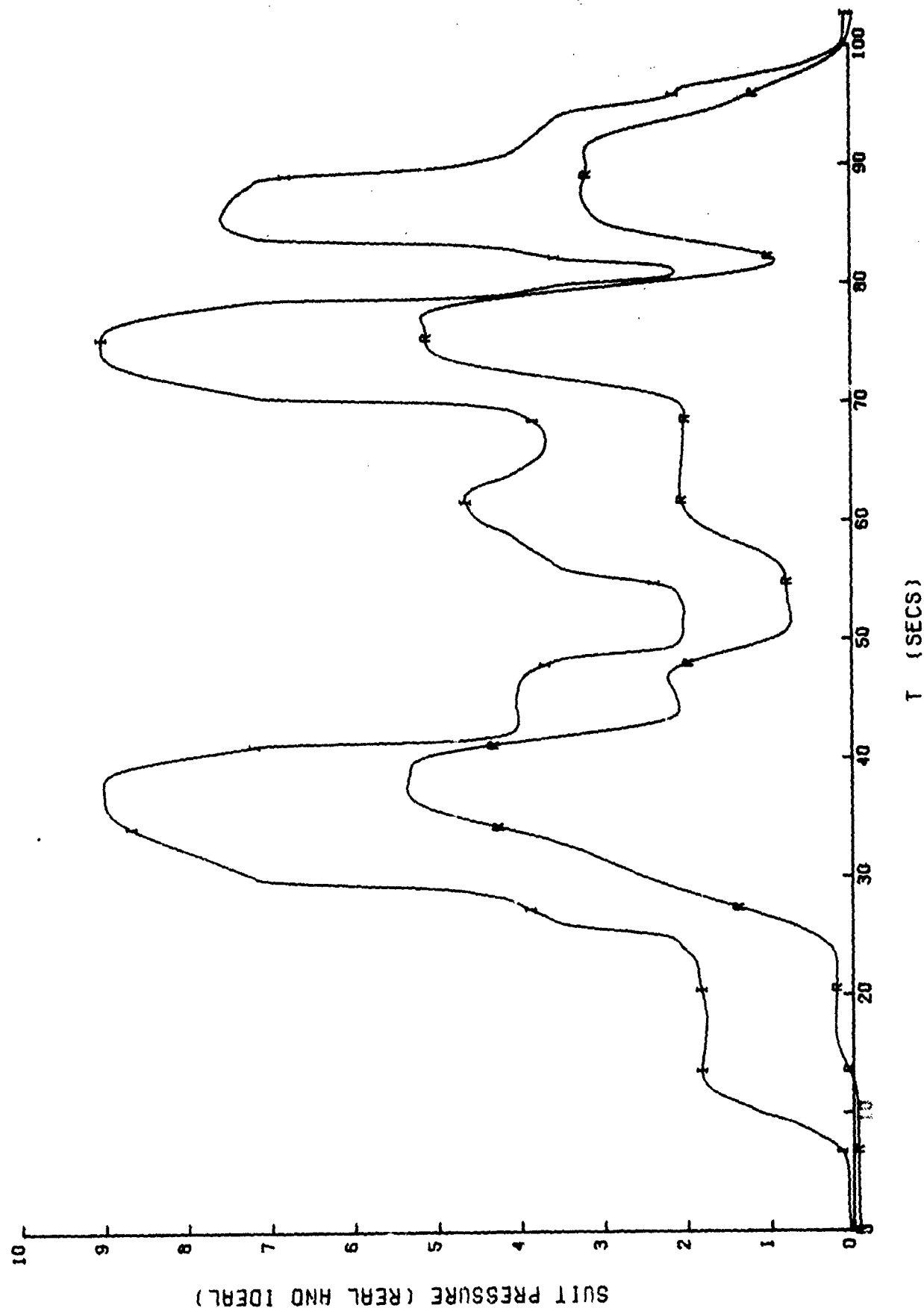
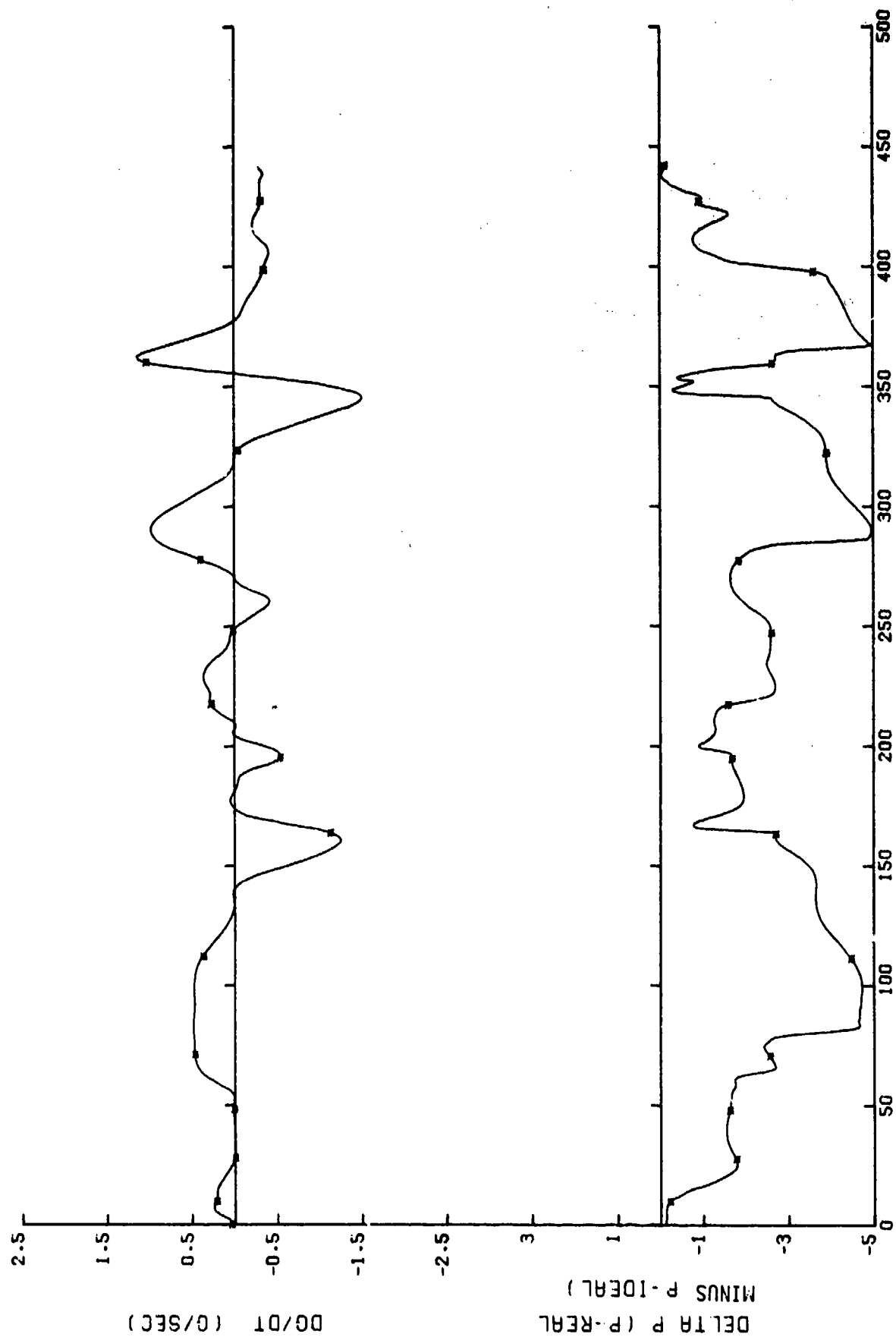


Figure 64. Bendix failure #2: SACM suit pressure profile comparison with G vector misalignment.
[Curves are: I and R. For "Key," refer to Table 2.]



INTEGRAL OF G DT FROM 0 TO T

Figure 65. Bendix failure #2: suit pressure deviation and dG/dt for the G vector misalignment SACH. [Curves are: * For "Key" refer to Table 2]

total performance scores on line 33 of the PETs (Vol. I, Table 2; and Vol. II, Table 4) indicates the performance decrement is not too serious. The value of the accompanying curves is readily apparent in this case.

1.4.3.1 ALAR AGV Failure #1 Flow Characteristics (Figs. 66 - 67)

The decrement in open-flow performance accounts for 10% of the PET score reduction. The leakage flow through the bellows and the very late initiation of pressurization are apparent in Figure 66. The latter characteristic is primarily responsible for the higher (less desirable) total score on line 12 of the PET (Table 4).

1.4.3.2 ALAR AGV Failure #1 Low G-Onset-Rate Characteristics (Figs. 68 - 71)

ALAR failure #1 resulted in a very slight, but recognizable improvement in low G-onset performance. Apparently, the leakage induced through the bellows was enough to fill the median-sized anti-G suit (AGS), used during the 0.1 G/sec onset-rate tests. During normal operation, the mass (Item 3, Fig. 23, section 1.3) seals the exhaust valve (Item 10, Fig. 23) at 1.4 to 1.5 G. Normally, pressurization begins considerably later, as the acceleration force on the mass opens the inflation valve (Item 19, Fig. 23). In this failure case, the leakage flow fills the suit much earlier, forcing exhaust-valve control of the suit pressure at all times (i.e., during both ascending and descending G profiles). The result is some improvement in linearity and a significant improvement in hysteresis (Vol. II: Fig. 71; and Vol. I: Fig. 10).

1.4.3.3 ALAR AGV Failure #1 High G-Onset-Rate Characteristics (Figs. 72 - 78)

The high G-onset-rate performance of ALAR failure #1 suffers a slight overall decrement from normal operation. The late turn-on is very apparent in Figure 73, resulting in a degraded linearity (line 22) and onset-rate influence (line 26) scores on the PET (Table 4). The source-pressure influence (line 23) and 3 sigma (line 24) scores in Table 4 were improved because of the concentration of activity (and error) around the 6-G level.

1.4.3.4 ALAR AGV Failure #1 SACM Characteristics (Figs. 79 - 86)

Most of the PET score degradation occurs on the SACM tests. Since the ideal pressures are derived from the 0.1 G/sec tests, the large response deadband induced by this failure resulted in a very poor comparison. Examination of Figures 79, 81, 83, and 85 discloses the very good descending-G response of this failure and the very poor ascending-G response.

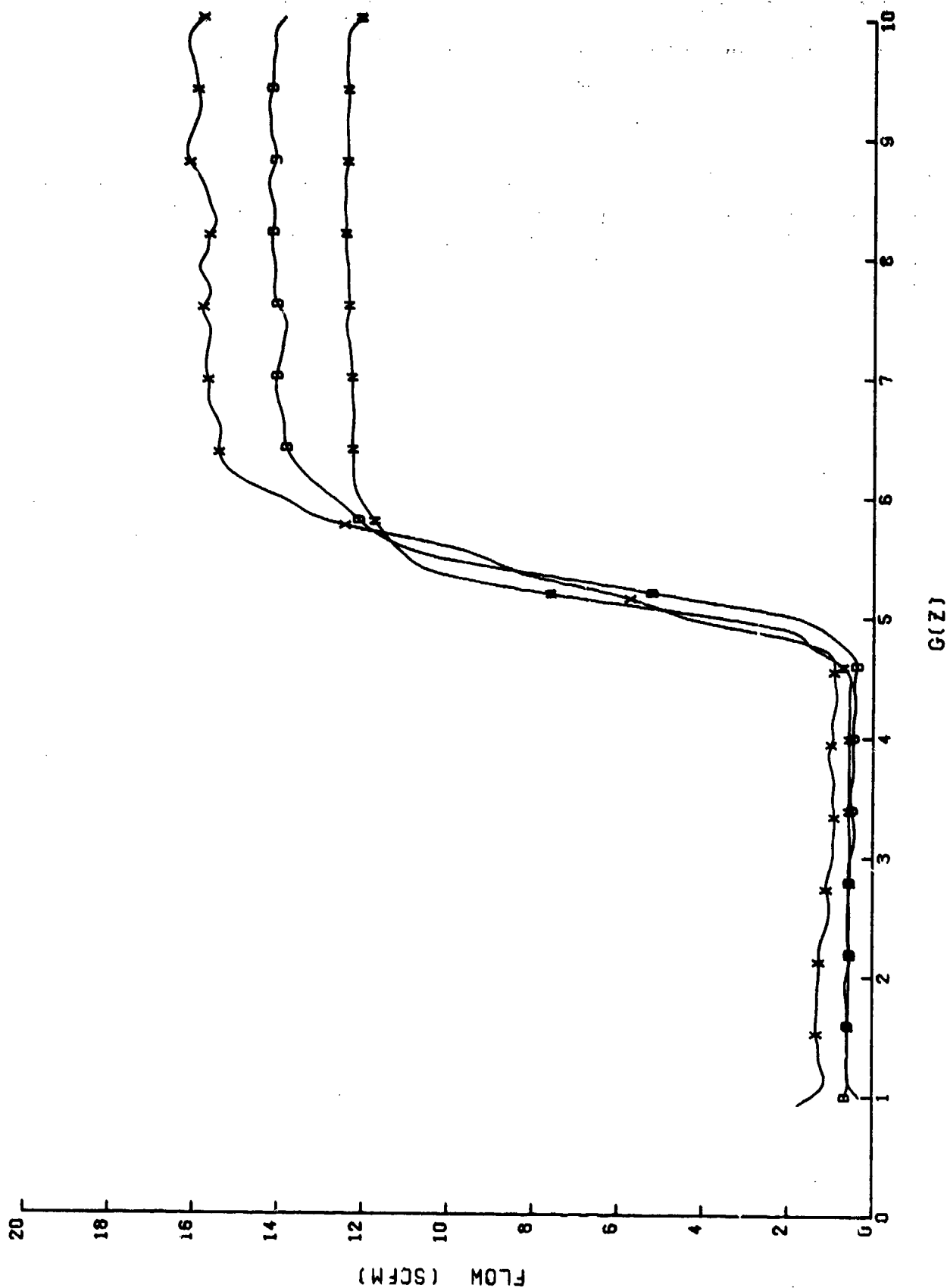


Figure 66. ALAR failure #1: flow as a function of source pressure.
 [Curves are: N, D, and X. For "Key," refer to Table 2.]

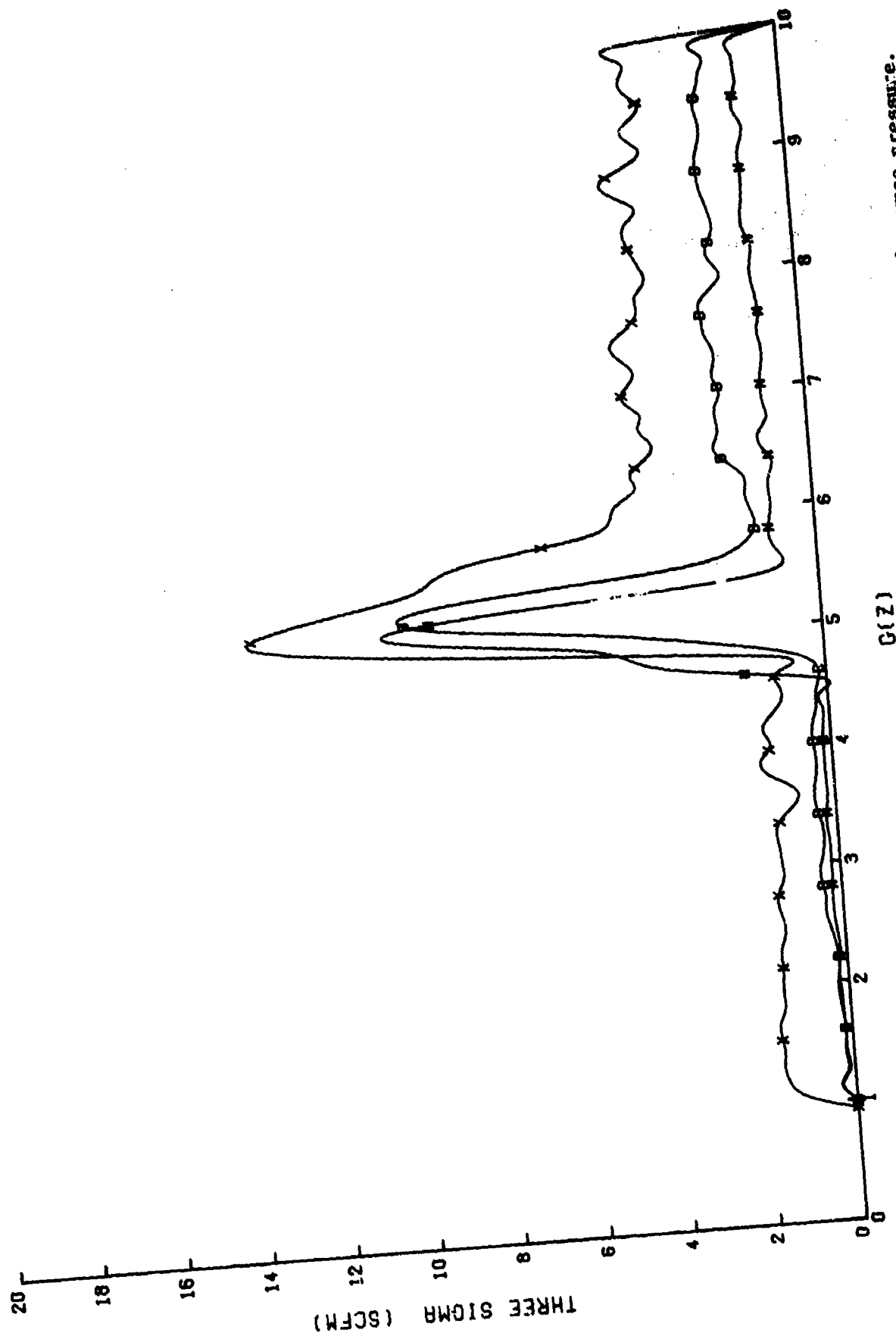


Figure 67. ALAR failure #1: variation (three sigma) in flow as a function of source pressure.
 [Curves are: N, D, and X. For "key," refer to Table 2.]

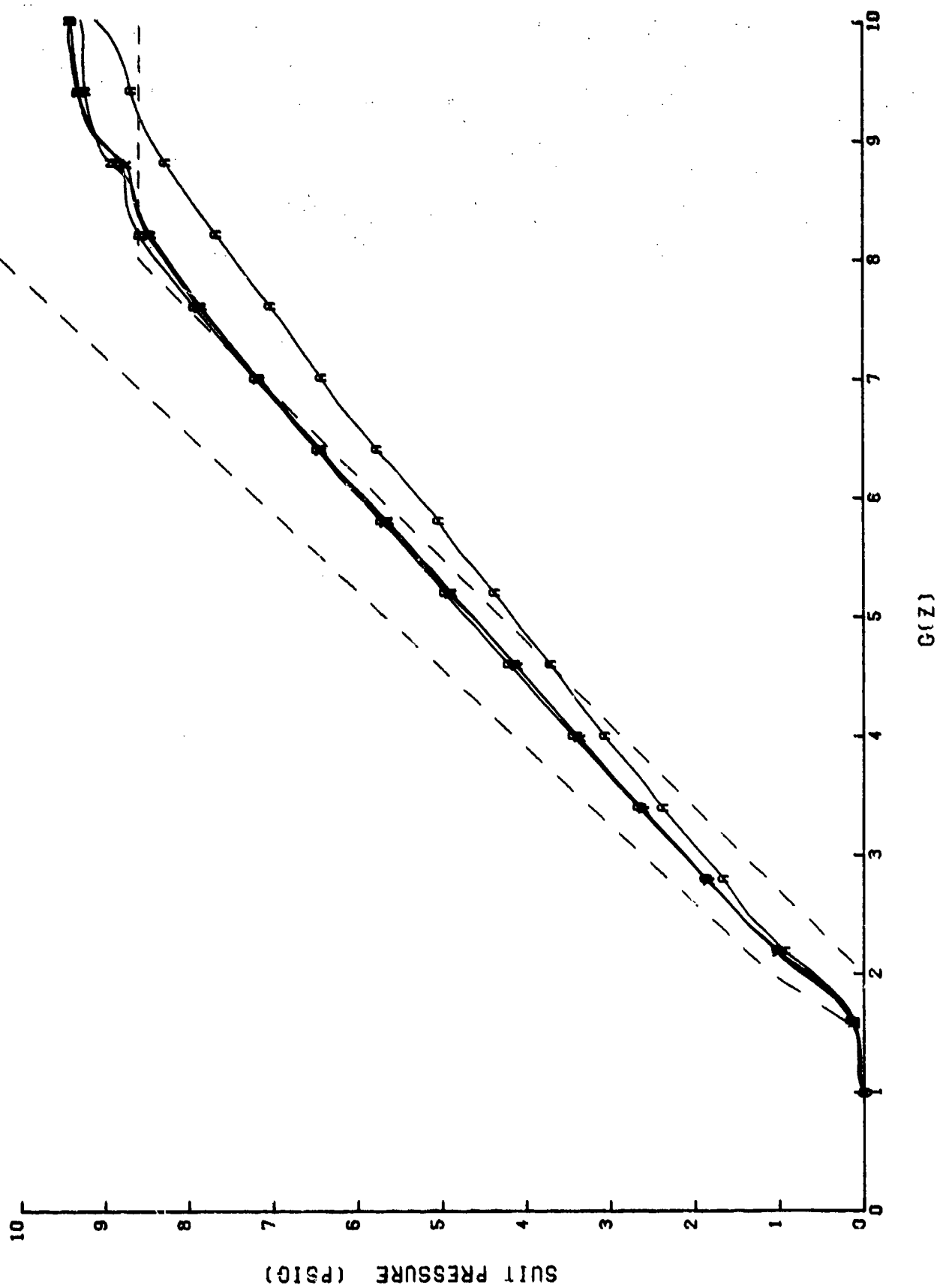


Figure 68. ALAR failure #1: 0.1 G/sec suit pressure profile as a function of source pressure.
[Curves are: N, D, X, and A. For "Key," refer to Table 2.]

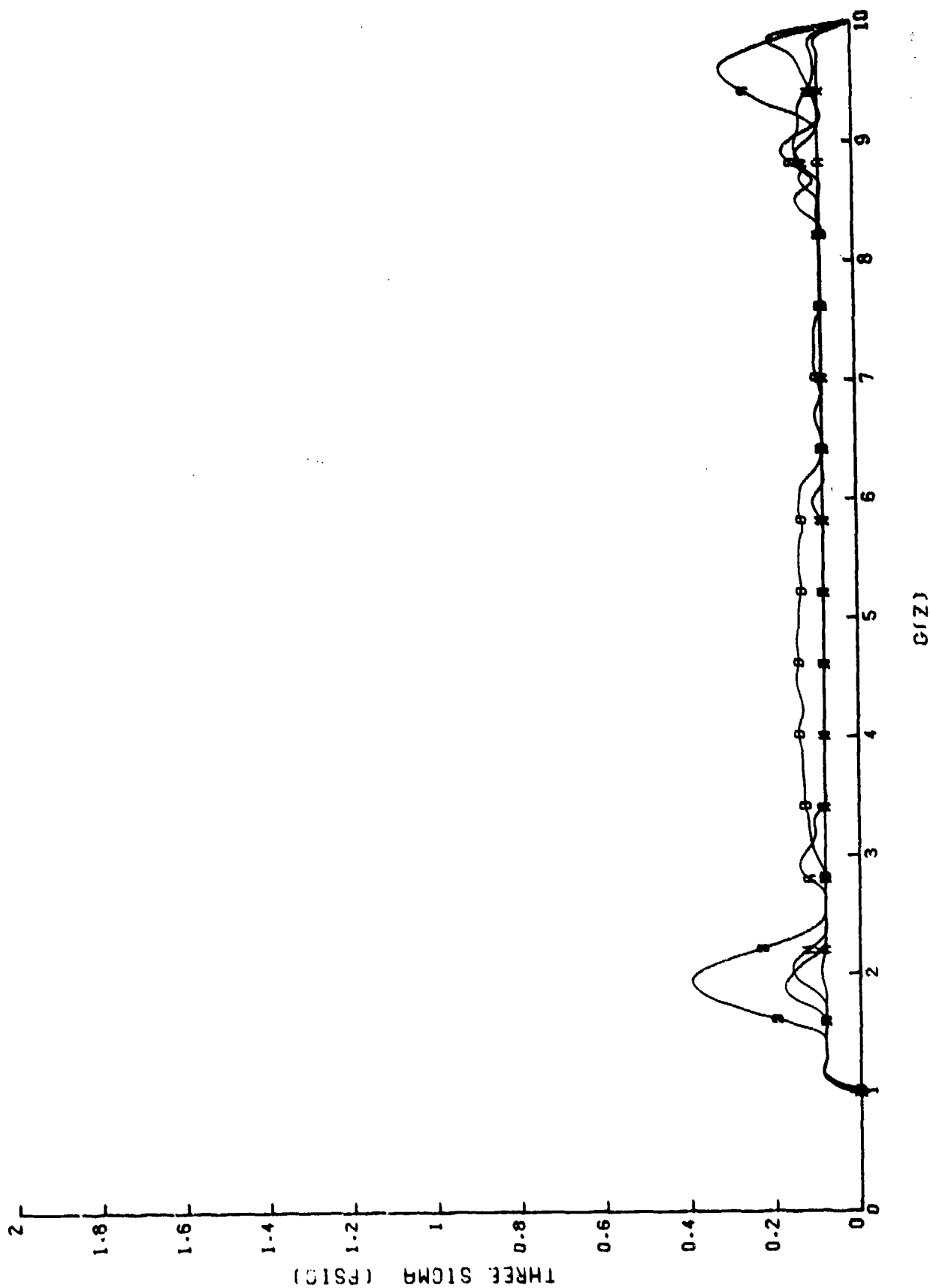


Figure 69. ALAR failure #1: 0.1 G/sec suit pressure variation as a function of source pressure.
[Curves are: N, D, X, and A. For "Key," refer to Table 2.]

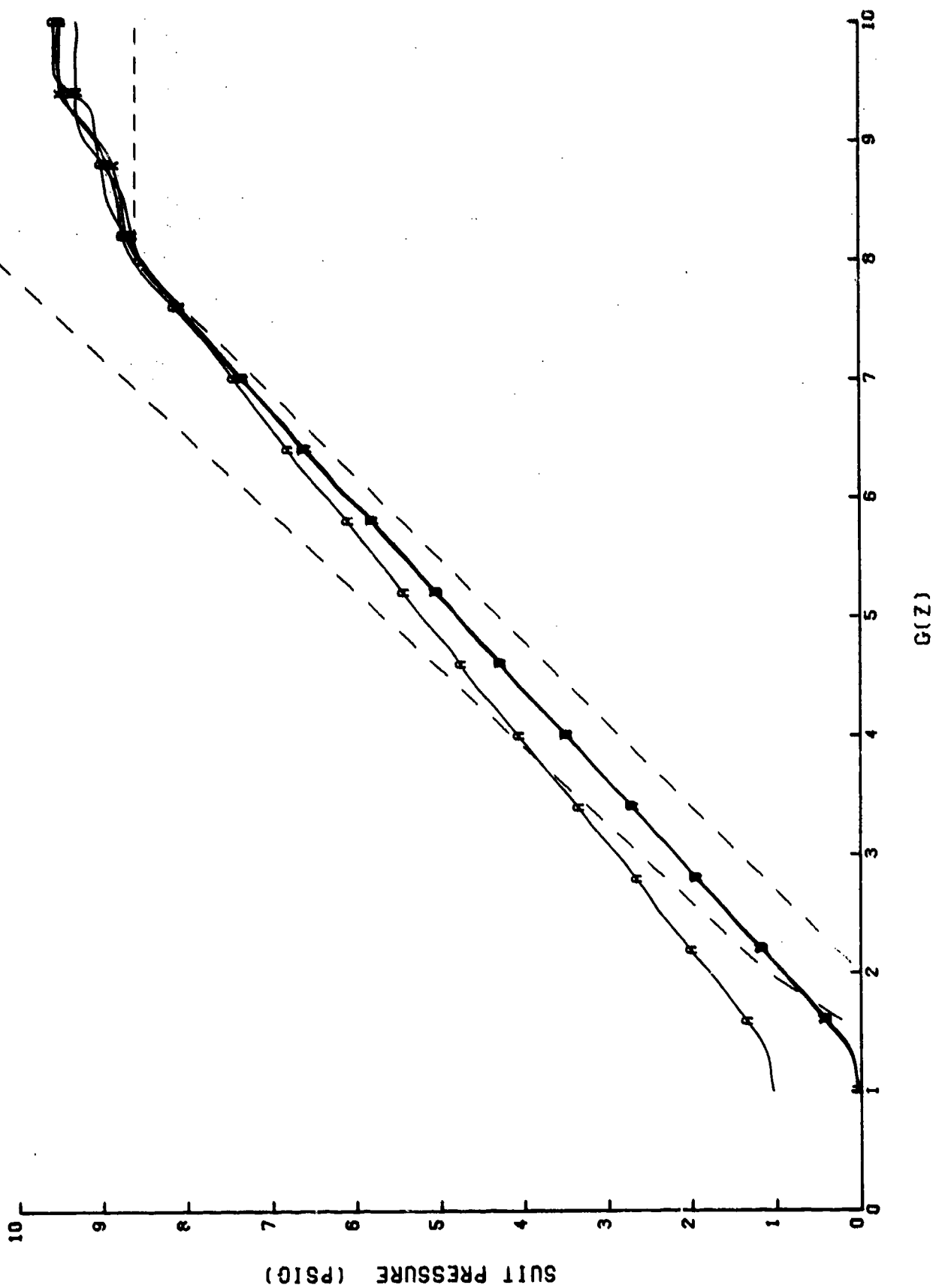
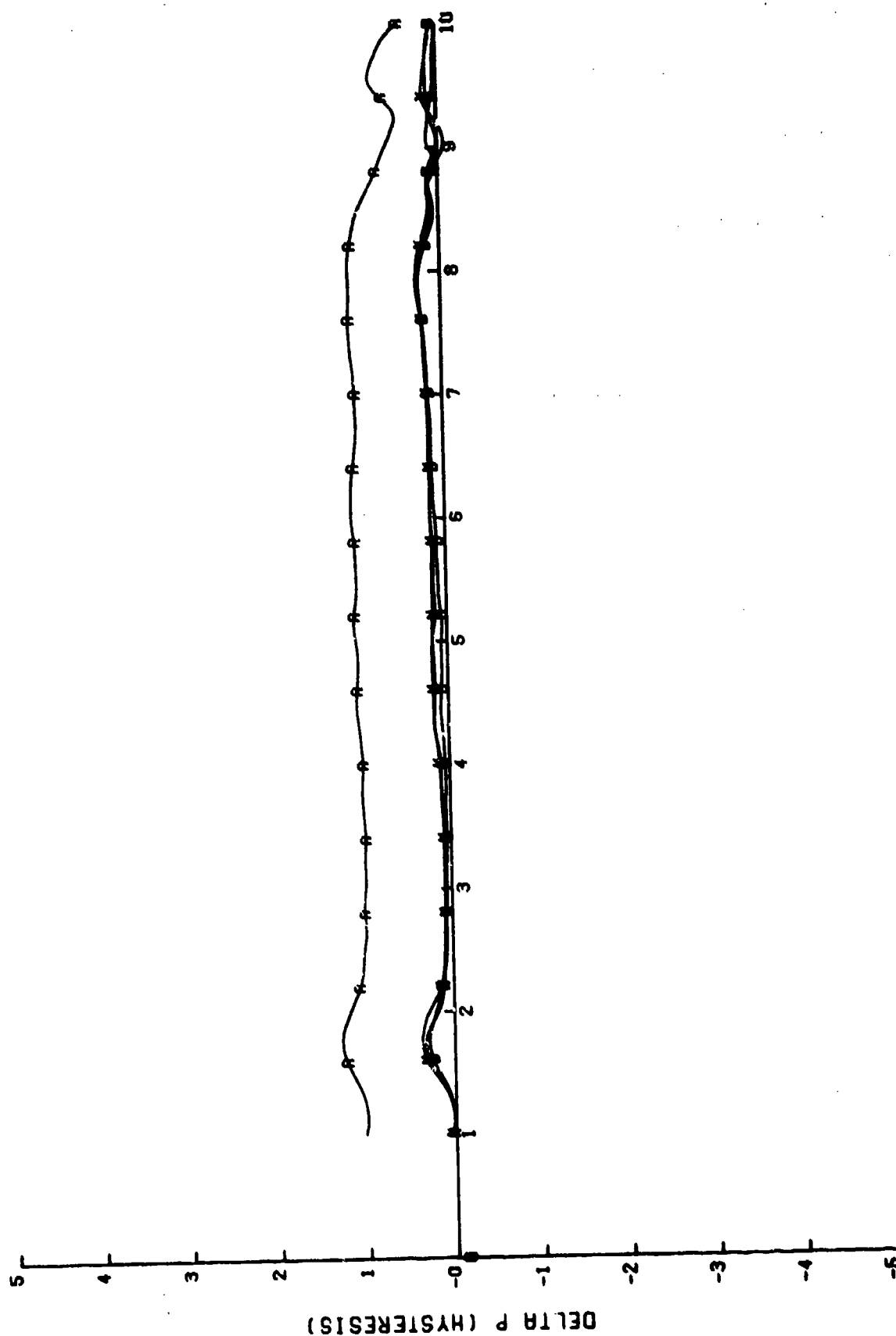


Figure 70. ALAR failure #1: 0.1 G/sec decreasing suit pressure profile as a function of source pressure. [Curves are: N, D, X, and A. For "Key," refer to Table 2.]



$G(Z)$

Figure 71. ALAR failure #1: 0.1 G/sec suit pressure hysteresis as a function of source pressure.
[Curves are: N, D, X, and A. For "Key," refer to Table 2.]

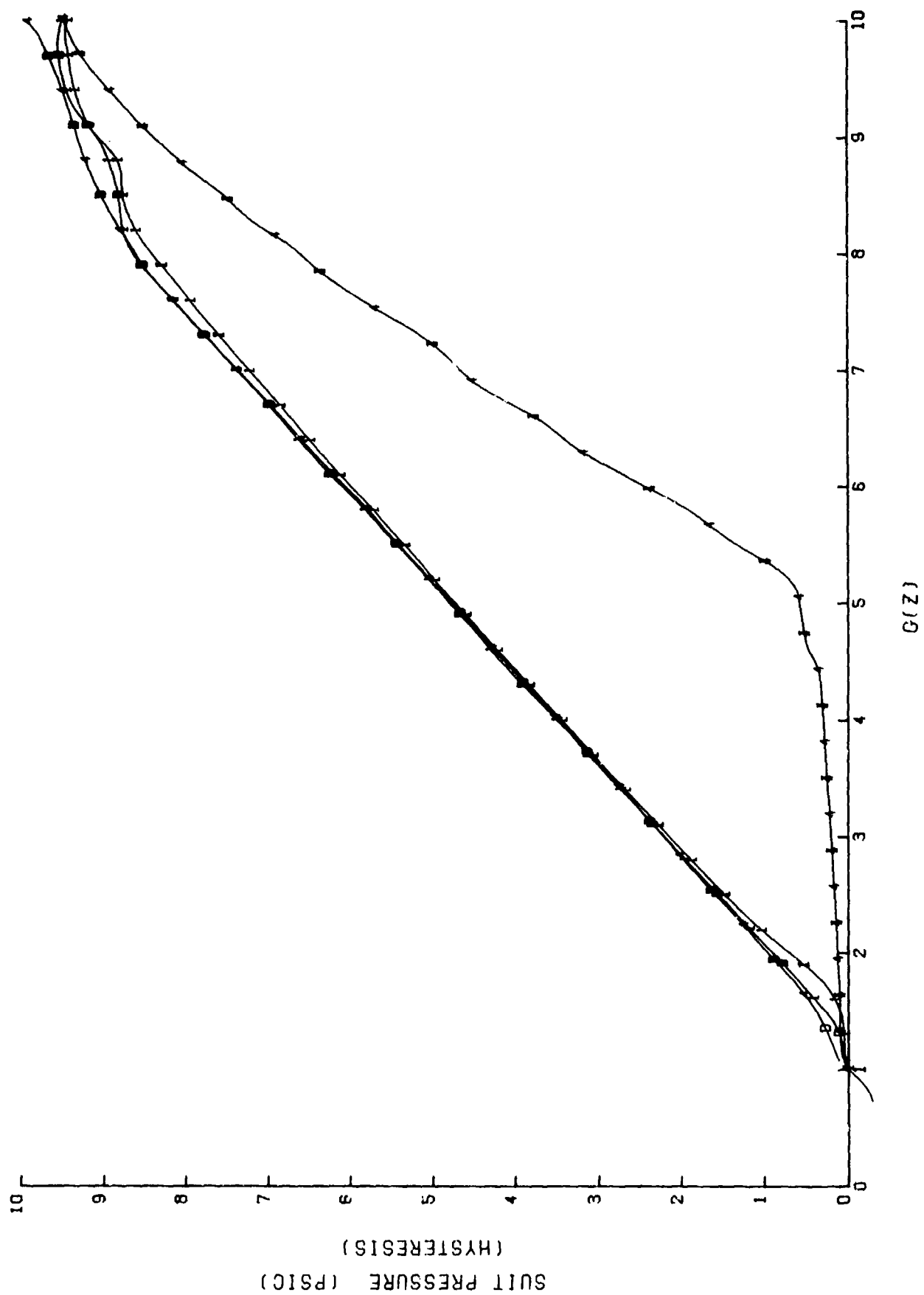


Figure 72. ALAR failure #1: suit pressure profile comparison as a function of onset rate.
[Curves are: 11, 4I, 1D, and 4D. For "Key," refer to Table 2.]

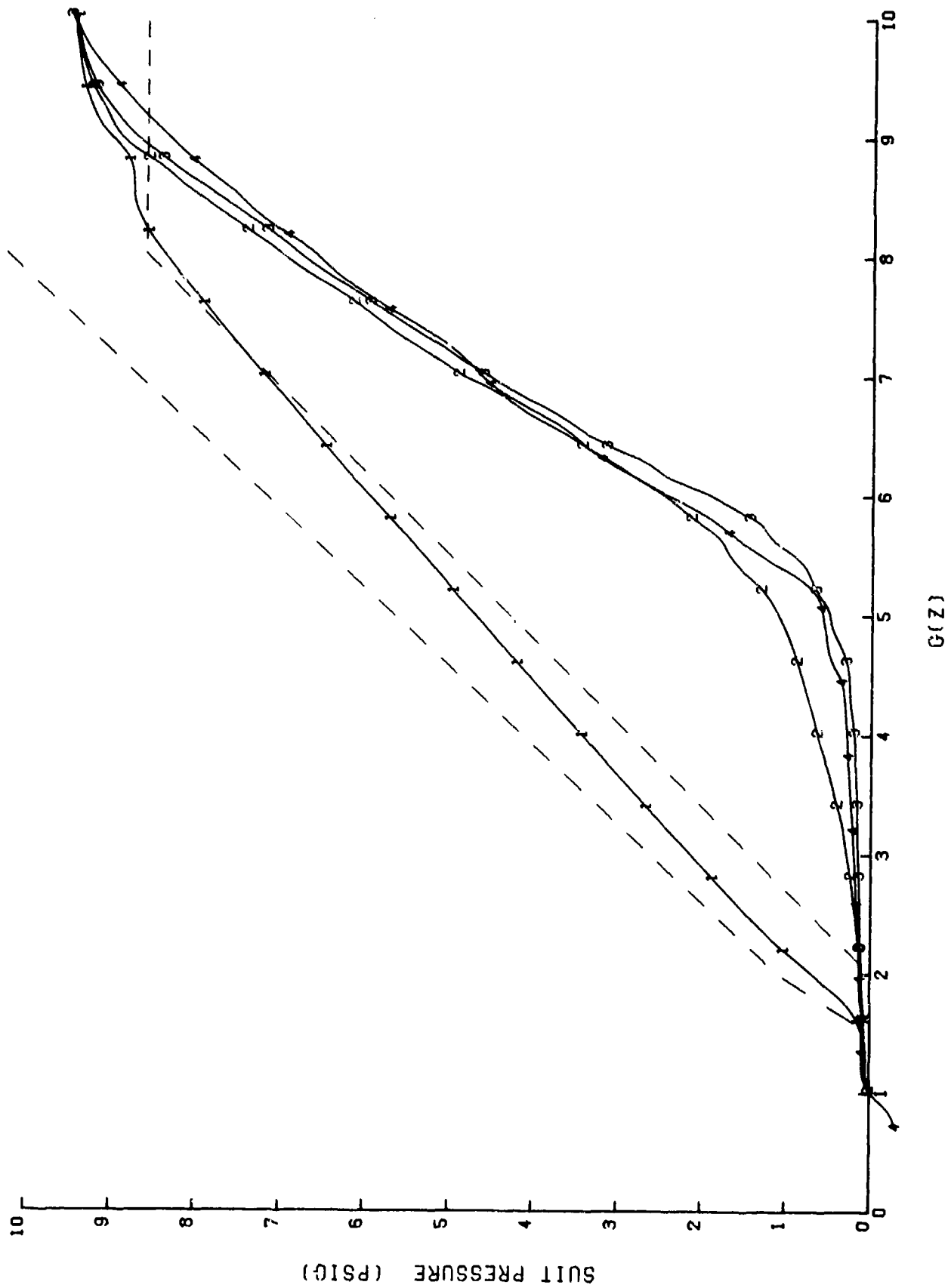


Figure 73. ALAR failure #1: suit pressure profile as a function of G-onset rate.
[Curves are: 1, 2, 3, and 4. For "Key," refer to Table 2.]

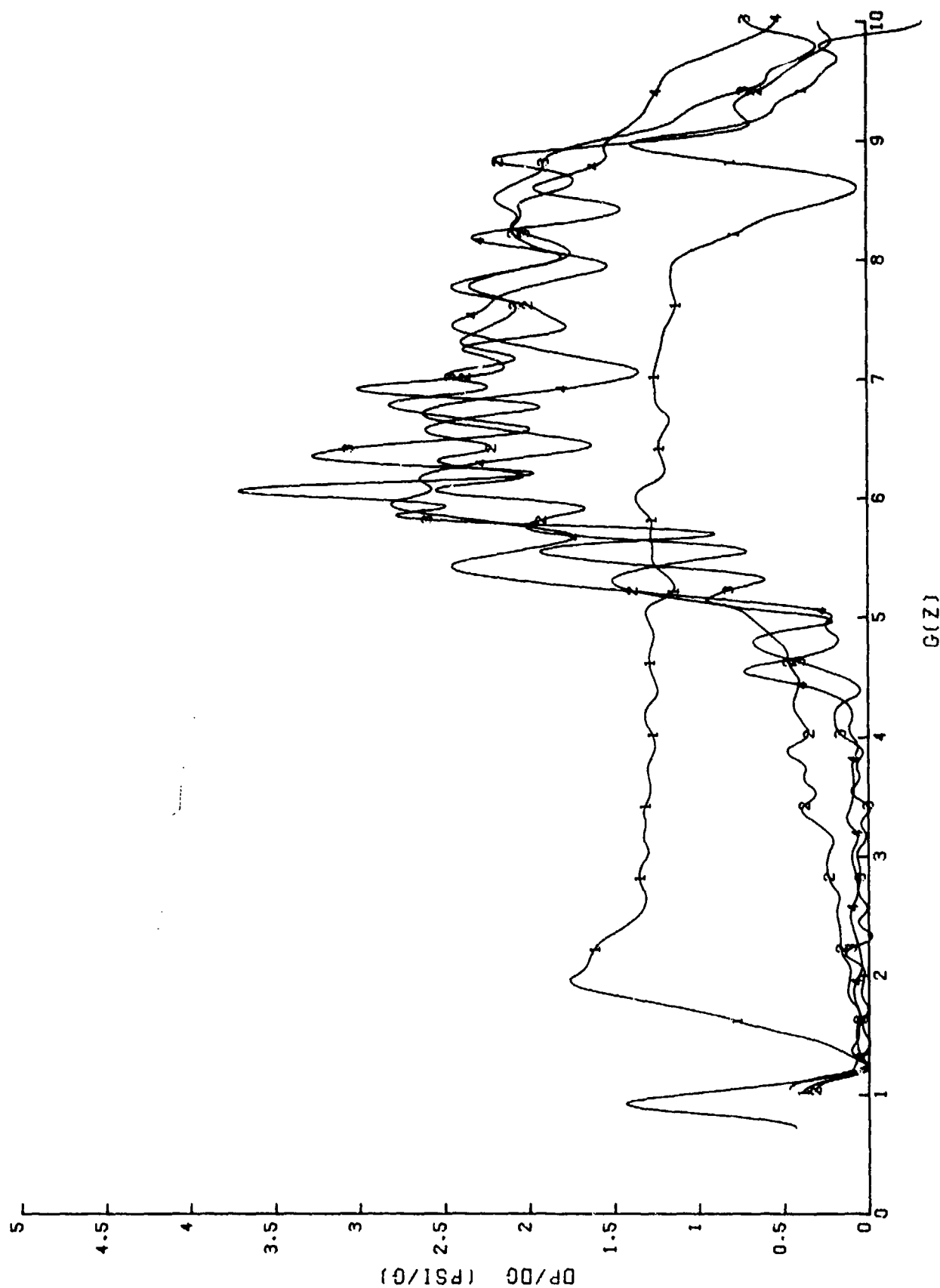


Figure 74. ALAR failure #1: dp/dG as a function of G -onset rate.
 [Curves are: 1, 2, 3, and 4. For "Key," refer to Table 2.]

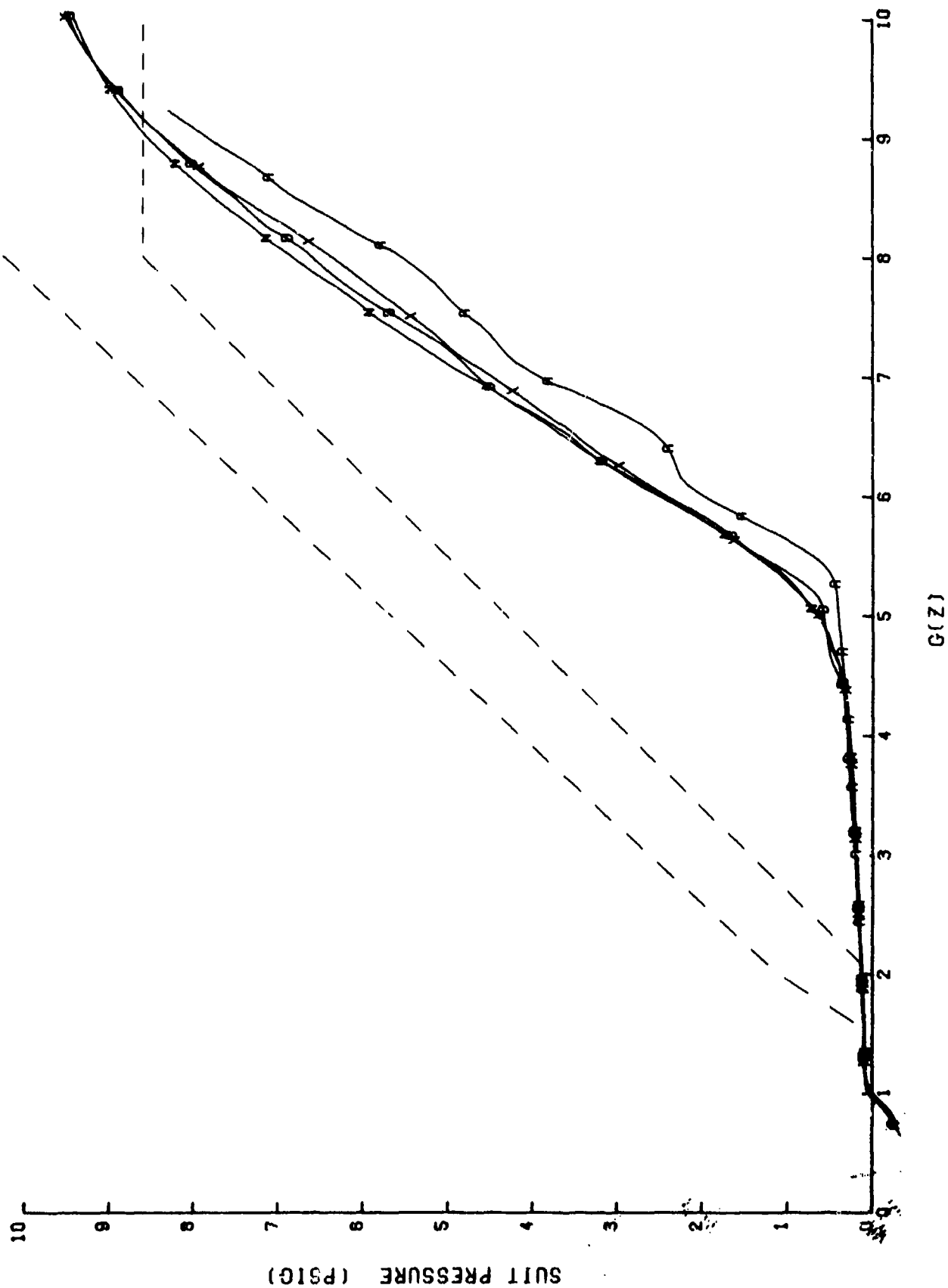


Figure 75. ALAR failure #1: 1.5 G/sec suit pressure profile as a function of source pressure.
[Curves are: N, D, X, and A. For "Key," refer to Table 2.]

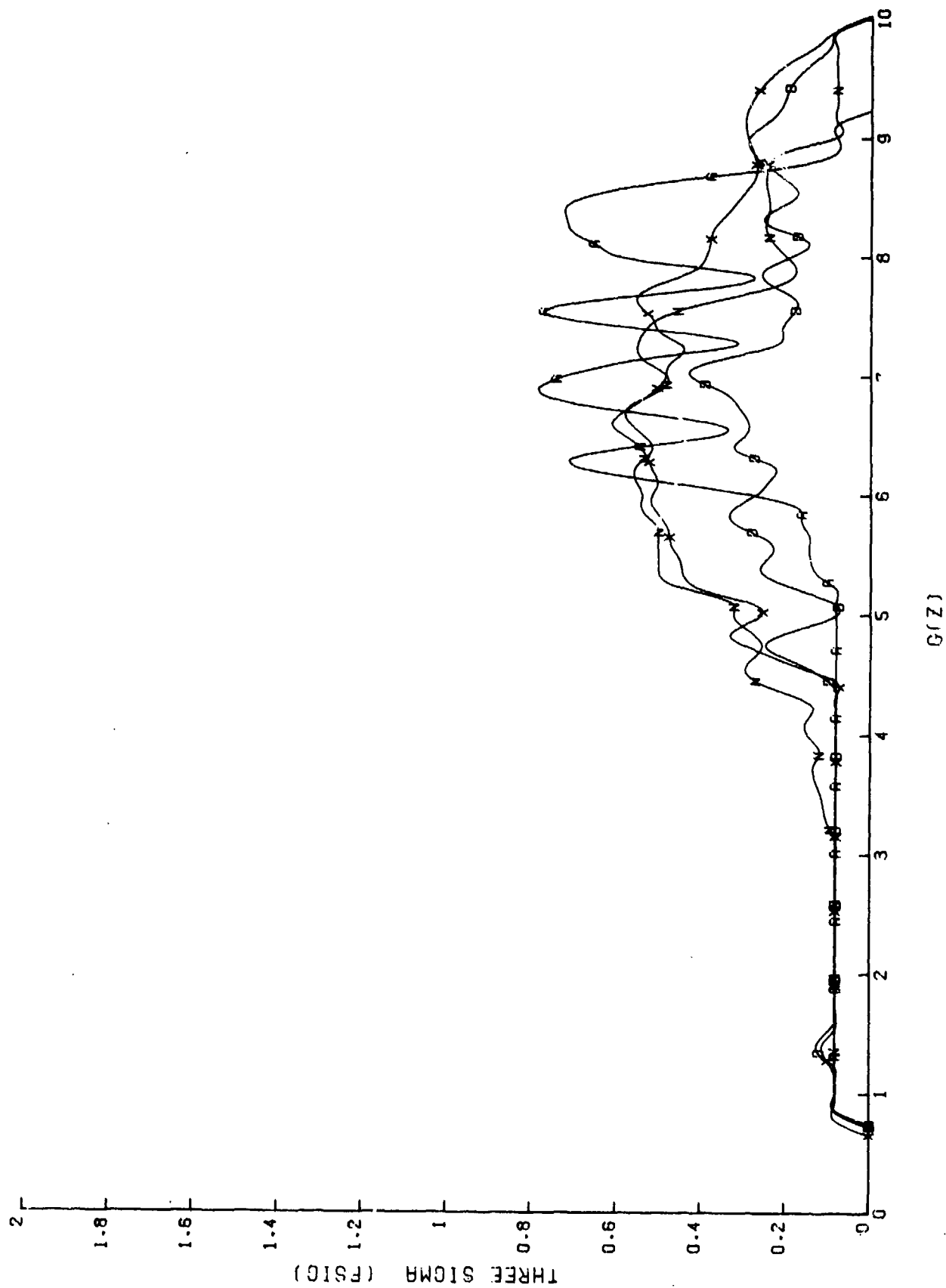


Figure 76. ALAR failure #1: 1.5 G/sec suit pressure variation as a function of source pressure. [Curves are: N, D, X, and A. For "Key," refer to Table 2.1.]

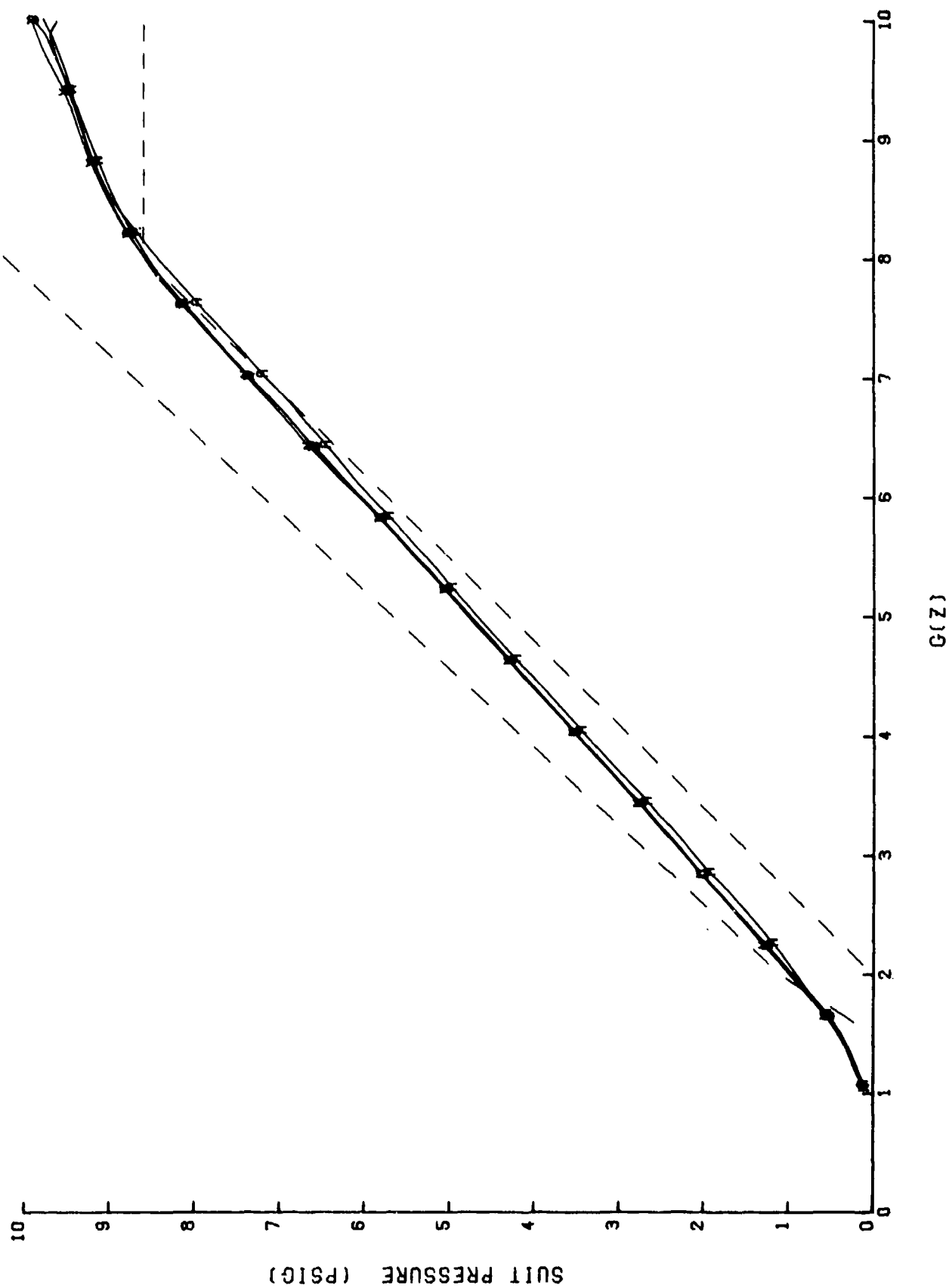
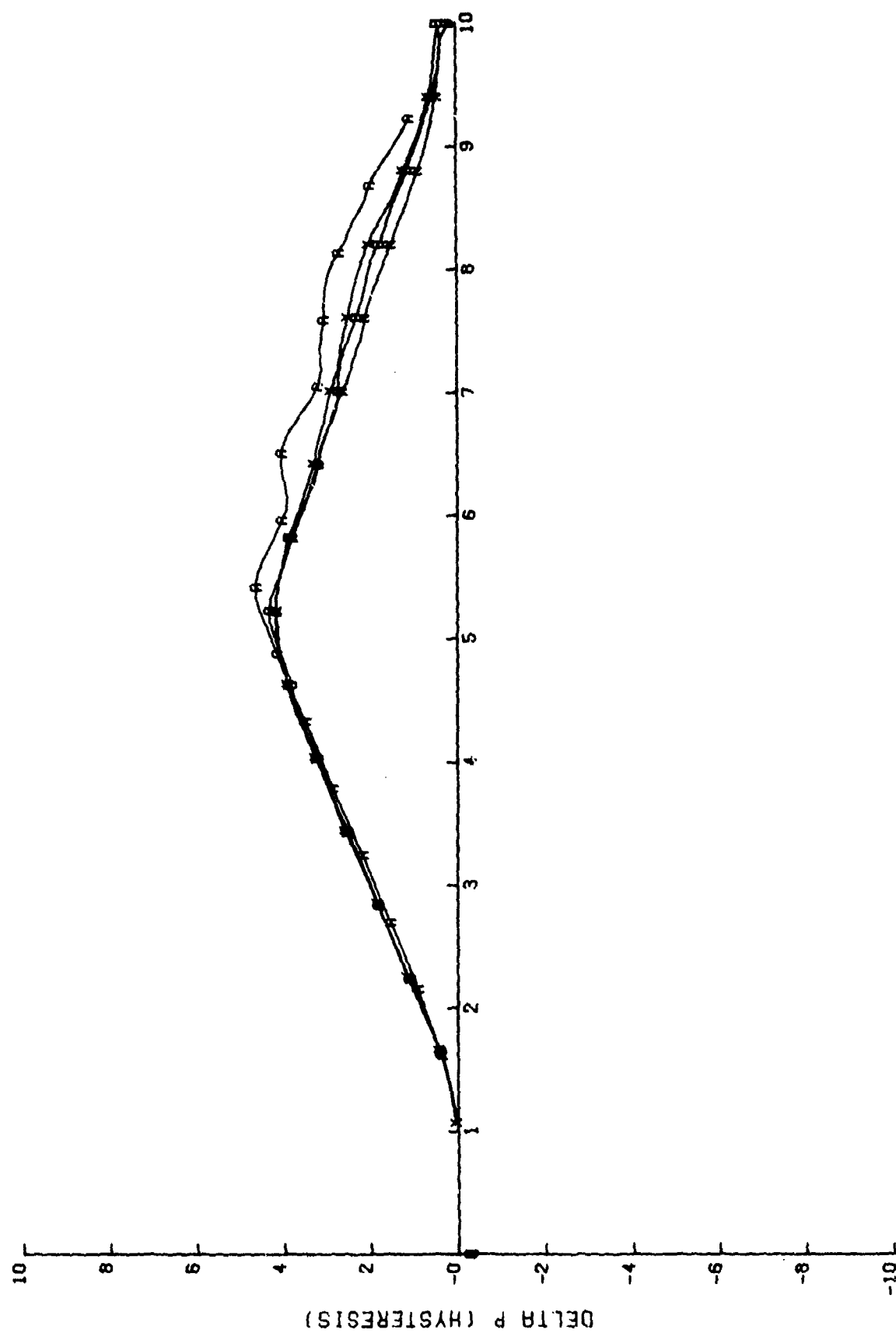


Figure 77. ALAR failure #1: -1.5 G/sec decreasing suit pressure profile as a function of source pressure. [Curves are: N, D, X, and A. For "Key," refer to Table 2.]



G(Z)

Figure 78. ALAR failure #1: 1.5 G/sec suit pressure hysteresis as a function of source pressure.
[Curves are: N, D, X, and A. For "Key," refer to Table 2.]

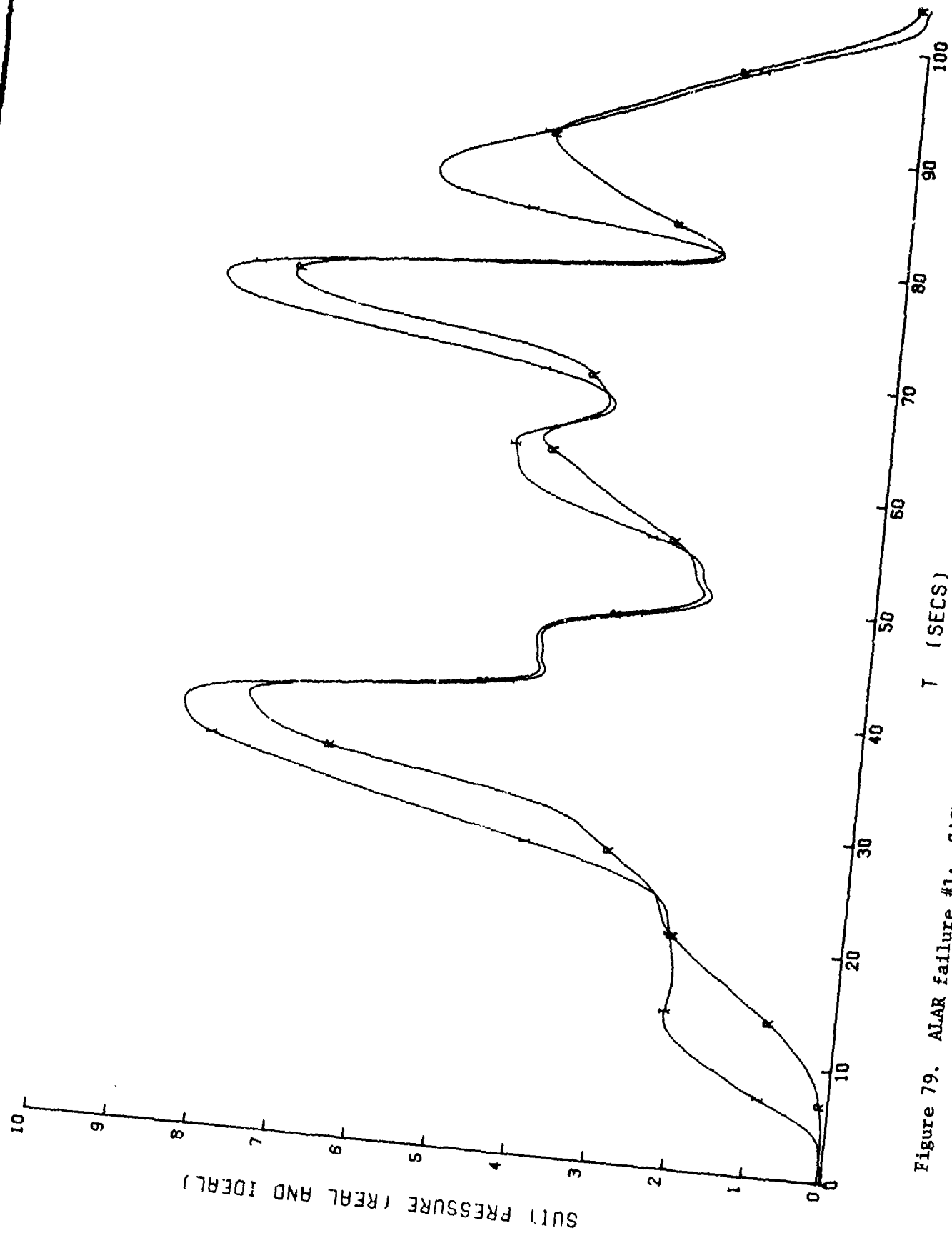
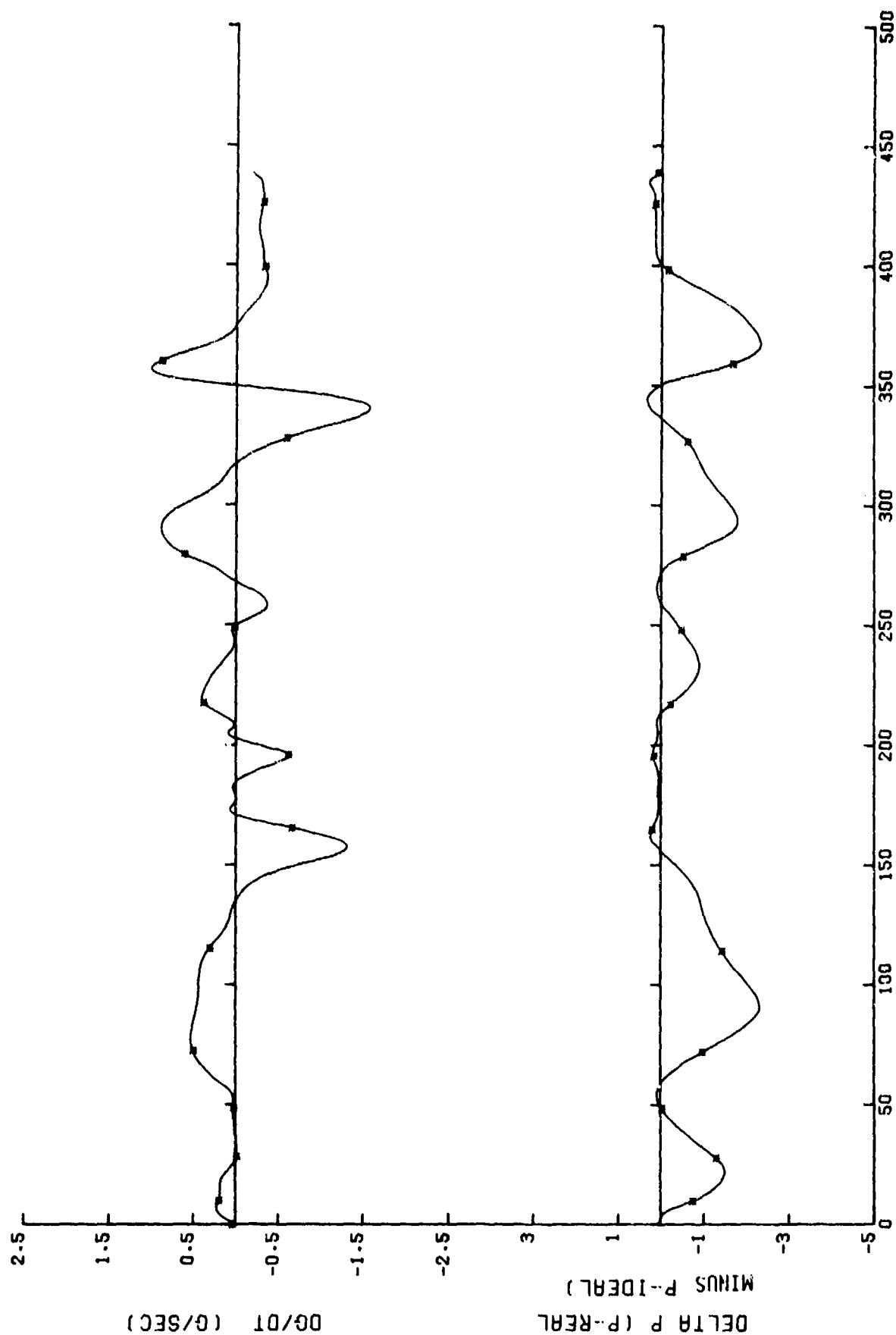


Figure 79. ALAR failure #1: SACM suit pressure profile comparison with minimum source pressure and maximum suit volume. [Curves are: I and R. For "Key," refer to Table 2.]



INTEGRAL OF G DT FROM 0 TO T

Figure 80. ALAR failure #1: suit pressure deviation and dG/dt for the minimum source pressure, maximum suit volume SACM. [Curves are: *. For "Key," refer to Table 2.]

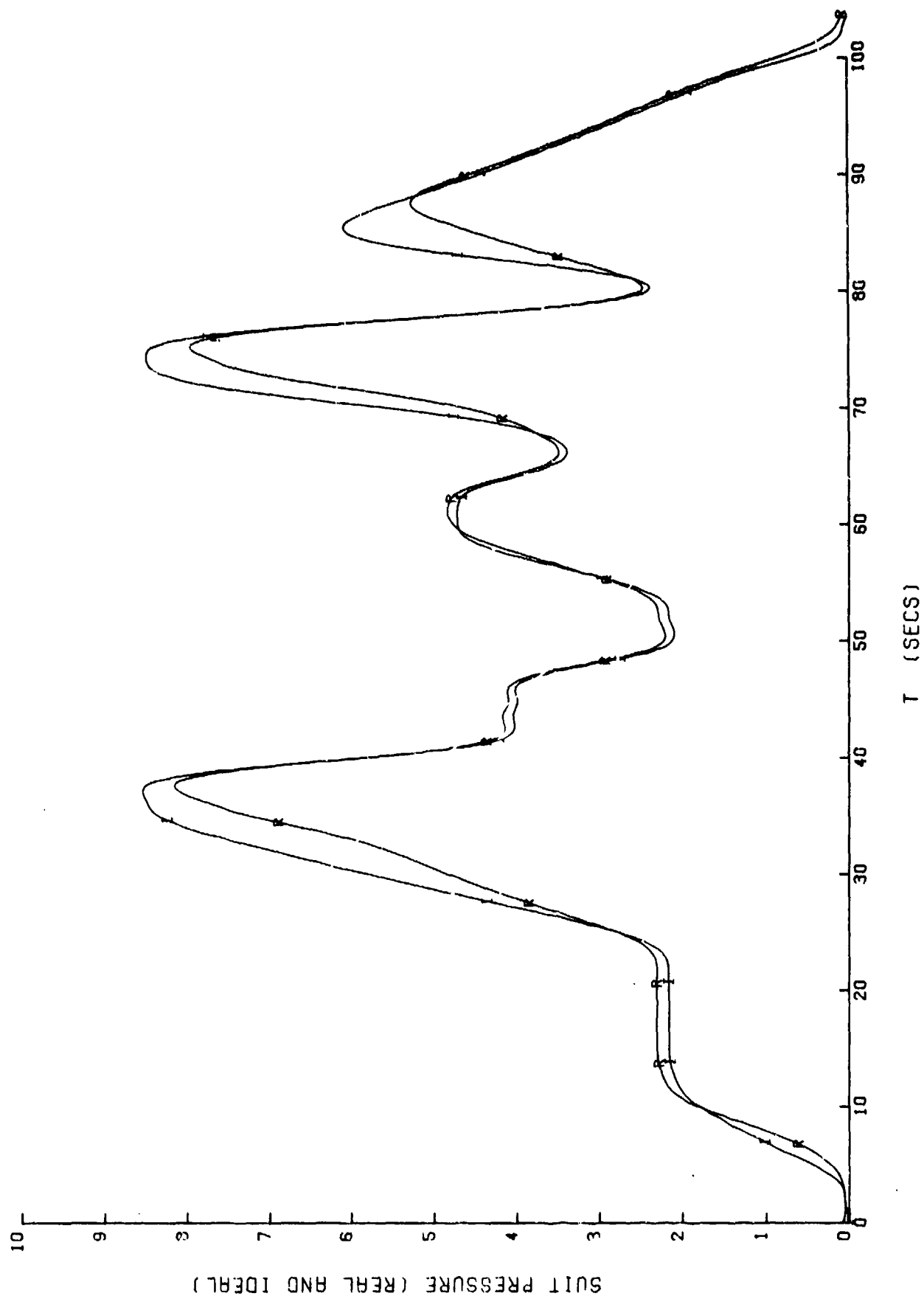


Figure 81. ALAR failure #1: SACM suit pressure profile comparison with maximum source pressure and minimum suit volume. [Curves are: I and R. For "Key," refer to Table 2.]

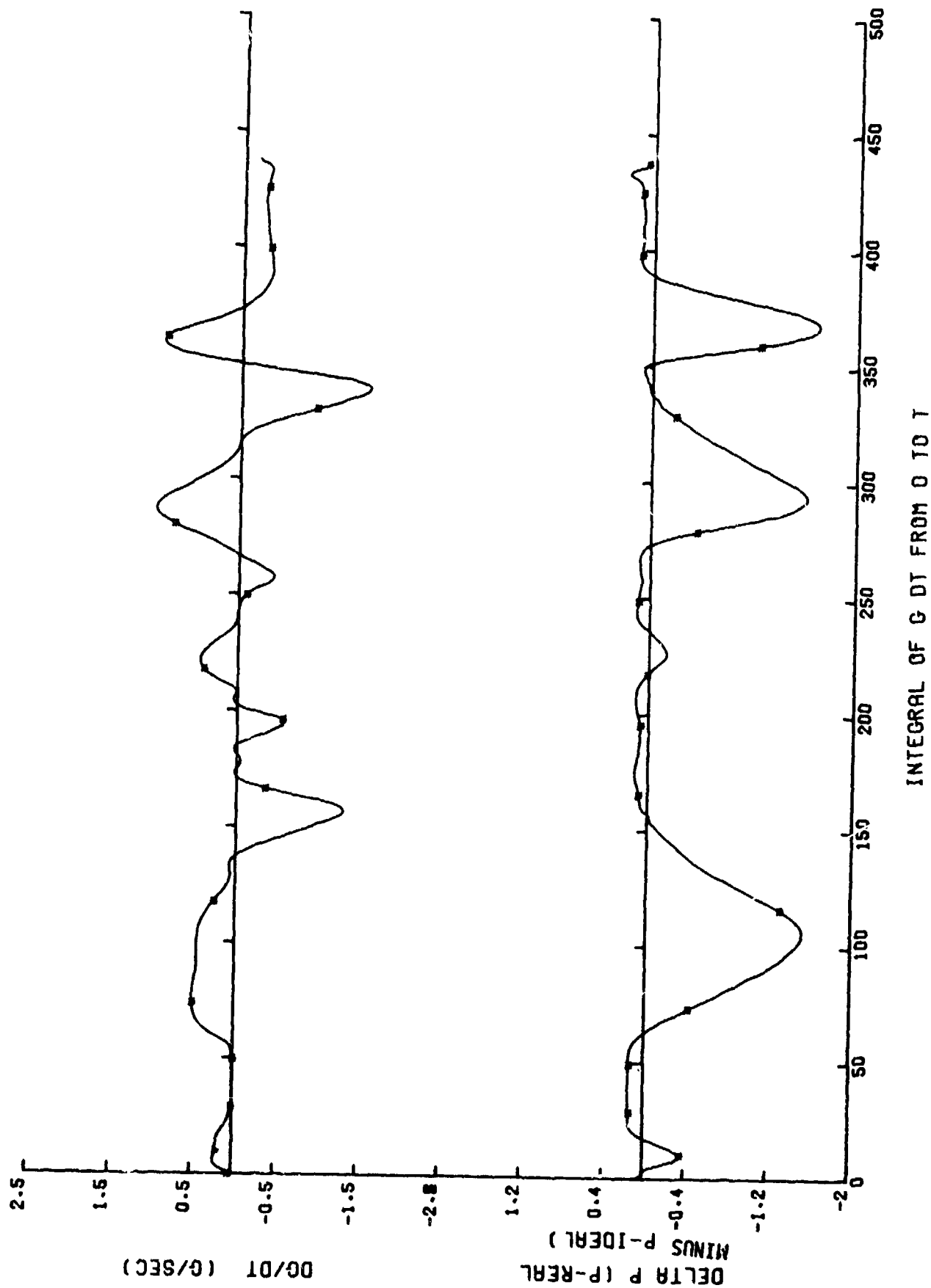


Figure 82. ALAR failure #1: suit pressure deviation and dg/dt for the maximum source pressure, minimum suit volume SACK. [Curves are: * For "Key." Refer to Table 2.1]

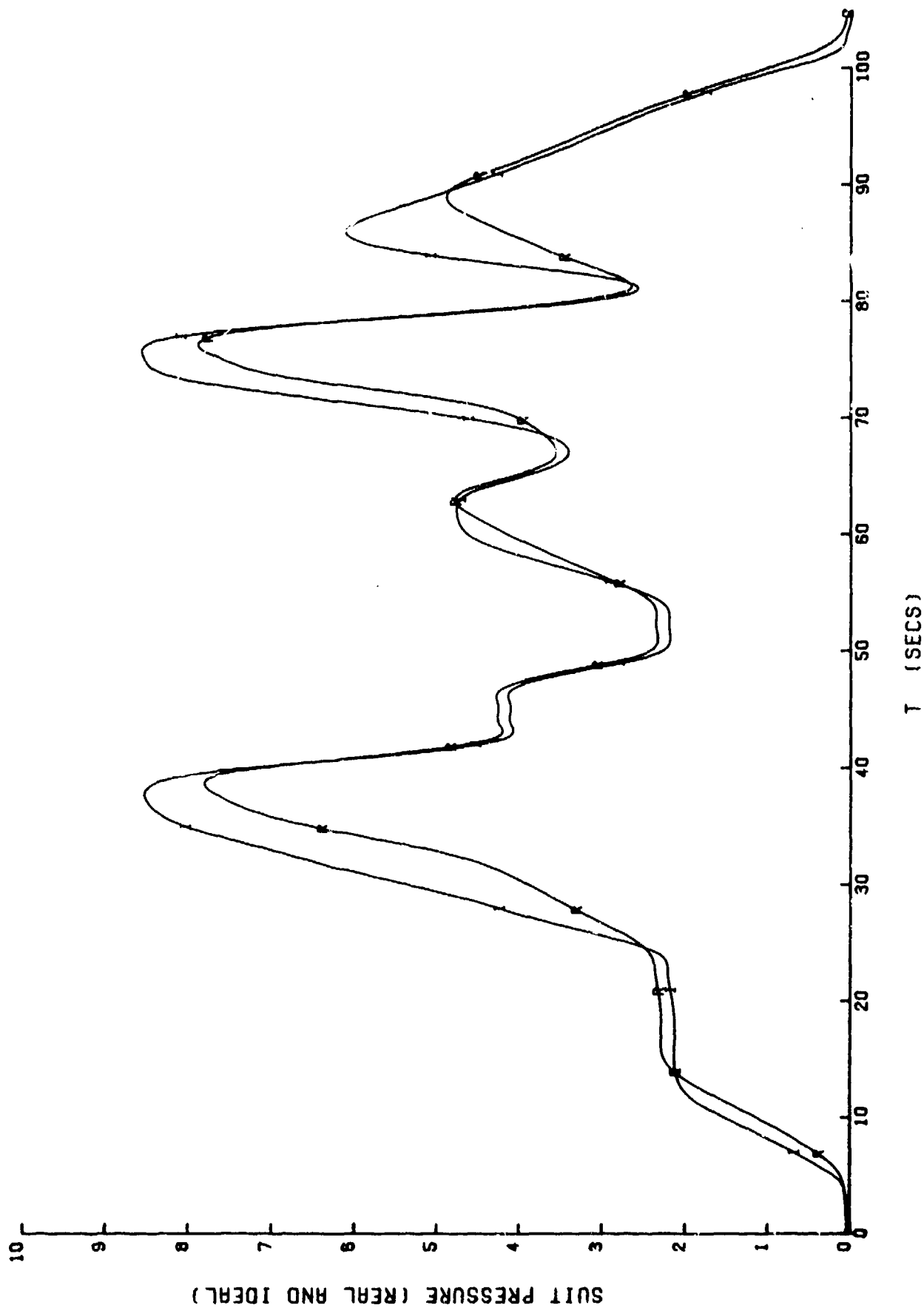
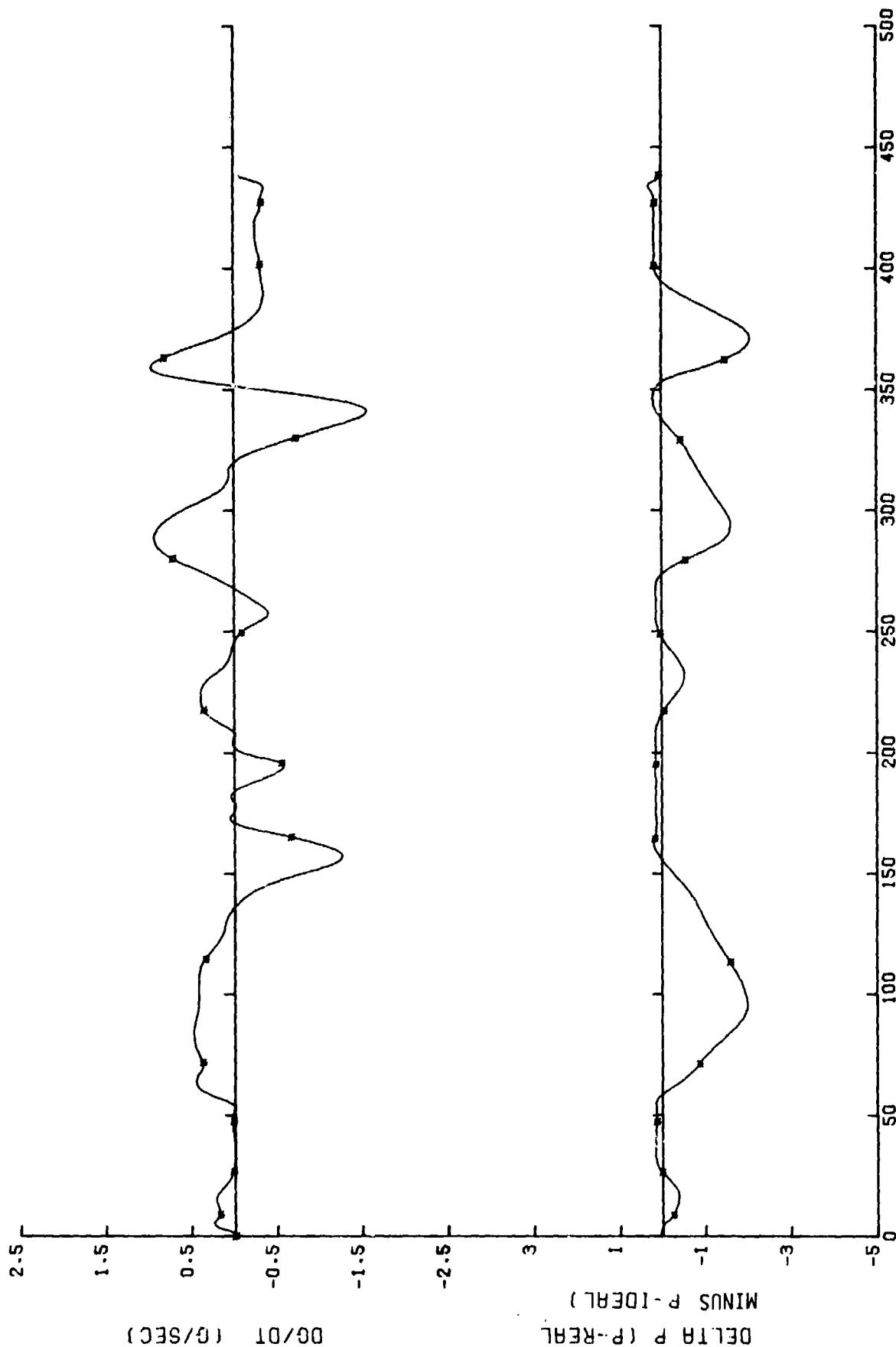


Figure 83. ALAR failure #1: SACM suit pressure profile comparison with median source pressure and suit volume. [Curves are: I and R. For "Key," refer to Table 2.]



INTEGRAL OF G DT FROM 0 TO T

Figure 84. ALAR failure #1: suit pressure deviation and dG/dt for the median source pressure and suit volume SACM. [Curves are: *, For "Key," refer to Table 2.1]

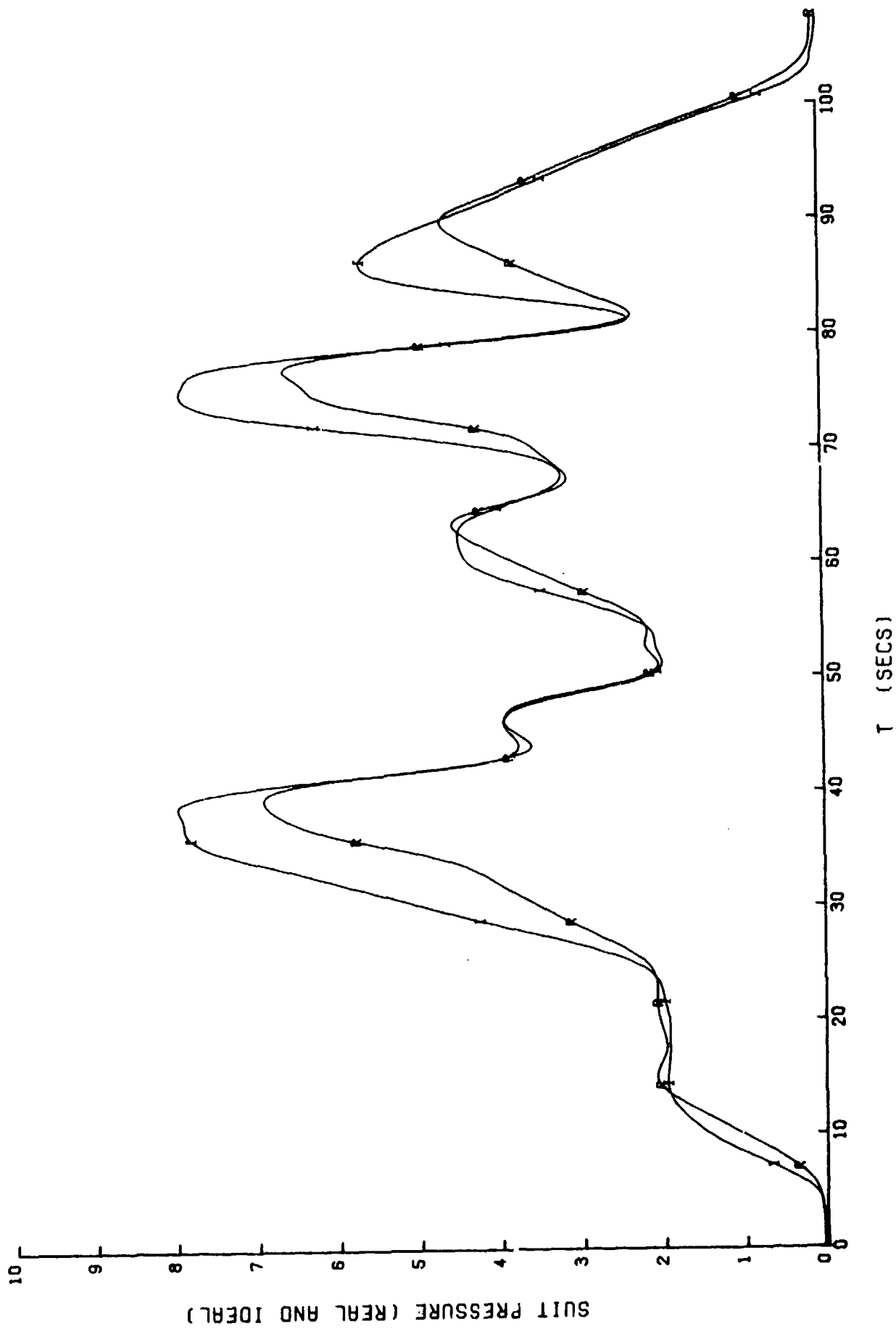
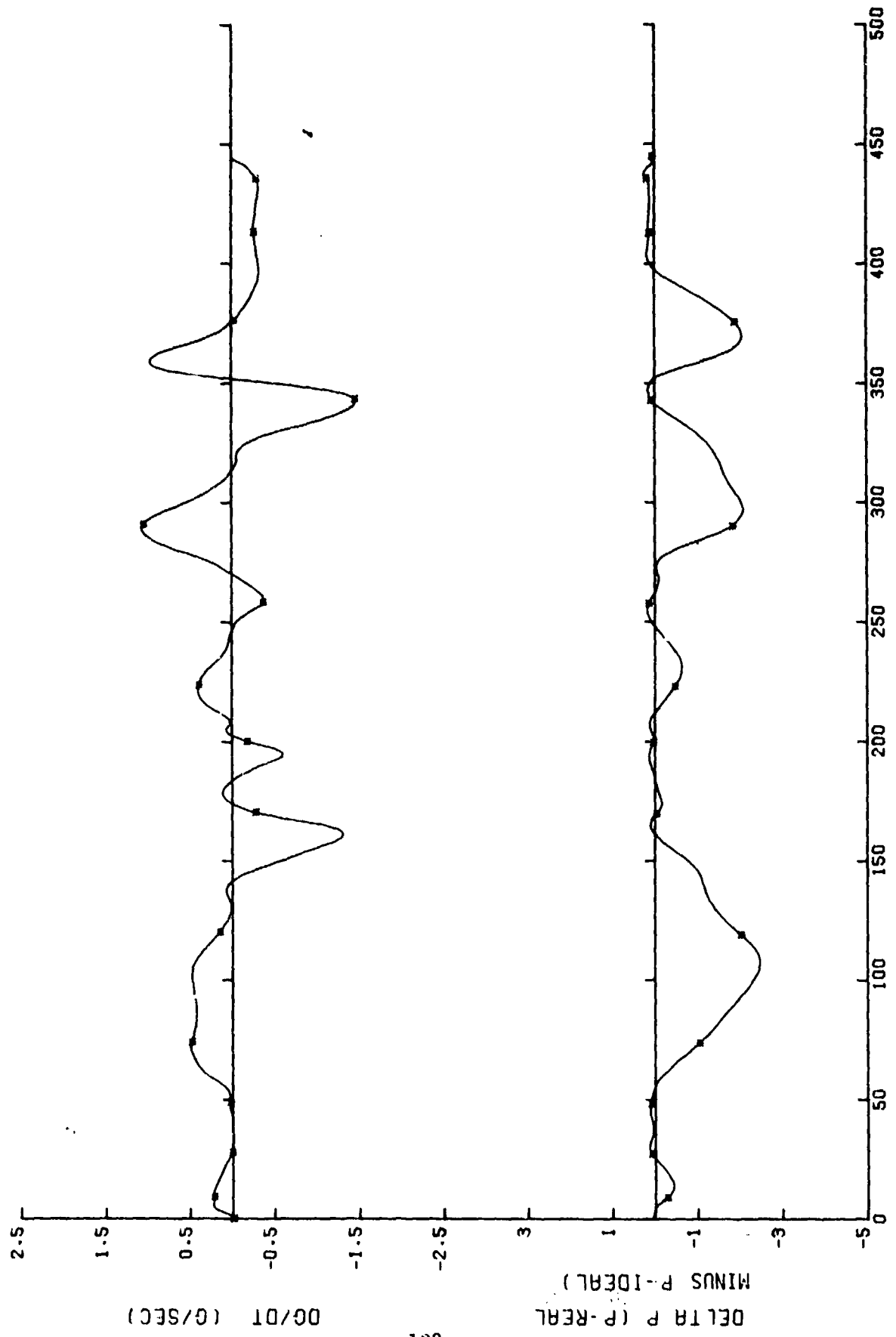


Figure 85. ALAR failure #1: SACM suit pressure profile comparison with G vector misalignment.
[Curves are: I and R. For "Key," refer to Table 2.]



INTEGRAL OF G DT FROM 0 TO T

TABLE 4. ALAR AGV FAILURE #1 PERFORMANCE EVALUATION TABLE

TEST STANDARDS:

1. SPMIN = 30. PSIG
2. SPMID = 125. PSIG
3. SPMAX = 300. PSIG
4. THETA = 20. DEGREES
5. SVMIN = 6. LITERS
6. SVMID = 10. LITERS
7. SVMAX = 14. LITERS

CHARACTERISTIC NUMBERS:

8. XSPMX = 1.0000
9. XSPMN = 1.0000
10. XTHTA = 1.0000
11. DESIGN TOTAL: 3.000
12. XFLBR = 3.919
13. XDELF = 2.029
14. XDDL F = 2.231
15. XSIGF = 0.396
16. FLOW TOTAL: 8.575
17. XCCP1 = 0.012
18. XDDP1 = 0.896
19. XSGP1 = 0.909
20. XDPP1 = 0.651
21. LOW-ONSET TOTAL: 2.468
22. XCCP2 = 6.095
23. XDDP2 = 2.128
24. XSGP2 = 1.687
25. XDPP2 = 4.449
26. XTDP2 = 16.328
27. HIGH-ONSET TOTAL: 30.687
28. XIDPA = 3.723
29. XIDPB = 6.670
30. XIDPC = 5.192
31. XIDPD = 6.361
32. SACM TOTAL: 21.946
33. VALVE: ALAR FAILURE #1 TOTAL: 66.676

1.4.4 SVTP Failure Testing Conclusions

All three of the AGV failures tested were clearly indicated on the PETs (Tables 2, 3, and 4) and supported by GVALVPGM graphic documentation. The authors agree that the system is somewhat subjective, and could probably be improved with extended study (i.e., by analyzing the results from a much larger number of valves).

2. SPECIFIC EQUIPMENT EVALUATIONS

2.1 The CWU-9/P Undergarment G-Effects Tests

The item under test was a two-piece, quilted, anti-exposure undergarment designed to be worn under a flight suit. The jacket, designated the "Liners, Flyers, CWU-9/P Jacket," was manufactured by Gibraltar Industries, Inc. The trousers, designated the "Liners, Flyers, CWU-9/P Trousers," were manufactured by Lankford Manufacturing Company, Inc. Both garments were of "medium" size and were labeled in accordance with MIL-L-27546C (Naval Publications and Forms Center, 5801 Tabor Ave., Philadelphia, Pa. 19120).

The purpose of these tests was to establish the relative anti-G suit to skin interface force difference (if any), with and without the exposure suit, over a span of suit pressures.

2.1.1 Test Instrumentation and Calibration

For these tests, a 0 to 30 psia transducer (Giannini model 451212-4) was used to monitor anti-G suit pressure. This transducer was calibrated from 0 to 10 psig, prior to each work shift, using the pressure calibration system installed in the USAFSAM/VNB centrifuge facility.

The transducers used to monitor anti-G suit to mannequin interface force were Houston Scientific Model 1200-15C force gages especially calibrated for this purpose [Houston Scientific (the HSI Corporation), 4202 Directors Row, Houston, Tex. 77018]. These force buttons were calibrated prior to each work shift, for a 0- to 10-lb span, using a lead weight.

All data from these tests were recorded on the USAFSAM/VNB Control-Room Brush-Chart system. Data were recorded on six channels: suit pressure, right thigh force, left thigh force, right calf force, left calf force, and abdominal force.

Anti-G suit volumes were determined using the "known volume-pressure drop system" developed by Technology Incorporated for this purpose.

All tests were conducted under static (1 G_z) conditions; for, as previously determined, a G_z field would have no significant influence on the test data or validity. Prior to each test series (with, or without, exposure suit), the suit was so fitted to the mannequin that the suit volume was ± 7.7 liters, to provide uniformity of the suit fit on the mannequin.

2.1.2 Test Methods

The test subject for these tests was a Fiberglas mannequin with strain-gage-type force buttons mounted in the abdomen, left and right thighs, and left and right calves. The mannequin was fitted with a CSU 13A/P "medium" anti-G suit, and the suit volume adjusted to 7.7 liters. The mannequin was mounted in a seat and the suit was evacuated with a mild vacuum. Suit pressure was then slowly increased, in 1-psig steps, from 0 to 10 psig, and

corresponding force-gage readings were recorded. Two more sets of data, taken in this configuration, were recorded with measurements at 0, 5, and 10 psig.

The anti-G suit was removed from the mannequin and the exposure suit installed. The anti-G suit was installed over the exposure suit and readjusted to a 7.7 liter fit. A set of data identical to the first test (without exposure suit) were recorded. Three separate iterations of this test sequence were made to establish an adequate statistical data base.

2.1.3 Data Presentation

The data from the foregoing tests were taken from the Brush charts at each test point and were recorded in tabular form. These data are presented in Tables 5 - 10.

The minimum, mean, and maximum data points for each test pressure point were calculated and normalized for each force-button location (Figs. 87 - 91).

2.1.4 Discussion and Conclusions

The data in Figures 87 - 91 show graphically the results of these tests. Previous testing by this contractor has shown that the force buttons, used to measure interface force, exhibit good linearity and fair repeatability from one run to the next--as long as the suit is not moved on the mannequin. If, however, as in these tests, the suit is removed and reinstalled, a significant change results in the pressure-force data. For this reason, several runs were made and mean values used. The maximum and minimum data points for each test pressure are also shown to indicate the amount of variation in data. We suspect that this variation is caused by slight differences in the location and orientation of the suit bladders to the force buttons. Slightly more variation appears in readings when the exposure suit is installed than when it is not. This variation is probably due to the tendency of the suit bladders to slip more on the surface presented by the exposure suit.

Also, the force buttons seem to have a tendency to exhibit a slightly higher force when the exposure suit is installed. In the opinion of the investigating team, this increase is a product of the measurement technique and does not predict a real increase in force on a human subject. We suspect that this effect is caused by the exposure suit forming a small "tent" over the force button, which protrudes above the surface of the mannequin skin, presenting a slightly larger contact area to the suit bladder. This judgment is empirically based on results of previous testing with these force buttons. Also, the mannequin is a comparatively rigid body, and only approximates the condition of the anti-G suit to human interface--facts which should be considered when applying the results of these tests to results with a human subject.

Lacking clear correlation between the CWU-9/P and the changes in suit to mannequin interface force in these test results, we concluded that the exposure suit had no significant effect on anti-G suit performance.

TABLE 5. FIRST SET OF RUNS WITHOUT EXPOSURE SUIT

<u>RUN</u>	<u>P_s</u>	<u>ABDOMEN</u>	<u>LEFT</u>		<u>RIGHT</u>	
			<u>Thigh</u>	<u>Calf</u>	<u>Thigh</u>	<u>Calf</u>
1	0	0	0.18	0.3	0.2	0.2
	1	0.7	0.8	1.3	1.0	0.6
	2	1.4	1.55	2.1	1.8	1.1
	3	2.1	2.3	3.0	2.6	1.65
	4	2.6	2.95	2.85	3.3	2.1
	5	3.2	3.6	4.7	4.0	2.6
	6	3.8	4.3	5.6	4.8	3.1
	7	4.4	5.0	6.45	5.5	3.6
	8	5.0	5.8	7.4	6.2	4.1
	9	5.5	6.4	8.2	6.8	4.6
	10	6.1	7.1	9.1	7.5	5.0
2	0	0	0.1	0.25	0.15	0.2
	5	3.2	3.6	4.6	4.15	2.7
	10	6.05	7.05	9.0	7.65	5.1
3	0	0	0.05	0.25	0.15	0.15
	5	3.2	3.7	4.9	4.2	2.8
	10	5.95	6.85	9.1	7.55	5.45

P_s = source pressure

TABLE 6. SECOND SET OF RUNS WITHOUT EXPOSURE SUIT

<u>RUN</u>	<u>P_s</u>	<u>ABDOMEN</u>	<u>LEFT</u>		<u>RIGHT</u>	
			<u>Thigh</u>	<u>Calf</u>	<u>Thigh</u>	<u>Calf</u>
1	0	-0.05	0	0.15	0.35	1.1
	1	0.6	1.0	1.1	1.3	1.8
	2	1.3	1.8	1.95	2.0	2.45
	3	1.9	2.6	2.9	2.85	3.2
	4	2.5	3.3	3.7	3.6	3.9
	5	3.1	4.0	4.6	4.3	4.6
	6	3.6	4.8	5.5	5.0	5.3
	7	4.2	5.4	6.35	5.7	5.95
	8	4.8	6.1	7.2	6.4	6.6
	9	5.35	6.8	8.0	7.0	7.3
	10	5.95	7.5	8.85	7.7	7.95
2	0	-0.05	0	0.2	0.35	1.1
	5	3.1	3.95	4.7	4.2	4.7
	10	5.95	7.45	8.95	7.6	8.0
3	0	-0.05	-0.05	0.15	0.35	1.15
	5	3.1	4.0	4.8	4.3	4.65
	10	5.95	7.45	9.05	7.6	8.0

P_s = source pressure

TABLE 7. THIRD SET OF RUNS WITHOUT EXPOSURE SUIT

<u>RUN</u>	<u>P_s</u>	<u>ABDOMEN</u>	<u>LEFT</u>		<u>RIGHT</u>	
			<u>Thigh</u>	<u>Calf</u>	<u>Thigh</u>	<u>Calf</u>
1	0	0.05	0.05	0.15	0.45	0.45
	1	0.8	1.05	1.2	1.55	1.15
	2	1.55	1.9	2.2	2.5	1.75
	3	2.15	2.7	3.15	3.2	2.3
	4	2.8	3.5	4.1	4.1	3.0
	5	3.4	4.2	5.0	4.95	3.6
	6	4.0	5.0	6.0	5.7	4.3
	7	4.65	5.75	7.0	6.6	4.95
	8	5.2	6.5	7.8	7.25	5.5
	9	5.8	7.15	8.75	8.0	6.2
	10	6.35	7.8	9.6	8.7	6.7
2	0	0	0.05	0.2	0.5	0.5
	5	3.3	4.25	5.1	5.0	3.7
	10	6.3	7.85	9.55	8.8	6.7
3	0	0	0.05	0.25	0.5	0.5
	5	3.2	4.2	5.15	5.05	3.65
	10	6.2	7.8	9.6	8.8	7.75

P_s = source pressure

TABLE 8. FIRST SET OF RUNS WITH EXPOSURE SUIT

<u>RUN</u>	<u>P_s</u>	<u>ABDOMEN</u>	<u>LEFT</u>		<u>RIGHT</u>	
			<u>Thigh</u>	<u>Calf</u>	<u>Thigh</u>	<u>Calf</u>
1	0	0	0	0.15	0.4	0.9
	1	0.7	0.8	1.2	1.3	1.4
	2	1.3	1.6	2.3	2.2	2.0
	3	2.0	2.4	3.3	3.0	2.6
	4	2.6	3.2	4.4	3.8	3.2
	5	3.2	3.9	5.3	4.6	3.8
	6	3.8	4.7	6.35	5.4	4.4
	7	4.3	5.35	7.25	6.1	4.95
	8	4.9	6.2	8.3	6.9	5.5
	9	5.5	6.8	9.2	7.6	6.2
	10	6.0	7.55	10.1	8.3	6.6
2	0	0	0	0.25	0.4	0.9
	5	3.0	3.85	5.3	4.6	3.7
	10	5.9	7.55	10.1	8.3	6.5
3	0	0	0	0.25	0.35	0.95
	5	3.1	3.95	5.4	4.65	3.8
	10	5.9	7.5	10.1	8.25	6.35

P_s = source pressure

TABLE 9. SECOND SET OF RUNS WITH EXPOSURE SUIT

<u>RUN</u>	<u>P_s</u>	<u>ABDOMEN</u>	<u>LEFT</u>		<u>RIGHT</u>	
			<u>Thigh</u>	<u>Calf</u>	<u>Thigh</u>	<u>Calf</u>
1	0	0	0	0.2	0.35	1.2
	1	0.5	1.0	1.15	1.4	1.9
	2	1.15	1.85	2.15	2.4	2.55
	3	1.7	2.6	3.05	3.25	3.2
	4	2.3	3.6	4.0	4.15	3.85
	5	2.85	4.1	4.9	4.9	4.5
	6	3.4	4.85	5.7	5.7	5.1
	7	3.95	5.6	6.7	6.5	5.7
	8	4.6	6.3	7.45	7.25	6.3
	9	5.0	7.0	8.35	8.0	6.85
	10	5.6	7.7	9.2	8.75	7.4
2	0	0	0	0.3	0.4	1.3
	5	2.75	4.0	4.9	5.0	4.45
	10	5.5	7.6	9.25	8.8	7.1
3	0	0	0	0.35	0.4	1.3
	5	2.8	4.1	5.0	5.05	4.3
	10	5.5	7.7	9.25	8.85	6.9

P_s = source pressure

TABLE 10. THIRD SET OF RUNS WITH EXPOSURE SUIT

<u>RUN</u>	<u>P_s</u>	<u>ABDOMEN</u>	<u>LEFT</u>		<u>RIGHT</u>	
			<u>Thigh</u>	<u>Calf</u>	<u>Thigh</u>	<u>Calf</u>
1	0	0	0.05	0.25	0.45	0.95
	1	0.85	1.2	1.2	1.6	1.3
	2	1.6	2.2	2.0	2.6	1.65
	3	2.4	3.2	3.0	3.6	2.0
	4	3.1	4.1	4.0	4.6	2.3
	5	3.9	5.0	4.85	5.6	2.6
	6	4.5	5.8	5.75	6.5	2.85
	7	5.3	6.7	6.5	7.4	3.15
	8	6.0	7.5	7.4	8.3	3.4
	9	6.5	8.4	8.3	9.3	3.65
	10	7.35	9.15	9.15	10.05	3.8
2	0	0.1	0.05	0.35	0.50	1.15
	5	3.75	5.1	4.8	5.7	2.55
	10	7.2	9.2	9.5	10.0	3.7
3	0	0.05	0.05	0.4	0.5	1.0
	5	3.8	5.0	4.9	5.4	2.55
	10	7.35	9.2	9.2	10.1	3.7

P_s = source pressure

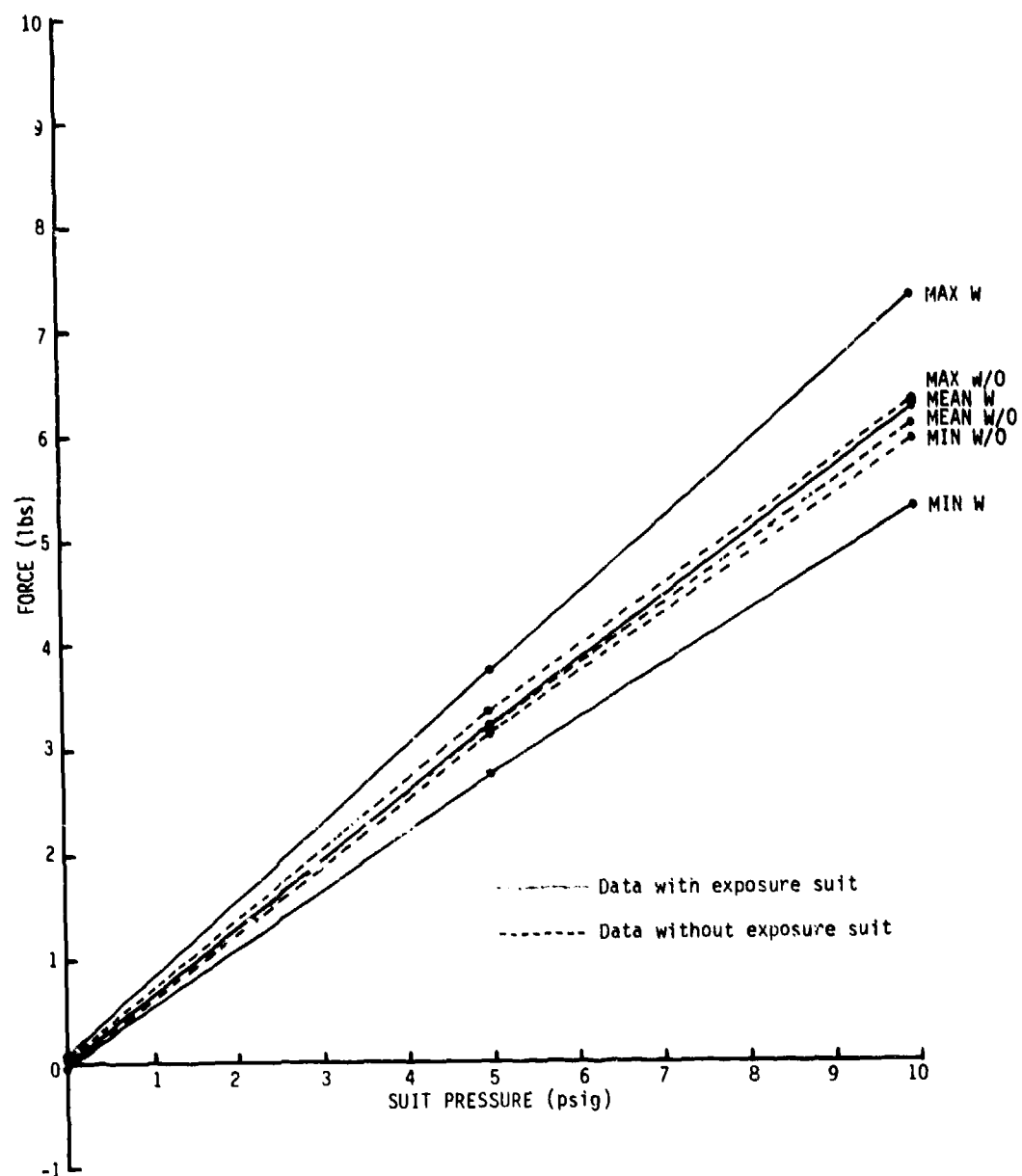


Figure 87. Normalized exposure suit abdomen force.
[Key: W = with suit; W/O = without suit.]

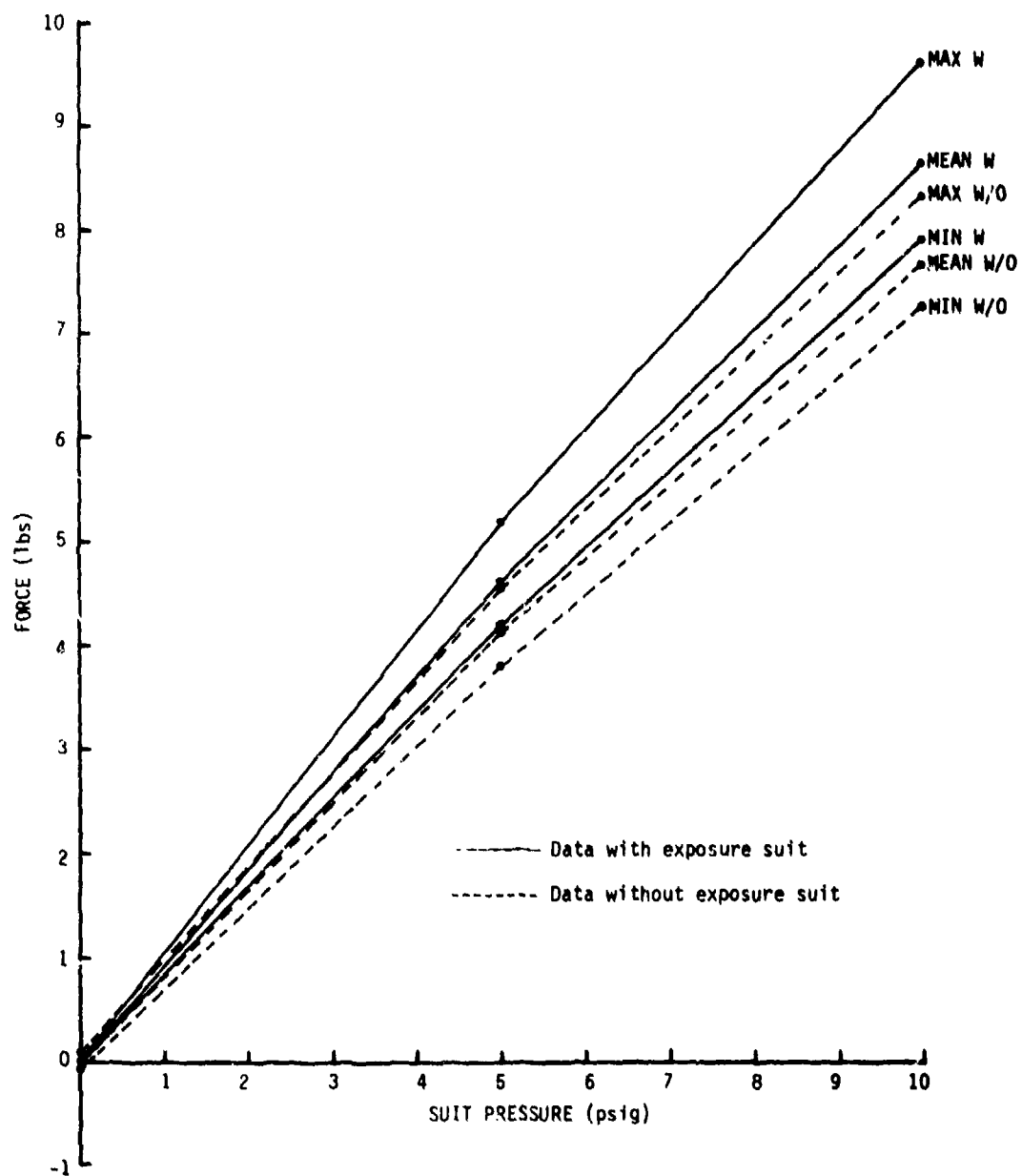


Figure 88. Normalized exposure suit right thigh force.
[Key: W = with suit; W/O = without suit.]

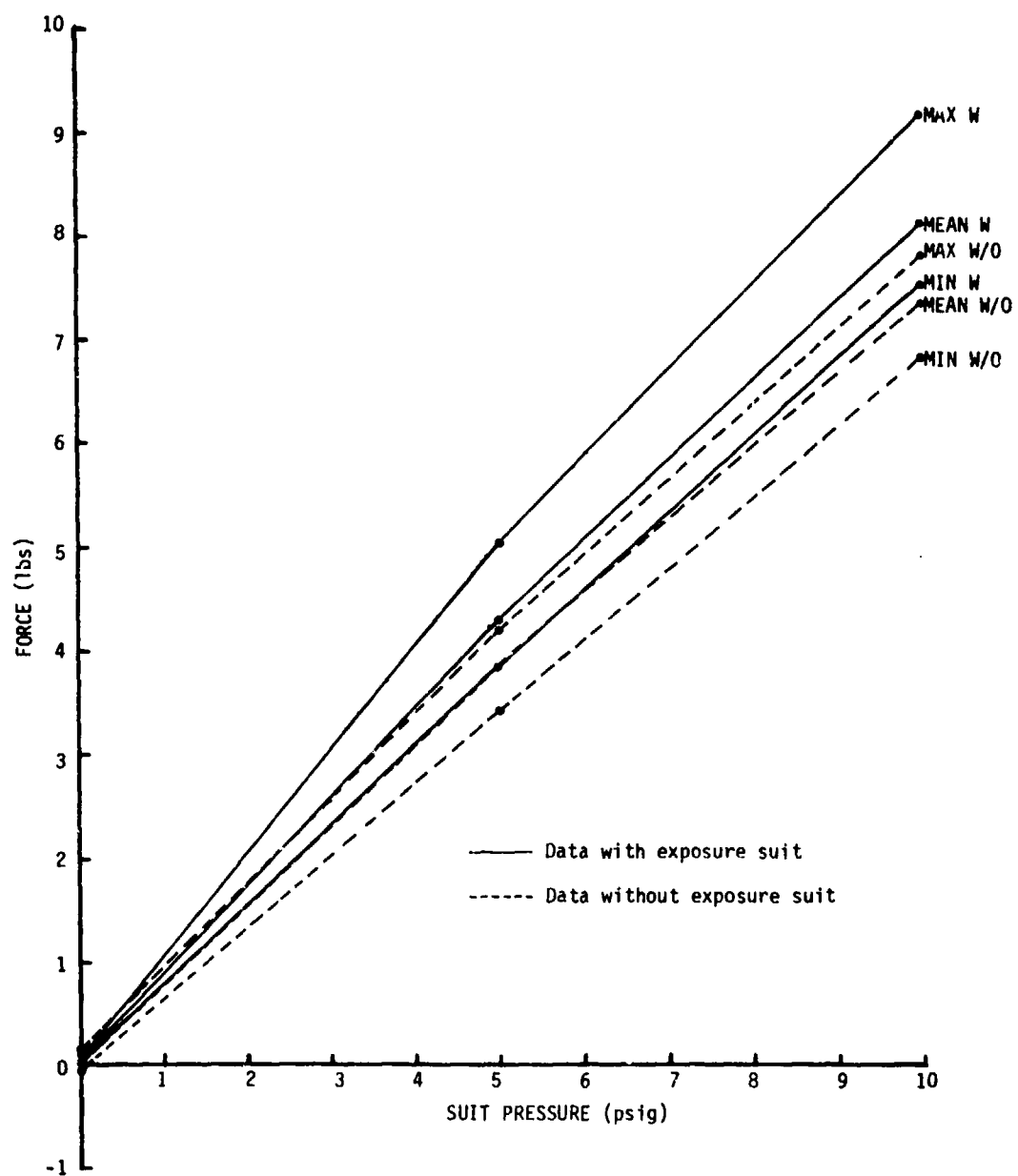


Figure 89. Normalized exposure suit left thigh force.
[Key: W = with suit; W/O = without suit.]

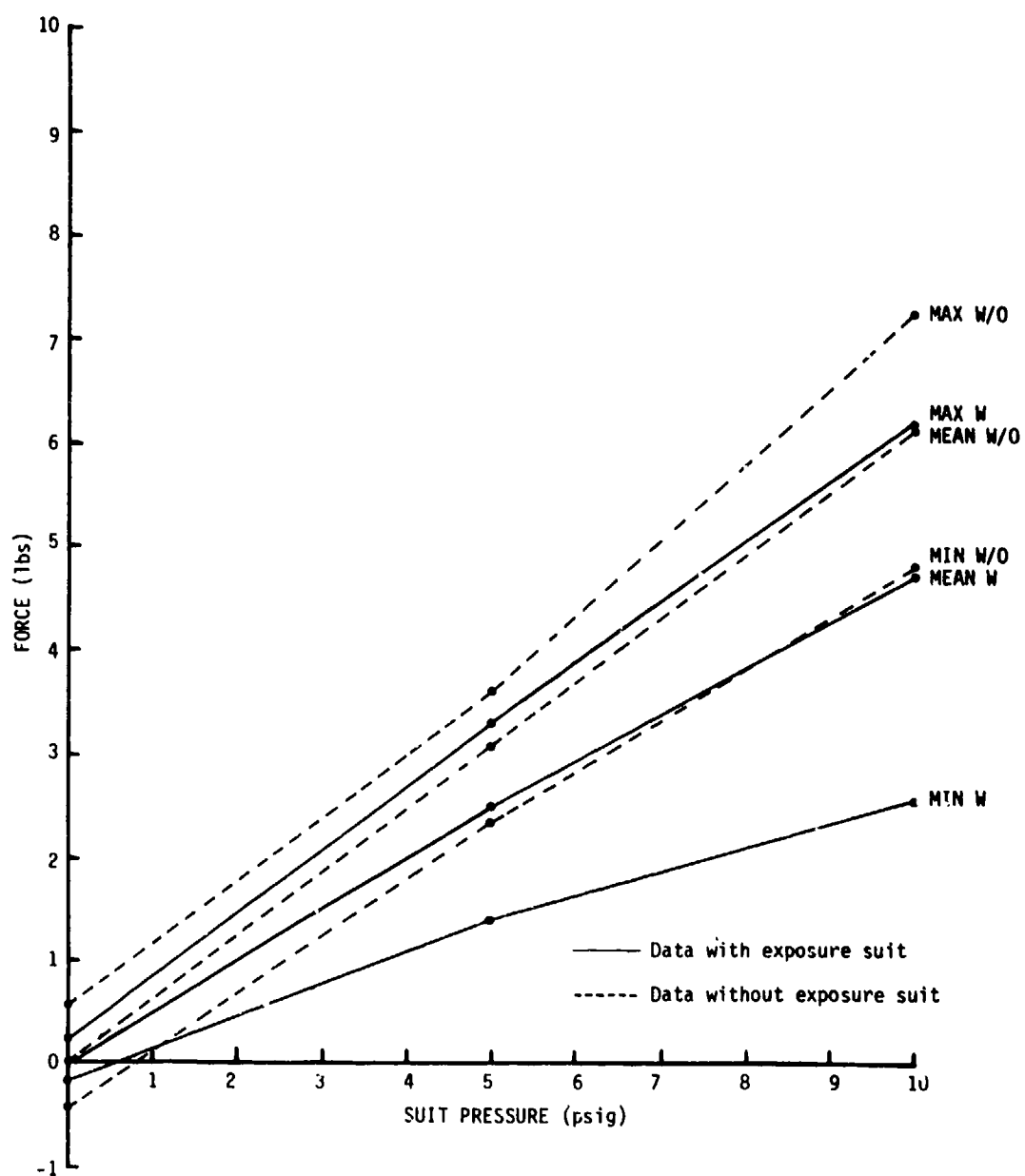


Figure 90. Normalized exposure suit right calf force.
[Key: W = with suit; W/O = without suit.]

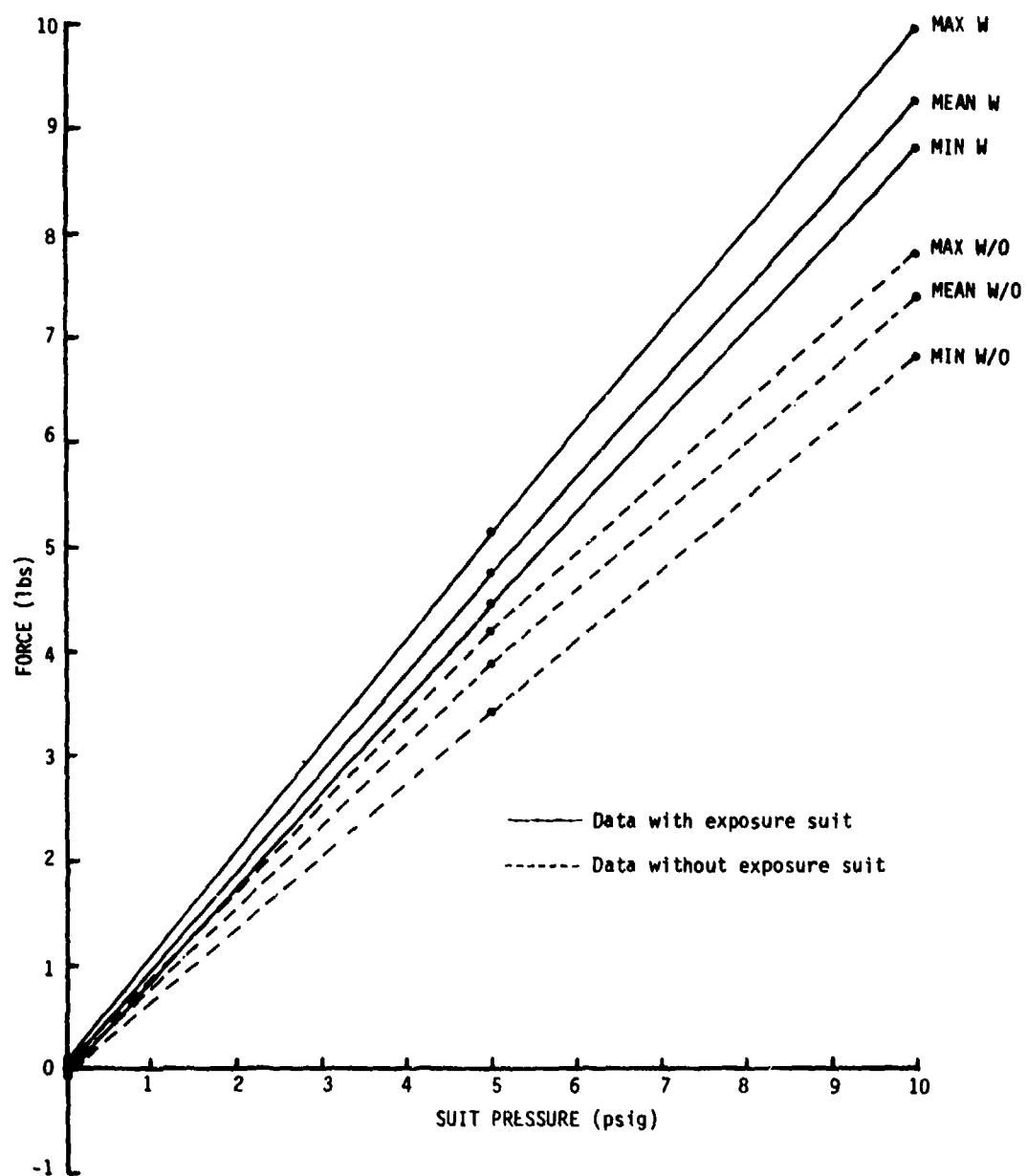


Figure 91. Normalized exposure suit left calf force.
[Key: W = with suit; W/O = without suit.]

2.2 G-Sensitivity Evaluation of the Statham PM131TC Pressure Transducer

The purpose of this test was to quantify the acceleration sensitivity of the Statham model PM131TC pressure transducer (Gould, Inc., Measurement Systems Div., Oxnard, Calif.). Linearity and sensitivity were also evaluated.

2.2.1 Test Configuration for the PM131TC Pressure Transducer

All tests were conducted with the transducer installed in the gondola of the USAFSAM human centrifuge. Pressure stimulus was provided by the Datametrics pressure calibration system, installed in the gondola [Datametrics (a subsidiary of ITE Imperial Corp.), 340 Fordham Rd., Wilmington, Mass. 01887]. All stimulus pressures were maintained at the stated value, ± 0.02 psig. Excitation for the transducer was applied through the centrifuge slip-rings from a laboratory power supply located in the control room and maintained at $+5.0 \pm 0.02$ VDC. For purposes of acceleration testing, the axes of the transducer were defined as: +Z with the pressure port vertical and on top of the transducer, +X parallel to a line from pin 4 to pin 2, and +Y parallel to a line from pin 3 to pin 4. The PM131TC was so mounted in the gondola as to experience the same acceleration forces as the gondola accelerometer.

2.2.2 Test Protocol of the PM131TC Pressure Transducer

The linearity and sensitivity of the PM131TC were determined by manually recording the transducer's response to stimulus (in 1.0-psig steps) from 0 to 20 psig, both ascending and descending. The acceleration sensitivity was determined by subjecting the transducer to three ascending and three descending 0.1 G/sec acceleration profiles from 1 to 11 G along each axis, in each direction, with 0-, 10-, and 18-psig stimulus applied. This protocol resulted in 108 recorded acceleration data runs.

2.2.3 Data-handling Techniques for the Performance Evaluation of the PM131TC Pressure Transducer

The data from the linearity and sensitivity tests were analyzed using a TI59 hand calculator. First, the mean and hysteresis were calculated, in 1-psig steps, for each ascending and descending pressure pair. The maximum hysteresis in all six sets of data was determined in 1-psig steps. Finally, a 62-point (the 63rd point was lost) linear regression was run of the ascending and descending means first calculated.

Data from the G-sensitivity tests were recorded on analog magnetic tape, converted to digital data in the USAFSAM/BRP analog laboratory. The digitized data was then processed through the BRP digital facilities. All data in each set (for three ascending and three descending runs, testing a particular axis sensitivity at a particular pressure stimulus) were normalized to the mean of all 1-G data. The mean and the $\pm 3\sigma$ points for all higher G levels in that set were then calculated and plotted (Figs. 92 - 109). In each case, the abscissa represents the acceleration level, while the ordinate represents the deviation in equivalent psig from the 1-G output of the transducer.

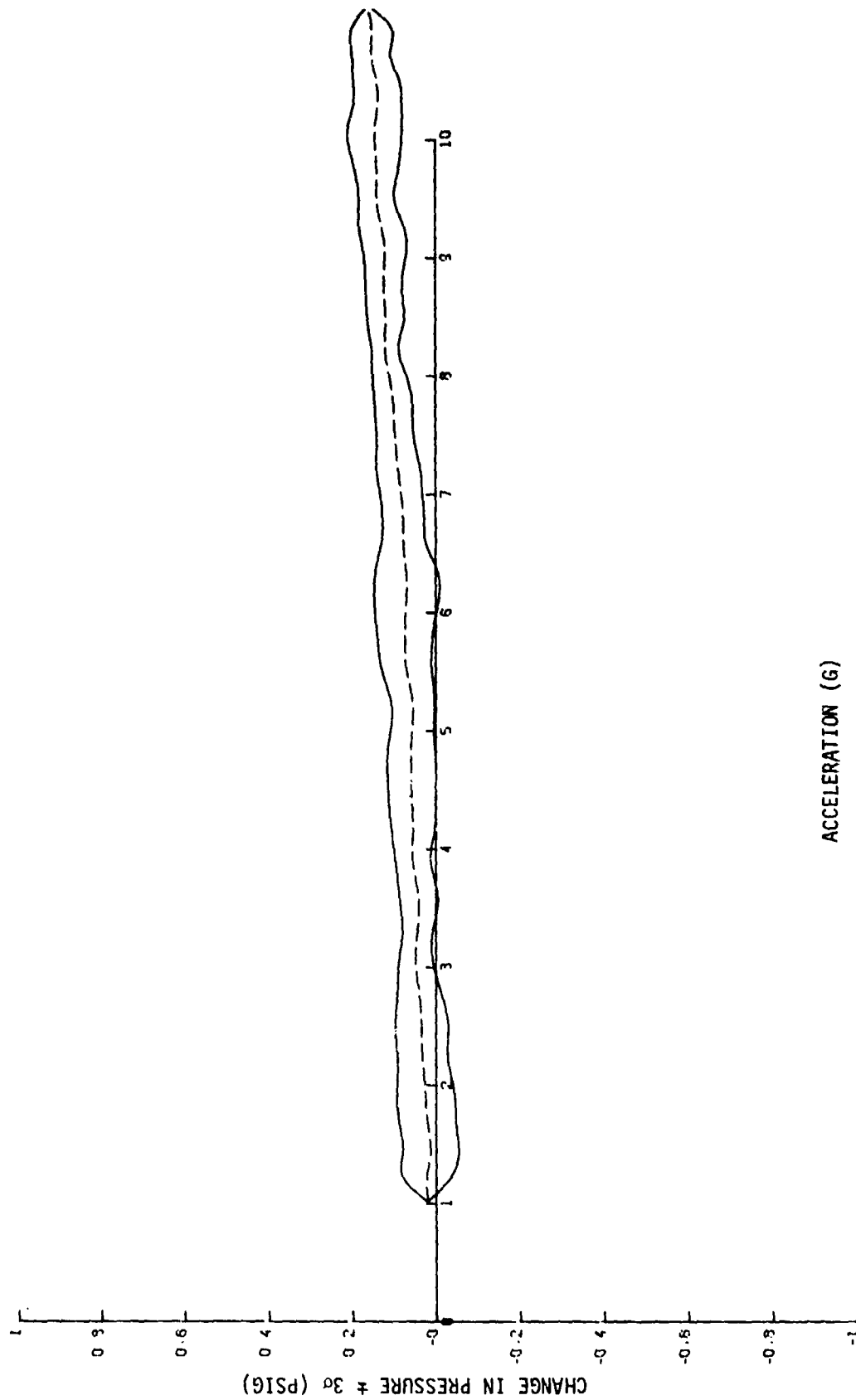


Figure 92. Acceleration influence on the +Z axis of the PM131TC-3644 transducer with 0-psig stimulus.

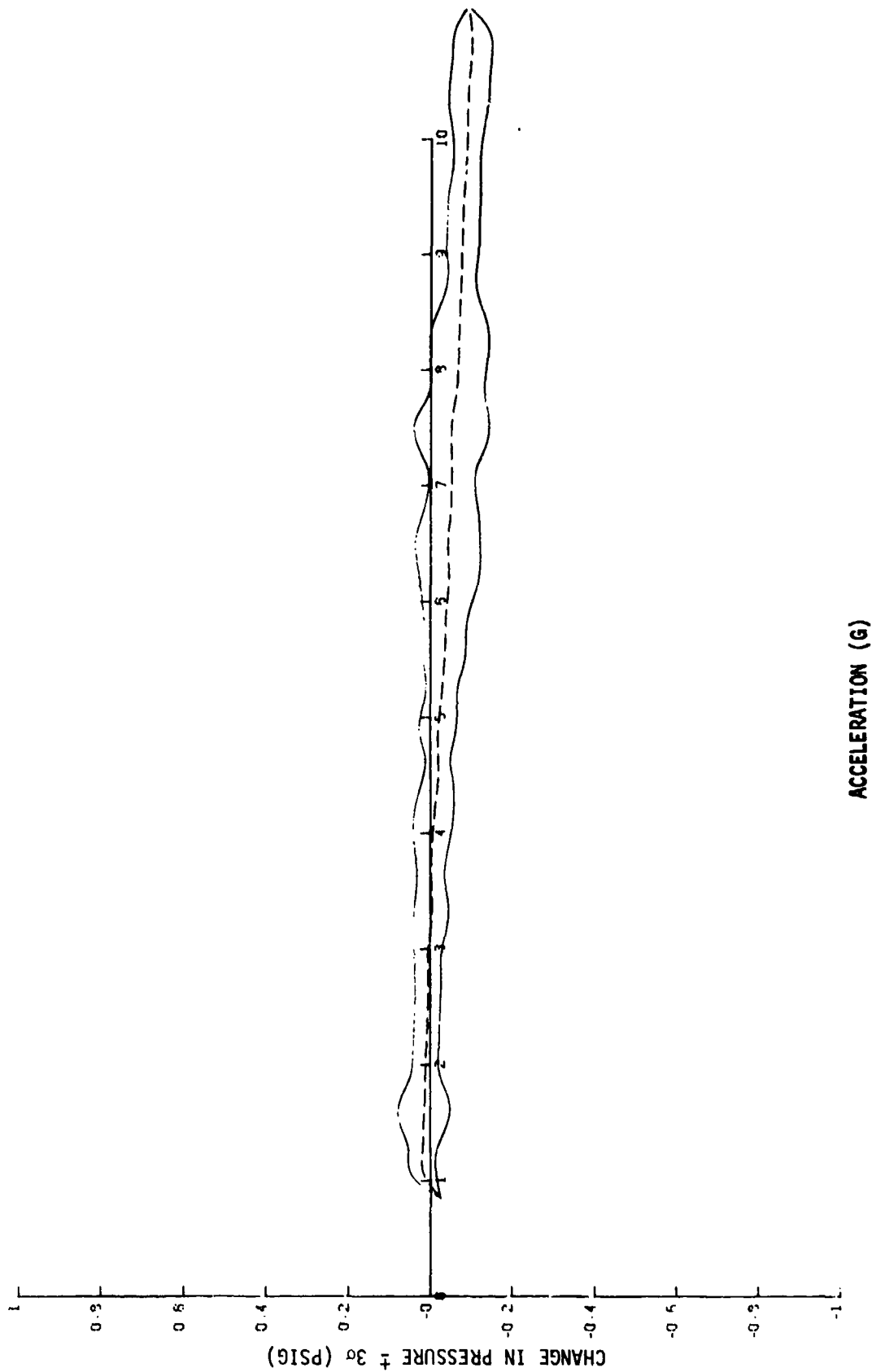


Figure 93. Acceleration influence on the -Z axis of the PM131TC-3644 transducer with 0-psig stimulus

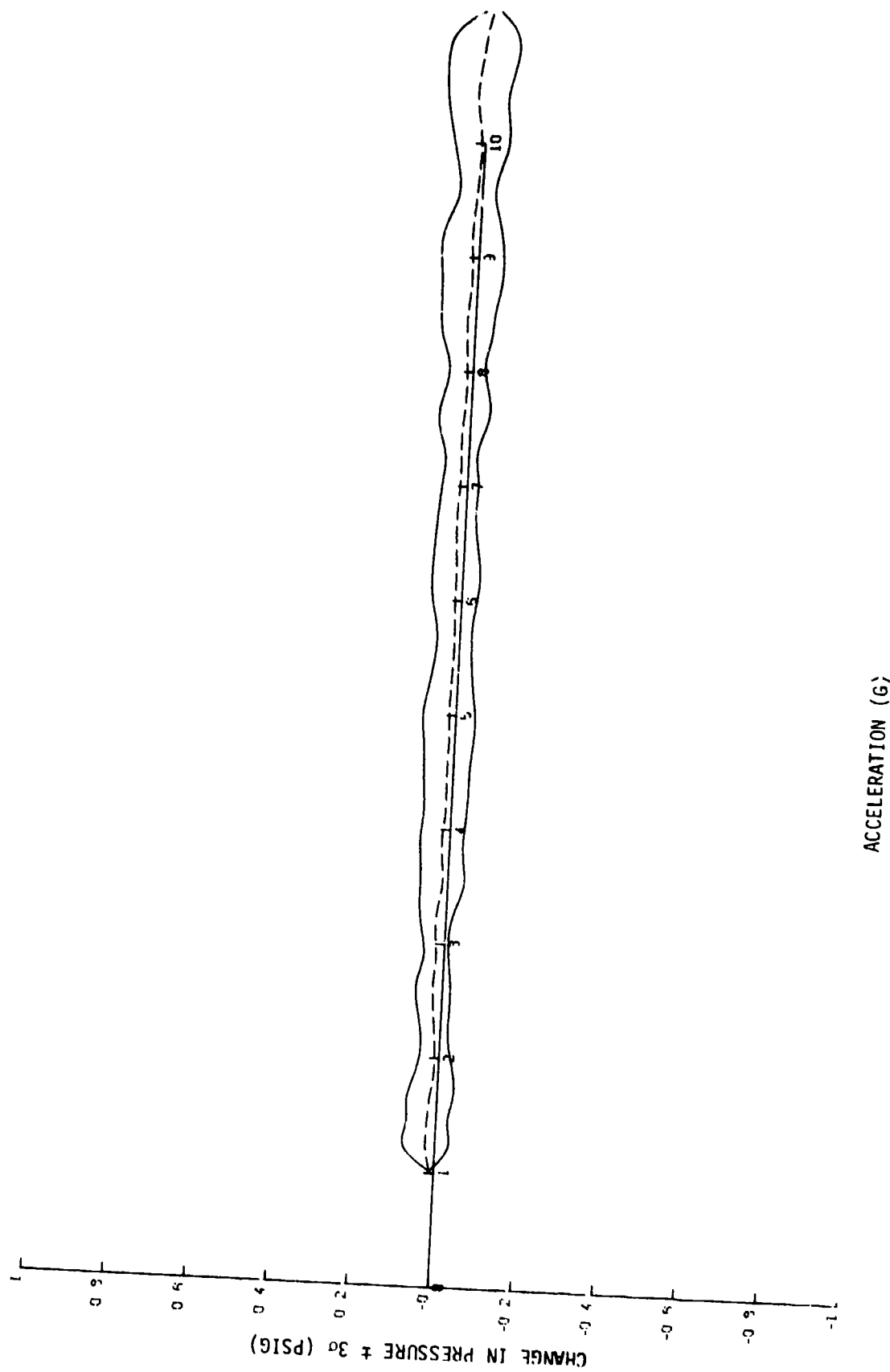


Figure 94. Acceleration influence on the +Y axis of the PM131TC-3644 transducer with 0-psig stimulus

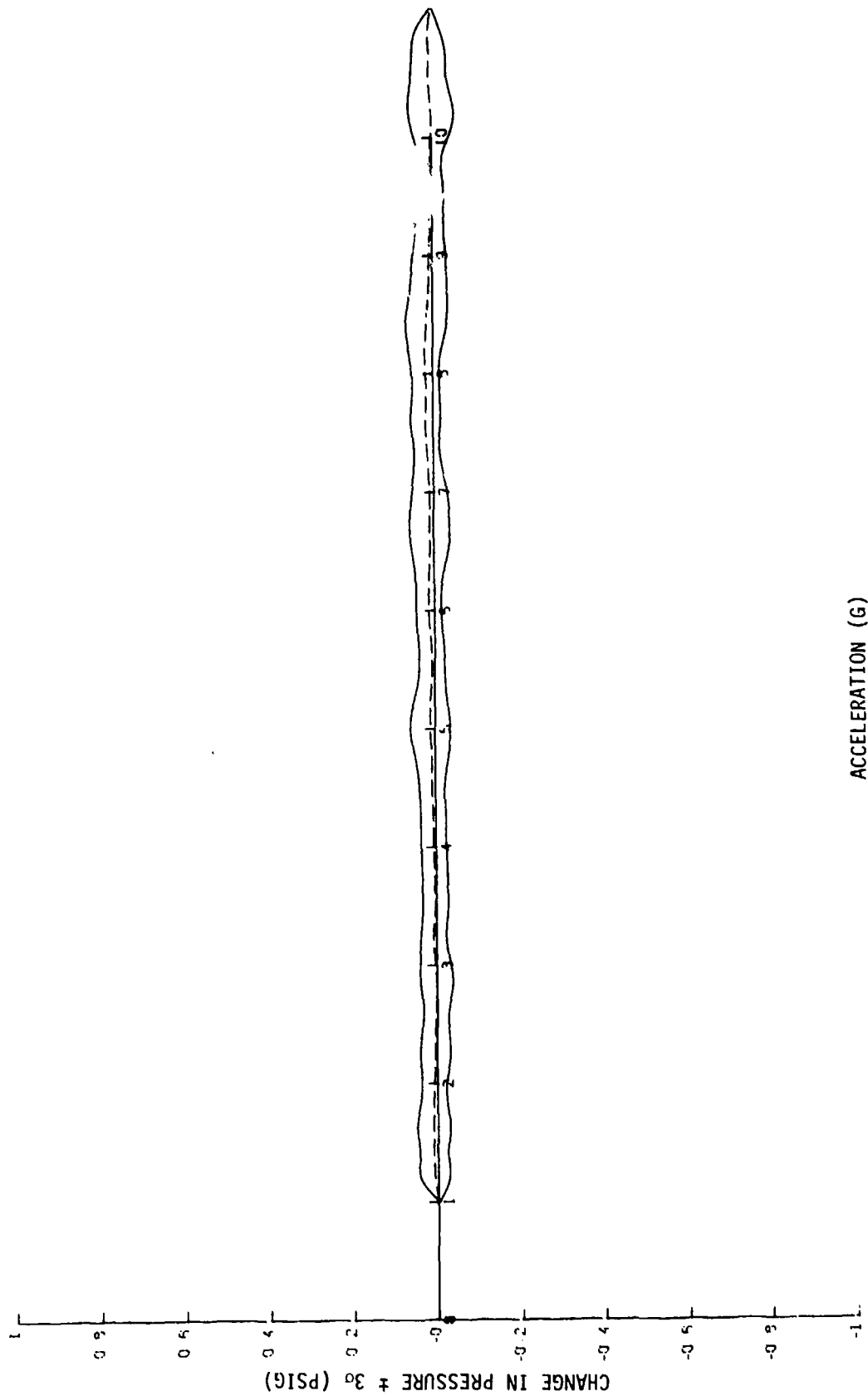


Figure 95. Acceleration influence on the -Y axis of the PM131TC-3644 transducer with 0-psig stimulus.

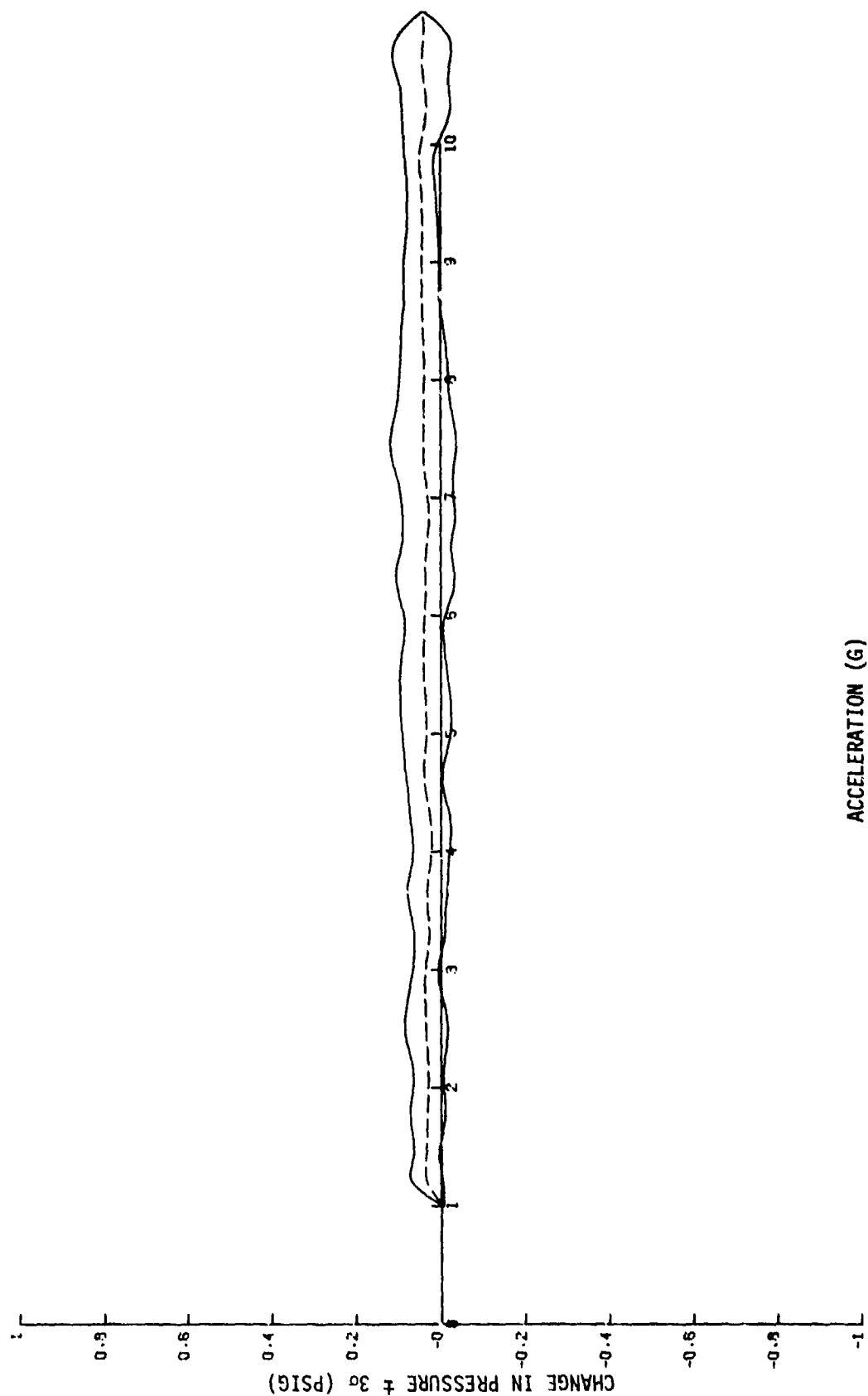


Figure 96. Acceleration influence on the +X axis of the PM131TC-3644 transducer with 0-psig stimulus.

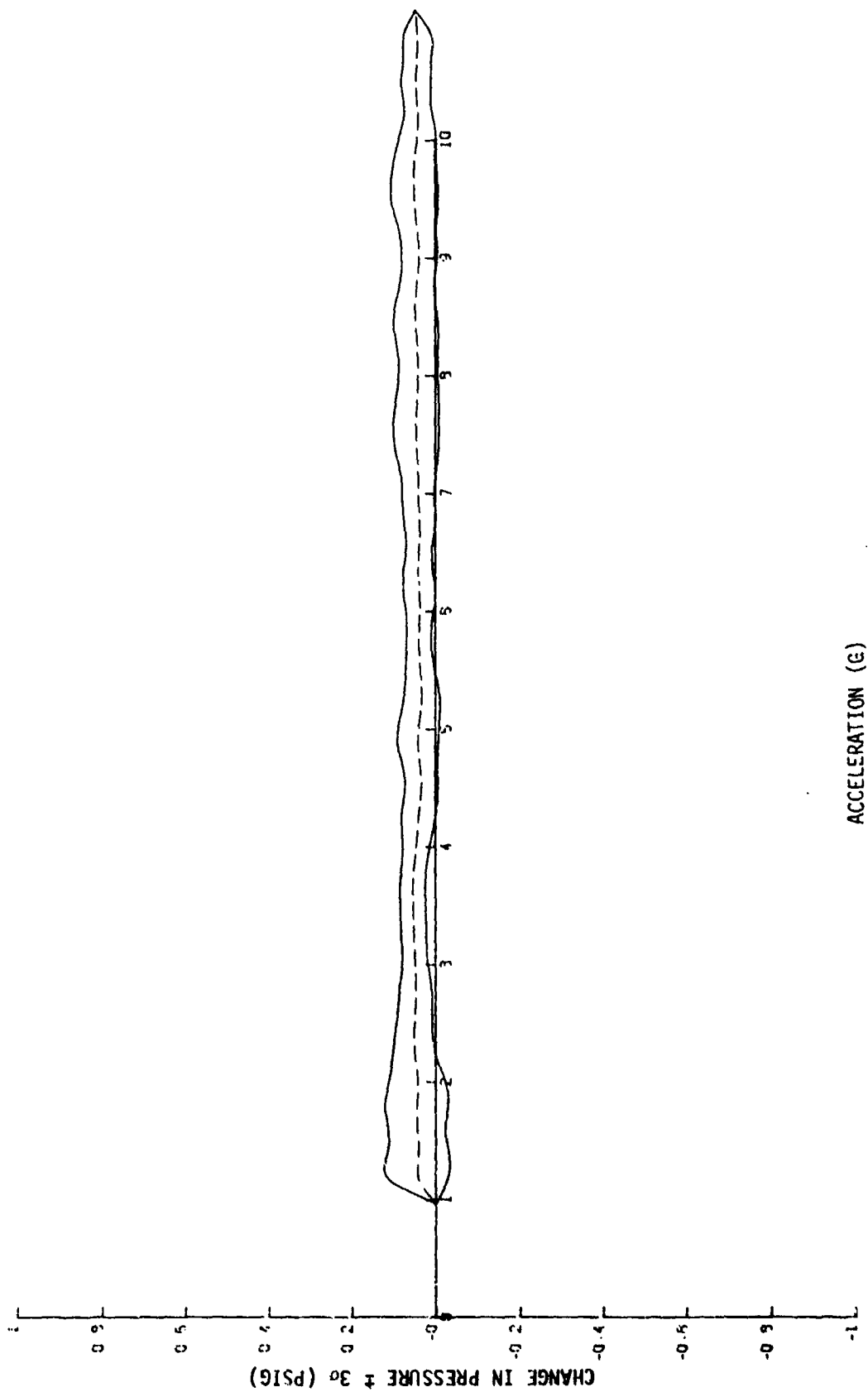


Figure 97. Acceleration influence on the -X axis of the PM131TC-3644 transducer with 0-psig stimulus

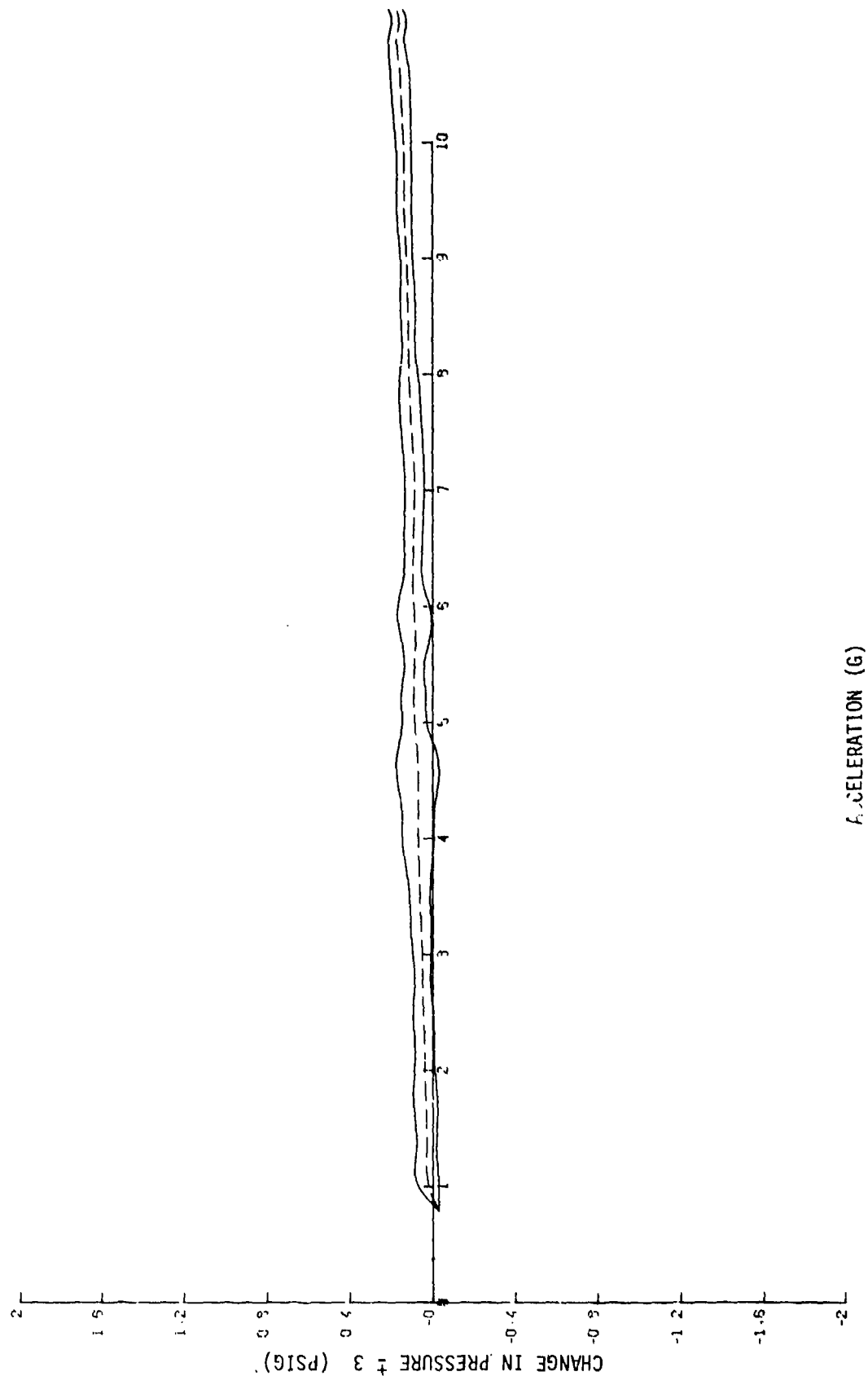


Figure 98. Acceleration influence on the +Z axis of the PM131TC-3644 transducer with 10-psig stimulus.

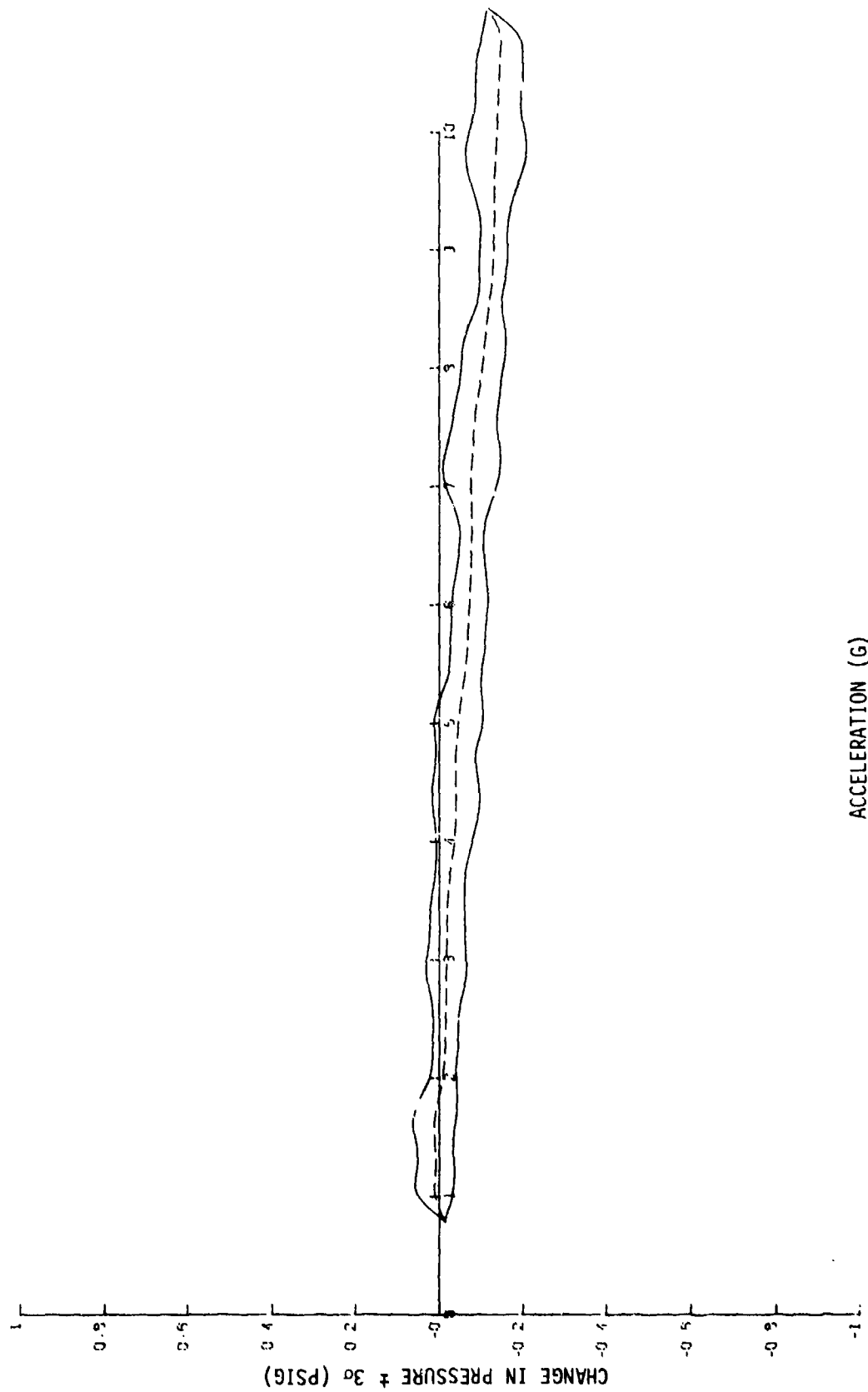
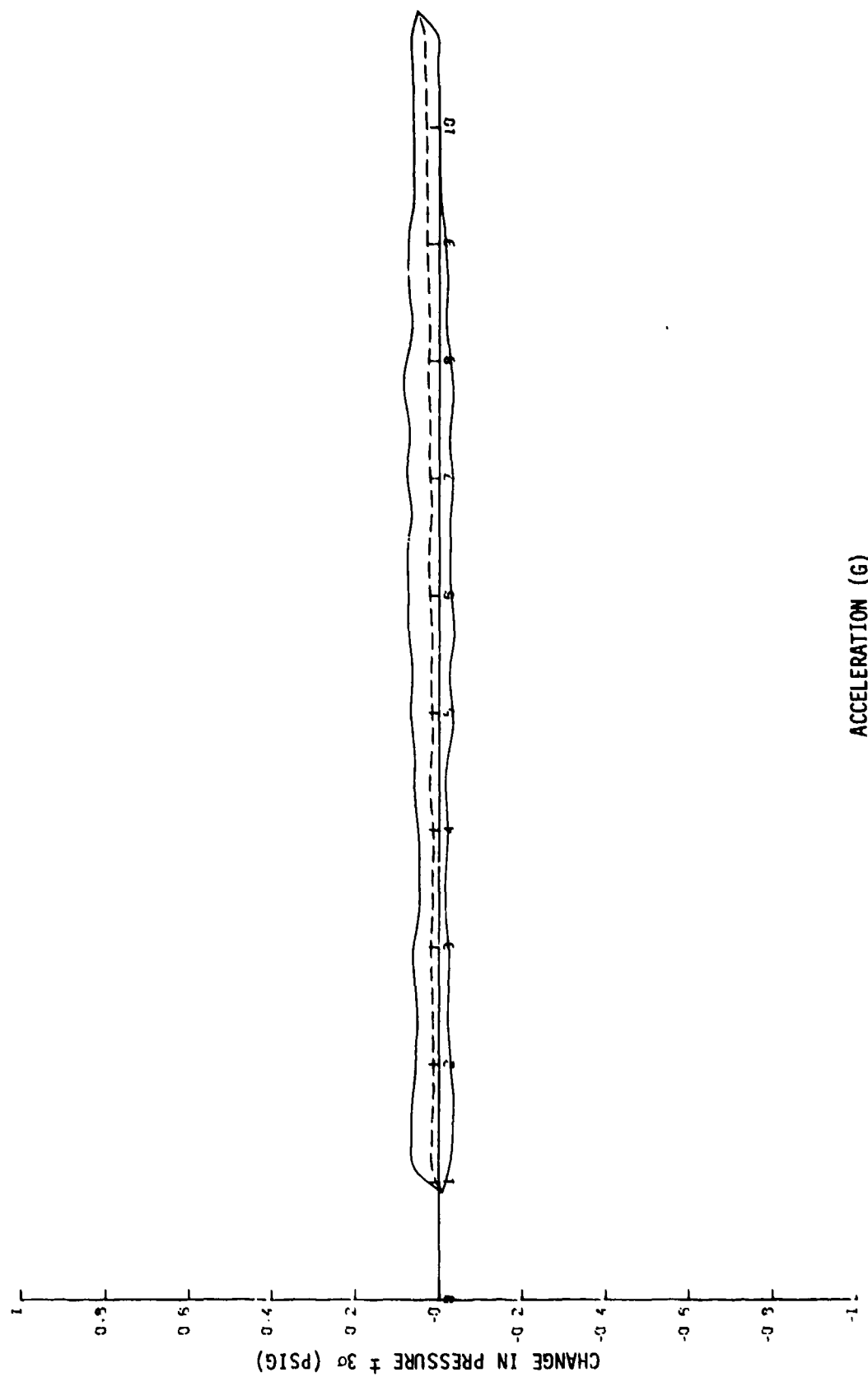


Figure 99. Acceleration influence on the -Z axis of the PM131TC-3644 transducer with 10-psig stimulus.



ACCELERATION (G)

Figure 100. Acceleration influence on the +Y axis of the PM131TC-3644 transducer with 10-psig stimulus.

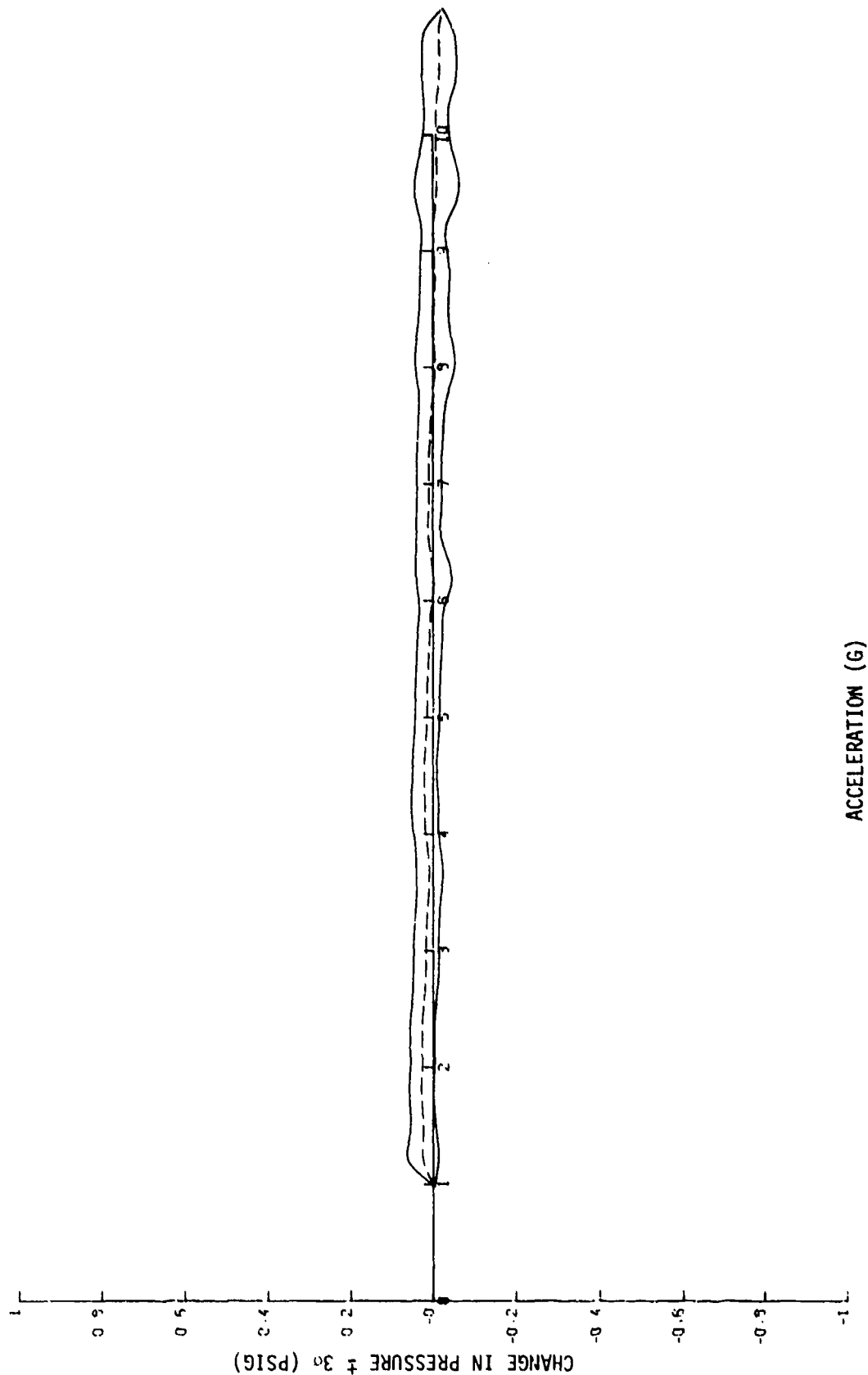


Figure 101. Acceleration influence on the -Y axis of the PM131TC-3644 transducer with 10-psig stimulus.

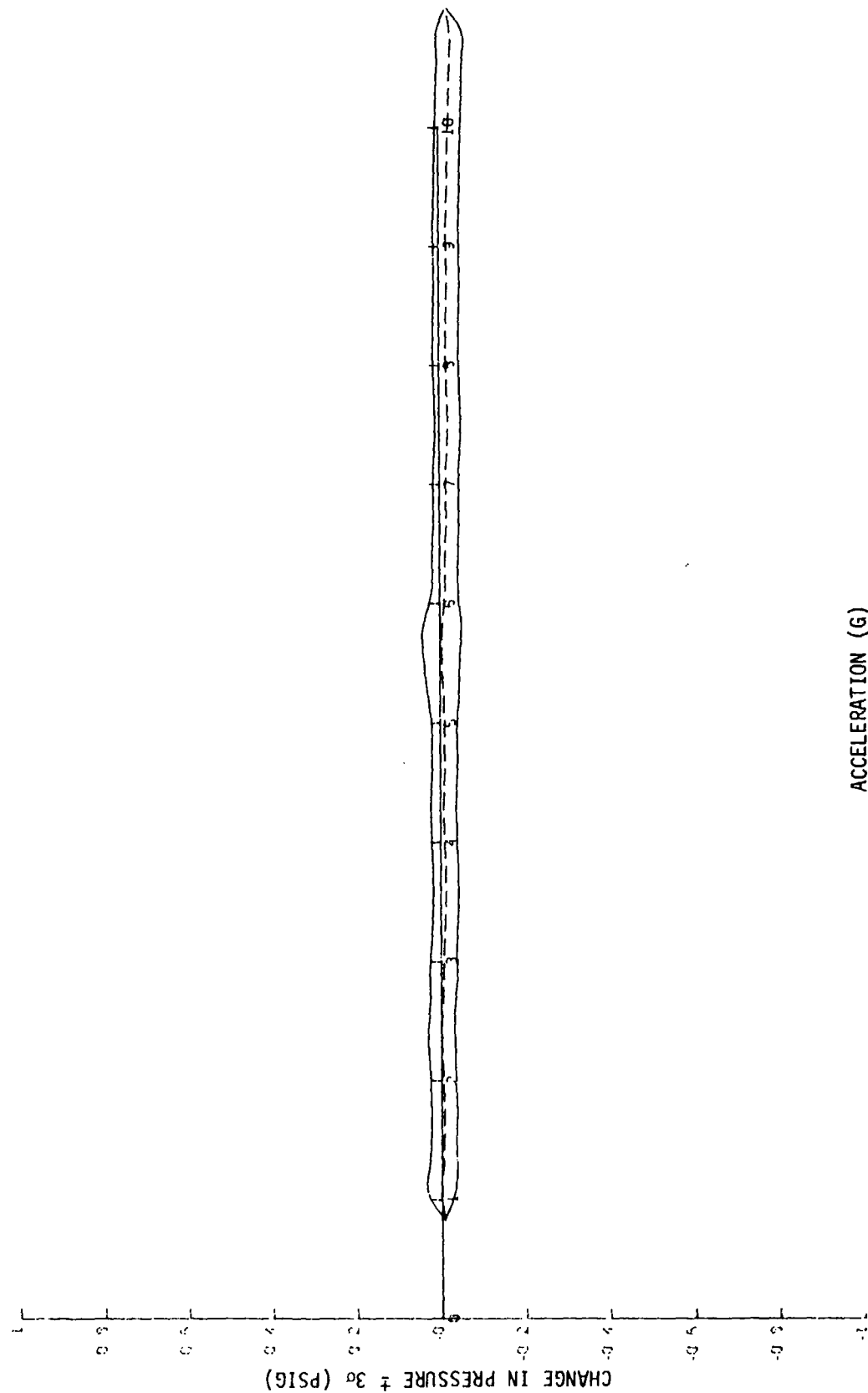


Figure 102. Acceleration influence on the +X axis of the PM31TC-3644 transducer with 10-psig stimulus.

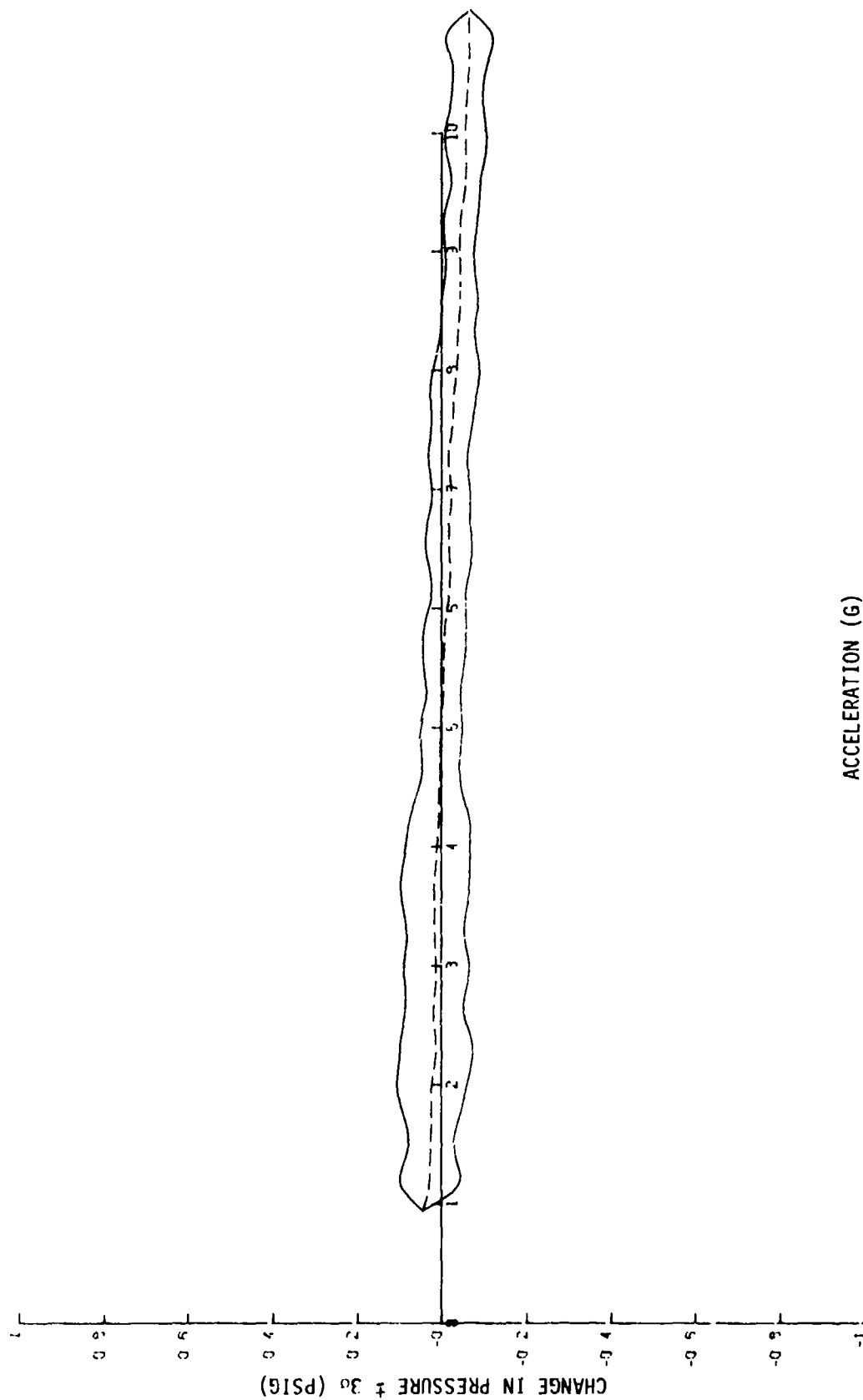


Figure 103. Acceleration influence on the -X axis of the PM131TC-3644 transducer with 10-psig stimulus.

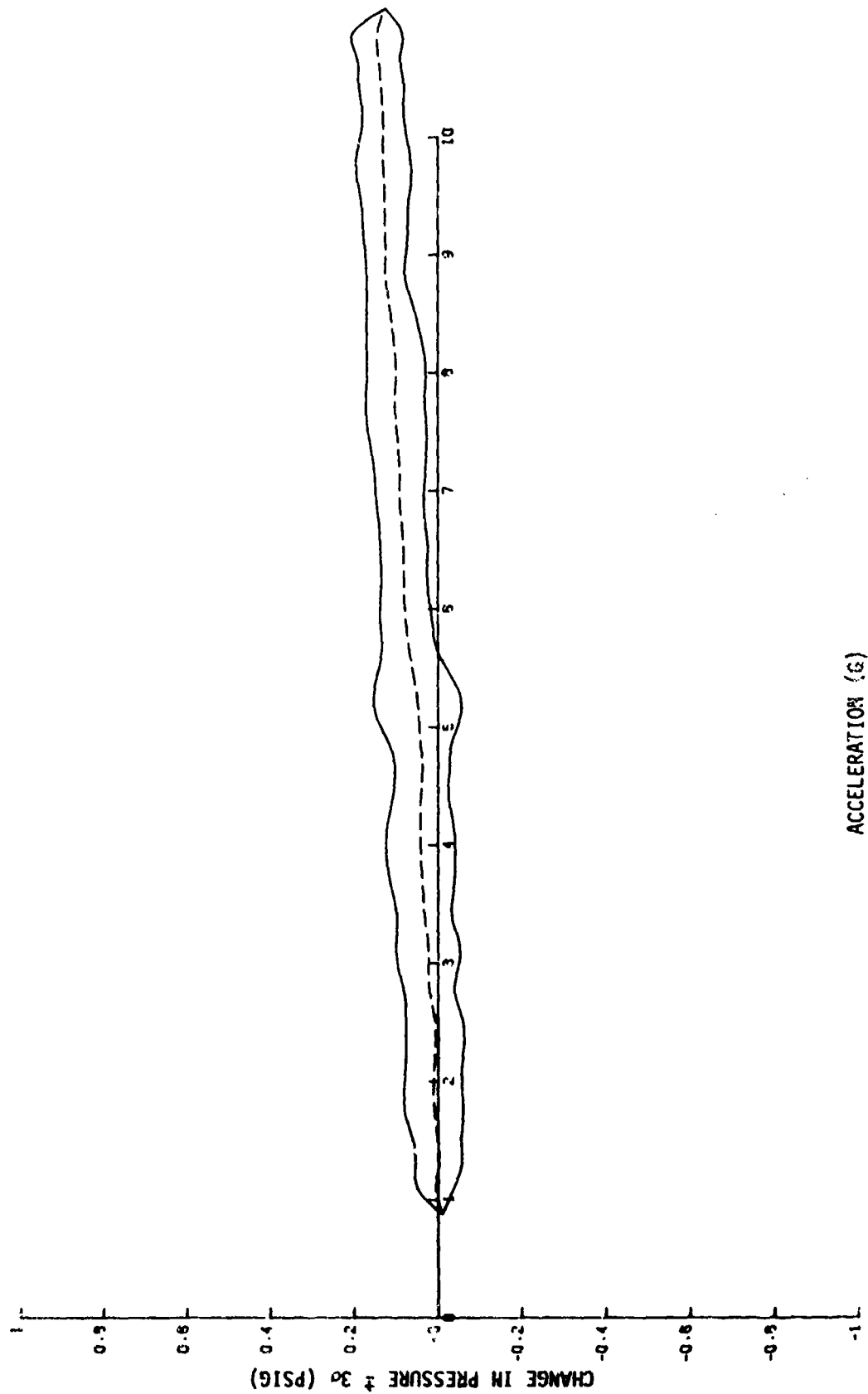


Figure 104. Acceleration influence on the +Z axis of the PM1311C-3644 transducer with 18-psig stimulus.

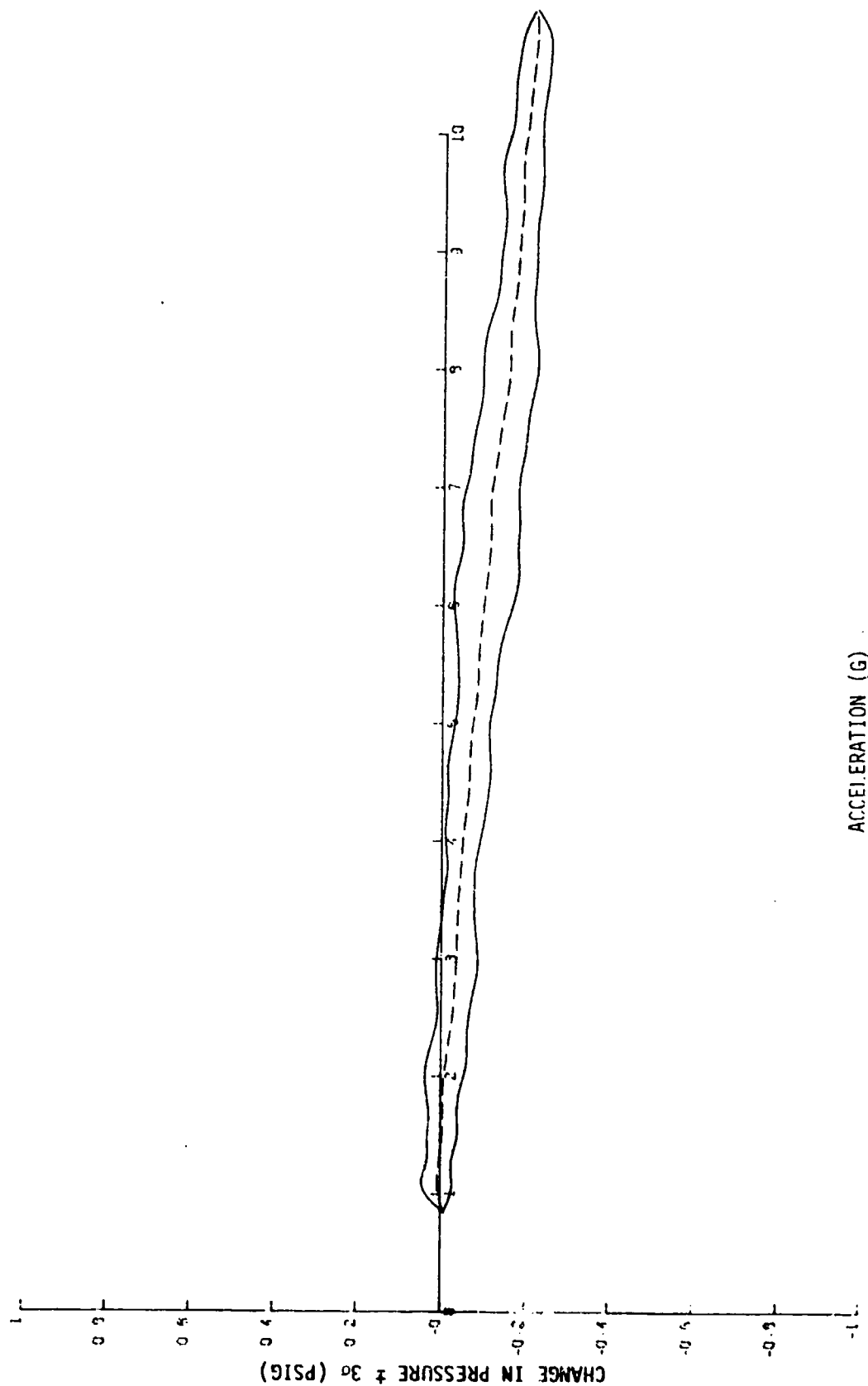


Figure 105. Acceleration influence on the -Z axis of the PM131TC-3644 transducer with 18-psig stimulus.

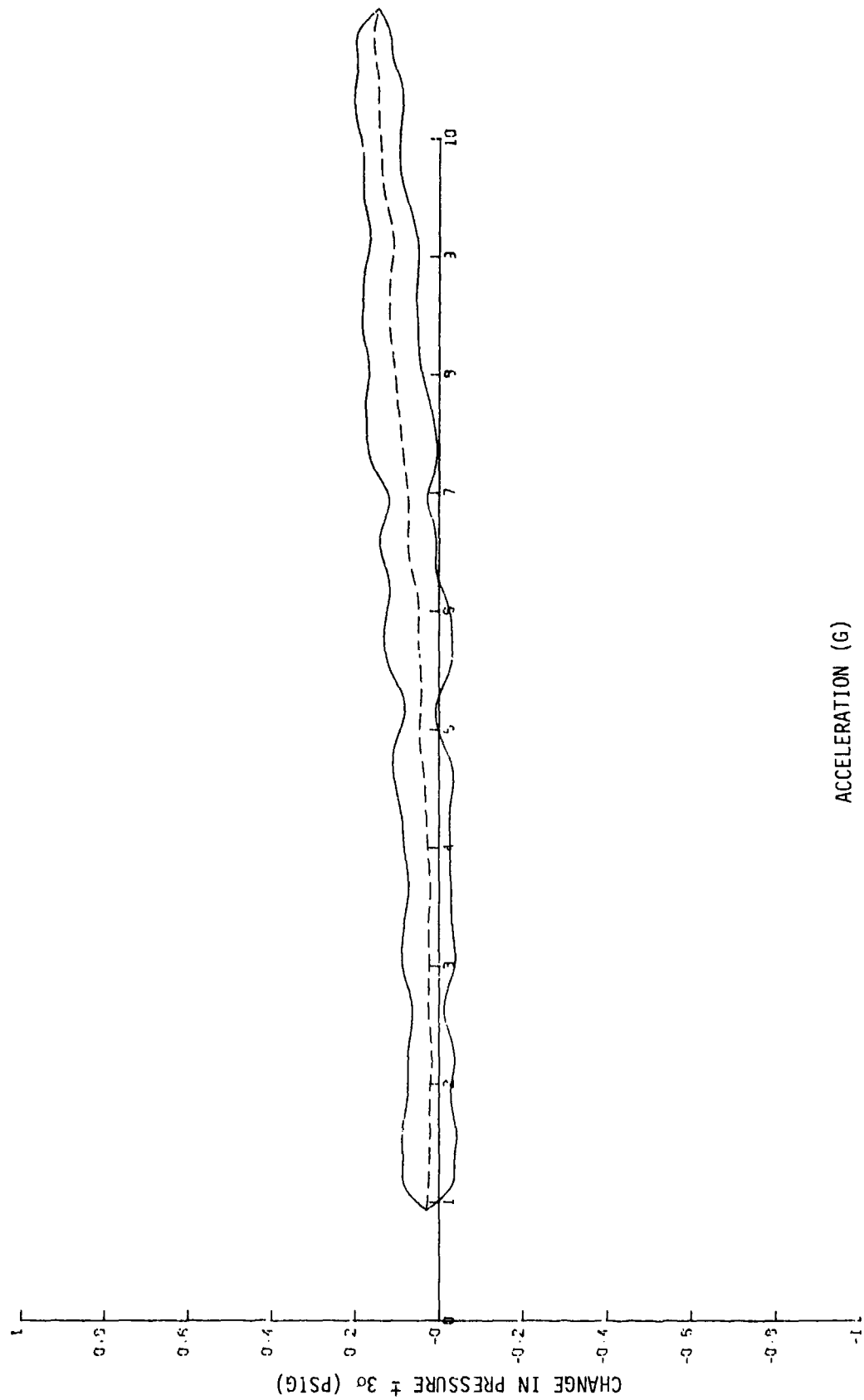


Figure 106. Acceleration influence on the +Y axis of the PM131TC-3644 transducer with 18-psig stimulus.

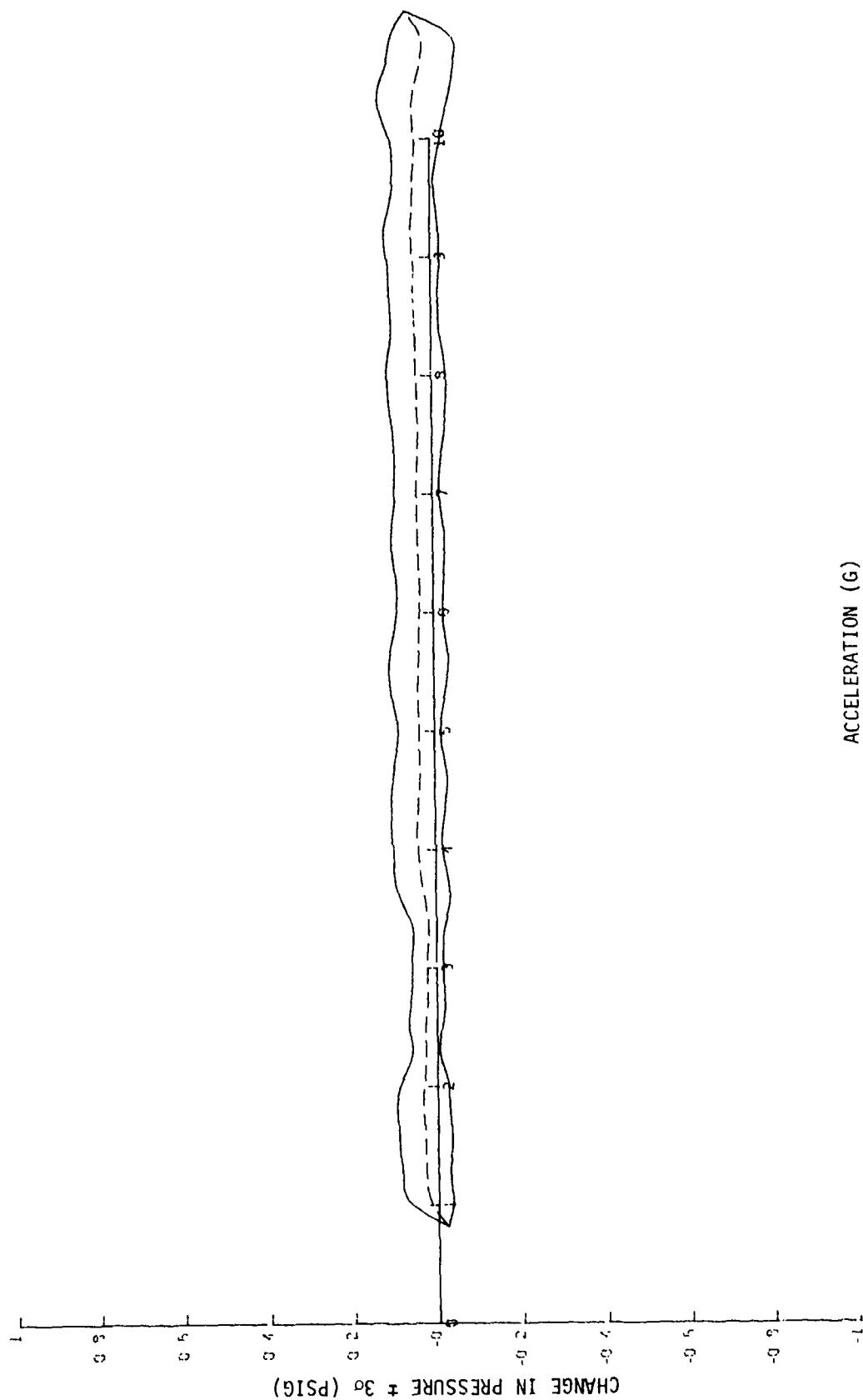


Figure 107. Acceleration influence on the -Y axis of the PM131TC-3644 transducer with 18-psig stimulus.

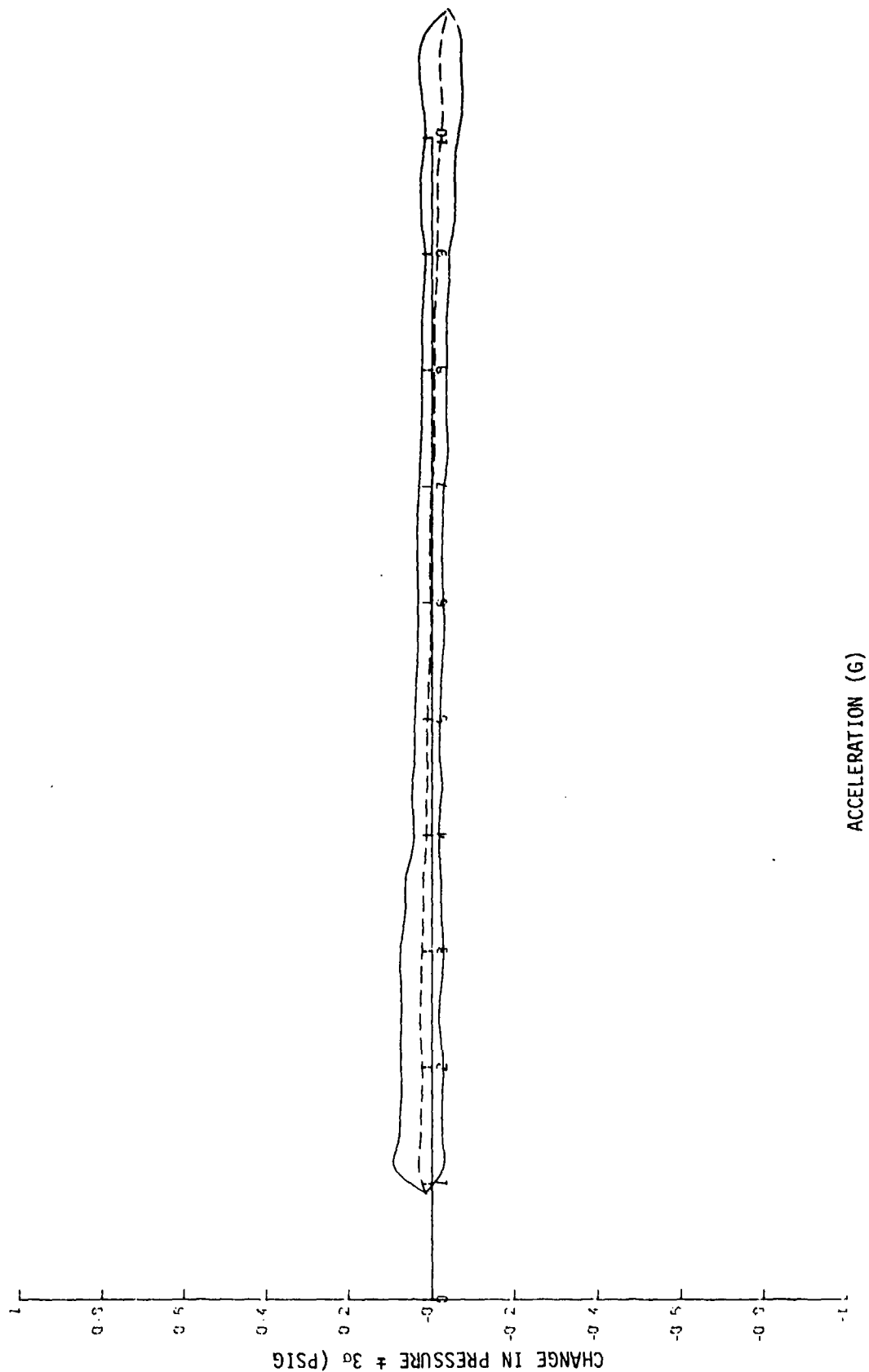


Figure 108. Acceleration influence on the +X axis of the PM131TC-3644 transducer with 18-psig stimulus.

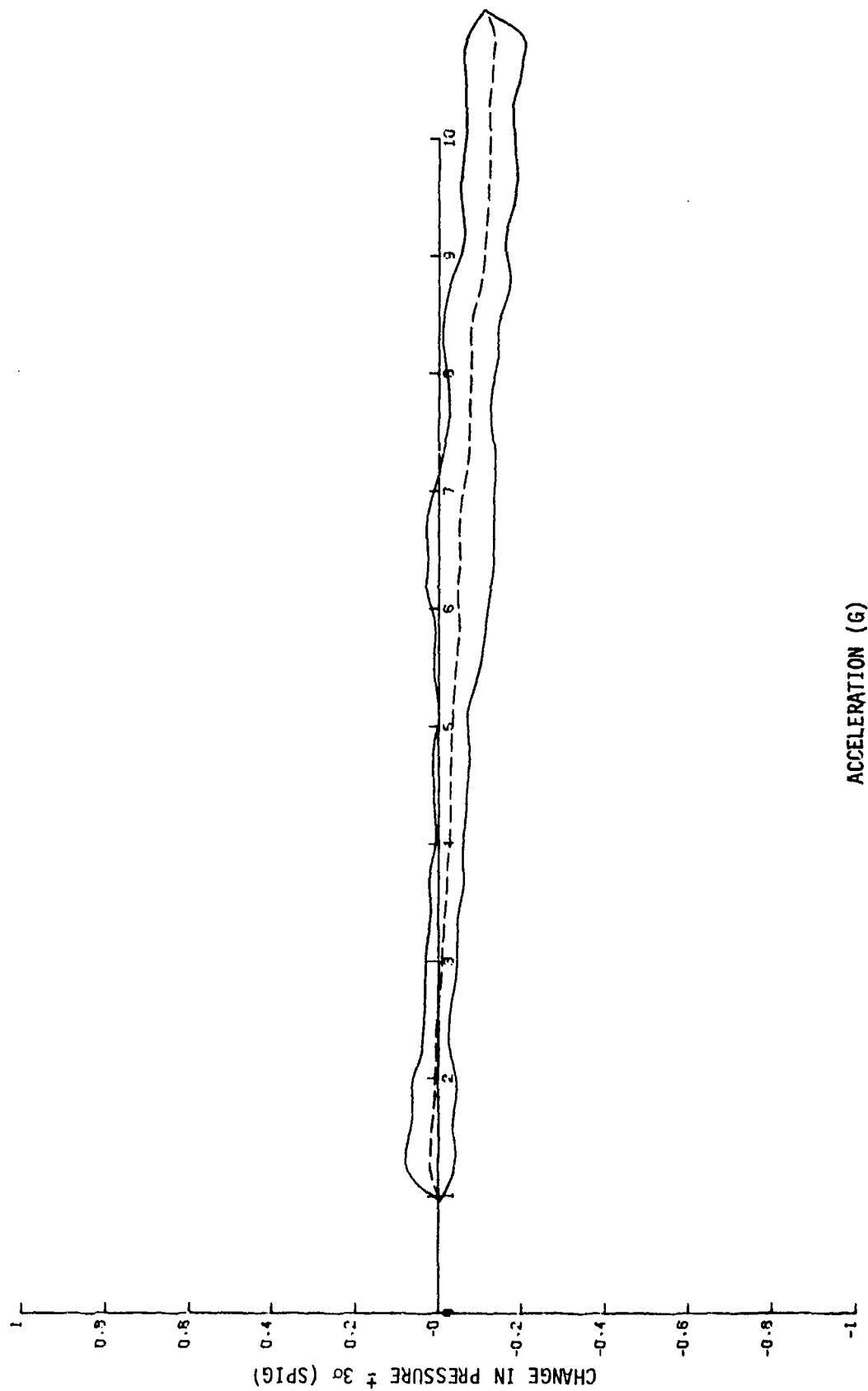


Figure 109. Acceleration influence on the -X axis of the PM131TC-3644 transducer with 18-psig stimulus.

2.2.4 Performance Evaluation of the PM131TC Pressure Transducer

The PM131TC (serial no. 3644), using 5.00 VDC excitation, responds as:

$$E = 0.9415 P + 0.6458,$$

where E is the output voltage in millivolts, and P is the pressure stimulus in pounds per square inch. The maximum hysteresis was 0.04 mV at 6 psig, constituting 0.13% of full scale. The maximum deviation from the least squares straight line through the data was found at the same point and was 0.06% of full scale.

The only axis indicating any significant acceleration sensitivity was the Z axis, with up to 1% of full-scale (i.e., up to 0.2 psig) error occurring (i.e., a maximum of 0.1%/G, or 0.02 psig/G). The -X axis and +Y axis show inconsistent tendencies to respond to acceleration but at lower levels. Since these errors, at 10 G, are on the order of ten times the apparent accuracy of the transducer, the investigator is cautioned to consider their effect on his data.

2.3 Ready Pressure AGV Mannequin Test

The performance of the ready pressure valve (RPV) has been tested and analyzed by SVTP and GVALVPGM (refer to Vol. I, section 5.4). The obvious extension of that analysis is to investigate the application of the protective pressure at the equipment-subject interface.

That interface was simulated using a CSU-13A/P anti-G suit on a Fiberglas mannequin. The transfer of protective pressure was monitored, using four force gages located on the abdomen, left thigh, right thigh, and right calf.

2.3.1 RPV Mannequin Test Protocol

The RPV mannequin (RPM) test was conducted in four phases on the USAFSAM human centrifuge. During each phase, a CSU-13A/P AGS was mounted on a Fiberglas dummy which was equipped with surface force gages. These force gages were on the abdomen, left thigh, right thigh, and right calf. The mannequin was mounted in an upright seat in the centrifuge gondola. (The instrumentation configurations and calibration are essentially described in Vol. I, section 3; and in Vol. II, section 2.1.)

Phase I generated the ideal (I) or control case which served as a baseline for detecting change in performance. In this phase, the valve-suit-mannequin system was subjected to three trapezoidal 0.1 G/sec G profiles. The source pressure to the AGV during this phase was 125 psig.

Phase II generates the median (D) data set, using a valve source pressure of 125 psig, and a set of three 1.5 G/sec (High G) trapezoidal G profiles (i.e., a linear increasing G profile followed by a linear decreasing G profile).

Phase II generates the maximum (X) data set, using 300 psig for valve source pressure and a High G profile set.

Phase IV generates the minimum (N) data set, using 30-psig source pressure with the High G profiles.

2.3.2 Description of the RPV Mannequin Test Data

Analog data recorded at the USAFSAM/VNB centrifuge facility is converted to digital data, using the USAFSAM/BRP analog-to-digital support facility. The digitized data, recorded on magnetic tape, serves as a data base for the RPM program. The 0.1 G/sec onset data (group I) is digitized at 20 samples/sec, thus giving approximately 2,000 samples for one increasing or decreasing low-G-onset data set. The 1.5 G/sec onset data (groups D, X, and N) are digitized at 80 samples/sec, which gives approximately 500 samples for one increasing or decreasing high-G-onset data set.

The six channels of data digitized and processed by the RPM program are:

- a) acceleration;
- b) suit pressure;
- c) abdomen force;
- d) left thigh force;
- e) left calf force; and
- f) right thigh force.

The data sets collected consisted of:

a) five sets of data, collected as calibration (CAL) runs; those CAL runs pertinent to this study are:

Run 1--acceleration at 1 G, suit pressure at 0 psig, and the four force-gage channels at 0 psi;

Run 2--acceleration at 10 G and suit pressure at 10 psig; and

Run 5--the four force-gage channels at 9 psi;

b) a total of six data sets, collected on each of the four test cases listed in section 2.3.1--three on the increasing slope of the trapezoidal profile, interspaced with three sets collected on the decreasing slopes. Prior to digitizing the test data set, the CAL runs were digitized at the sampling rate required by the G-onset rate used in the particular test case. In all test cases, data were collected at G-intervals of: 1 - 11 G (increasing), and 11 - 1 G (decreasing). The G intervals used in the RPM program are: 1 - 10 G (increasing), and 10 - 1 G (decreasing).

2.3.3 Data Analysis

The computer program designed to analyze these data is designated the "RPM Program." It assumes the first sets will be the CAL runs, and reduces them to an arithmetic mean and a standard deviation. The standard deviation is checked for excessive variance (a value of greater than 2.5333). If excessive variance is found in the CAL runs, the following data are considered invalid and new data are required for further processing. Otherwise, RPM begins data processing.

Then, each test data set is calibrated using the means reduced from the CAL runs, and is assigned the values of the standards stimulating that channel on that run. The formulas utilized in data calibration are:

$$G1 = (RH - RL) / (CH - CL)$$

$$G2 = RH - (G1) \times (CH).$$

Then, the calibrated value = $G1 \times (\text{digitized value}) + G2$,

where RH = real high,

RL = real low,

CH = actual calibrated high, and

CL = actual calibrated low.

Values used for normalizing the force gage channels to the suit pressure channel are then calculated. These values are taken directly from the calibrated data sets, according to the following formulas on each test data set:

$$\text{NORM1} = N_L = \text{Low norm value} = \frac{\text{sum of first val of 3 incr G runs}}{3}$$

$$\text{NORM2} = N_H = \text{High norm val} = \frac{\text{sum of first val of 3 decr G runs}}{3}$$

The remainder of the RPM Program works with data points selected from the calibrated data sets. From each channel, of each run, for each whole G value (i.e., 1, 2, ..., 10), a mean is calculated for digitized data within the span $G \pm 0.05$. These mean values are then entered into an array designated the "H" array.

Each column pair (i.e., the ascending and descending partners in a trapezoidal profile) of the H array is normalized according to the formula:

$$Ci = (Fi - F1) (N_H - N_L) / (F_N - F_1) = N_L,$$

in which

Ci = corrected array element value,

Fi = original array element value,

F_1 = the first array element in the ascending column (corresponds in time to N_L),

F_N = the last array element in the descending column (corresponds in time to N_H),

N_L = low normalization value (as already explained), and

N_H = high normalization value (as already explained).

At this point, one full (calibrated and normalized) test case has been stored in the holding array (H) in such a manner that the number of values around each G-level is known. An arithmetic mean is calculated for each of six runs at each G-level and stored in the "A" array. This A array is dimensioned A(10,5,8) or A(G-level, data channel, table), where data channels 1 to 5 are: 1--suit pressure; 2--abdomen force; 3--left thigh force; 4--left calf force; and 5--right thigh force. [NOTE: Information from the original channel 1 (acceleration) is contained in the gravity-level dimension of this array.]

The eight tables of the A array are filled so that:

- a) Test Case I yields Tables 1 and 2,
- b) Test Case D yields Tables 3 and 4,
- c) Test Case X yields Tables 5 and 6, and
- d) Test Case N yields Tables 7 and 8.

The odd-numbered tables will contain increasing run data, and the even-numbered tables will contain decreasing run data. Each table of the A array contains the sum of the C averages about each G level (1 - 10, and 10 - 1) for three runs. [NOTE: each test case is made up of three runs increasing, and three runs decreasing.] The cells of the A array are now divided by three to give the average pressure for the three runs they (the cells) represent.

Since the first test case is considered to be the optimal case, the comparison of the suit pressure and the four bladders, in test cases D, X, and N to test case I, is of special interest. Therefore, an R array is set up such that the various tables (6 in all) hold the residuals from the optimal case (or test case I).

2.3.4 Data Presentation

The output of the RPM Program consists of 10 tables and 10 graphs. Tables 11 - 15 contain the reduced data (from the program's A array) for the suit pressure and the four force gages. The columns represent the test conditions, while the rows represent the discrete G-levels at which the data were averaged. Figures 110 - 114 (graphic representations of Tables 8 - 12, respectively) permit easier visual interpretation of what is really happening across the four test cases.

TABLE 11. RPV MANNEQUIN TEST SUIT PRESSURE RESPONSE (PSIG)

G LEVEL	TEST CASE			
	I	P	X	N
[INCREASING G]				
1	0.207	0.154	0.206	0.238
2	0.390	0.524	0.392	0.485
3	1.384	1.058	1.042	1.149
4	2.934	2.394	2.452	2.564
5	4.495	4.097	4.113	4.148
6	6.020	5.505	5.520	5.575
7	7.485	6.981	7.070	7.137
8	8.818	8.510	8.552	8.607
9	9.721	9.712	9.632	9.646
10	10.172	10.380	10.211	10.254
[DECREASING G]				
10	10.382	10.957	10.833	10.801
9	9.909	9.911	9.905	9.859
8	8.916	8.630	8.675	8.605
7	7.569	7.303	7.333	7.291
6	6.148	6.016	6.028	6.030
5	4.793	4.743	4.732	4.733
4	3.431	3.410	3.402	3.408
3	2.070	2.051	2.061	2.042
2	0.760	0.843	0.842	0.841
1	0.493	0.430	0.428	0.433

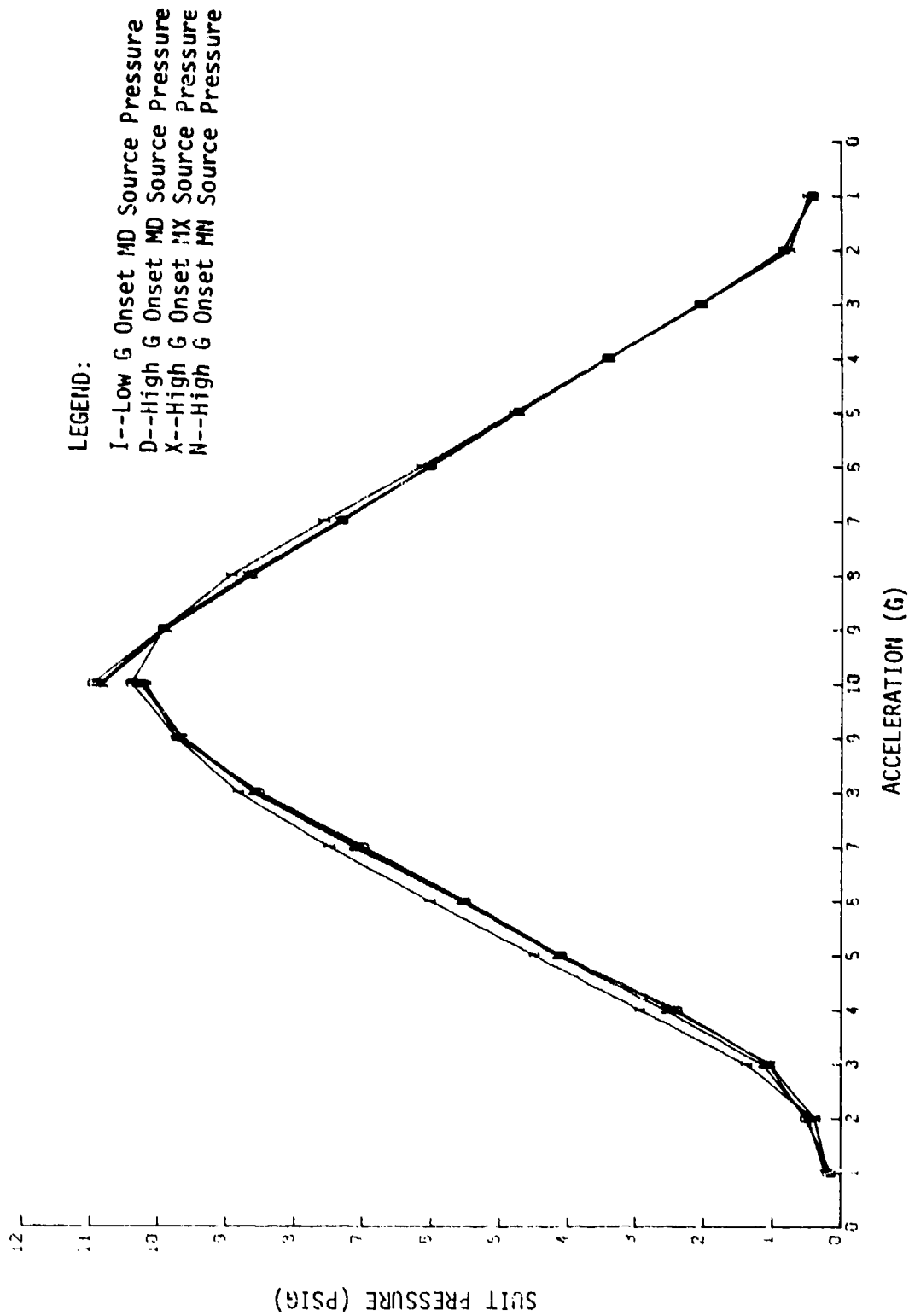


Figure 110. RPV mannequin test suit pressure response for four test cases.

TABLE 12. RPV MAINEQUIN TEST ABDOMINAL FORCE RESPONSE (PSI)

G LEVEL	TEST CASE			
	I	D	X	N

[INCREASING G]

1	0.146	0.140	0.205	0.234
2	0.394	0.557	0.387	0.477
3	1.531	1.073	1.022	1.111
4	3.108	2.360	2.386	2.510
5	4.650	3.987	3.987	4.973
6	6.194	5.491	5.484	5.571
7	7.642	6.902	7.005	7.107
8	8.924	8.319	8.378	8.485
9	9.783	9.505	9.467	9.523
10	10.217	10.197	10.063	10.149

[DECREASING G]

10	10.431	11.043	10.839	10.847
9	9.990	10.213	10.142	10.125
8	9.119	9.139	9.074	9.063
7	7.907	7.971	7.900	7.877
6	6.633	6.843	6.745	6.727
5	5.305	5.625	5.503	5.493
4	3.992	4.314	4.161	4.151
3	2.584	2.849	2.702	2.662
2	0.984	1.256	1.130	1.092
1	0.598	0.676	0.530	0.522

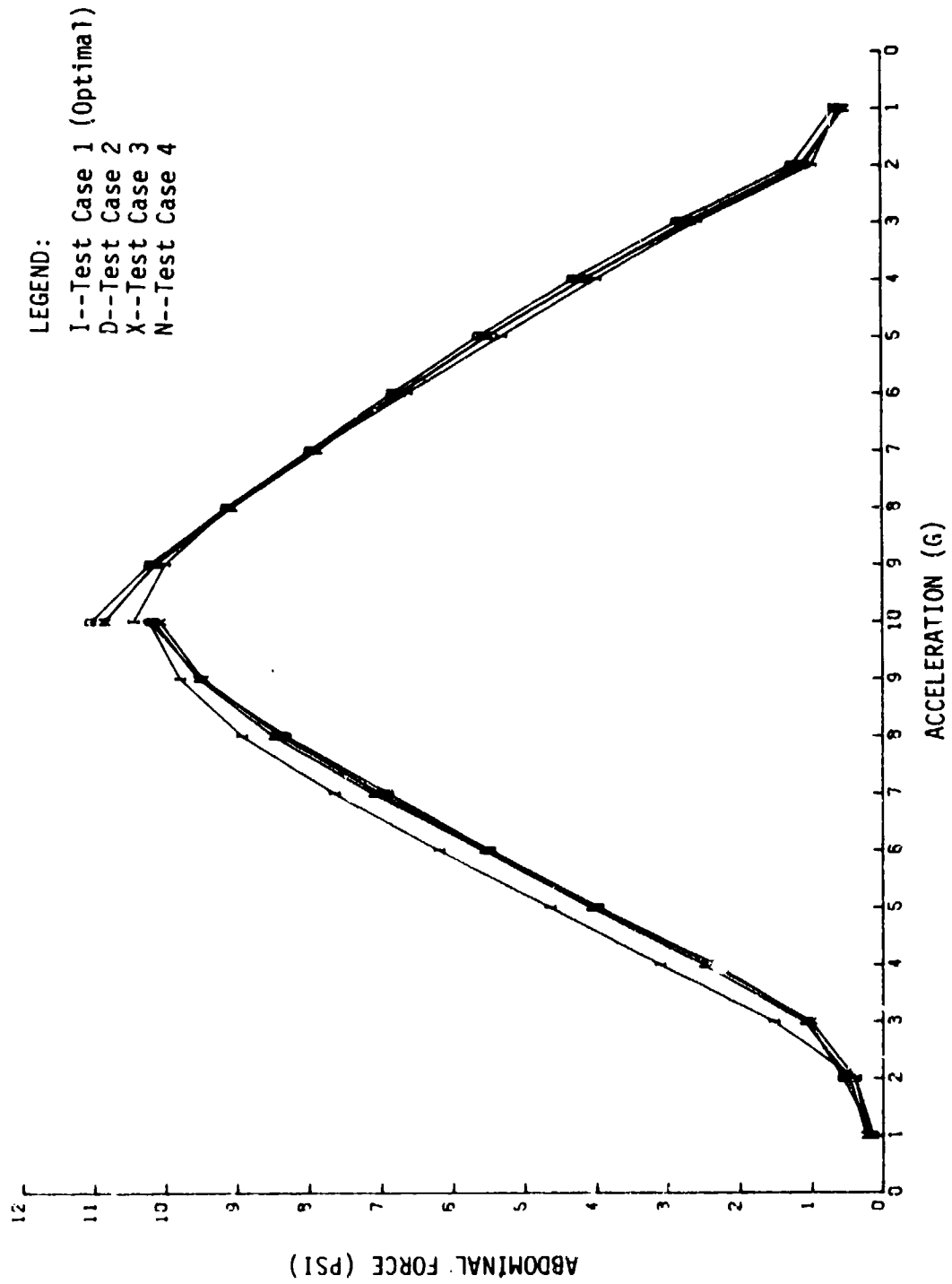


Figure 111. RPV annequin test abdominal force response for four test cases.

TABLE 13. RPV MANNEQUIN TEST LEFT THIGH FORCE RESPONSE (PSI)

G LEVEL	TEST CASE			
	I	D	X	N

	[INCREASING G]			
1	0.186	0.101	0.215	0.242
2	0.435	0.551	0.466	0.564
3	1.548	1.141	1.163	1.274
4	3.150	2.460	2.534	2.651
5	4.685	4.107	4.113	4.184
6	6.154	5.493	5.489	5.554
7	7.500	6.889	6.918	7.008
8	8.760	8.278	8.325	8.410
9	9.621	9.431	9.377	9.406
10	10.077	10.102	9.969	10.031

	[DECREASING G]			
10	10.344	10.968	10.822	10.816
9	9.885	10.073	10.051	10.046
8	8.975	8.958	9.009	9.002
7	7.723	7.737	7.822	7.830
6	6.400	6.541	6.647	6.670
5	5.059	5.304	5.425	5.461
4	3.740	3.982	4.121	4.176
3	2.359	2.588	2.723	2.761
2	0.937	1.186	1.249	1.276
1	0.575	0.609	0.611	0.620

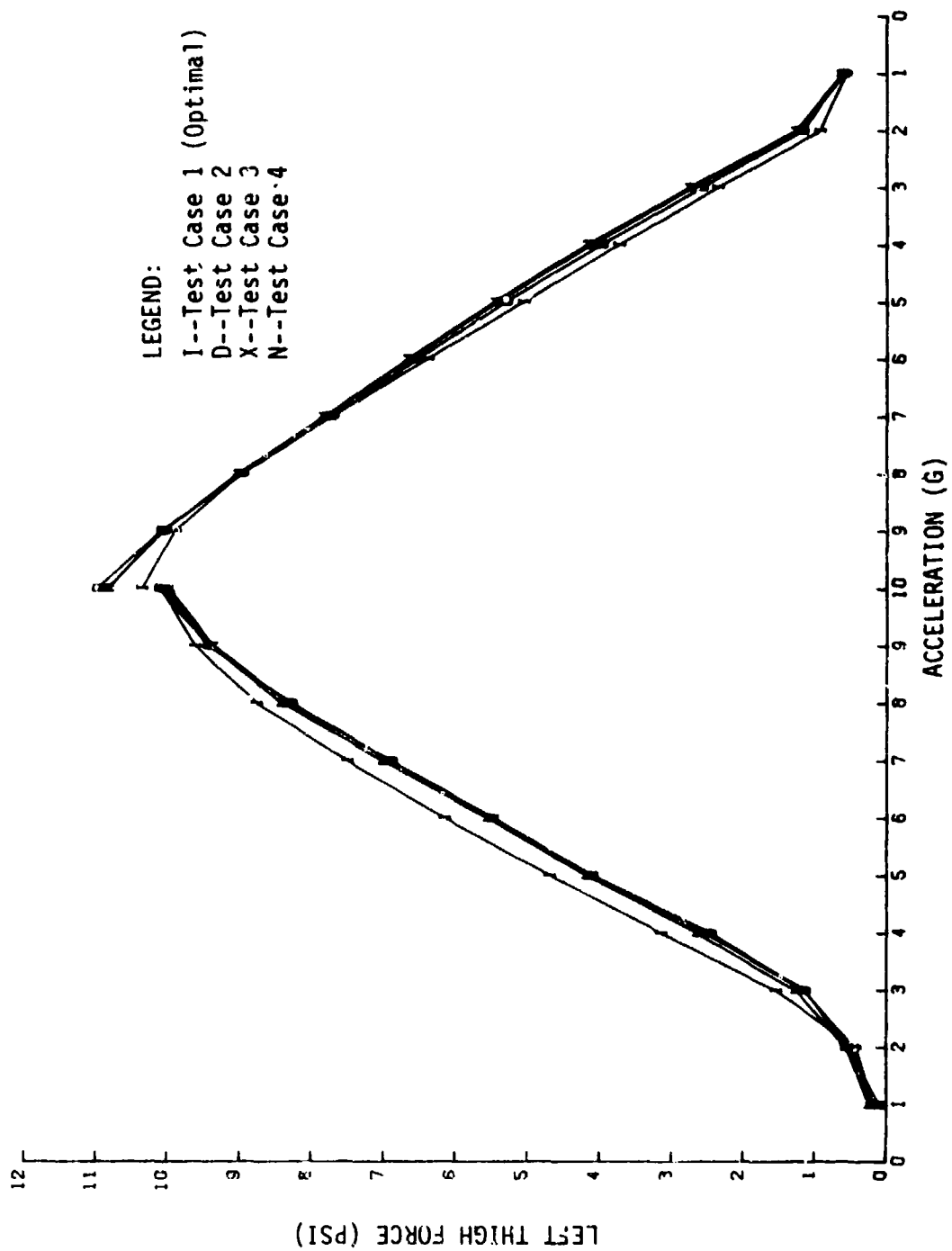


Figure 112. RPV mannequin test left thigh force response for four test cases.

TABLE 14. RPV MANNEQUIN TEST LEFT CALF FORCE RESPONSE (PSI)

G LEVEL	TEST CASE			
	I	D	X	N

[INCREASING G]				
1	0.175	0.101	0.214	9.232
2	0.407	0.541	0.456	0.564
3	1.514	1.166	1.234	1.359
4	3.126	2.518	2.667	2.797
5	4.705	4.238	4.331	4.404
6	6.210	5.695	5.745	5.821
7	7.566	7.117	7.210	7.272
8	8.830	8.508	8.557	8.646
9	9.675	9.634	9.564	9.598
10	10.117	10.264	10.088	10.155

[DECREASING G]				
10	10.390	11.015	10.859	10.852
9	10.030	10.266	10.203	10.186
8	9.234	9.253	9.235	9.213
7	8.088	8.074	8.063	8.045
6	6.823	6.895	6.890	6.888
5	5.486	5.639	5.631	5.618
4	4.084	4.260	4.265	4.263
3	2.595	2.788	2.800	2.786
2	1.095	1.342	1.337	1.322
1	0.708	0.739	0.718	0.702

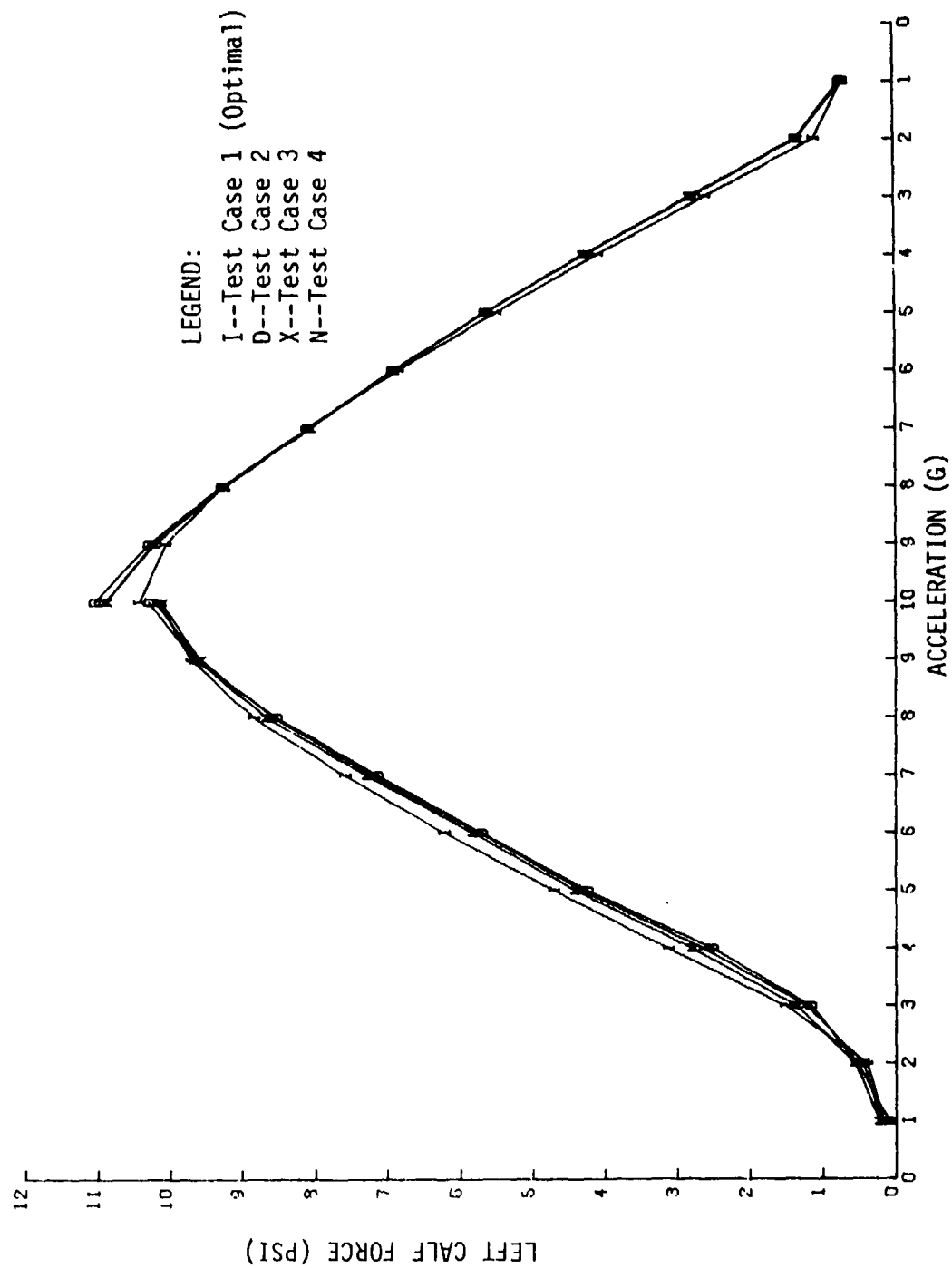


Figure 113. RPV mannequin test left calf force response for four test cases.

TABLE 15. RPV MANNEQUIN TEST RIGHT THIGH FORCE RESPONSE (PSI)

G LEVEL	TEST CASE			
	I	D	X	N
[INCREASING G]				
1	0.173	0.088	0.185	0.237
2	9.461	0.603	0.486	0.612
3	1.652	1.237	1.307	1.435
4	3.310	2.745	2.890	3.042
5	4.881	4.462	4.581	4.672
6	6.370	5.941	6.033	6.125
7	7.727	7.316	7.463	7.562
8	8.970	8.748	8.835	8.919
9	9.790	9.883	9.830	9.870
10	10.205	10.523	10.365	10.424
[DECREASING G]				
10	10.340	10.332	10.782	10.780
9	9.886	10.013	9.980	9.981
8	8.976	8.887	8.903	8.887
7	7.735	7.644	7.674	7.663
6	6.431	6.428	6.456	6.474
5	5.105	5.154	5.185	5.194
4	3.734	3.796	3.843	3.866
3	2.308	2.359	2.413	2.422
2	0.834	0.933	0.990	1.009
1	0.483	0.411	0.455	0.482

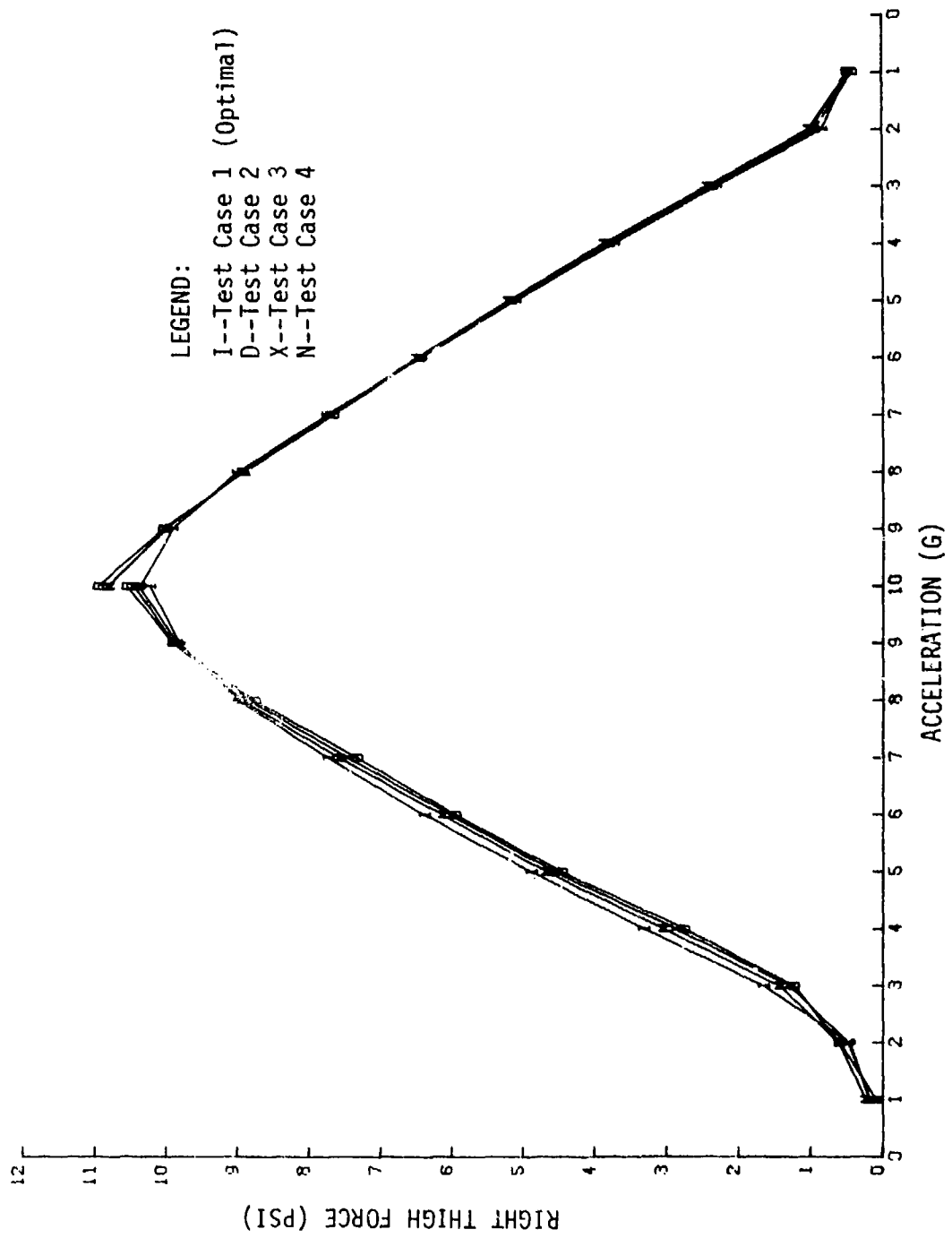


Figure 114. RPV mannequin test right thigh force response for four test cases.

Tables 16 - 20 contain columns showing the residuals (from the program's R array), from the optimal test case I, for each of the less than optimal test cases (D, X, and N); and Figures 116 - 119 are, again, plots of the corresponding tables. The residual plots, which permit easier visual interpretation, are actually expansions of the response differences in Tables 11 - 15 and Figures 110 - 114.

2.3.5 RPV Mannequin Test Conclusions

Reviewing Figures 110 - 114 yields an excellent overview of the RPV performance. The tables are presented for examination, in which more subtle characteristics may be found.

The residual plots probably overstate their case. In no case does a pressurization lag exceed 0.75 psig. That maximum occurs in the abdominal bladder and corresponds to a 0.5 psig lag in suit pressure. The apparent tendency of the AGS to maintain pressure on the mannequin is obvious when Figures 116 - 119 are compared with Figure 115. This "mechanical" response was noted and discussed in detail on the preceding contract (refer to SAM-TR-78-12: TEHG, Vol. III: Anti-G Suits).

2.4 ALAR "High Flow" and "Special" Examinations

Two design modifications to the ALAR 8400A AGV were tentatively tested by the staff of USAFSAM/VNB. These modifications have been designated the "High Flow" and the "Special." The PTAP examination of these valves had three phases: First, the mechanical differences between the two modified valves and a standard 8400A were cataloged. Second, the open-flow capacity of the two modified valves was measured. Third, the effect of spring shim thickness on first-stage regulator output pressure was examined.

2.4.1 Design Modifications

The design modifications associated with the "High Flow" and the "Special" are summarized in Table 21. The "item numbers" references in that table may be correlated with those in Figure 23, section 1.3.

The modification to the bellows assembly [Item 18] increases the flow capacity between the first- and second-stage regulators. The modification to the bellows seat [Item 21] increases the flow capacity out of the second stage to the suit. The additional holes in the second-stage body [Item 23] increase the flow capacity to the suit. The shims [Item 28] increase the first-stage regulator output pressure, thus increasing flow capacity of the second stage. The enlarged spool assembly [Item 29] and spool seats [Item 34] increase the flow capacity of the first stage and increase the first-stage regulating surface. The additional holes in the main body [Item 46] increase the flow capacity between the first- and second-stage regulators. The ventilated spaces increase the exhaust flow capacity of the valve.

2.4.2 Open-flow Capacity of "High Flow"

The open-flow capacity of each of the valves was statically tested using the press-to-test button. In each case, the button was manually depressed to the mechanical limit of its travel. The results are shown in Table 22. The "Special" provides 11%, 44%, and 44% flow increases over the "High Flow" for source pressures (P_S) of 30, 125, and 300 psig, respectively.

Recalling that the major differences between the "Special" and "High Flow" are the shims [Item 28] and bellows seat [Item 21], the effects of these modifications were examined. In the 30-psig tests, no significant changes were detected. In the 125-psig and 300-psig tests, the first-stage regulator shim [Item 28] produced slightly more than half the increased flow capacity.

2.4.3 First-stage Regulator Shim Effect

In order to optimize the first-stage regulator performance, an ALAR 8400A was modified to allow measurement of the first stage regulation pressure. The effects of various shim thicknesses were measured under static conditions (Table 23). All tests were run using 125-psig source pressure. Spot checks were made using 30 psig and 300 psig, with no noticeable changes.

2.5 Accelerometer Calibration

The primary objective of this effort was to define a procedure for calibration of the accelerometers used on the USAFSAM/VNB human centrifuge. The initial approach was to define the acceleration environment experienced by the gondola accelerometer, allowing its calibration in place. This approach became prohibitively complicated. An alternate approach is presented here which removes the accelerometer to a location for which the acceleration environment is easily defined.

2.5.1 Gondola Acceleration Environment

The resultant acceleration through any specified point is the vector sum of all acceleration vectors through that point. In the case of the USAFSAM human centrifuge, an adequate assumption is that (for most purposes) the acceleration vectors in the gondola are limited to the acceleration of gravity (\vec{g}) and the centrifugal acceleration (\vec{a}) generated by the rotation of the system. These two vectors may be considered perpendicular, with negligible error, and the resultant through any point defined by a vector of magnitude

$$|A| = \sqrt{a^2 + g^2},$$

located in a plane, defined by the vectors a and g , at an angle

$$\theta = \tan^{-1} g/a$$

from \vec{g} . Using this definition, θ also approximates the roll angle of the gondola.

TABLE 16. RPV MANNEQUIN TEST SUIT PRESSURE RESIDUALS (PSIG)

G LEVEL	TEST CASE		
	D-I	X-I	N-I
[INCREASING G]			
1	-0.053	-0.001	0.031
2	0.134	0.003	0.096
3	-0.342	-0.342	-0.235
4	-0.540	-0.482	-0.370
5	-0.398	-0.382	-0.347
6	-0.516	-0.500	-0.446
7	-0.503	-0.414	-0.348
8	-0.308	-0.267	-0.211
9	-0.009	-0.090	-0.075
10	0.207	0.039	0.082
[DECREASING G]			
10	0.575	0.451	0.419
9	0.003	-0.004	-0.050
8	-0.286	-0.241	-0.311
7	-0.261	-0.236	-0.278
6	-0.132	-0.120	-0.118
5	-0.051	-0.061	-0.060
4	-0.021	-0.028	-0.022
3	-0.019	-0.009	-0.028
2	0.083	0.082	0.081
1	-0.063	-0.065	-0.060

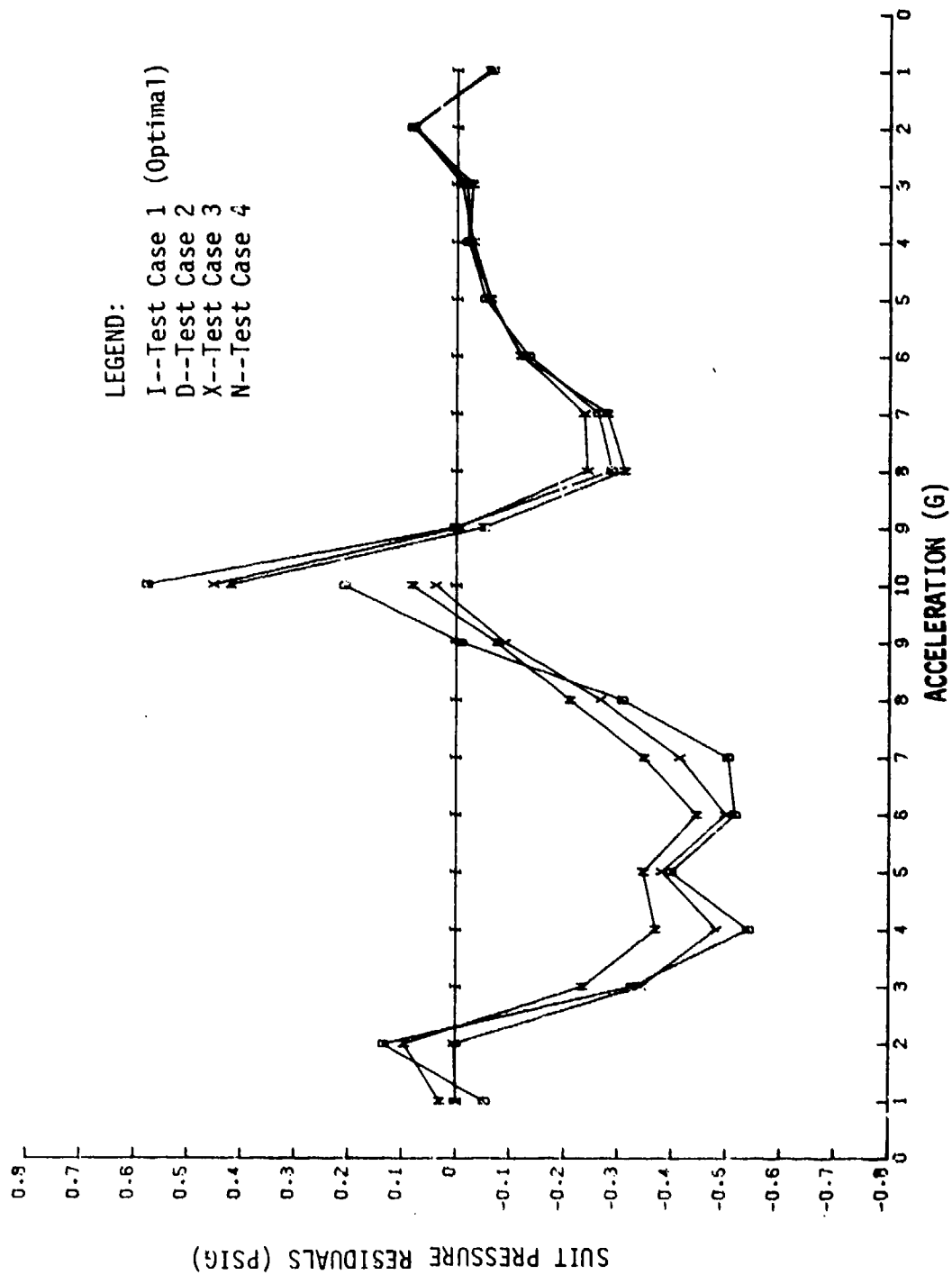


Figure 115. RPV mannequin test suit pressure residuals.

TABLE 17. RPV MANNEQUIN TEST ABDOMINAL FORCE RESIDUALS (PSI)

G LEVEL	TEST CASE		
	D-I	X-I	N-I
[INCREASING G]			
1	-0.006	0.059	0.088
2	0.163	-0.007	0.082
3	-0.458	-0.509	-0.420
4	-0.748	-0.722	-0.598
5	-0.662	-0.663	-0.571
6	-0.704	-0.710	-0.623
7	-0.740	-0.637	-0.535
8	-0.605	-0.546	-0.438
9	-0.278	-0.316	-0.260
10	-0.020	-0.153	-0.068
[DECREASING G]			
10	0.511	0.408	0.416
9	0.222	0.152	0.135
8	0.020	-0.045	-0.056
7	0.054	-0.008	-0.031
5	0.210	0.112	0.094
5	0.320	0.197	0.188
4	0.322	0.169	0.160
3	0.265	0.117	0.077
2	0.272	0.146	0.108
1	0.078	-0.068	-0.076

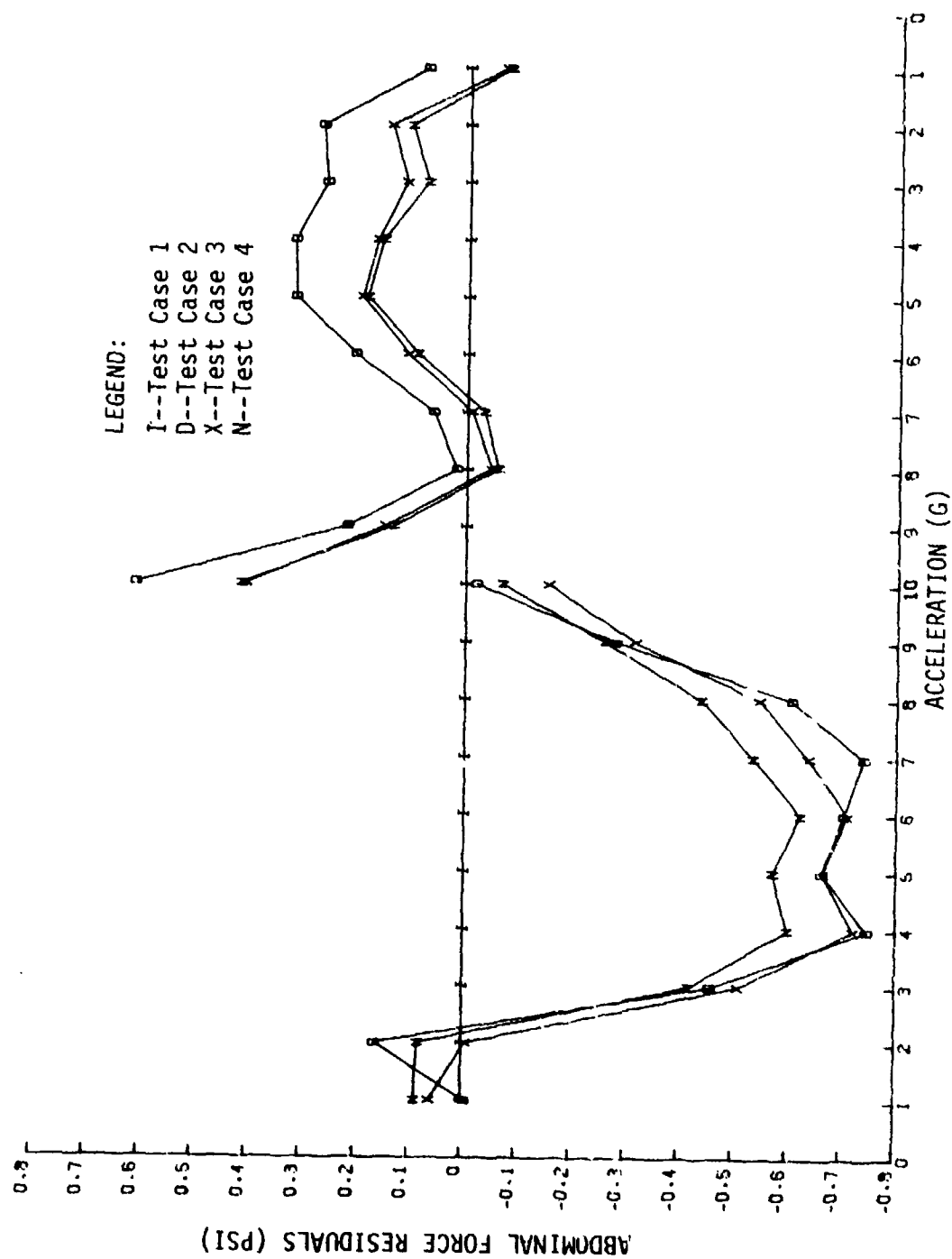


Figure 116. RPV mannequin test abdominal force residuals.

TABLE 18. RPV MANNEQUIN TEST LEFT THIGH FORCE RESIDUALS (PSI)

G LEVEL	TEST CASE		
	D-I	X-I	N-I
[INCREASING G]			
1	-0.085	0.029	0.056
2	0.116	0.032	0.130
3	-0.407	-0.385	-0.274
4	-0.690	-0.616	-0.499
5	-0.578	-0.573	-0.501
6	-0.658	-0.662	-0.597
7	-0.611	-0.582	-0.492
8	-0.482	-0.435	-0.350
9	-0.150	-0.244	-0.215
10	0.025	-0.108	-0.046
[DECREASING G]			
10	0.624	0.478	0.472
9	0.188	0.166	0.161
8	-0.017	0.035	0.027
7	0.014	0.098	0.106
6	0.141	0.248	0.270
5	0.246	0.366	0.402
4	0.242	0.382	0.436
3	0.229	0.364	0.402
2	0.248	0.311	0.338
1	0.034	0.036	0.045

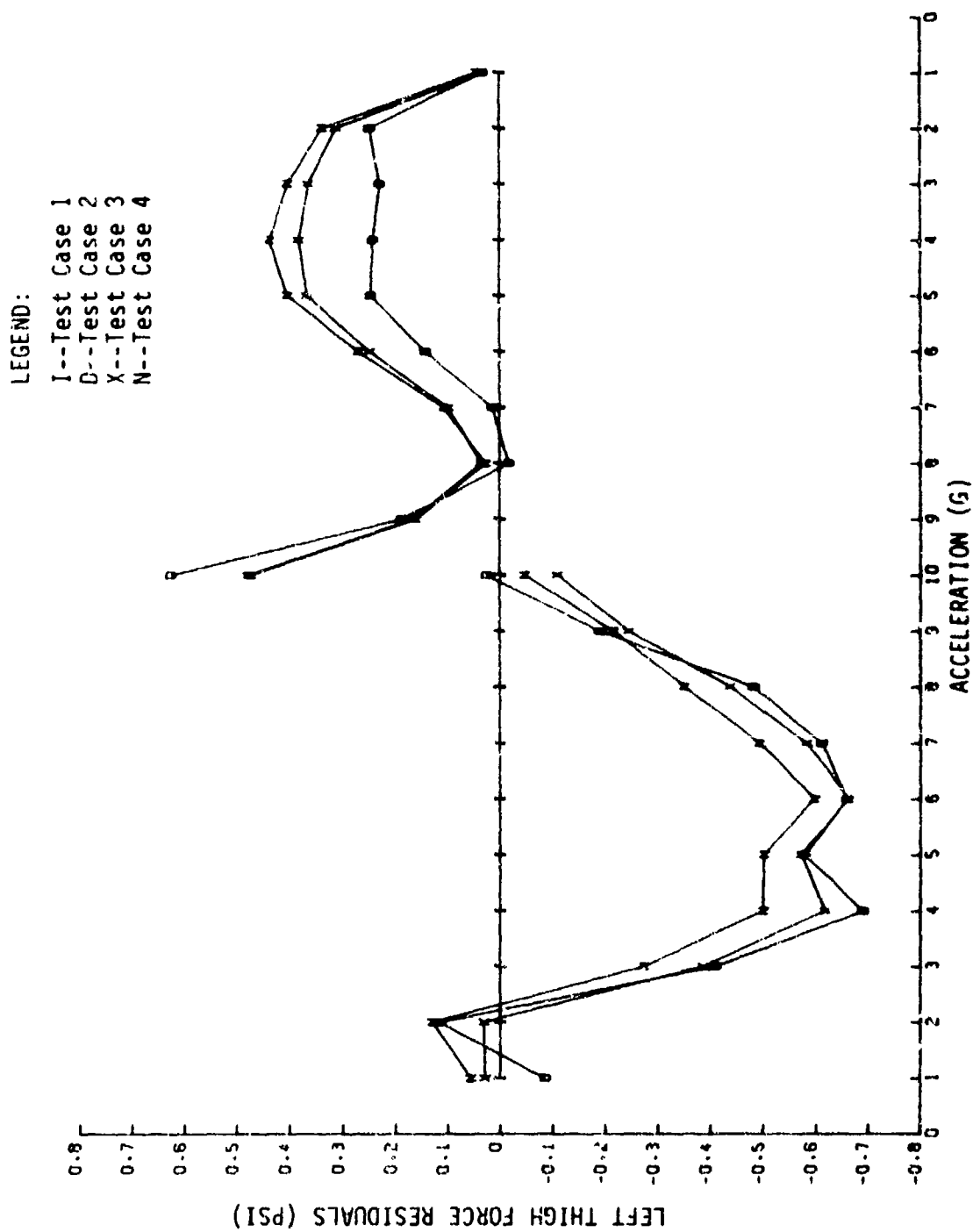


Figure 117. RPV mannequin test thigh force residuals.

TABLE 19. RPV MANNEQUIN TEST LEFT CALF FORCE RESIDUALS (PSI)

G LEVEL	TEST CASE		
	D-I	X-I	N-I
[INCREASING G]			
1	-0.074	0.039	0.057
2	0.134	0.049	0.158
3	-0.348	-0.280	-0.155
4	-0.608	-0.459	-0.329
5	-0.467	-0.374	-0.301
6	-0.515	-0.465	-0.388
7	-0.450	-0.357	-0.294
8	-0.322	-0.273	-0.184
9	-0.041	-0.111	-0.077
10	0.147	-0.029	0.038
[DECREASING G]			
10	0.624	0.469	0.462
9	0.236	0.173	0.156
8	0.019	0.001	-0.021
7	-0.013	-0.024	-0.043
6	0.072	0.066	0.055
5	0.153	0.144	0.132
4	0.176	0.182	0.179
3	0.194	0.205	0.191
2	0.247	0.243	0.227
1	0.030	0.010	-0.006

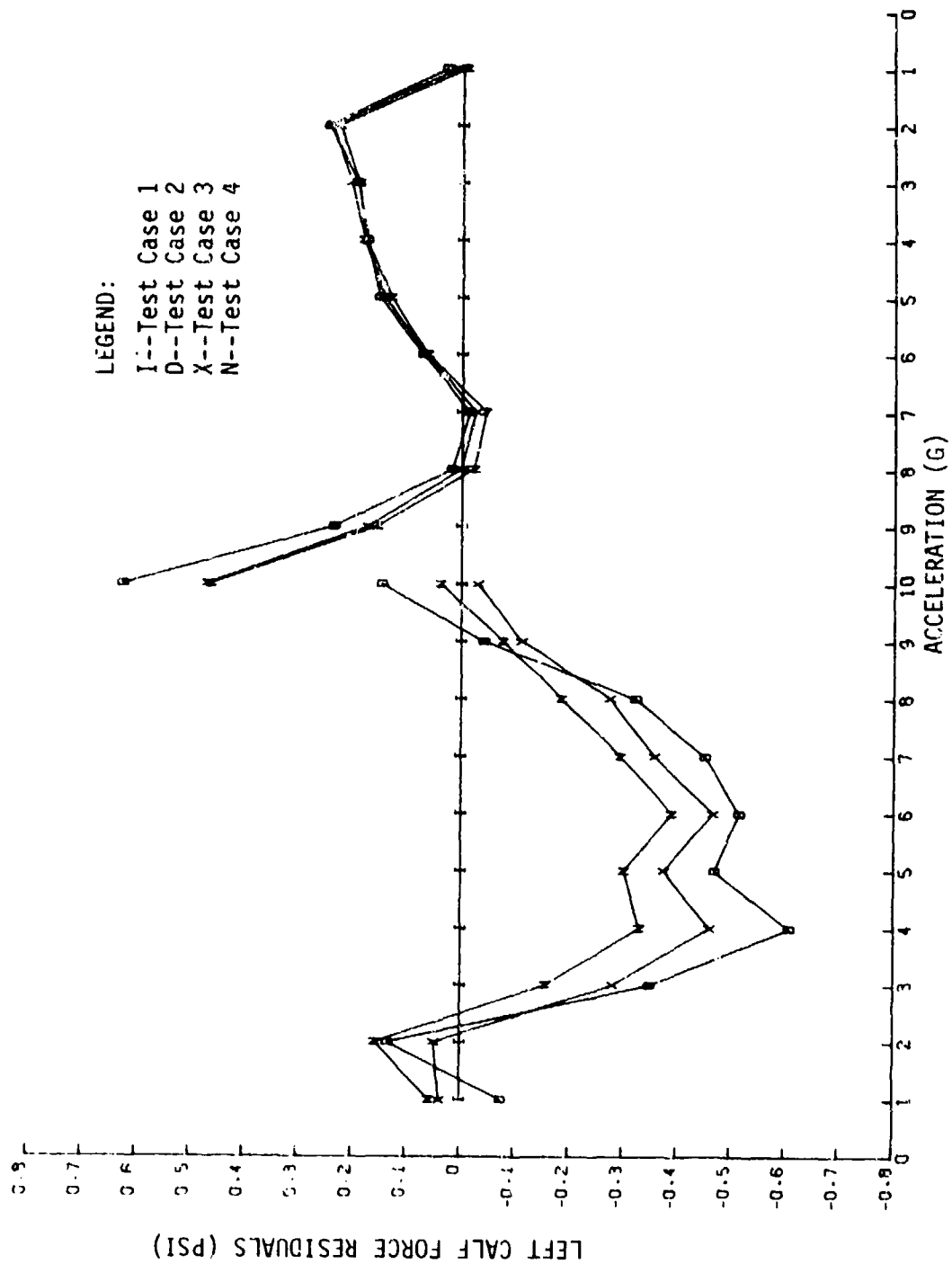


Figure 118. RPV mannequin test left calf force residuals.

TABLE 20. RPV MANNEQUIN TEST RIGHT THIGH FORCE RESIDUALS (PSI)

G LEVEL	TEST CASE		
	D-I	X-I	N-I
[INCREASING G]			
1	-0.085	0.012	0.064
2	0.142	0.026	0.151
3	-0.415	-0.345	-0.217
4	-0.565	-0.420	-0.268
5	-0.419	-0.300	-0.209
6	-0.438	-0.346	-0.253
7	-0.411	-0.264	-0.165
8	-0.223	-0.135	-0.051
9	0.093	0.040	0.080
10	0.318	0.160	0.220
[DECREASING G]			
10	0.592	0.442	0.439
9	0.127	0.094	0.094
8	-0.089	-0.073	-0.089
7	-0.092	-0.062	-0.073
6	-0.002	0.026	0.043
5	0.049	0.080	0.088
4	0.062	0.109	0.132
3	0.051	0.105	0.114
2	0.099	0.155	0.174
1	-0.072	-0.027	-0.001

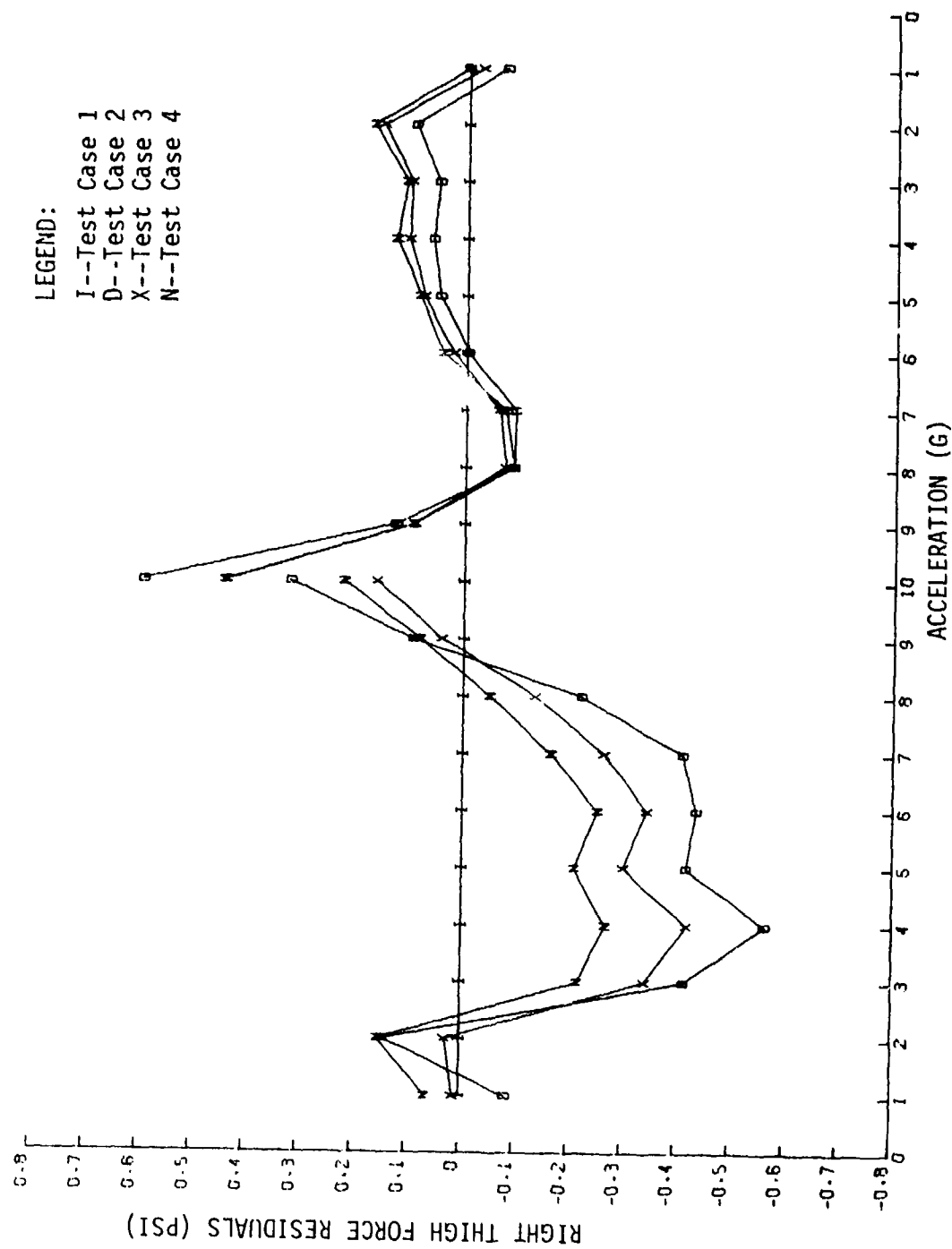


Figure 119. RPV mannequin test right thigh force residuals.

TABLE 21. ALAR "HIGH FLOW" AND "SPECIAL" DESIGN MODIFICATIONS

Item No.	Description	Valves		
		Standard	"Special"	"High Flow"
18	Bellows assembly	No change	Half-circle cut, 9/64 in. deep in the 4 sides of base plate	Same as special valve
21	Seat, for bellows	No change	Bellows post support bar cut down to 0.050 in.	No change
23	Body, second stage	4 flow holes, 0.228 in.	8 flow holes, 0.228 in.	Same as special valve
28	Shim	None	0.115 in.	0.030 in.
29	Spool assembly	Spool is 0.260 in.	Spool is 0.434 in.	Same as special valve
34	Seat, spool, 2 ea.	0.265 in. opening	0.437 in. opening	Same as special valve
36	Screen assembly		None	None
46	Body assembly, main	4 holes (0.169 in.) between first- and second-stage chambers	10 holes (0.169 in.) between first- and second-stage chambers	Same as special valve
--	Spacer, ventilated	None	1/8 in. spacer with large vent holes mounted between main body assembly [46] and weight [2]	None

TABLE 22. ALAR "HIGH-FLOW" AND "SPECIAL"
OPEN-FLOW CAPACITIES

DESCRIPTION	SOURCE PRESSURE		
	30 psig	125 psig	300 psig
"High Flow"	12.2	17.0	18.0
"High Flow"	13.6	20.5	22.0
"Special"			
Shim [Item 28]	13.6	24.5	26.0
"Special"	15.0	20.0	21.5
"High-flow"			
Shim [Item 28]			

[Item 28: Consult Figure 23, and Table 18.]

TABLE 23. ALAR 8400A FIRST-STAGE REGULATOR SHIM EFFECT

Shim Thickness (in.)	First-stage Regulator Output (psig)
0	12.5
15	12.5
50	15.0
100	16.0
115	17.0
178	19.5
188	19.5
203	24.0
218	125.0 (source pressure)
241	125.0 (source pressure)

The magnitude of the centrifugal acceleration vector is commonly defined as

$$a = \omega^2 R,$$

where ω equals the angular velocity of the system in rad/sec, and R equals the radius of rotation (in some convenient dimension) of the specified point. The determination of R makes prohibitively complex the expression describing the acceleration environment of the accelerometer in the gondola.

The accelerometer is normally located on the forward wall of the gondola, at a position which approximates the elevation of a subject's heart from the gondola floor. This position places the accelerometer approximately $10\text{--}47/64 \pm 1/64$ in. (27.265 ± 0.040 cm) above the center of rotation of the gondola. The accelerometer is approximately $20\text{ ft } 2\text{--}17/64$ in. $\pm 3/64$ in. ($6.15355\text{ m} \pm 0.0012\text{ m}$) from the centrifuge center of rotation when the system is at rest. The obvious change (shortening) in radius as the gondola rotates would, if not accounted for, introduce an error of unacceptable magnitude. Therefore, the rotation of the gondola must be predicted; and, at this point, the theoretical expression became unmanageable.

Obviously, a significant acceleration gradient exists in the gondola due to the differences in radii of rotation of the various locations. A subject's feet may experience at least 10% more acceleration than his head! The physical structure, equipment, and instrumentation experience an even larger gradient due to their wider distribution.

At this point, the difference between the center of mass and the center of gravity must be considered. These two points only coincide in a uniform acceleration field. In the case of the gondola, this field occurs only when the gondola is at rest. When an acceleration gradient is applied to the system, the gondola will rotate to align the center of gravity and the axis of rotation. The center of gravity can (and in the case of the gondola, does) move a considerable distance from the center of mass. Furthermore, this movement is not perpendicular to the gondola floor and through the centerline of gondola rotation. Empirical data indicate errors in excess of 4° between actual and theoretical roll angles. These errors can result in as much as 20% error in acceleration reading (although usually the resulting errors are much smaller) for low-G levels. At this point, attempts to calibrate an accelerometer, theoretically or empirically, in the gondola were abandoned.

2.5.2 Dynamic Calibration

Two means of transducer calibration are available. Both techniques involve rotating the transducer so that the sensitive axis is perpendicular to the natural G vector, and adjusting the variable resistor marked "Z" for a zero output from the transducer.

Coarse adjustment of the "S" (span) control on the transducer may be accomplished by aligning the sensitive axis of the transducer with the G field and adjusting "S" for the proper response. The acceleration of gravity for the USAFSAM human centrifuge was calculated, using Helmert's equation, an assumed altitude of 594 ft, and a latitude of $29^\circ 20' 30''$ (longitude is

approximately $98^{\circ}26'30''$). This estimated value is 979.214 cm/sec^2 (32.126 ft/sec^2 , or 0.9985 G) compared to a standard of 980.665 cm/sec^2 (32.174 ft/sec^2 , or 1.0 G).

Greater resolution may be obtained by installing the accelerometer in a special bracket, manufactured by the PTAP crew, which locates the sensitive axis of the accelerometer $13 \text{ ft } 9 \text{ in.} \pm 0.1 \text{ in.}$ ($419.10 \pm 0.25 \text{ cm}$) from the center of rotation (CR). In this case, the "S" and "Z" controls may be adjusted to respond according to Table 24, using the rotational speed of the system as a standard. Estimated error of this approach is 0.149% .

2.6 Continuous ECG Recordings in Primates

2.6.1 Objective

The purpose of this investigative effort was to examine some of the problems VNB has experienced while performing long-term (6 months) ECG monitoring in animals. This portion of the report covers two areas: first, a discussion of various types of percutaneous lead devices; and second, a discussion of silver and silver-silver chloride electrodes. Recommendations are made and methods are suggested in both areas.

2.6.2 ECG From Chronically Implanted Electrodes

Using chronically implanted electrodes for ECG eliminates many of the problems associated with conventional surface electrodes; namely, daily skin preparation, electrode attachment, impedance variations, and electrode impedance measurements. Most importantly, consistent repeatable ECG measurements can be obtained. With implanted electrodes, the most difficult problem, of course, is the data recovery method--which is limited to telemetry or hard wire. Telemetry has several distinct disadvantages for long-term (6 months) monitoring. The first disadvantage is that the power consumption for transmitting the data over long periods necessitates using rechargeable batteries and a convenient method of recharging. A power loop transmitter placed over the skin and an inductive coil placed beneath the skin, with associated circuitry for charging the device (6,9), adds immensely to the volume and complexity of the circuit to be implanted. The second disadvantage is the surgical implantation of the telemetry/power-supply device, which is certainly more extensive and traumatic than the implantation of subcutaneous electrodes. Since the ECG is the only anticipated parameter to be measured in the near future, it is advisable to keep the surgical procedures at a minimum and to continue using a hard-wire system.

A. Percutaneous Leads: Using a hard-wire system, the problem now becomes one of finding a biologically inert feed-through, and

EDITOR'S NOTE: For the convenience of the reader, the author has included "References," No. 1-18 (section 2.6.5), which pertain specifically to the material in section 2.6.

TABLE 24. ACCELEROMETER CALIBRATION VALUES FOR LOCATION
13 FT 9 IN. \pm 0.1 IN. (419.10 \pm 0.25 CM) FROM
THE CENTER OF ROTATION

	Centrifugal Acceleration		Angular Velocity	
	(G)	(ft/sec ²)	(rad/sec)	(rpm)
0		0	0	0
1		32.174	1.530	14.607
2		64.348	2.163	20.658
3		96.522	2.649	25.301
4		128.696	3.059	29.215
5		160.870	3.420	32.663
6		193.044	3.747	35.781
7		225.218	4.047	38.648
8		257.392	4.327	41.316
9		289.566	4.589	43.822
10		321.740	4.837	46.193
11		353.914	5.073	48.447
12		386.088	5.299	50.601
13		418.262	5.515	52.668
14		450.436	5.724	54.656
15		482.610	5.924	56.574
16		514.784	6.119	58.430
17		546.958	6.307	60.228
18		579.132	6.490	61.974
19		611.306	6.668	63.672
20		643.480	6.841	65.326

maintaining the percutaneous lead system. Given that one has a biologically inert material, the development of infection due to rejection has been minimized; but disruption of the skin outlet interface may occur, due to mechanical stress applied to the leads, thus causing drainage. Chronic infectious drainage can cause the infection process to follow the leads deep into the animal, causing death or local necrosis, and disrupting the percutaneous leads (13).

In the development of a biologically inert percutaneous lead system, various types of materials have been used, including Teflon, silicone, velour, epoxies, titanium, and pure carbon (1-3, 13-18). Of these materials, pure carbon and velour seem to be best suited for a natural ingrowth of subcutaneous tissue and the formation of a bacteria-proof barrier.

The velour technique, which is presently being used by VNB, is usually a matter of securing the velour fabric around the lead system with a medical grade of silicone adhesive, Dow Corning Type A (Dow Corning, Inc., Midland, Mich.). The literature indicates that adherence of the tissue to the fabric is good, producing a bacteria-proof seal; however, the silicone adhesive tends to fail, causing drainage and subsequent infection. The tissue-velour interface tends to be delicate and is subject to disruption by mechanical trauma (13). Nevertheless, this method appears to be fairly successful and simple for obtaining a percutaneous lead system.

During the past decade, several types of high purity (90-99%) carbon have been developed in the interest of biomedical applications (2,4). This high purity carbon, having extremely low chemical reactivity, is presently being used in human subjects for prosthesis, cardiac assist devices, dental implants, and percutaneous lead devices. The fact that high purity carbon is biologically inert is well documented (2-4,8,10), and apparently seems to be "number one" candidate for many of the percutaneous lead problems. In work done at Rancho Los Amigos Hospital, Downey, California, carbon devices have been implanted in human subjects for over 3 years. These patients have been exposed to full daily activities, including sporting activities.

The mechanical stability of these devices is very good, and consequently they do not need additional support. The devices are not perfect, however, and are subject to disruption due to mechanical stress; but apparently they do not cause a drainage problem when disrupted (5,11).

One property of vitreous carbon is very low resistivity-- 10^{-3} ohm-cm (2,8). Consequently, to use this material for a percutaneous lead system, an electrical connector must be used in conjunction with the carbon device for electrical insulation. Earlier pure carbon devices were molded and then fired (vitreous carbon) to their final form. The problem with vitreous carbon is that about 40% shrinkage occurs during the firing process; and consequently, maintaining accurate dimensions for an electrical connector feed-through is difficult. Also, in its final form, vitreous carbon is very hard, and thus difficult to machine.

Another process has been developed whereby high-purity carbon is deposited (pyrolite carbon) on a substrate base, and subsequently the dimensions of the device are precisely controlled. A pyrolytic carbon device can be deposited on a substrate base having a feed-through for a miniature multi-pin connector

(female end). These pyrolite carbon devices are custom-made for a selected connector by General Atomic Co. (Medical Products Div., 11388 Sorrento Valley Rd., San Diego, Calif. 92121) for approximately \$30.00 each. General Atomic has already produced this type of device, using miniature electrical connectors with as many as 200 pins. These percutaneous devices are presently being used in subjects for chronic nerve implants for external visual stimulus (5). The connector, a Cannon NJS series (9-, 24-, or 72-pin), can be obtained--unterminated, or terminated with individual wires, or as a one-piece multiconductor cable--for approximately \$30.00 each (ITT Cannon Electric, 666 E. Dyer Rd., Santa Ana, Calif. 92702). The contractor recommends ordering the connector terminated with individual 30-gage insulated wires of a specified length (long enough to reach from exit site to electrode site). In this way, the feed-through connector device can be obtained as a sealed, moisture-proof unit. Ordering the connector in the 9-pin configuration is also advisable, to allow a sufficient number of electrodes for measuring the ECG or VCG, if desired. (However, consideration should be given to future experiments, in which case the 9-pin configuration would be insufficient.)

B. Silver and Silver-Silver Chloride Electrodes: When electrodes come in contact with an electrolyte, a voltaic cell is created at the electrode-electrolyte interface. This effect, known as polarization, is a function of temperature, of the concentration of the electrolyte, and of the manner in which the metal reacts with the electrolyte. Because the temperature and concentration of the electrolyte are fixed for this particular application, only the type of metal and its reaction to the electrolyte (NaCl) will be considered.

The effects of polarization are usually minimized by the fact that this potential occurs at each electrode, and the net difference between electrodes should be zero--assuming electrodes are identical in material, size, and shape, and are immersed in the same electrolyte. In practice, however, an unstable residual potential difference will exist. This residual is probably due to slight differences in surface contamination and irregularities in the metal electrode (7). If these potential differences were stable, they could simply be removed by ac coupling the ECG signal at the preamplifier. Actually, these potentials are not stable, vary constantly in a random fashion, and cannot be completely filtered out by the high-pass filter, which is usually set at 0.05 Hz for the ECG.

When silver is used as the electrode, metallic silver combines with a chloride ion of the electrolyte, releasing an electron and eroding silver away from the electrode. The polarizing potential, developed at the silver surface, is approximately 0.8 V, with residual potential differences of 95 mV (18).

The conventional method of eliminating the polarization potential in silver electrodes is to remove the electrode-electrolyte interface by plating the silver with silver chloride, thus providing a non-polarizable electrode. The AgCl maintains a high concentration of ionized Ag and Cl at the Ag-AgCl interface, and current flow at the AgCl-electrolyte interface is maintained by diffusion of the chloride ions (12). Unlike the Ag electrodes, current flow in the Ag-AgCl electrodes does not result in an irreversible electrochemical reaction. Silver chloriding silver electrodes reduces the residual potential difference to approximately 2.5 mV.

Another advantage of chloriding silver electrodes is that even though the process raises the overall electrode impedance, the capacitive effects are decreased for the lower frequencies, thus decreasing impedance nonlinearities. There is an optimum amount of chloride plating to obtain the lowest possible impedance while reducing electrode capacitance, as will be explained later.

Ag-AgCl electrode pellets are produced commercially by combining Ag and AgCl (about 60/40), thus eliminating the plating process. However, because of the number of experimental animals involved and because the electrodes will be chronically implanted, the contractor suggests that VNB continues to use the silver electrodes, but that they be plated with AgCl as follows:

The electrode lead must be soldered to the silver electrode. All of the wire not used in making the connection should be covered with polyvinylchloride (PVC) insulation. A medical grade adhesive, Dow Corning Type A (Dow Corning, Inc., Midland, Mich.), is used to seal the solder connection and the insulation. This adhesive will protect the solder connection and the electrode lead from electrolyte infiltration and subsequent eroding potentials.

The electrode surface is then polished with an emory cloth and washed to free the surface of contaminants. The electrode is then placed in a clean, nonmetallic container of fresh 0.9% NaCl solution and connected to the positive terminal of a constant current source. A larger bare silver electrode (approximately 1.0 in.²), also cleaned as just described, is placed at the opposite end of the container. The lead of this electrode is connected to the negative end of the constant current source. A milliammeter is placed in series with the electrode to be plated for determination of applied current.

The literature indicates (7) that the optimum electrode impedance can be achieved by using a current density in the range of 500 - 2000 mA-sec/cm², and should be applied at a rate greater than 5 mA/cm². Using a 6-mm-diam. electrode ($A = 0.28 \text{ cm}^2$) and an arbitrary current density of 1000 mA-sec/cm² at a rate of 7.5 mA/cm², 2.1 mA of current should be applied between the electrodes for 133 sec. Each electrode should be plated in this manner, and fresh NaCl should be used for each plating process. After plating, the electrodes should be handled with some degree of care, since the AgCl surface can be removed by abrasion. A small electrode (3-mm-diam., for example) could be used without degrading the amplitude or fidelity of the ECG. For a 3-mm electrode, with all other factors remaining constant, 0.53 mA should be applied for 133 sec.

2.6.3 Animal Instrumentation

Given the chlorided electrodes with leads and the percutaneous device with connector and leads, the animal can be instrumented for ECG by introducing the percutaneous leads subcutaneously at the exit site and bringing them out at the electrode site. The excess lead from each lead is then trimmed off and dressed for soldering, and all but approximately 2 in. trimmed off the electrode lead. A small piece (approximately 1/2 in.) of polyolefin heat-shrinkage tubing, Alpha FIT-300-1/8 (Alpha Wire, 711 Linderwood Ave., Elizabeth, N.J. 07207), is placed over one of the lead wires. The wires are

then soldered together, leaving only a small length (approximately 1/8 - 3/16 in.) of exposed wire. This shrinkable tubing is then slid over the exposed wire, and heat is applied at approximately 275°F at the splice. Care should be exercised so that the excessive heat is not applied to the PVC insulation of the leads. The polyolefin tubing has different characteristics from normal PVC heat-shrinkable tubing in that when heat is applied to polyolefin, the outer wall shrinks, but the inner wall melts, thus providing a moisture-proof, encapsulating jacket.

After the connectors have been positioned and sutures applied, a protective cap should be placed over the electrical connector to protect the pins. This protective cover should be kept in place when measurements are not being made.

2.6.4 Conclusions

In conclusion, we recommend using pyrolytic carbon percutaneous devices designed specifically for use with the miniature connector discussed in this report. We feel this device is a biologically compatible feedthrough which will facilitate physiologic measurements. Adequate protection for the connector, especially with the animal unrestrained, should result in a maintenance-free percutaneous lead system. We also recommend silver chloriding the silver electrodes, as VNB has done in the past (refer to section 2.6.2, B). The use of polyolefin tubing to obtain a waterproof seal will decrease the time required in instrumenting the animal, and will allow repeated use of the electrodes, percutaneous connector, and leads.

2.6.5 References

1. Al-Nakeeb, S., P. T. Pearson, and N. R. Cholvin. A thoracic percutaneous lead system: development and evaluation. *J Biomed Mater Res* 6:245-265 (1972).
2. Benson, J. Elemental carbon as a biomaterial. *J Biomed Mater Res Symposium* (Aug. 3-7, 1970, New England College, Henniker, N.H.), No. 2 (part 1), 41-47, 1971.
3. Bokros, J. C., et al. Prosthesis made of carbon. *Chemtech* 7:40-49 (1977).
4. Bokros, J. C., L. D. LaGrange, and F. J. Schoen. Control of structure of carbon for use in bioengineering. In Q. L. Walker (ed.). *Chemistry and physics of carbon*, vol. 9. N.Y.: Dekker, 1972.
5. Bokros, J. C. General Atomic Corporation, Division of Medical Products, San Diego, Calif. 92138. Personal communication, 1978.
6. Fryer, T. B., et al. Multichannel implantable telemetry system. NASA Tech Brief ARC-11079, Dec 1977.
7. Geddes, L. A. *Electrodes and the measurement of bioelectric events*. N.Y.: Wiley-Interscience, 1972.

8. Kedefors, R., and J. B. Reswick. A percutaneous electrode for long-term monitoring of bioelectric signals in humans. Med Biol Eng 8:129-135 (1970). [Now: Med Biol Eng Comput]
9. Kojima, G. K. Batteryless implanted echosonometer. NASA Tech Brief ARC-11035, Dec 1977.
10. Laenger, C. J., et al. A new communication method for deaf-blind people. Southwest Research Institute Technical Report 13-9134, 1974.
11. Laenger, C. J. Southwest Research Institute, San Antonio, Tex. Personal communication, 1978.
12. Miller, H. A., and D. C. Harrison. Biomedical electrode technology. N.Y.: Academic Press, Inc., 1974.
13. Miller, J., and C. E. Brooks. Problems related to the maintenance of chronic percutaneous electronic leads. J Biomed Mater Res Symposium (Aug. 3-7, 1970, New England College, Henniker, N.H.), No. 2 (part 1), 41-47, 1971.
14. Mooney, V., et al. Percutaneous implant devices. Ann Biomed Eng 5:34-46 (1977).
15. Mooney, V., et al. The use of pure carbon for permanent percutaneous electrical connector systems. Arch Surg 108:148-153 (1974).
16. Owen, L. J. Skin implant multiwire connector. NASA Tech Brief KSC-11030, Spring 1977.
17. Rogers, A., and L. B. Morris. Percutaneous leads for power and control of artificial hearts. Trans Am Soc Artif Intern Organs 13:146-150 (1967).
18. Vasco, K. A., and R. O. Rawson. A chronic non-reactive percutaneous lead system. Trans Am Soc Artif Intern Organs 13:143-145 (1967).

2.7 Control Center Data Distribution System Study

The patch panel system, presently installed at the USAFSAM human centrifuge control console, has several undesirable physical and electrical qualities. Technology Incorporated was assigned the task of locating, evaluating, and recommending a suitable replacement for the patchcord programming system. In addition to the resulting recommendation, this report includes a drawing of a suggested physical arrangement and a generalized block diagram of the recommended electrical arrangement.

2.7.1 Undesirable Characteristics

The more annoying of the electrical inadequacies of the present system is the problem of poor electrical contact between the patch panel receptacles and the patchcord tips. Poor contact causes erratic changes

in the signal levels whenever the console is bumped or the patchcords are moved. Perturbations of the signals during several tests have been painstakingly traced to the patch panel.

The physical construction of the present patch panel system creates several recurring problems--one is the force required to insert or remove patchcord tips; and another, the poor arrangement of the signal processing inputs and outputs. The force required to patch or unpatch the tips frequently results in broken patchcords; and the poor arrangement almost always results in a maze of tangled patchcords.

2.7.2 Recommendations

Specification sheets and other literature pertaining to patchcord programming systems were solicited from 43 manufacturers of such systems. The manufacturers were selected from those listed in the 20th edition of the Electronic Engineer's Master, Technical Publications, Inc., 645 Stewart Ave., Garden City, N.Y. 11530).

Initially, much consideration was given to obtaining a shielded system identical to the one presently installed at the data collection center. This purchase would have been an advantage because spare patchboards are either on hand or available. However, according to the manufacturer, Amp Inc. (Box 3608, Harrisburg, Pa. 17105), the data center system was obsolete. The production department of Amp Inc. advised that a system (identical to the one presently installed at the data collection center) could be fabricated; but it would require "intensive labor," and so would tend to be cost prohibitive.

The better patchcord programming systems available are of the shielded type with all contact surfaces gold plated; and such systems yield a good signal-to-noise ratio with little crosstalk. These are the qualities required for best results in signal processing at the centrifuge console.

After the available literature on several systems from various manufacturers had been studied, the patchcord programming system recommended was the 960 system manufactured by Amp Inc. The 960 system is of the preprogrammable, removable type, and has the format of 30 holes vertical by 32 holes horizontal. The external dimensions of the patchcord (including the frame) are 16-13/64 in. high by 14-47/64 in. wide (41.2 cm high X 37.4 cm wide). The front of the 960 system patchboard extends 2-1/4 in. (5.7 cm) forward from the panel on which it is mounted. Dividing the patch panel into its various system inputs and outputs sections, by contrasting color patterns, tends to increase the speed and ease of reprogramming for various tasks. Amp Inc. can silk-screen the patchboard according to any convenient pattern furnished by the buyer of the system at additional cost. Technology Inc. recommends that several patchboards be purchased so that they can be preprogrammed for each test protocol. Then repatching between tests and experiments would consist of simply removing one patchboard and replacing it with the proper one. This approach would insure standardization of the patching procedures and also save time.

A suitable enclosure for mounting the system is manufactured by the Premier Metal Products Company (Div. of Sunshine Mining Co., 381 Canal Place,

Bronx, N.Y. 10451). The stock number is TIC 21-19-13; and the dimensions are 21 in. high by 19 in. wide by 13 in. panel-to-panel depth (53.3 cm X 48.3 cm X 3.3 cm).

The new patch-panel system should be located in approximately the same position as the presently installed patch panel. The rear frame of the patch panel should be physically located in the enclosure, such that easy access for troubleshooting and/or wiring is afforded.

The physical arrangement of the inputs and outputs of the various data systems (Fig. 120) is the composite of the better features of several arrangements studied for this report. Figure 121 is a block diagram of the proposed centrifuge data distribution system. Special consideration was given to arranging the inputs and outputs of the various systems to be programmed by the patch panel. The inputs and outputs that are more frequently patched into each other are placed either adjacent to each other, or as close as physically feasible.

The 16 BNC connectors, that in the present system provide access to systems external to the patch panel, are very useful; and this arrangement should be retained in the new system. An additional recommendation is that several MS-type connectors be placed at the convenient locations, either on the console or the patchboard system enclosure, and wired to the available patch panel contacts. This arrangement would allow flexibility in patching external systems, such as tracking tasks to the centrifuge. Several nonpolarized capacitors should be wired between ground and convenient patchboard contacts to provide ac bypass to ground and/or glitch filtering, as required.

An arrangement for monitoring the outputs of the signal conditioners should be provided. It should be able to switch select all 16 preamplifiers, instead of just 12, as in the current system.

Patchable access to permanently installed digital multimeters (DMM's) would be very useful for monitoring signal levels, determining resistances, or checking the continuity of signal pairs.

The signals from the accelerometers are usually patched into channel 1 of the data recording systems, and this arrangement should also be kept in the new system. Hard wiring into channel 1 is not recommended. Because the patchboards are pre-programmable and quickly changeable, the selector switch (presently used to select either the gondola accelerometer or the animal end accelerometer) is not necessary.

One final consideration that may be of some future value is the utilization of a few spare, or seldom used, signal pairs for an instrumentation ground. These signal pairs would be useful for patching through a ground to the signal patch panels on the centrifuge to provide an instrumentation ground separate from the power ground.

2.8 Closed-Loop Centrifuge Control Study

2.8.1 Objective

The purpose of this study was to perform circuit analysis, circuit design, and troubleshooting on an Air Force developed electronic method for closed-loop control of the human centrifuge.

HUMAN END SLIP RINGS Signal Pairs 1 through 14					Connectors BNC 1 - 8	
PREAMPLIFIER INPUTS Channel 1 through 16						
Meter Volts	HUMAN END SLIP RINGS Signal Pairs 15 through 27				Signal Pairs to Gondola Special 8 Pairs	
	ANIMAL END SLIP RINGS Signal Pairs 1 through 14					
PREAMPLIFIER INPUTS Channel 1 through 16						
Meter mV	ANIMAL END SLIP RINGS Signal Pairs 15 through 17				Connectors BNC 9 - 16	
PREAMPLIFIER OUTPUTS MULTIPLE (COMMON) OF 5 PER OUTPUT Channels 1 through 16						
8 CHANNEL BRUSH RECORDER INPUTS			8 CHANNEL BRUSH RECORDER OUTPUTS			
SIGNAL PAIRS TO DATA COLLECTION CENTER Pairs 1 through 32						
EXCITATION FROM TRANSDUCER OR CARRIER Preamplifiers 1 through 16						
BALANCE POTS	+DC	EVENT MARKERS FOR BRUSH RECORDER RIGHT AND LEFT 9 each	MULTIPLES (COMMON)	MEDI SCOPE	CONNECTOR J8	J1 CONNECTOR MS16-26 26 Pins
TOTAL 8	TOTAL 16		Nine Sets of Four	8 Ch.	40 Available	Spare 13
						J2 CONNECTOR MS16-26 26 Pins
						Spare 13
						J3 CONNECTOR MS16-26 26 Pins
CAPA- CITORS Total 9	Spare Meter Spare	Spare 14		GROUND Total 21		Spare 38
						G

Figure 120. Recommended arrangement of new patchcord programming system.
[POTS = potentiometers]

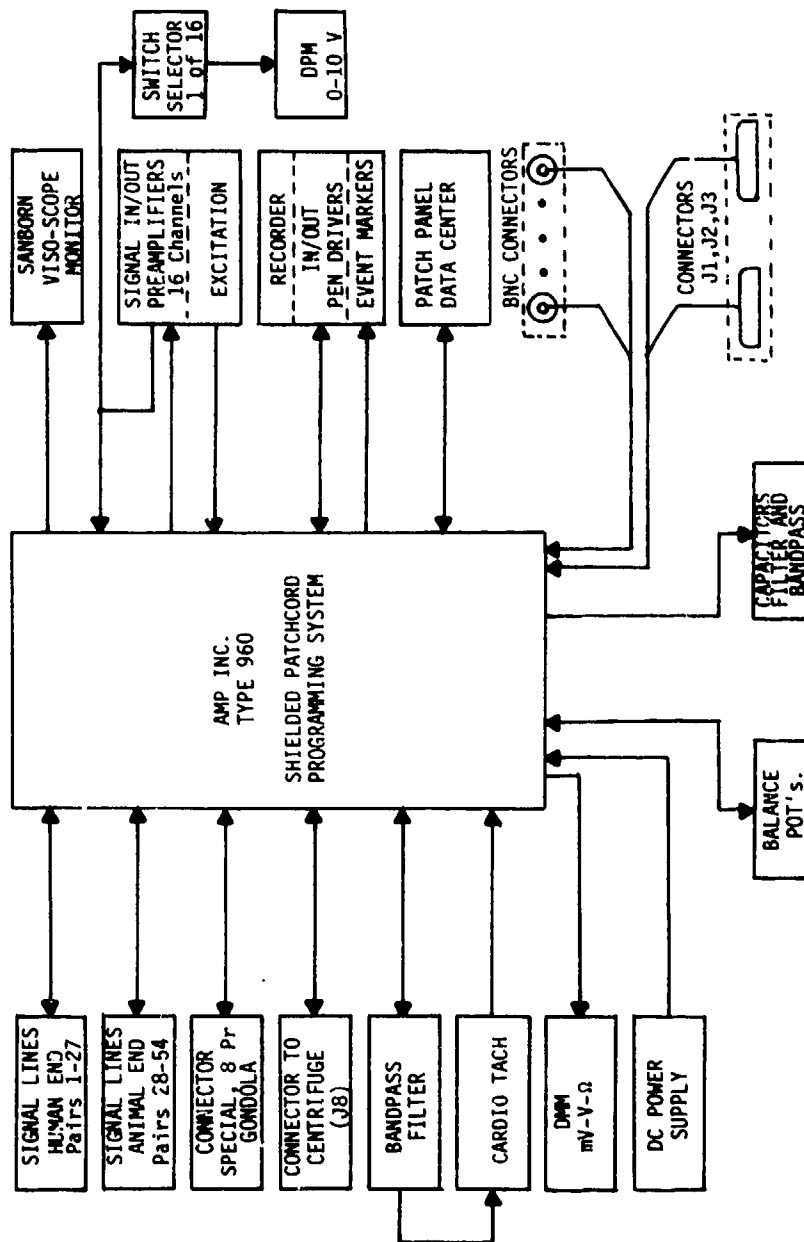


Figure 121. New patchcord programming system.
[POTS = potentiometers]

2.8.2 Normal Centrifuge Operation (Figs. 122 - 125)

Pressurized hydraulic fluid for the drive system is supplied by 5 variable volume pumps which are driven by 4 electric motors. The pressurized hydraulic fluid turns the 8 fluid motors, which, in turn, drives the rotor arm through gear trains. The motor speed, which is proportional to fluid flow through the motors, is adjusted by means of a servo control, which varies the output volume of the pumps. The motor inlet pressure is controlled by the onset pressure control, A207 (Fig. 122), which determines the pressure (between 0 psi and 5000 psi) at which the onset relief valves (RV-3 through RV-7, in Fig. 125), vent the pump output to the main reservoir. As shown in Figure 125, when the 4-way valves (DCV-1 through DCV-5) are in the spring offset position (solenoids L-7, L-8, L-403, L-404, L-405, not energized), this pressure is reservoir pressure. When these solenoids are energized by the pressure command, the pilot pressure to the onset relief valves is determined by the setting of the electrically operated relief valve, B-402 (Fig. 125). B-402 is adjustable between 0 psi and 5000 psi by the onset pressure control, A-207.

Deceleration of the rotor arm is accomplished by depressurizing the hydraulic motor inlets and restricting the motor outlets so that the motors, as they are driven by the moving rotor arm, pump the fluid against a back pressure, thus resulting in a braking torque. This motor outlet pressure is controlled by brake pressure control signals, which determine the pressure at which the brake relief valves will vent hydraulic fluid to the main reservoir.

Specifically, the hydraulic fluid flows from the outlet ports of fluid motors MF-1 through MF-8 (Fig. 124) through the return manifold, through the three braking relief valves (RV-8, RV-9, and RV-10), which are designed to relieve at their spring setting (5000 psi) or at their pilot pressure (0 to 5000 psi), whichever is lower. When 4-way valve DCV-7 is in its spring-offset position, it blocks the flow of pilot fluid through the three braking relief valves. When DCV-7 is activated (first ready status) by L-401, pilot pressure flows from the three braking relief valves, through the three check valves (CV-22, CV-23, and CV-24), through DCV-7 itself, to electrically adjustable relief valve B-401. B-401 is adjustable between 0 psi and 5000 psi by deceleration pressure control A-206 (Fig. 122) on the console. The closure of K-322 (first ready) contacts energizes relays K-308, K-226, K-309, and onset pressure control A-207. Relay K-226 is energized through K-4 contacts (which remain closed until final ready status), thereby energizing deceleration pressure control A-206 and preventing pressurization of the main hydraulic pumps.

The momentary closure of pressure switch S-212 (Fig. 123) energizes and locks K-323, the contacts of which energize the solenoids (L-7, L-8, L-403, L-404, and L-405) of the pump vent valves DCV-1 through DCV-5. These valves allow onset pressure control A207 to control relief valves RV-3 through RV-7 which, in turn, control pump outlet.

Momentary closure of hydraulic brake switch S-208 energizes K-226 and opens the normally closed contacts K-226 which, in turn, causes K-323 to be deenergized and depressurizes the system. During the time of S-208 closure, the deceleration pressure control A-206 is energized and hydraulic braking is available.

2.8.3 Closed-Loop Control System Developed by the Air Force

The closed-loop control system, developed by the Air Force, utilizes a control stick command voltage and feedback voltage from an accelerometer (Fig. 126). The design intent was that, when these two signals were in equilibrium, the gondola would reach a G-level proportional to the control stick position.

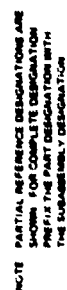
The closed-loop control circuit, which takes the place of the onset pressure control A-207 and the deceleration pressure control A-206, has two outputs. When the control stick voltage (V_r) is greater than the accelerometer feedback voltage (V_a), voltage is applied to the onset relief valve B-402. When V_r is less than V_a , voltage is applied to the brake pressure valve B-401. Also, when the closed-loop control system was tested, hydraulic brake switch S-208 (console) and the pressurize switch S-212 (console) were each shorted to the closed position at all times, and the normally closed contacts of K-226 were externally shorted. These are the contacts that open and break the pressurization circuit when the hydraulic brake switch is momentarily closed. In other words, with the control circuit wired in this configuration, the hydraulic system cannot be depressurized when the hydraulic brake is applied ($V_r < V_a$).

The centrifuge has many electrical and hydraulic interlocks, many of which were designed for subject safety, and several of which were designed to prevent damage to the hydraulic system itself. For example, the contacts of K-4, which energize the deceleration pressure control for hydraulic braking and prevent the system from being pressurized, are normally closed until first ready status. Under the test configuration just discussed, the interlocking safety features of K-4, S-208, and K-226 are circumvented. The contractor feels that these interlocks should not be bypassed and that the hydraulic system should be depressurized before applying the hydraulic brake. Operation of the centrifuge without these designed safety interlocks could cause catastrophic damage to the hydraulic system.

2.8.4 Design Modifications

The contractor feels that the electronic circuit of the control system developed by the Air Force is a workable design that, with certain modifications, can be used in the closed-loop control system. These modifications must provide three modes of operation--pressurization and onset pressure control, depressurization, and hydraulic brake control--which possibly could be accomplished by comparing the control voltage (V_r) with the accelerometer voltage (V_a). When $V_r \geq V_a$, the pressure switch S-212 would close and the gondola would accelerate until $V_r = V_a$. The position of the control stick would represent a certain G level. When $V_r < V_a$, by some small fixed difference, S-211 would be opened and the system depressurized. This small voltage difference would allow for minor adjustments in G level by pressurizing and depressurizing the system, without applying hydraulic braking. When $V_r \ll V_a$ by some larger but fixed difference, the system would be depressurized and hydraulic braking applied in proportion to the difference between V_r and V_a . The contractor feels that all three modes (pressurization, depressurization, and hydraulic braking) are necessary for operating the gondola on an SACM profile.

In addition to having control over the gondola via the emergency kill, the pilot controls (already described) should also be designed for manual over-ride at the console.



184

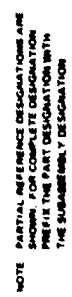


Figure 123. Electrical rotor arm drive subsystem (Part II).
[TO 43D8-7-2-2, AFLC/Hill AFB, Ogden, Utah]

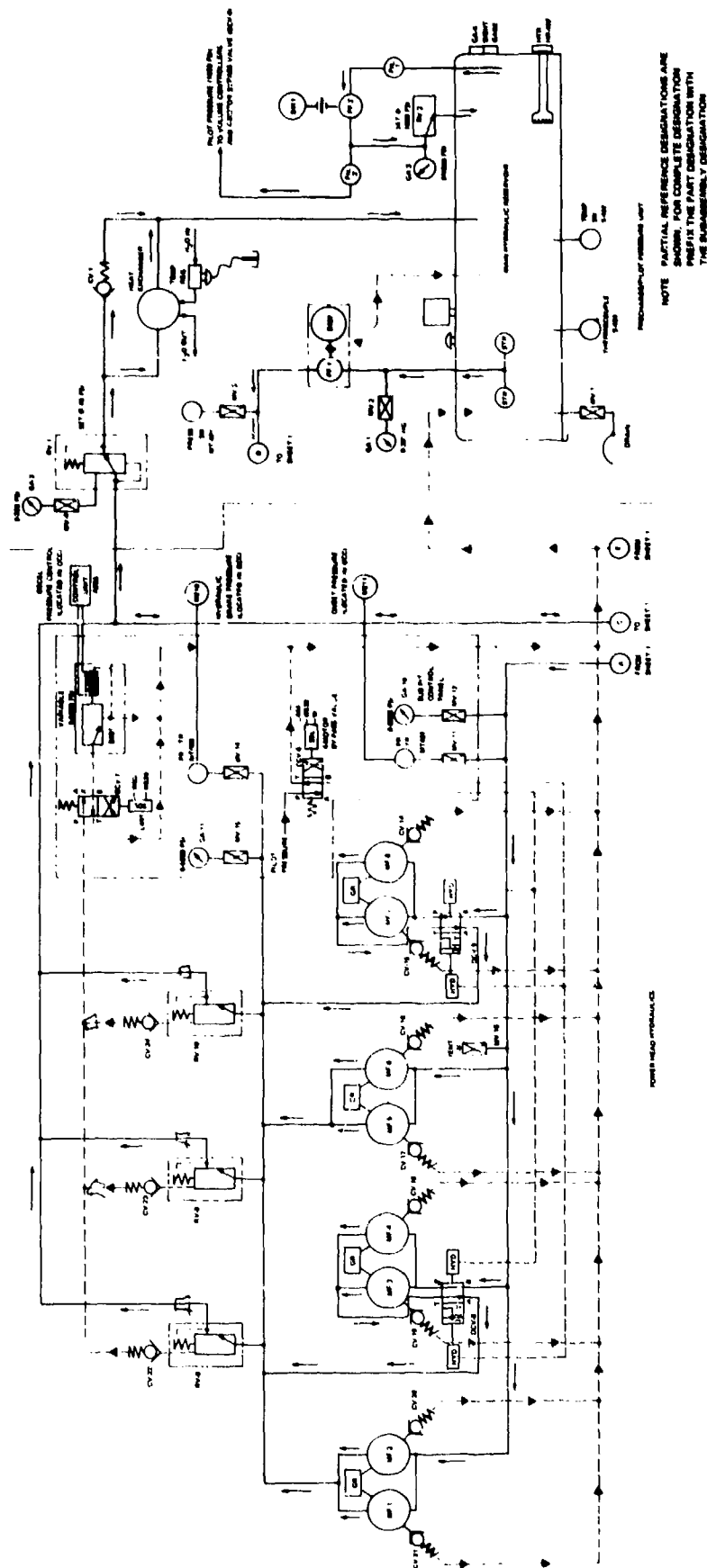
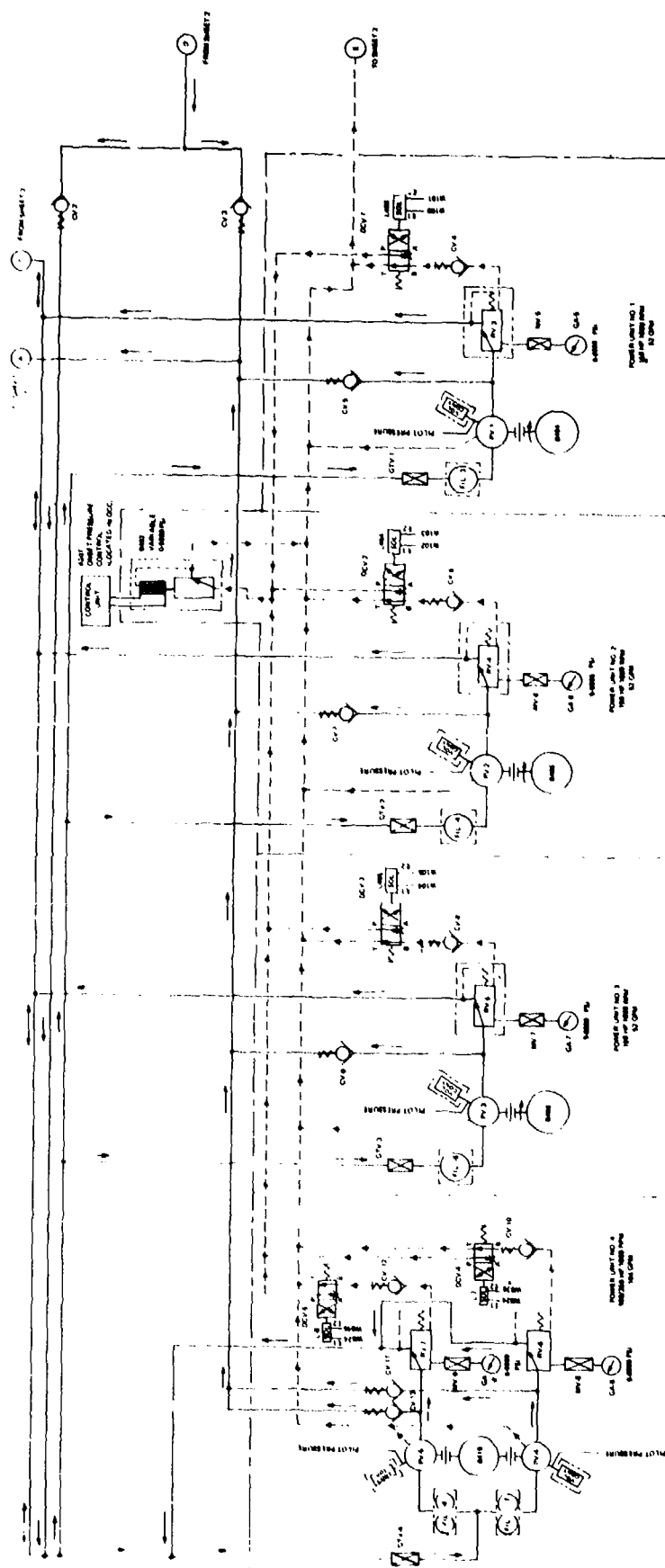


Figure 124. Hydraulic rotor arm drive subsystem (Part I).
[TO 43D8-7-2-2, AFLC/Hill AFB, Ogden, Utah]



NOTE: PARTIAL REFERENCE DESIGNATIONS ARE SHOWN. FOR COMPLETE DESIGNATION, REFER TO THE PART DESIGNATION WITHIN THE SUB-ASSEMBLY DESIGNATION.

Figure 125. Hydraulic rotor arm drive subsystem (Part II).
[TO 43D8-7-2-2, AFLC/Hill AFB, Ogden, Utah]

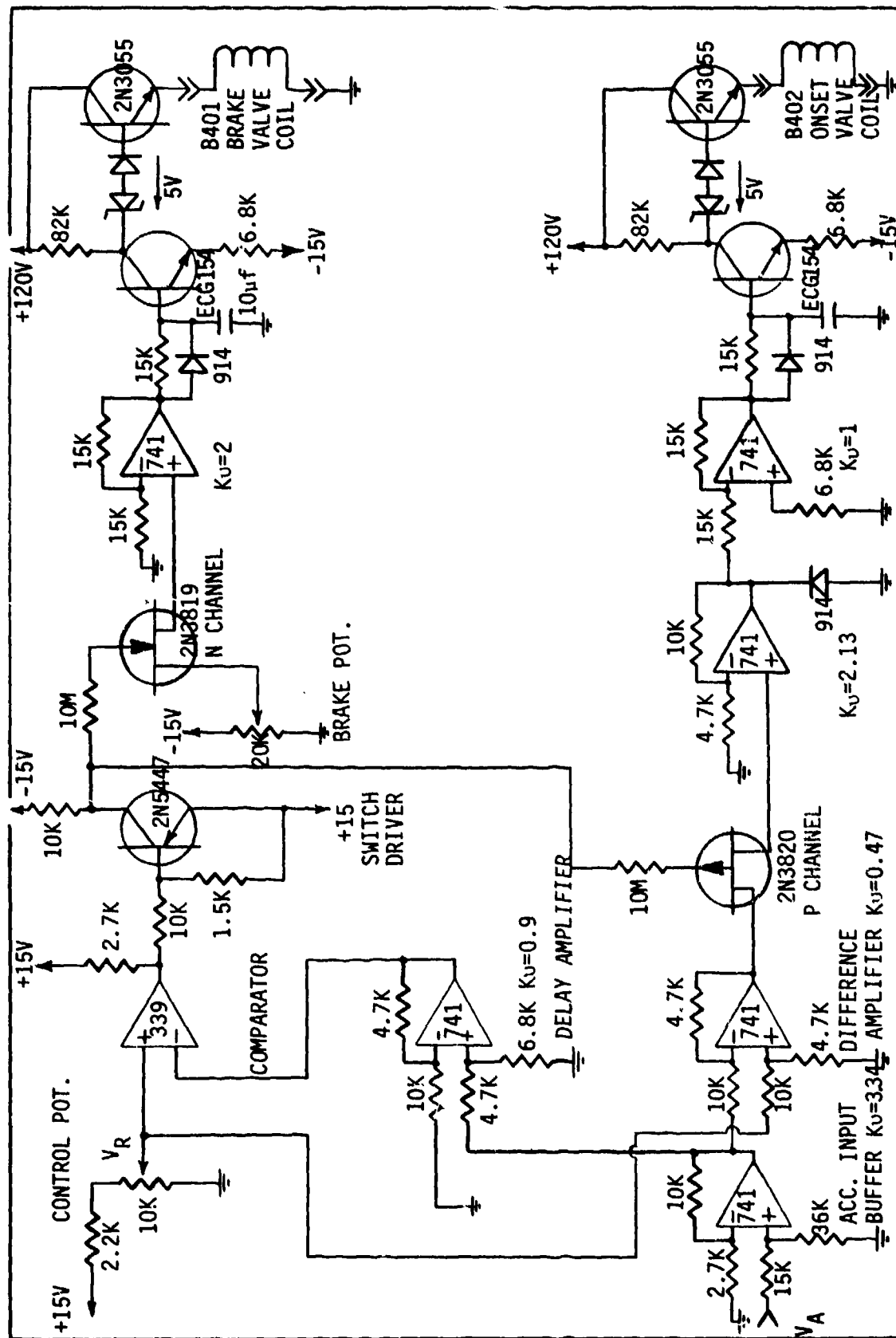


Figure 126. Air Force closed-loop control circuit.

Additional design modifications in the Air Force developed system should also include hysteresis and temperature compensation of the electrolytic valves (B-401 and B-402) employed in the A-206 and A-207 control circuitry. These changes are not essential in the initial design stages, and could easily be incorporated after the design concept has been proven.

In conclusion, we recommend making the following design changes on the closed-loop control system developed by the Air Force:

- (1) pressurization and onset pressure control with control stick voltage V_r greater than accelerometer voltage V_a ;
- (2) depressurization and subsequent deceleration with control stick voltage V_r slightly less than accelerometer voltage V_a ;
- (3) hydraulic braking proportional to the difference between V_r and V_a for large $|V_r - V_a|$; and
- (4) hysteresis and temperature compensation for control valves B-401 and B-402.

2.9 Medilog Recorder G-sensitivity Tests

2.9.1 Introduction

The Medilog recorder is a miniature 4-channel tape recorder designed specifically for monitoring of ambulatory subjects. Data is recorded on a 2-hr or 24-hr recorder, and is recovered from the Oxford reproduce unit at a rate of 60 times real-time of the recorded tape.

The purpose of these tests was to determine the sensitivity of the Medilog 4-24 tape recorder to various levels of G forces on the three orthogonal axes. The recorder selected for these tests was a 24-hr recorder (S/N 06481) with the following preamplifier configuration: channel 1--EG2 (ECG); channel 2--AM3 (acceleration); channel 3--AM3 (G-suit pressure); and channel 4--AT2 (temperature).

2.9.2 Test Protocol and Configurations

A. Time base expansion test: Since the recorded data cannot be recovered from the recorder on a real-time basis, and the fact that the record unit has an upper frequency response limitation (100 Hz on the EG2, and 4 Hz on the AM3) precluded the use of time code recording and the correlation of real-time events with recorded test data--all events during the centrifuge runs were correlated to recorded G levels (channel 3). Also, the 60 times real-time reproduction speed necessitated using a second instrumentation recorder to obtain a 32:1 expansion of all test data.

The test configuration for the time base expansion is shown in Figure 127. Signal amplitudes and frequencies were selected to be compatible with actual recorded data for channels 1 and 2 (ECG and pressure respectively). Amplitudes

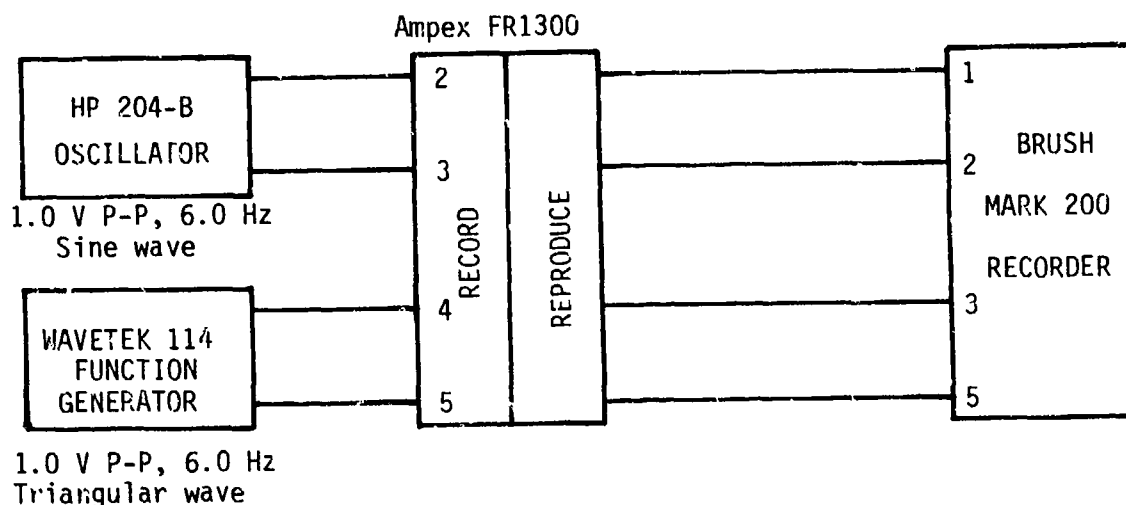


Figure 127. Time base expansion test configuration.

and frequencies for channels 3 and 4 were selected as a matter of convenience. Test signals were recorded at a speed of 60 ips and were reproduced at 1-7/8 ips for a time base expansion of 32:1. All test signal frequencies and amplitudes were monitored with a Systron Donner 6152 A counter and a Tektronix 564 oscilloscope during both record and reproduce modes.

B. Medilog recorder and reproducer tests: This experiment was designed to test the Medilog for fidelity of record and reproduction of signals while being exposed to various levels of G forces.

The recorder axis orientation is shown in Figure 128, and the test configuration in Figure 129. The 10 Hz sine wave was selected for channel 1; for this sine wave was well within the bandpass of the EG2 amplifier, and the reproduced signal (10 X 60/32 = 18.75) was fast enough to be counted on the frequency counter but slow enough to copy on the Brush recorder. The 0.1 Hz triangular signal was selected because it was within the bandpass of the AM3 recorder and would allow an easy method for testing amplitude variation in the Medilog recorder. The signals for channels 1 and 3 were differential inputs, with the tape recorder common used as the reference ground. These signals were sent through the instrumentation slip rings, but were monitored in the gondola at the recorder input--before and after the centrifuge runs--with a Tektronix 564 scope. The input signal frequency for channel 1 was monitored at the console with a Systron Donner 6152A counter.

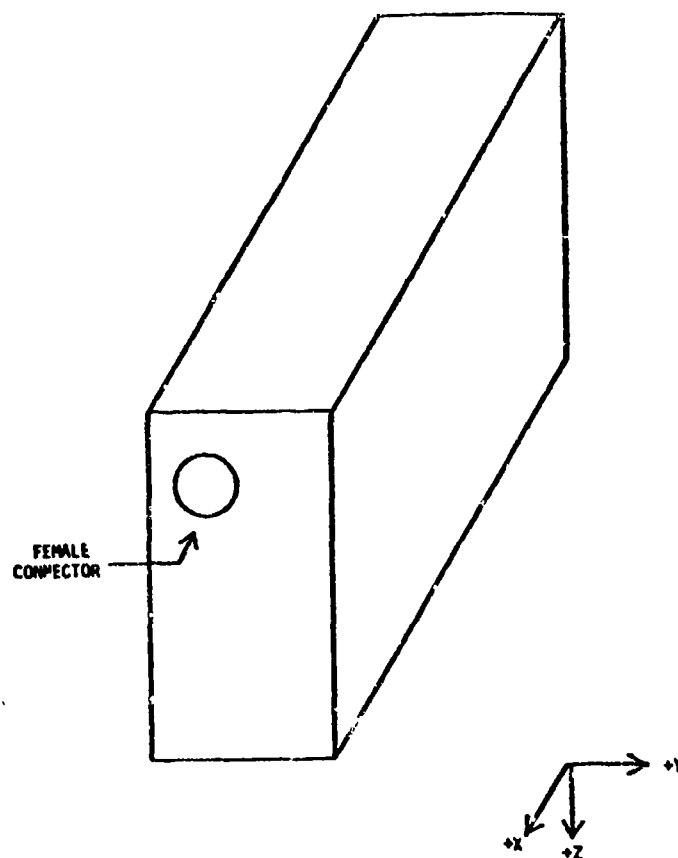


Figure 128. Recorder axis orientation.

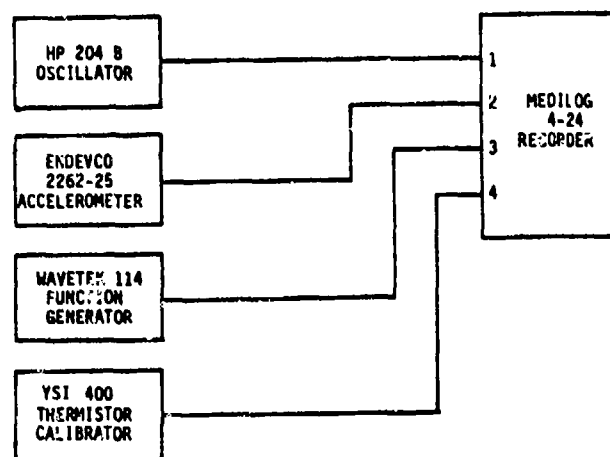


Figure 129. Medilog recorder test configuration.

TABLE 25. ORDER OF AXIS TESTING AND TEST SIGNALS

AXIS	CHANNEL 1 (10 Hz)	CHANNEL 2	CHANNEL 3 (0.1 Hz)	CHANNEL 4
+Z	1 mV p-p	1-10 G	8 mV p-p	37°C
-Z	"	"	"	40°C
+X	"	"	"	33°C
-X	"	"	"	34°C
+Y	"	"	"	27°C
-Y	"	"	"	30°C

The Medilog recorder was exposed to 1 min of acceleration, from 2 to 10 G and back to 2 G, in 2-G increments (Table 25). The recorded test tape was then reproduced from the Oxford reproduce unit at 60 times real time and re-recorded on the Ampex FR1300 at 60 ips. This test setup is shown in Figure 130, and the test conditions are described in Table 26. The 6152A counter time base was set on 10-sec count to provide at least 3 frequency counts at each G level. The digital multimeter was used to indicate different G levels and to insure that frequency counts were not taken between different G levels.

2.9.3 Test Results

A. Time base expansion: Test results from the time base expansion test (Fig. 127) are shown in Table 27. The actual measurement of the 600 Hz signal, reduced by 32, should be 18.75 Hz; however, the resolution of the counter is only provided for 0.1 Hz, so percent error is not shown for this frequency. The 6 Hz signal for channels 2 and 3 should be 0.1875 Hz. This frequency was determined by strip-chart measurement and chart speed. The amplitude of all signals was approximately 1.05 V peak-to-peak, and did not vary significantly throughout the test. The absolute amplitude of each signal was not considered important for this test, and only the variations in the frequency during the test were considered. This test indicates that no appreciable frequency or amplitude error would be introduced into the Medilog recorder test by using a 32:1 time base expansion.

B. Medilog recorder-reproducer: The recorded data tape was reproduced and re-recorded using the test configuration of Figure 130. The mean frequency count for the G level in each axis is shown in Table 28. The standard deviation of frequency for any G level was less than 0.1 Hz, and was usually less than 0.06 Hz.

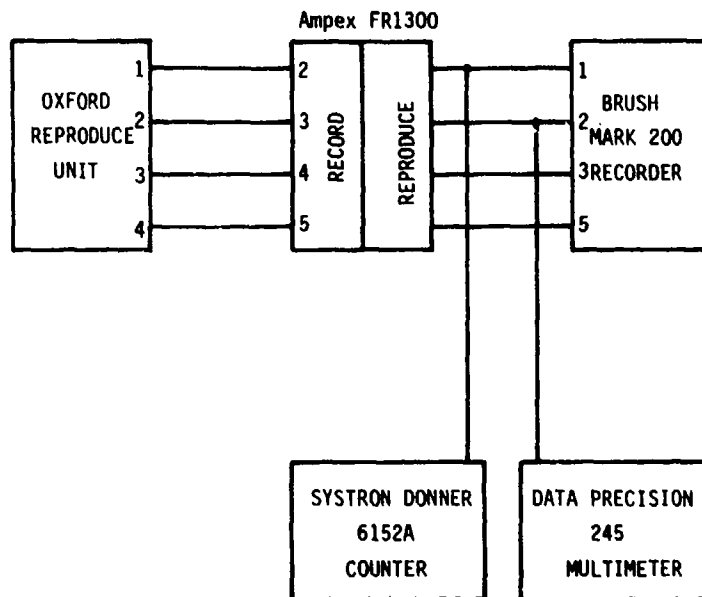


Figure 130. Oxford reproduce and re-record test configuration.

TABLE 26. OXFORD REPRODUCE TEST SETUP

CHANNEL	AMPLIFIER	GAIN	FILTER
1	PD-2	MAX	MIN (both filters)
2	PM-3	MAX	5 (MAX)
3	PM-3	MAX	0 (MIN)
4	PM-3	MAX	5 (MAX)

TABLE 27. TIME BASE EXPANSION ACCURACY

CHANNEL	FREQUENCY (Hz)		PERCENT ERROR
	Input	Output	
1	600	18.7	--
2	6	0.188	0.27
3	6	0.188	0.27
4	600	18.7	--

TABLE 28. REPRODUCED FREQUENCY (MEAN)

G	+Z	-Z	+X	-X	+Y	-Y
1	16.93	16.60	16.60	16.60	16.64	16.60
2	17.04	16.68	16.54	16.60	16.70	16.63
4	18.19	16.73	16.64	16.75	16.80	16.80
6	18.43	16.80	16.75	16.83	16.90	17.03
8	18.48	16.95	16.85	16.90	17.02	18.50
10	18.52	17.05	16.92	17.00	17.08	18.53
8	18.50	16.95	16.82	16.88	16.93	18.47
6	18.48	16.87	16.70	16.80	16.85	18.43
4	18.45	16.78	16.60	16.73	16.87	18.45
2	18.45	16.65	16.56	16.63	16.63	18.47
1	18.47	16.57	16.57	16.68	16.56	18.43

TABLE 29. PERCENT ERROR IN FREQUENCY REPRODUCTION
AT 1-G START OF RUN

AXIS	PERCENT ERROR
+Z	-9.71
-Z	-11.47
+X	-11.47
-X	-11.47
+Y	-11.25
-Y	-11.47

TABLE 30. PERCENT ERROR CHANNEL 1 REPRODUCE NORMALIZED TO
1-G START OF RUN

G	+Z	-Z	+X	-X	+Y	-Y
1	0	0	0	0	0	0
2	0.65	0.45	-0.36	0	0.36	0.18
4	7.35	0.75	0.24	0.90	0.96	1.20
6	8.83	1.20	0.90	1.36	1.56	2.59
8	9.13	2.11	1.51	1.81	2.28	11.45
10	9.39	2.71	1.93	2.41	2.64	11.60
8	9.27	2.11	1.33	1.69	1.74	11.27
6	9.13	1.66	0.60	1.20	1.26	11.02
4	8.98	1.06	0	0.75	0.84	11.14
2	8.98	0.30	-0.24	0.18	-0.06	11.27
1	9.07	-0.18	-0.18	0.45	-0.48	11.02

The 1-G level (start of the run) shows that the reproduced frequency was lower than the expected 18.75 Hz. This systematic error indicates that the recorder-reproducer combination of speed is different from the specified value. Specifically, the record speed is too fast and/or the reproduce speed is too slow. This error in reproduction (shown in Table 29) is normalized to 18.75 Hz, and indicates an error in frequency reproduction of approximately -11%. Consequently, if the recorded ECG is used to derive heart-rate information, the same -11% error can be expected.

To separate this systematic tape recorder error from the G-induced error, each axis run was normalized to the 1-G frequency output at the start of the run. This error (shown in Table 30) indicates that an error in frequency reproduction for all axes reaches a maximum at the 10-G level. The error for -Z, X, -X, and Y is only slight (a maximum of 2.7% for -Z with little hysteresis) compared to that for Z and -Y. The Z and -Y axes show considerable error (9.39% and 11.6%, respectively) and a considerable amount of hysteresis. From the axis orientation (Fig. 128), nothing indicates a Z, -Y G relationship which would affect record speed. It should be pointed out that the Z-axis run was conducted on one day, and the remainder of the axes were tested on consecutive runs of the next day.

Interestingly, the G-induced error is the opposite direction of the systematic system error. Since we have no reason to suspect a change in reproduce speeds due to G levels (other than possible random changes), this finding indicates the record speed in all axes is reduced as a result of G forces. This conclusion accounts for the almost linear change (minus a small hysteresis) in tape speed with respect to G for the -Z, X, -X, and Y axes, but does not explain the large error and hysteresis observed in the Z and -Y axes. The only explanation for these deviations is the possibility of random variations in tape recorder speed. Since the tape recorder has a phase-locked loop speed control, speed variations should not occur in the recorder. We should also point out that, before the test, the record head and guides were cleaned and a fresh set of batteries were installed in the recorder.

Test signal amplitudes were also observed for variations due to G forces. The contractor feels that the amplitude variations in the test signals, due to G, were inconsequential. In fact, amplitude variations in the AM3 (channel 3) were virtually nonexistent, and only minor variations were observed in the EG2 (channel 1). One problem did occur in the initial tests with regard to amplitude variations--which appeared large (30% - 40%), with occasional dropout at 1 G. Although a bad cassette proved to be the cause, the possible problem area is one of which VNB should be aware. The contractor suggests that each cassette be tested briefly before being used in the field. This test could be made by simply recording and reproducing the calibration signals before each subject is instrumented.

2.9.4 Conclusions

The large systematic errors observed in the system can probably be isolated to the recorder or reproduce units. Since VNB has two 24-hr recorders and one 2-hr recorder, a common signal should be recorded

on a single channel of each recorder simultaneously. The signal should be monitored with a frequency counter during recording and reproducing. Using the three recorded tapes, and the two reproduce speeds, a process of elimination could indicate recorder, reproducer, or a combinational error of the two. For example, if the two 24-hr tapes are reproduced at the same but lower than expected frequency, the reproduce speed should be adjusted for the desired frequency output. If, however, the two 24-hr tapes are different in response, with only one reproducing as expected, we would suspect that the record speed of the second recorder needed adjustment. This suspicion should be confirmed by checking the accuracy of the 2-hr recorder before any adjustments are made. By using this process, a logic table could be used in isolating the recorder(s) and/or the reproduce unit, which are operating at the incorrect speed. Continued investigation into the speed (frequency) error of the Medilog recorder system is beyond the scope of this effort.

ABBREVIATIONS, ACRONYMS, AND SYMBOLS

ac	alternating current
ACM	Aerial Combat Maneuver
Ag	silver
Ag-AgCl	silver-silver chloride
AgCl	silver chloride
AGS	anti-G suit
AGV	anti-G valve
AWG	American Wire Gage
BRP	Data Processing Branch, Data Sciences Division, USAFSAM
BNC	Bayonet "N" Type Connector
CAL	calibration
CR	center of rotation
dc	direct current
dG/dt	rate of change of acceleration with respect to time
DMM	digital multimeter
dP/dG	rate of change of pressure with respect to acceleration
ECG	electrocardiogram
FAIL	failures
GVALVPGM	a specialized FORTRAN IV and IBM Assembly computer program for the analysis of anti-G valve data recorded in accordance with the SVTP
GVALPROC	an IBM procedure, written in IBM JCL, which utilizes analog-to-digital tapes
G _z	acceleration along the Z axis (head to foot) [also: G(Z)]
Hz	Hertz (cycles per second)
ips	inches per second
m	meter
mA	milliampere

MS	Military Standard (when used as a prefix for an electrical connector)
mV	millivolt
NAILSC	Naval Aviation Integrated Logistics Support Center
OP TIME	operating time (flight hours)
OTH/MAL	other malfunctions
PET	Performance Evaluation Table
p - p	peak-to-peak
P _s	source pressure
psig	pounds per square inch gage
PTAP	Procedural Tests for Anti-G Protective Devices
PVC	polyvinylchloride
RPM	ready pressure anti-G valve mannequin
RPV	ready pressure valve
SACM	Simulated Aerial Combat Maneuver
SAM	School of Aerospace Medicine (Brooks AFB, Tex.)
SVTP	Standardized Anti-G Valve Test Protocol
V	volt
V _a	accelerometer voltage
VCG	vector cardiogram
VDC	volts (direct current)
VNB	Biodynamics Branch, Crew Technology Division, USAFSAM
V _r	control voltage
WRT	with respect to

[How to order Appendix A

RE: The USAF School of Aerospace Medicine's Technical Report Series
on Procedural Tests for Anti-G Protective Devices--
Volume I (SAM-TR-79-30), and Volume II (SAM-TR-79-31).

APPENDIX A:

In order for comprehensive information on this research
to be readily accessible, microfiche have been made of
this Appendix. The microfiche are available through:

The Strughold Aeromedical Library
Documentation Section (USAFSAM/TSK)
USAF School of Aerospace Medicine
Brooks AFB, Texas 78235